Fall 12-16-2016

Pancreatic Cancer Invasion of the Lymphatic Vasculature and Contributions of the Tumor Microenvironment: Roles for E-selectin and CXCR4

Maria M. Steele
University of Nebraska Medical Center

PANCREATIC CANCER INVASION OF THE LYMPHATIC VASCULATURE AND CONTRIBUTIONS OF THE TUMOR MICROENVIRONMENT: ROLES FOR E-SELECTIN AND CXCR4

By

Maria M. Steele

A DISSERTATION

Presented to the Faculty of

the University of Nebraska Graduate College

in Partial Fulfillment of the Requirements

for the Degree of Doctor of Philosophy

Cancer Research Graduate Program

Under the Supervision of Professor Michael A. Hollingsworth

University of Nebraska Medical Center

Omaha, NE

November, 2016

Supervisory Committee

Michael A. Hollingsworth, Ph.D.

Kaustubh Datta, Ph.D.

Angie Rizzino, Ph.D.

Joyce C. Solheim, Ph.D.

PANCREATIC CANCER INVASION OF THE LYMPHATIC VASCULATURE AND CONTRIBUTIONS OF THE TUMOR MICROENVIRONMENT: ROLES FOR E-SELECTIN AND CXCR4

Maria M. Steele

University of Nebraska, 2016

Advisor: Michael A. Hollingsworth

ABSTRACT

As the fourth leading cause of cancer-related deaths, pancreatic cancer is one of the most lethal forms of cancers in the United States. Lymphatic vessel invasion and subsequent metastasis to the lymph nodes are early and significant events observed during pancreatic cancer progression and are used to determine patient prognosis and therapy selection. Although clinicians and researchers recognize the importance of lymph node involvement for patient prognosis and therapy selection, the biological mechanisms that govern lymphatic invasion and metastasis and the contributions of the pancreatic tumor microenvironment to these processes remain poorly understood. In this dissertation, we characterize the interactions of lymphatic endothelial cells with pancreatic tumor cells and pancreatic fibroblasts, showing that while both cell types accelerate lymphangiogenesis, pancreatic fibroblasts are the major recruiters of lymphatic endothelial cells. Additionally, we evaluated pancreatic tumor cell invasion of lymphatics and demonstrated that adhesion protein E-selectin regulates pancreatic tumor adhesion to and transendothelial migration across a lymphatic endothelium. Blockade of E-selectin using a novel glycomimetic inhibitor, GMI-1271, significantly impaired these processes if pancreatic tumor cells expressed the proper E-selectin ligands. E-selectin blockade *in vivo* significantly impaired pancreatic tumor metastasis to a number of organs sites including the lymph nodes. This

impairment of metastasis through the lymphatic vasculature by GMI-1271 was not due to changes in lymphatic vessel density, but rather tumor cell interactions with the lymphatic endothelium.

Chemokine receptor CXCR4 and its ligand CXCL12 have also been implicated in facilitating pancreatic tumor progression and metastasis. Using a novel small molecule inhibitor of both CXCR4 and E-selectin, we demonstrated that CXCR4 blockade significantly impairs pancreatic tumor cell adhesion and transendothelial migration across a lymphatic endothelium independent of tumor cell expression of E-selectin ligands. *In vivo* blockade of both CXCR4 and E-selectin moderately impaired pancreatic tumor metastasis. However, this inhibition of metastasis through GMI-1359 administration did not prolong animal survival even when administered in combination with chemotherapy and immunotherapy. Examination of pancreatic tumor microenvironment following GMI-1359 treatment revealed significant changes to the cell cellular composition: drastically reduced desmoplasia and lymphatic vascular densities. Further studies are ongoing to evaluate GMI-1359 efficacy in combination with immunotherapy in spontaneous mouse models of pancreatic cancer. Altogether, our data demonstrates that lymphatic biology and function is affected by both pancreatic tumor cells and pancreatic fibroblasts, and that factors expressed by the lymphatic endothelium ((E-selectin and CXCR4) may be targetable for the treatment of pancreatic cancer.

ACKNOWLEDGEMENTS

Firstly, I would like to acknowledge my advisor, Dr. Tony Hollingsworth. I think the single most important lesson I learned under your mentorship is how to step back and examine the big picture. Early during my graduate studies, I spent a lot of time focused on very specific mechanisms within pancreatic cancer. However, you challenged me to evaluate how a single mechanism impacts the whole disease including the tumor, the local tumor microenvironment, and the distant metastatic microenvironment, resulting in novel and exciting questions regarding pancreatic cancer. I am a better scientist because of this. Also, thank you for all your time and efforts in teaching me the skills necessary to pursue a career in science: critical thinking, experimental design, scientific writing, and much more. I have had many unique opportunities since joining your laboratory such as participating in the rapid autopsy program, collaborating with a drug company, learning live cell imaging, and developing various *in vivo* experiments. For these opportunities and your mentorship, I am very grateful.

I would also like to acknowledge my supervisory committee members, Drs. Kaustubh Datta, Angie Rizzino, and Joyce Solheim. Thank you for all your wonderful ideas, advice, and support through the years. Each of you has unique mentorship styles which has enabled me to evaluate problems from different perspectives and made me a more well-rounded scientist.

Over the years, I have had the opportunity to work with many talented individuals within the Hollingsworth laboratory. I thank all of my labmates for being so generous with their time in helping me with my studies. In particular, all the *in vivo* studies would not have been possible without all of your help and for that I am truly grateful. Also, thank you for all of your insights and troubleshooting suggestions over the years: you are all so very knowledgeable and I have learned so much from my discussions with each of you. Thank you for being such wonderful colleagues. Dr. Jim Grunkemeyer and Kelly O'Connell – thank you for all your help in the

process of imaging mice and administering treatments when I was unavailable. The drug trial studies would have come to a standstill if not for your help. I would also like to specially acknowledge Dr. Darci Fink. As a talented scientist, your studies on lymphatic biology were an invaluable resource for my own work. Moreover, thank you for working with me to assemble a comprehensive review of the role of lymphatics in pancreatic cancer - that work would not have been possible without your help.

I would also like to thank Dr. Erin Wuebben for all of her insight and support. You are a fantastic scientist and an even better friend. Thank you so much for helping me to survive graduate school!

I would like to thank my family for all their encouragement. To my parents, especially, you have both always provided me with unyielding support and encouragement. I am a determined and hardworking person because you both were fantastic examples of these qualities. You never let me quit anything and always encouraged me to put in the hard work necessary to get through graduate school and life. Your love and support means the world to me. Thank you. Additionally, to all my siblings – Michael, Tim, Joe, Sam, and Becky – thank you for keeping life fun and exciting. Graduate school was not such an arduous process with all of you around.

Lastly, I would like to acknowledge my husband, Mark. Thank you for encouraging me to pursue a career in science. I know these past few years have been as hard on you as they have been on me. When I was frustrated and felt like a failure, you picked me up then made me laugh; I am so grateful that you have been there to support me. Your own intelligence keeps me on my toes and challenges me to learn new things. I would not be the scientist or person I am today without you. Thank you for all your love and support.

TABLE OF CONTENTS

LIST OF FIGURES

LIST OF TABLES

ABBREVIATIONS

Ang-1, 2	Angiopoietin-1, -2
APC	Antigen-presenting cell
BSA	Bovine serum albumin
BVD	Blood vessel density
CA19-9	Sialyl-Lewis A; Carbohydrate antigen 19-9
CAF	Cancer-associated fibroblast
CCL21	C-C motif chemokine ligand 21
CCR7	C-C motif chemokine receptor 7
CD11b	Cluster of differentiation 11b (macrophage/monocyte marker)
CD11c	Cluster of differentiation 11c (dendritic cell marker)
CD19	Cluster of differentiation 19
CD133	Cluster of differentiation 133; Prominin 1
CD3	Cluster of differentiation 3 (T cell marker)
CD31	Cluster of differentiation 31 (endothelial cell marker)
CD335	Cluster of differentiation 335
CD4	Cluster of differentiation 4
CD45	Cluster of differentiation 45 (leukocyte marker)
CD8	Cluster of differentiation 8
CFDA-SE	Carboxyfluorescein diacetate succinimidyl ester
CM	Conditioned media
CT	Computerized tomography
CTLA-4	Cytotoxic T-lymphocyte-associated protein 4
CXCL12	C-X-C motif chemokine ligand 12
CXCR4	C-X-C motif chemokine receptor 4
CXCR7	C-X-C motif chemokine receptor 7

Cy5.5, 7	Cyanine 5.5, 7
DAB	3,3'-Diaminobenzidine
DAPI	4’,6-diamidino-2-phenylindole
DC	Dendritic cell
DMEM	Dulbecco’s Modified Eagle Medium
EBM-2	Endothelial basal medium-2
ECM	Extracellular matrix
EDTA	Ethylenediaminetetraacetic acid
EGF	Epidermal growth factor
EGM-2MV	Endothelial growth media-2 for microvascular endothelial cells
ELISA	Enzyme-linked immunosorbent assay
ERK1/2	Extracellular signal-regulated kinase 1/2
EUS	Endoscopic ultrasound
FAP	Fibroblast activation protein
FBS	Fetal bovine serum
FDG-PET	Fluorodeoxyglucose-positron emission tomography
FFPE	Formalin-fixed, paraffin-embedded
FGF-2	Fibroblast growth factor-2
FGFR	Fibroblast growth factor receptor
FITC	Fluorescein isothiocyanate
FOLFIRINOX	Folinic acid (leucovorin), fluorouracil, irinotecan, oxaplatin
Gem	Gemcitabine
GMI-1271 or 1271	GlycoMimetics Inhibitor – 1271 (E-selectin antagonist)
GMI-1359 or 1359	GlycoMimetics Inhibitor – 1359 (dual E-selectin and CXCR4 antagonist)
GPCR	G-protein-coupled receptor
Gr-1	Granulocyte-differentiation antigen-1

H&E	Hematoxylin and Eosin
HCl	Hydrochloric acid
HGF	Hepatocyte growth factor
hLEC	Human adult dermal lymphatic microvascular endothelia cells
HRP	Horseradish peroxidase
hTERT	Human telomerase reverse transcriptase
HuFF	Human neonatal foreskin fibroblast
HUVEC	Human umbilical vascular endothelial cell
ICAM-1	Intercellular adhesion molecule 1
IDO	Indoleamine 2,3-dioxygenase
IFNγ	Interferon γ
IGF-1, 2	Insulin-like growth factor-1, -2
IgG	Immunoglobulin G
IL-1β	Interleukin-1beta
IL-4, -6, -8, -10	Interleukin 4, 6, 8, 10
KPC	*LSL-Kras*$^{G12D/+}$*;LSL-Trp53*$^{R172H/+}$*;Pdx-1-Cre* (spontaneous PDAC mouse model)
K-Ras	Kirsten-rat sarcoma viral oncogene homolog
LAG-3	Lymphocyte-activation gene 3
LEC	Lymphatic endothelial cell
LVD	Lymphatic vessel density
LYVE-1	Lymphatic vessel endothelial hyaluronan receptor 1
Mac-1	Macrophage-1 antigen
MDSC	Myeloid-derived suppressor cell
MHC-I, II	Major histocompatibility complex-I, -II
mm^3	Cubic millimeters
MMP	Matrix metalloproteinase

mMWNT	Magnetic multiwalled carbon nanotubes
MOPS	3-(N-morpholino)propanesulfonic acid
MRI	Magnetic resonance imaging
mRNA	messenger RNA
NGF	Nerve growth factor
NK cell	Natural killer cell
Nrp-1, 2	Neuropilin-1, -2
OD	Optical density
$p16^{Ink4a}$/CDKN2A	p16/cyclin-dependent kinase inhibitor 2A
PanIN	Pancreatic intraepithelial lesion
PAR-2	Protease-activated receptor-2
PBS	Phosphate-buffered saline
PDAC	Pancreatic ductal adenocarcinoma
PDGF-BB	Platelet-derived growth factor-BB
PDGFR	Plate-derived growth factor receptor
PD-L1	Programmed death-ligand 1
PE	Phycoerythrin
PEGylation	Polyethylene glycol addition
PECAM-1	Platelet endothelial cell adhesion molecule; CD31
PerCP	Peridinin chlorophyll protein complex
PET	Polyethylene terephthalate
PFA	Paraformaldehyde
Prox-1	Prospero homeobox protein 1
PSC	Pancreatic stellate cell
PVDF	Polyvinylidene fluoride
qRT-PCR	Quantitative reverse transcription polymerase chain reaction

RCC	Renal cell carcinoma
RIPA	Radioimmunoprecipitation assay buffer
RPMI	Roswell Park Memorial Institute medium
RTKI	Receptor tyrosine kinase inhibitor
s.d.	Standard deviation
SDF-1	Stromal cell-derived factor 1
SDS	Sodium dodecyl sulfate
Shh	Sonic hedgehog
$sLe^{A/X}$	Sialyl $Lewis^{A/X}$
TAM	Tumor-associated macrophage
TBS	Tris-buffered saline
TBST	Tris-buffered saline with 0.1% Tween-20
TEM	Transendothelial migration
TGF-β	Transforming growth factor beta
TIE2	Tyrosine kinase with immunoglobulin-like and EGF-like domains 2
TLA	Tertiary lymphoid aggregate
TNFα	Tumor necrosis factor alpha
T_{reg}	T regulatory cell
uPA	Urinary plasminogen activator
VE-cadherin	Vascular endothelial cadherin; cadherin-5
VEGF-A, C, D	Vascular endothelial growth factor A, C, D
VEGFR-1,2,3	Vascular endothelial growth factor receptor 1, 2, 3

CHAPTER 1:

Introduction

Excerpts from this chapter have been edited from:

Fink, DM[1], Steele, MM[1], and Hollingsworth, MA (2015). The lymphatic system and pancreatic cancer. Cancer Lett; ePublished.

[1]Authors contributed equally to this publication

Selected sections from this chapter authored by Maria Steele (in "The lymphatic system and pancreatic cancer" review) were also previously used (with the permission of Maria Steele) in the dissertation of Darci Fink (entitled "Inflammation- and cancer-associated neurolymphatic remodeling and cachexia in pancreatic ductal adenocarcinoma). These sections are indicated in this chapter by quotation marks.

I. Pancreatic Cancer Background

Pancreatic ductal adenocarcinoma (PDAC) is the fourth leading cause of cancer-related deaths in the United States (1) and results in over 330,000 deaths annually worldwide (2). Unfortunately, the 5-year survival rate for patients with pancreatic cancer is a dismal 6% and the median survival time is only 6 months (3). Unlike the stable or decreasing trends of incidence and death rates for other cancers, the incidence of PDAC continues to rise. It is predicted that by 2030 PDAC will become the second leading cause of cancer-related deaths in the United States (4). Current therapies for the treatment of PDAC are inadequate. The only curative option is surgical resection, but only 15% of patients present with localized, resectable disease (5, 6). Standard of care chemotherapy, gemcitabine, does little to extend the survival of patients with metastatic disease (7, 8). Combinatorial treatment of gemcitabine with other drugs such as cisplatin (9), capecitabine (10), and nab-paclitaxel (11) have also proven unsatisfactory. A newly developed drug regimen, FOLFIRINOX, has improved median survival from 6 months to 11 months; however severe side effects limits which patients can endure this therapy (12). These dismal facts regarding PDAC and PDAC therapy underscore the critical need for a better understanding of PDAC biology in order to develop new and effective therapies.

As previously mentioned, the only curative option for PDAC is surgery, but for more than 85% of newly diagnosed patients, surgery is not an option as the disease has already spread to regional (i.e. lymph nodes) or distant locations (i.e. liver, lung, bone marrow) (1). The ability to diagnosis PDAC at early stages has proven to be quite difficult. Patients with early stage PDAC do not present with any obvious symptoms. Even at late stage disease, PDAC symptoms are very similar to those of other more common gastrointestinal maladies such as weight loss, fatigue, nausea, appetite loss, and abdominal/back pain; this confounds proper diagnoses (5). Multiple imaging modalities are used to diagnosis PDAC including endoscopic ultrasound (EUS), magnetic resonance imaging (MRI), computed cosmography (CT), and fluorodeoxyglucose-positron emission tomography (FDG-PET); however, by the time imaging is performed PDAC has already

metastasized (13). Many researchers are evaluating potential biomarkers within the blood and urine, but currently none consistently and accurately indicate the presence of PDAC especially at early stages (14). Even when PDAC is diagnosed at localized stages, many of these patients still succumb to recurrent disease suggesting that the identification of metastatic disease at diagnosis also requires improvement (15). Deeper examination of PDAC progression and biology will ultimately lead to the development of better biomarkers and imaging modalities for the early detection of PDAC.

Histological examination of PDAC progression has revealed that noninvasive precursor lesions known as pancreatic intra-epithelial neoplasias (PanINs) arise from the ductal epithelium of the pancreas. As PanIN lesions progress from benign PanIN 1 to more concerning PanIN 3 lesions, the ductal epithelium displays increasing cellular atypia and hyperplasia (3). Genetic studies have demonstrated that there are accompanying genetic aberrations that drive PanIN progression and development of PDAC. The most common genetic aberration found in PDAC patients is an activating mutation within the *Kras* gene (16-20). This mutation is found in early, low grade PanIN lesions and promotes the accumulation of other genetic aberrations necessary for PDAC development (21-23). These *Kras*-accompanying mutations are often inactivation mutations in tumor suppressor genes $p16^{INK4a}$*/CDKN2A*, *p53*, or *SMAD4/DPC4*, all of which are frequently found in PDAC patient samples (16, 24-30). Similar to mutant *Kras* expression, these inactivated tumor suppressor genes can also found in precursor PanINs and cooperate with *Kras* mutations to induce PanIN transformation and PDAC development (26, 31, 32).

II. Lymphatic System and Pancreatic Cancer

"Cancer metastasis into and through the lymphatic vasculature and lymph nodes occurs frequently (>70%) in PDAC patients (5, 28, 33) and is strongly correlated with poor prognosis (34-37). Evaluating lymph node status has proven to be a significant factor when determining therapy selection for cancer patients (38-40). Furthermore, lymph nodes are often the first site of metastatic

growth, suggesting the importance of these organs in tumor progression (41). The lymphatic vasculature offers the most direct route from the primary tumor to these frequently-invaded draining lymph nodes during PDAC dissemination. Although lymph node involvement is a crucial determinant of PDAC prognosis and therapy, the role of the lymphatic system in PDAC progression is often overlooked. A better understanding the processes of lymphatic invasion and lymph node metastasis in PDAC will significantly contribute to our overall understanding of this deadly disease and provide the groundwork for the development of novel efficacious therapies."

i. Normal Lymphatic Structure and Biology

"The lymphatic system is responsible for maintenance of tissue fluid homeostasis, absorption of dietary fat, and leukocyte and antigen transport from tissues to lymph nodes for the initiation of immune responses (42-44). Originating in nearly all vascularized tissues, blind-ended lymphatic capillaries, or initial lymphatics, are specialized for the uptake of interstitial fluids, macromolecules, antigens, and leukocytes. They are composed of a single layer of lymphatic endothelial cells (LECs) with discontinuous intercellular junctions and lack a basement membrane (45, 46). The endothelial membrane of the initial lymphatics is attached to the extracellular matrix (ECM) *via* anchoring filaments, which facilitate the opening of the lymphatic lumen during increased interstitial fluid pressure (47, 48). Upon entry into the lymphatic capillaries, lymph and its macromolecular and cellular contents are transported to larger pre-collecting lymphatic vessels and then to collecting vessels, composed of not just the endothelial layer, but also smooth muscles to facilitate flow and bi-leaflet valves to prevent backflow (49-51). The afferent collecting lymphatics enter the lymph nodes where the lymph is filtered and processed for immunity purposes. Upon exiting the lymph nodes through the efferent collecting vessels, the lymph passes through the major trunks of the lymphatic system, the thoracic duct and the right lymphatic trunk, and is then returned to the venous circulation (43, 52)."

"The network of lymphatic vasculature and lymph nodes responsible for draining the pancreas is quite complex. In the normal pancreas, the lymphatic vessels are typically located near

blood vessels and are often found in the interlobular spaces of the pancreas (53). Classification of pancreatic nodes has not been uniformly standardized, although pancreatic lymph nodes are generally divided into regions based upon their location around the pancreas and the areas of drainage of the pancreas: head/neck, body/tail, left side, or right side (reviewed in (54, 55)). Studies correlating primary tumor location and lymph node involvement following resection have helped to identify the regional patterns and probabilities of lymph node metastasis, but more analysis will need to done for consistent accurate prediction of lymph node involvement (56-59)."

ii. Lymphangiogenesis and Pancreatic Cancer

Lymphangiogenesis is the growth of new lymphatic vessels from preexisting vessels and is a crucial biological process during wound healing, inflammation, and malignancy (60). Under pathological conditions, lymphangiogenesis is primarily driven by binding of vascular endothelial growth factor-A (VEGF-A), -C, and -D to respective vascular endothelial growth factor receptors-2 (VEGFR-2) and -3 and co-receptor neuropilin-2 (Nrp-2) (61-66) and binding of angiopoietin-1 (Ang-1) and -2 to tyrosine kinase with immunoglobulin-like and EGF-like domains-2 (TIE2) receptor (67, 68). Additionally, numerous other growth factors have also been implicated in promoting lymphangiogenesis including but not limited to fibroblast growth factor -2 (FGF-2) (69), hepatocyte growth factor (HGF) (70), insulin-like growth factor-1 (IGF-1) and -2 (71), nerve growth factor (NGF) (72), epidermal growth factor (EGF) (73-75), and platelet-derived growth factor-BB (PGF-BB) (76, 77). Sources for these pro-lymphangiogenic factors include LECs (autocrine mechanisms) as well as cells within inflammatory and tumor microenvironments (paracrine mechanisms) such as fibroblasts (75, 78-81), macrophages (82-85), dendritic cells (83), and tumor cells (86-91).

In many malignancies, new lymphatic vessel growth occurs not only within primary tumor sites but also pre-metastatic lymph nodes (41, 43, 52, 92-94). The reasons for tumor-induced lymphangiogenesis at these sites extend beyond the simple explanation of increasing potential escape routes for tumor dissemination to lymph nodes. Firstly, lymphangiogenesis augments the

transport of tumor-derived factors, such as cytokines, antigens, growth factors, and exosomes, to the lymph nodes. These factors are necessary for pre-conditioning of the lymph node metastatic niche prior to tumor arrival (41, 95, 96). Secondly, higher lymphatic vessel densities increase trafficking of immune-suppressing leukocytes from tumors to lymph nodes where they inhibit anti-tumor response (97). Thirdly, lymphangiogenesis may also serve to exacerbate immunosuppression as LECs cross-present scavenged tumor antigens to induce T cell tolerance, and they also express immune checkpoint inhibitory molecules to prevent T cell activity (98-100). Fourthly, increased lymphatic vessel density, strengthens the chemotactic gradients needed to guide tumor cells to distant organs including the lymph nodes (101, 102). Lastly, lymphangiogenic vessels exhibit increased expression of cell adhesion molecules, integrins, and chemokines which promote LEC-tumor cell communication and interaction during transendothelial migration and dissemination (103, 104). Altogether, this suggests that lymphangiogenesis supports tumor progression, and that anti-lymphangiogenic therapies may be effective treatment options for cancer patients. Targeting the lymphatic system for the treatment of cancer progression and metastasis is discussed in greater details in Chapter 6.

The incidence and significance of lymphangiogenesis in pancreatic cancer progression is a contested area of research. Several studies have demonstrated a correlation between lymphatic vascular density (LVD) at the primary site and incidence of lymphatic invasion and lymph node metastasis in pancreatic cancer patient samples (94, 105). Additionally, expression levels of pro-lymphangiogenic factors VEGF-C and -D and receptor VEGFR-3 have also been shown to correlate with increased LVD, lymphatic invasion, and lymph node metastasis of pancreatic cancer (94, 106, 107), but not with hematogenous invasion and metastasis (94). Correspondingly, *in vivo* deletion of VEGF-C or -D significantly decreased LVD and impaired lymph node metastasis of pancreatic cancer (108, 109). However, one study by Sipos *et al*. did not observe overexpression of VEGF-C or -D in PDAC patient samples (110). Moreover, they did not find any correlation

between LVD or pro-lymphangiogenic factor expression and lymph node metastasis or patient outcome (110). Their findings suggest that PDAC metastasis is independent of lymphangiogenesis and that metastasis to the lymph node occurs solely through pre-existing lymphatic vessels. More work will need to be done to determine the role of lymphangiogenesis in tumor progression and whether this process can be targeted for the treatment of PDAC.

iii. PDAC Invasion of Lymphatic Vessels and Metastasis

a. Background

"Lymphatic vessel invasion and subsequent metastasis to the lymph nodes are early and significant events frequently observed during pancreatic cancer progression (5, 28). Although lymphatic invasion and metastasis to the lymph nodes does not directly contribute to PDAC morbidity in patients, these pathologies are important indicators of the metastatic potential of this disease. In the clinical setting, lymph node status is used to assess disease progression, to select appropriate therapies, and to predict survival (39, 40). Nearly all studies concur that lymph node status correlates with poor prognosis for pancreatic cancer patients (34, 36, 37, 111). Studies also agree that invasion of lymph nodes by PDAC occurs most frequently through the lymphatic vasculature rather than through direct/contiguous extension of the primary tumor to the lymph node (112-114). However, the prognostic value of mode of lymph node invasion is arguable: some studies report poorer overall survival in patients with lymphatic vessel-directed metastasis as compared to direct invasion (114), while other reports show no survival difference between the two modes of lymph node invasion (112, 113). Although lymph node invasion by PDAC occurs most frequently through the lymphatic vasculature, the LVD at the tumor site has not been conclusively correlated with either lymph node metastasis or prognosis due to conflicting study results (105, 106, 110, 115). This is also true for studies examining the expression of pro-lymphangiogenic factors such as VEGF-C and -D (88, 110, 116) (and in pancreatic endocrine tumors (117)). The lack of standardized protocols for quantifying LVD in patients makes comparative analysis among collected data sets difficult. Some studies enumerate only intratumoral lymphatics in whole tumor

sections, while others examine tumor margins for peritumoral lymphatics, and still others examine the sum of lymphatic vessels in both regions. In the continued absence of a standardized method, LVD has limited value as a metric for assessing pancreatic cancer progression. “

“PDAC tumors are often hypovascular with only sporadic blood and lymphatic vessels found among the tumor cells (81). These intratumoral lymphatic vessels are typically collapsed and nonfunctional due to direct compression by the tumor cells and the high internal pressure of the PDAC tumor microenvironment (116, 118, 119). However, even in the absence of functioning intratumoral lymphatic vessels, tumor cells are still capable of disseminating to lymph nodes, although identification of reliable sentinel lymph nodes remains challenging (56). The lymphatic vessels located at the tumor margins are frequently described as enlarged with open lumens capable of being filled with tumor cells (116, 118), and drainage studies show that these peritumoral lymphatic vessels are, in fact, functional (119). Sipos and colleagues demonstrated that even in the absence of elevated LVD values and active lymphangiogenesis, PDAC patients still frequently presented with lymph node metastases (110). This suggests that PDAC cells are capable of invading the pre-existing lymphatic vasculature, especially enlarged vessels at tumor margins, and necessitates examination of the mechanisms regulating lymphatic invasion.”

b. Mechanisms/Players

“Mechanisms regulating lymphatic invasion are not completely understood, but are gaining increasing research interest. Most of our knowledge of vascular invasion has come from studies of the blood vasculature that are now being extended to studies of lymphatic vessel properties and function. Initially, invasion of lymphatic vessels by tumor cells was considered a passive process with increased interstitial fluid pressure driving tumor cells into draining lymphatic vessels (120). Although increased interstitial pressure may contribute to tumor cell invasion, the concept of lymphatic-mediated tumor metastasis as a process that utilizes a “path of least resistance” is greatly oversimplified, and proteomics studies have identified distinctions between primary pancreatic

tumors and their corresponding lymph node lesions (121). Comparisons of pancreas tumors with and without lymph node metastases revealed differences in protein expression intrinsic to these two pathological tumor presentations (122). In an effort to better understand the potential drivers of lymphatic metastasis, results of studies of leukocyte intravasation into lymphatic vessels are now being examined for commonalities to tumor cell intravasation. Three key molecular players of invasion have emerged as likely candidates in the regulation of tumor-lymphatic interactions and metastasis: chemokine signaling, paired binding of adhesion protein partners, and alterations in lymphatic vessel barrier integrity."

1. Chemokines

"Chemokines secreted by lymphatic endothelial cells contribute to inflammation and initiation of immune responses in part by regulating the chemotaxis of antigen presenting cells to the lymph nodes. These same molecules are also being studied for similar roles in tumor metastasis to lymph nodes. Two widely researched candidate chemokines are CCL21 and CXCL12 and their respective G-protein coupled receptors (GPCRs), CCR7 and CXCR4."

"During normal immune responses, lymphatic endothelial cells secrete CCL21 to increase migration of $CCR7^{+}$ dendritic cells (DCs) toward the vessel and then to guide DCs to the lymph nodes (123, 124). Tumor cells, including those of pancreatic cancer, overexpress CCR7 and are capable of responding to CCL21 cues to facilitate their dissemination to the lymph nodes (125-128). Guo, *et al.*, noted a correlation between CCR7 expression in tumor cells and frequency of lymph node metastasis in pancreatic cancer patients (129). Sperveslage, *et al.*, confirmed these results and also demonstrated that lymphatic vessels of PDAC patients had significantly higher expression of CCL21 compared to lymphatic vessels of the normal pancreas. Expression of CCL21 in lymphatic vessels correlated with increased lymphatic invasion and lymph node metastasis in these patients, as did overexpression of CCR7 in pancreatic tumor cells *in vivo* (130)."

"The expression of CCL21 in lymphatic endothelial cells is regulated by numerous inflammatory cytokines including tumor necrosis factor α (TNFα) and interleukin-1β (IL-1β) and is also influenced by increases in transmural flow (131), both of which are often present in tumor microenvironments. *In vitro* co-culture work has demonstrated that CCR7-expressing tumor cells have increased chemotaxis toward CCL21-expressing lymphatic endothelial cells (104, 132, 133). This chemotactic axis is used by tumor cells specifically for invasion into lymphatic vessels; tumor cell chemoattraction to blood endothelial cells does not use this mechanism (104, 134). Blocking CCR7 or CCL21 expression and/or function inhibits lymphatic vessel invasion and metastasis to the lymph nodes *in vitro* and *in vivo* (133, 135, 136). This chemokine signaling axis appears to be regulated by and to work in concert with VEGF-C to synergistically promote lymphatic invasion of $CCR7^+$ and VEGFR-3^+ tumor cells (104)."

"Another chemokine axis that influences lymphatic metastasis is the CXCL12-CXCR4 axis. It has been widely documented that CXCR4-expressing tumor cells, including PDAC cells, home to organs with high CXCL12 expression, such as the lungs, bone marrow, and lymph nodes (128, 137-139). In PDAC patient tissues, high expression of CXCR4 was found in tumors, while lymph nodes expressed high levels of CXCL12 (137, 140). This expression pattern positively correlated with increased LVD values in the pancreas, lymph node metastasis frequency, and poor disease prognosis. Tumor-associated, but not normal uninflamed, LECs secrete ample amounts of CXCL12 in the tumor microenvironment and attract $CXCR4^+$ tumor cells to lymphatic vessels and lymph nodes (101, 141). Blocking the CXCR4-CXCL12 signaling axis has resulted in impaired lymph node metastasis in numerous tumor models (142-144). An *in vitro* breast cancer model demonstrated that CXCL12-treated LECs permitted greater transendothelial migration by breast cancer cells, and this permissiveness could be reversed by blocking CXCR4 in the LECs (145). An *in vivo* model of melanoma demonstrated that stem-like, dual positive $CD133^+/CXCR4^+$ tumor cells were strongly associated with CXCL12-producing LECs and that these cells were resistant to

chemotherapy (101). Combinatorial treatment with a CXCR4 antagonist relieved this resistance and increased the efficacy of chemotherapy thereby reducing tumor growth and metastasis. This study suggested that CXCL12 secretion from lymphatic vessels supported a pro-metastatic and pro-survival niche for tumor cells. Further studies are required to elucidate whether or not these types of mechanisms are employed in PDAC and/or its tumor microenvironment."

2. Adhesion Proteins

"Physical interactions between tumor cells and lymphatic endothelial cells may be another crucial regulator of tumor cell intravasation. Adhesion molecules such as E-selectin, intercellular adhesion molecule 1 (ICAM-1), and vascular adhesion molecule 1 (VCAM-1) are typically used by DCs and other immune cell types to gain entry into inflamed lymphatic vessels during migration toward lymph nodes (131, 146). Mounting evidence indicates that these same leukocyte adhesion molecules may also be important for controlling tumor cell entry into lymphatic vessels (147-149). In a non-inflamed state, the lymphatic endothelium does not express or only very weakly expresses these adhesion molecules (146, 150). Inflammatory conditions—such as those found during infection or tumor development—or a wound healing response quickly increase the expression of these molecules on the lymphatic endothelium (131, 146). Increased transmural flow, also characteristic of an inflamed microenvironment, upregulates ICAM-1 and E-selectin expression on an *in vitro* lymphatic endothelium resulting in increased DC binding (131). A recent report shows that binding and transendothelial migration of breast cancer cells is also influenced by *in vitro* fluid flow, although the mechanisms governing these behaviors have not been elucidated (150). When placed in co-culture with tumor cells, LECs display marked upregulation of adhesion molecules. Kawai, *et al.* (2008 and 2009) have demonstrated that invasive breast cancer cells, which express the αLβ2 integrin ligand for ICAM-1, are capable of inducing the expression of E-selectin and ICAM-1 on lymphatic endothelial cells. They also demonstrated that blocking ICAM-1 impaired the ability of these tumor cells to bind to a lymphatic endothelium (149, 151). Studies of the ability of adhesion proteins on lymphatic vessels to regulate tumor cell entry should be expanded to

pancreatic cancer cell lines to determine if PDAC tumor cells can use similar mechanisms to bind and gain access to the lymphatic vasculature."

3. Lymphatic Vessel Barrier Integrity

"The intrinsic cellular and molecular organizational characteristics of lymphatic vessels facilitate entry of immune cells and fluids from a collecting tissue bed—properties that may also allow these vessels to support tumor cell metastasis. The initial lymphatic capillaries within tissues are composed of only a single layer of endothelial cells with loose junctions between neighboring cells (44, 152). Unlike the tightly-formed, continuously-arranged junctions between neighboring endothelial cells of the blood vasculature (153), the junctional proteins—vascular endothelial cadherin (VE-cadherin), platelet/endothelial cell adhesion molecule-1 (PECAM-1; CD31), claudins, occludins, *etc*.—of initial lymphatic vessels are discontinuously arranged, creating gaps between overlapping lymphatic endothelial cells (45). These discontinuous junctions along with preformed openings in the basement membrane (46) enable uptake of macromolecules, fluids, and cells by the initial lymphatic capillaries. As lymph and cells are transported up the lymphatic vasculature to the collecting lymphatic vessels, the discontinuous intercellular junctions become more constant and successive to prevent leakage prior to arrival at the lymph nodes (45)."

"Data suggest that tumor cells are capable of modulating the barrier integrity of the lymphatic endothelium to further facilitate lymphatic vessel invasion (154). Lipoxygenase secretion by breast cancer cells has been shown to disrupt VE-cadherin junctions and induce endothelial cell repulsion, resulting in breaches in the lymphatic endothelium. Tumor-secreted VEGF-C also facilitates invasion by creating leaky lymphatic vasculature. VEGF-C induces the internalization of VE-cadherin, which, in turn, promotes tumor cell transendothelial migration (155, 156). In a pancreatic tumor model, inhibiting Ang-2 signaling with a soluble Tie-2 receptor decreased lymphatic-directed metastasis to the lymph nodes (86). This result may be explained by studies demonstrating that Ang-2 disrupts the barrier integrity of the lymphatic endothelium and

increases lymphatic permeability through phosphorylation of VE-cadherin resulting in button-junction formation in the initial lymphatic capillaries (157)."

III. Lymphatic Vasculature and the PDAC Microenvironment

"The PDAC microenvironment is arguably one of the most complex of any tumor microenvironment, replete with cancer associated fibroblasts (CAFs), immunosuppressive leukocytes, tumor-associated blood/lymphatic endothelial networks, and a considerably dense ECM compartment (**Figure 1**)." Collectively referred to as stroma, these components can comprise up to 80-90% of the tumor (29, 158, 159). The stroma not only facilitates PDAC progression and dissemination, it also has the capacity to influence the normal lymphatic vasculature within the pancreas.

i. Cancer-Associated Fibroblasts

One of the most striking features of PDAC tumors is the robust desmoplastic reaction observed within both the primary and metastatic sites. The major cellular component of desmoplasia is CAFs, also known as pancreatic stellate cells (PSCs) when specifically referring to PDAC. These PSCs have many tumor-supporting properties. Secretion of growth factors and cytokines from PSCs promotes PDAC cell proliferation, survival, migration, and invasion (160, 161). Reciprocally, PDAC cells secrete numerous factors that promote PSC proliferation and activation creating a positive feedback loop between the two cell types (162). *In vivo* orthotopic co-injection of PSCs with PDAC cells was shown to accelerate tumor growth and metastasis (160, 161, 163, 164), and these co-injected PSCs were also observed to accompany PDAC cells to metastatic sites (161). Additionally, activated PSCs secrete excessive amounts of ECM proteins which impede drug delivery to tumors (165). Acute pharmacological inhibition of morphogen sonic hedgehog (Shh) was shown to inhibit α smooth muscle actin (αSMA) + fibroblast proliferation in PDAC tumors which, in turn, improved tumor vascularity and chemotherapy delivery to tumors (165, 166). In regards to influencing tumor immunity, PSCs secrete numerous factors that suppress or modulate immune cell function such as tumor growth factor-β (TGF-β), TNFα, IL-1β, -6, and -8. (167-169).

Figure 1.1

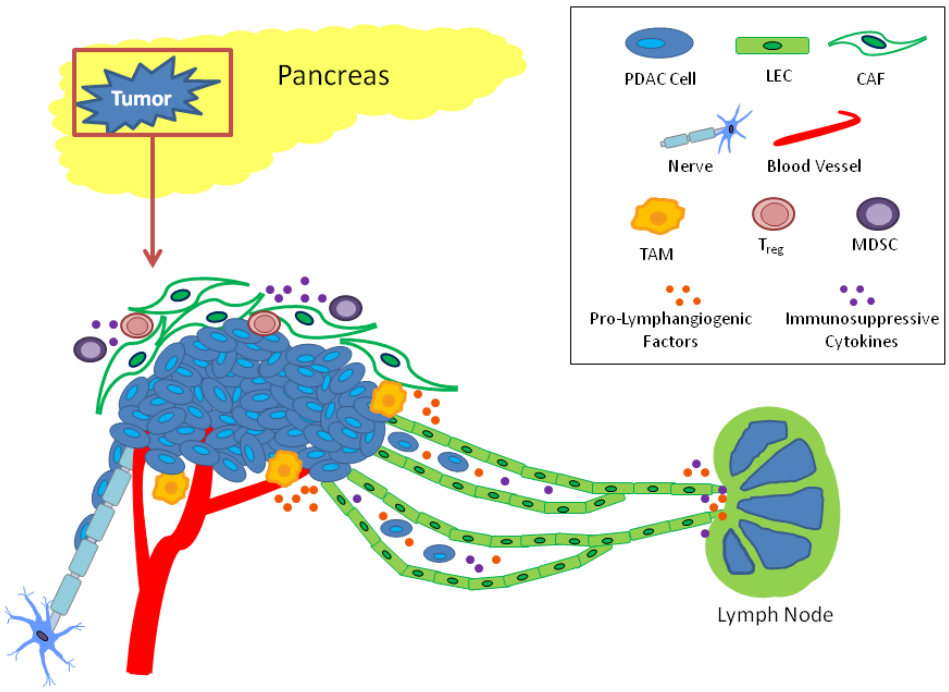

Figure 1.1 Pancreatic tumor microenvironment and lymph node metastasis.

"Cells of the tumor microenvironment are essential contributors to tumor growth, lymphatic invasion, and lymph node metastasis. CAFs and TAMs secrete pro-lymphangiogenic factors and proteases needed for lymphangiogenesis and metastasis. Lymphatic vessels act as conduits not only for tumor cell metastasis, but also for immunosuppressive cell and cytokine transport to lymph nodes. Nerves are also another route for pancreatic tumor metastasis and can communicate with lymphatic vessels to facilitate tumor metastasis from one network to the other."

These factors also promote recruitment and differentiation of immunosuppressive immune cells such as myeloid-derived suppressor cells (MDSCs) and regulatory T cells (T_{regs}) to PDAC tumor (80, 170). PSCs disrupt T cell recruitment to PDAC tumors and are capable of inducing T cell apoptosis (171-174). Depletion of fibroblast activation protein (FAP)+ fibroblasts was shown to significantly improve T cell infiltration and immunotherapy efficacy (171). Altogether, PSCs provide several mechanisms that drive tumor development and progression.

Although initially believed to be solely tumor-supportive cells, new evidence indicates PSCs may possess both pro- and anti-tumor properties. Recently a handful of studies have demonstrated that *in vivo* depletion of these cells accelerated PDAC progression and shortened survival time. Genetic ablation of αSMA+ fibroblasts resulted in more aggressive PDAC tumors including increased invasion and metastasis, increased hypoxia, and enhanced immunosuppression leading to reduced survival (175). Rhim et al. demonstrated that genetic knockout of sonic hedgehog (Shh) from PDAC tumor cells reduced αSMA+ PSC activation and proliferation resulting in poorly differentiated tumors with accelerated growth and metastasis and significantly shortened animal survival (176). This group's findings were confirmed using chronic administration of Shh antagonists (176). Lee et al. also confirmed Rhim's findings demonstrating Shh inhibition accelerates PDAC growth and Shh activation slows PDAC growth (177). Altogether, these studies suggest that PSCs have anti-tumor properties and complete loss of these cells leads to accelerated tumor progression. Interestingly, ablation of fibroblasts in these studies exposed other vulnerabilities of PDAC tumors: Odzemir et al. demonstrated that fibroblast-depleted PDAC tumors were more susceptible to anti-cytotoxic T-lymphocyte-associated protein 4 (CTLA-4) immunotherapy (175), and Rhim et al. demonstrated that VEGFR inhibitors reversed tumor aggressiveness following Shh-dependent depletion of fibroblasts (176). The fibroblast population comprising the PDAC tumor microenvironment is likely heterogeneous (178, 179). Currently the molecular markers of fibroblast subtype are poorly defined and are often expressed across multiple

types of fibroblasts as well as other cell types. The depletion or inhibition of a particular subtype or multiple subtypes will likely have significant consequences on tumor progression and survival outcomes. Much more work needs to be done to fully understand the pro- and antitumor properties of CAFs and CAF subtypes and whether these cells can be targeted for effective PDAC therapy.

"Due to their abundance in the PDAC microenvironment, PSCs also exert a strong influence over other microenvironmental cell types including the lymphatic endothelium (180). As one of the main protein regulators of desmoplasia, Shh signaling is PSCs lead to the creation of a pro-angiogenic and pro-lymphangiogenic stromal compartment (163, 181). When Shh signaling was inhibited in PSCs, LVD decreased and lymph node metastasis was reduced. Data such as these suggest that CAFs primarily influence the lymphatic endothelium *via* secretion of various effector proteins. It has been demonstrated that CAFs of various tumor types, including PDAC, secrete a wide range of pro-lymphangiogenic factors such as VEGF-C, VEGF-D (78, 79), VEGF-A (80), EGF (75), PDGF, and FGF (81). PSCs also secrete chemokines, including CXCL12, which has been shown to correlate with increased tumor aggressiveness, LVD values, and lymph node metastases in PDAC patient tissues (137, 171). In addition to their direct action on lymphatic endothelia, many of these same secreted factors as well as pro-inflammatory cytokines allow CAFs to indirectly support lymphangiogenesis and lymphatic vessel invasion through the recruitment of pro-lymphangiogenic immune cells such as tumor associated macrophages (TAMs) and DCs (182, 183). Lastly, CAFs secrete matrix metalloproteinases (MMPs) and other proteases that remodel the ECM of tumors (184). This remodeling promotes tumor invasion of stroma and tumor vasculature and releases sequestered growth factors and cytokines from the ECM for tumor growth, angiogenesis, and lymphangiogenesis. A recent study by Shi et al. highlights an additional protease-related mechanism by which PSCs may influence pancreatic cancer progression and lymphatic metastasis. Specific pancreatic stromal compartment deletion of protease-activated receptor-2

(PAR-2), a GPCR highly expressed in PDAC, resulted in decreased primary tumor size (due to anti-angiogenesis effects) but increased LVD and lymph node metastases (185)."

ii. Immune Cells and Immune Regulation

PDAC tumors are highly immunosuppressed microenvironments with pro-tumor mechanisms greatly outweighing anti-tumor mechanisms preventing the immune system from mounting an anti-tumor response (186). In addition to inducing immune suppression, tumor-infiltrating immune cells contribute to many other aspects of tumor progression including tumor growth, inflammation, angiogenesis, metastasis and chemoresistance (187, 188). During progression from precancerous PanIN lesions to invasive PDAC, there is a drastic infiltration of tumor-supporting MDSCs, T_{regs}, and TAMs (189-192), and their presence significantly correlates with disease stage and metastasis and negatively correlates with survival (189-191, 193, 194). Many of these immune-suppressing infiltrating leukocytes promote tumor immune evasion by impairing T cell recruitment or function. MDSCs discourage T cell recruitment to tumors, induce T cell apoptosis through production of nitric oxide and reactive oxygen species, activate inhibitory T_{regs}, interfere with interferon γ (IFNγ) signaling, and deplete metabolites necessary for T cell function and survival (195-199). Additionally, T_{regs} inhibit the adaptive immunity through secretion of immunosuppressive cytokines such as IL-10 and TGF-β and expression of high levels of co-inhibitory ligands (200). TAMs, another prominent immune cell type in the PDAC microenvironment, secrete ample amounts of immunosuppressive factors that impede T cell function directly and indirectly through preventing DC maturation necessary for T cell activation (201). These cells also secrete high levels of growth factors and cytokines that stimulate tumor growth, invasion, and angio- and lymphangiogenesis (201-206). Noticeably absent from the PDAC tumor microenvironment are cytotoxic and helper T cells. The abundant amounts of immunosuppressive cells and cytokines exclude T cells from contact with neoplastic PDAC cells and retain them either in the stromal compartment or at the tumor periphery (171, 172). These T cells are often of a naïve phenotype or are not activated (207, 208).

"One of the main functions of lymphatic vessels is to transport leukocytes to lymph nodes for immune response initiation, uniquely positioning LECs to modulate immune responses in ways that may support tumor progression. As immune cell trafficking conduits, LECs are responsible for the transport of both antigens and antigen presenting cells (APCs), such as DCs, to the lymph nodes for immune response optimization (124). By regulating the expression and secretion of various chemokines in response to inflammation, injury, or tumor development, LECs can alter the recruitment of immune cells to the lymph nodes, and, as a result, influence the ensuing immune response (reviewed (209, 210)). Partially due to lymphatic-directed recruitment, tumor-draining lymph nodes demonstrate a more immunosuppressive environment as compared to normal lymph nodes with an increased presence of T_{regs}, MDSCs, immature and tolerogenic DCs, and immunosuppressive cytokines (97, 131, 211, 212). These immunosuppressive cells and cytokines accumulate in the lymph as a result of increased lymphatic drainage from the tumor site (95). Within the lymph nodes TGF-β, a major driver of immune suppression, supports the differentiation and activation of T_{regs} as well as promoting tolerogenic and immature phenotypes of DCs (213). As T_{regs} differentiate and accumulate, they secrete more TGF-β to further drive immune suppression. IL-10 is another factor that supports the accumulation of immunosuppressive cells in the lymph nodes by promoting T_{reg} activity (214) and tolerogenic DC function (214, 215). Indoleamine 2,3-dioxygenase (IDO) increases the generation of T_{regs} in the lymph nodes (216, 217), while concurrently inhibiting effector T cell activity (218). Other factors implicated in the accumulation of immunosuppressive cells in lymph nodes include IL-4, VEGF-A, and prostaglandin E_2 (219)."

"In addition to cellular and cytokine transport, LECs also transport tissue antigens (and in the case of cancer, tumor antigens) from peripheral tissues to lymph nodes. Studies have demonstrated that LECs, particularly those in the lymph nodes, are capable of scavenging these tissue and tumor antigens and cross-presenting them on major histocompatibility complex-I (MHC-I) (98, 99). This can lead to immune tolerance through deletion of naive $CD8^+$ T cells as LECs lack

co-stimulatory molecules needed to activate the T cells and instead express programmed death-ligand 1 (PD-L1), an inhibitory signal for T cells (100). LECs can also present scavenged exogenous tissue/tumor antigens on MHC-II molecules and likely induce immune tolerance through interactions with the inhibitory lymphocyte activation gene-3 (LAG-3) protein on $CD8^+$ T cells (220). These studies shed light on the phenomenon that when tumor cells are denied lymphatic vessel experience, such as through direct implantation into lymph nodes, tumor immunity is impaired through a robust $CD8^+$ T cell response (221). LECs also modulate immune responses by inhibiting DC maturation (211). Binding of DCs to the lymphatic endothelium *via* macrophage-1 antigen (Mac-1) and ICAM-1-mediated interactions during transendothelial migration can reduce the expression of co-stimulatory molecules on DCs needed for T cell activation. Studies such as these inspire new ideas regarding increased lymphangiogenesis at the tumor periphery and draining lymph nodes, suggesting that it may influence tumor progression in two ways: 1) increasing metastatic routes for dissemination and 2) immune suppression through increased antigen scavenging and decreased DC maturation leading to T cell inhibition and immune tolerance (222). Further investigation is needed to substantiate the immunosuppressive properties of the lymphatic endothelium and its specific contribution to disease progression as a component of the tumor microenvironment."

"A reciprocal concept in relation to the capacity of LECs to affect immunity is that of immune cells inducing effects on LECs. One such tumor infiltrating immune cell type, TAMs, can be found in many tumor microenvironments, including PDAC (202, 203, 223, 224), and their presence often correlates with poor patient prognosis (225-227). TAMs promote tumor lymphangiogenesis through two mechanisms: paracrine secretion of pro-lymphangiogenic factors and transdifferentiation into LEC-like progenitor cells. TAMs secrete high levels of VEGF-C and -D, which, in turn, increases LVD in and around tumors (202-205). Indeed, TAM density has been shown to significantly correlate with increased LVD, lymphatic vessel invasion, and lymph node

metastasis in many cancers (202, 205, 228-230). Inhibition or depletion of TAMs from tumor microenvironments significantly reduced LVD values and decreased the incidence of lymph node metastases compared to tumors with TAMs present (231-233). However, depletion of TAMs did not completely inhibit lymph node metastasis as tumor cells were still able to invade pre-existing lymphatic vessels. These macrophages also secrete proteases such as MMP-2, MMP-9, and plasmin/urokinase plasminogen activator (uPA) that remodel the extracellular microenvironment and release sequestered growth factors for lymphangiogenesis (234, 235). The plasmin/uPA system is also important for the proteolytic maturation of VEGF-C and -D increasing their affinity for VEGFR-3 (236). It has yet to be determined if TAMs secrete any of the other factors known to promote lymphangiogenesis. The second way TAMs contribute to lymphangiogenesis is by transdifferentiating into LEC-like progenitors both in inflammatory and tumor settings (232, 237-239). Transdifferentiated macrophages undergo genetic reprogramming (237) with increased expression of lymphatic markers LYVE-1, Prox-1, podoplanin, and VEGFR-3 (232, 237, 240, 241). Expression of LEC markers enables TAMs to physically incorporate into the newly developing lymphatic vasculature. The percentage of transdifferentiated TAMs within these newly formed lymphatic vessels is often less than 10% (232, 240) suggesting the main mechanism by which TAMs promote tumor-associated lymphangiogenesis is through secretion of pro-lymphangiogenic factors."

IV. Summary

The lymphatic system almost certainly plays a significant role in PDAC progression, as dissemination to the lymph nodes is seen early and frequently in PDAC patients. Lymphatic vessels are routes for PDAC dissemination as they directly connect the primary tumor to the draining lymph nodes. Additionally, these vessels transport tumor-derived factors and immune cells to lymph nodes in order to make these organs more hospitable for tumor metastases. Lastly, the endothelial cells that comprise lymphatic vessels are known suppressors of the immune system through cross presentation and expression of co-inhibitory ligands. All these roles promote efficient PDAC

growth, dissemination, and immune suppression. However, the specific mechanisms governing lymphatic invasion and metastasis are sorely under-researched as are the contributions of the PDAC microenvironment to these processes. In this dissertation, we characterized the effects PDAC cells and pancreatic fibroblasts have on lymphatic endothelial cells in regards to recruitment, lymphangiogenesis, and invasion. Using novel small molecule inhibitors, we specifically focused on the roles of E-selectin and CXCR4 in regulating lymphatic invasion and metastasis and whether blocking the function of these proteins prolongs animal survival in PDAC-challenged mice.

CHAPTER 2:

Materials and Methods

I. Cell Lines and Cell Culture

i. Primary Human Lymphatic Endothelial Cells

Adult human dermal microvascular lymphatic endothelial cells (hLECs) were purchased from Lonza and cultured in EGM-2MV growth medium supplemented with 5% fetal bovine serum (FBS), growth factors (hEGF, VEGF, hFGF-B, R^3-IGF-1), ascorbic acid, hydrocortisone and antibiotics (GA-1000) per manufacturer's specifications. Cells were maintained in a 37º C humidified atmosphere at 5% CO_2. As an alternative source, hLECs were also purchased from PromoCell and maintained in culture as stated above. Primary hLEC cultures were used at passages 5-8. For serum starvation studies, hLECs were washed and media replaced with EBM-2 basal media for 24 hours.

ii. Primary Human Umbilical Vein Endothelial Cells

Primary human umbilical vein endothelial cells (HUVECs) were purchased from Lonza and cultured in EGM-2MV growth medium supplemented with recommended growth factors and antibiotics per manufacturer's specifications. Cells were maintained in a 37º C humidified atmosphere at 5% CO_2. Primary HUVECs were used at passages 4-9.

iii. Human Pancreatic Cancer Cell Lines

All human PDAC cell lines were maintained in RPMI medium supplemented with 7% FBS and 100 units penicillin/100 µg of streptomycin per 1 ml of culture media. Cells were stored in a 37º C humidified incubator with 5% CO_2. Human PDAC cell lines used include: S2-013, BxPC-3, Colo357, HPAF-II, T3M4, Hs667t, Capan-1 and MiaPaca-2. For serum starvation studies, FBS-containing RPMI was removed, cells were washed, and media replaced with RPMI containing no FBS.

iv. Mouse Pancreatic Cancer Cell Lines

Mouse pancreatic tumor cells KPC8060 and KPC8069 were derived from *LSL-Kras$^{G12D/+}$;LSL-Trp53$^{R172H/+}$;Pdx-1-Cre* (KPC) mouse tumors by our laboratory. KPC mice spontaneously develop PDAC tumors in a manner that recapitulates the human disease with

progression from precursor PanIN lesions to pancreatic cancer (242). Additionally, our laboratory has back-crossed (10 times) the KPC mouse into the C57BL/6 background. For tumor cell isolation, the pancreas was minced with scissors and then digested with 2 mg/ml collagenase A (Roche, Basel Switzerland) for 45 minutes to 1 hour at 37º C with shaking. Cells were cultured in DMEM containing 5% FBS and 100 units penicillin/100 μg of streptomycin per ml of media. KPC8060 and KPC8069 cell lines were evaluated for epithelial morphology and routinely passaged to discourage fibroblast growth.

v. Pancreatic Fibroblast Cells

Immortalized, non-transformed pancreatic fibroblast clones 13.34, 13.7, 13.8, and 13.9 were cultured in RPMI supplemented with 7% FBS and 100 units of penicillin/100 μg of streptomycin per ml of media. Cells were maintained in a 37º C humidified incubator with 5% CO_2. 13.34 pancreatic fibroblasts have been previously determined to be of an activated stellate cell phenotype (166). Additionally, 09-06 PC pancreatic fibroblasts (isolated from a pancreatic cancer patient during a Whipple procedure and immortalized with hTERT) and primary LM fibroblasts (isolated from a liver metastasis of a pancreatic cancer patient) were a generous gift from Dr. Quan Ly. These cells were also cultured in RPMI supplemented with 7% FBS and 100 units penicillin/100 μg of streptomycin per ml of media and stored in a 37º C humidified incubator with 5% CO_2. Dermal human foreskin fibroblasts (HuFF) were also cultured under the same conditions as above.

II. Conditioned Media Collection and Preparation

To create cellular conditioned media (CM), $3.2x10^4$ PDAC cells or pancreatic fibroblasts were plated per 1.0 cm^2 in tissue culture-treated plasticware. Following cell adhesion, media was changed to RPMI or EBM-2 supplemented with 0.2% FBS. Cells were allowed to condition the media for 24 hour. Media was then collected and passed through a 0.45 μm filter to remove cell debris prior to use.

III. Cell Lysates and Western Blotting

i. Whole Cell Lysates

Whole cell lysates were collected using a Radio Immuno Precipitation Assay (RIPA) lysis buffer (150 mM NaCl, 1% IGEPAL, 0.5% sodium deoxycholate, 0.1% SDS, 50 mM Tris base, pH 8.0) supplemented with a Roche mini PMSF tablet, and 1X Halt Protease and Phosphatase Inhibitor Cocktail (Thermo Fisher Scientific). Collected samples were then centrifuged at 10,000 rpm for 10 minutes at 4° C. Supernatants were collected and stored at -20° C.

ii. CA19-9 Western Blot

For CA19-9 western blotting of tumor cell lysates and conditioned media, 50 μg of protein or 30 μl of conditioned media were loaded onto 4-20% Tris-Glycine gradient gels (Bio-Rad Laboratories) under reducing conditions (2.5% dithiothreithol and 2.5% β-mercaptoethanol). Gels were run at 180 volts in SDS-PAGE running buffer (3 g/L Tris base, 14.4 g/L glycine, 1 g/L SDS). The proteins were then transferred to PVDF membranes for 1 hour at 0.35 amps in a Tris-glycine buffer (TBS; 1.4 g/L Tris base, 7.2 g/L glycine). The membranes were blocked for 2 hours with 5% nonfat dry milk diluted in TBS buffer (3.0 g/L Tris base, 150 mM NaCl, 3 mM KCl) containing 0.1% Tween-20 detergent (TBST). Following blocking, membranes were incubated with mouse anti-human sialyl Lewis^{A} (sLe^{A}) (CA19-9; 1:500) or loading control mouse anti-mouse β-actin (1:3000, Sigma) overnight at 4° C. After washing with TBST, the membranes were incubated with goat anti-mouse-HRP secondary antibodies (Jackson Labs) for 1 hour followed by exposure to chemiluminescence reagents (Thermo Scientific) for visualization.

iii. CXCR4 Western Blot

For CXCR4 western blots, 50 μg of protein were loaded into the wells of 10% Bis-Tris gels under reducing conditions in a 1X MOPS buffer (50mM Tris, 50 mM MOPS, 0.1% SDS, 1 mM EDTA). The gel electrophoresis and membrane transfer were performed as stated above. Membranes were blocked for 2 hours with 5% nonfat dry milk diluted in TBST followed by

incubation with rabbit polyclonal CXCR4 antibody (Abcam; 1:500) overnight at 4° C. After washing, the membranes were incubated with goat anti-rabbit-HRP secondary antibodies (Jackson Labs) for 1 hour followed by exposure to chemiluminescence reagents for visualization.

iv. Phospho-ERK and Total ERK Western Blot

Western blotting for phospho-ERK and total ERK was performed similarly to CXCR4 western blotting except a 5% bovine serum albumin (BSA) buffer (10 mM Tris base, 100 mM NaCl, 0.2% Tween-20) was used for blocking and primary antibody incubations and 1% BSA buffer for secondary antibody incubations. Rabbit polyclonal phospho- and total ERK antibodies (Cell Signal) were used at a 1:1000 dilution.

IV. Flow Cytometry

i. *In Vitro* Expression Studies

Cells were collected using TryLE Cell Dissociation Buffer (Invitrogen) and then washed with PBS containing 5% FBS. Following washing, cells were incubated with primary antibodies for 30 minutes at room temperature. Cells were then washed 2 times with PBS+5% FBS and appropriate fluorescently labeled AlexFluor secondary antibodies (Invitrogen; 1:500) added. Cells were incubated with secondary antibodies for 30 minutes at room temperature in the dark. Cells were then washed again and incubated for 10 minutes with 2% neutral buffered formalin diluted in PBS+2% FBS. Cells were washed and resuspended in PBS and then analyzed by flow cytometry. Primary antibodies included rabbit polyclonal anti-CXCR4 (Novus Biologicals; 1:200), mouse anti-human E-selectin (Santa Cruz; 1:100), and mouse and IgG controls (Jackson Labs; 1:1000).

ii. Immune Cell Identification

Cells isolated from KPC8060 orthotopic tumors were incubated with Live/Dead Aqua stain (Thermo Fisher Scientific) for 10 minutes in the dark then equally dispensed into the wells of a 96-well plate. Excess Live/Dead stain was washed with PBS+2% FBS. Cells were then incubated with fluorophore-conjugated primary antibodies (5 µl/sample) for 30 minutes in the dark at room

temperature followed by washing with PBS+2% FBS. Dr. Kamiya Mehla kindly developed and optimized the immune cell panel for the study (**Table 2.1**). Following washing, cells were fixed with 2% paraformaldehyde (PFA) for 10 minutes in the dark at room temperature. Cells were again washed and then resuspended in 150 µl PBS+1% FBS and taken to the Flow Cytometry Facility for analysis. Unstained immune cells and compensation beads (eBiosciences) were used at controls.

V. Methylene Blue Proliferation Assay

For analysis of the effects of E-selectin and CXCR4 blockade on cells, a methylene blue-based proliferation assay was adapted from (243). Briefly, $3x10^3$ cells were plated in the wells of a 96-well plate along with increasing doses of GMI-1271 or GMI-1359. Five replicate wells were set up per dose. At designated time points (2, 24, 48, 72, and 96 hours), cells were fixed with 10% neutral buffered formalin then stained with 1% methylene blue for 30 minutes. After staining, cells were washed 4 times with 0.01 M borate buffer (pH 8.5). The methylene blue dye was then eluted from the cells with 1:1 (v/v) solution of ethanol and 0.1 N HCl, and the absorbance at 650 nm was read. Increases in the OD values were plotted as cells proliferated over time.

VI. Inhibitor Dosing Assay

Cells were plated in the wells of 24-well plates and grown to 70% confluence. GMI-1271 or GMI-1359 at various concentrations was added to the wells. Cells were imaged every 24 hours for 96 hours and examined for changes in morphology and cell death. GMI-1271 and GMI-1359 are rationally designed glycomimetic small molecule inhibitors developed by GlycoMimetics, Inc. (Rockville, MD). GMI-1271 inhibits adhesion protein E-selectin with an IC50 of 2.4 µM. GMI-1359 inhibits both E-selectin (IC50: 1.0 µM) and chemokine receptor CXCR4 (IC50: 0.5 µM). To design GMI-1359, a CXCR4 blocking structure was added to the GMI-1271 scaffolding backbone.

Table 2.1 Panel of immune cell markers used for *in vivo* identification within tumors.

Panel 1		
Marker	**Fluorophore**	**Cell Type**
Live/Dead	Aqua	live vs. dead cells
CD11b	eFluor450	macrophages/monocytes
CD11c	PE-Cy7	DCs
Gr-1	FITC	MDSCs
F4/80	PE	macrophages
Panel 2		
Marker	**Fluorophore**	**Cell Type**
Live/Dead	Aqua	live vs. dead cells
CD3	PE	T cells
CD8	PerCP-Cy5.5	CD8+ T cells
CD4	APC-Cy7	CD4+ T cells
CD19	PE-Cy7	B cells
CD335	APC	NK cells

Table 2.1 lists the immune cell markers and conjugated fluorophores used to identify the immune cell composition of KPC8060 orthotopic tumors by flow cytometry.

VII. *In Vitro* Lymphangiogenesis Assays

i. Collagen-I Three-Dimensional Matrix

For analysis of *in vitro* tubulogenesis, $5x10^4$ hLECs were plated into the wells of a 48-well plate. When hLECs achieved a confluent monolayer, 100 μg/ml of rat tail collagen-I (BD Biosciences) was overlaid across the hLECs and allowed to form a three-dimensional matrix. Cells were imaged at 18 hours and tube number quantified. All treatments were performed in triplicate. For inhibitor studies, increasing doses of GMI-1271 or GMI-1359 were included during tubulogenesis.

ii. Growth Factor Reduced Matrigel Three-Dimensional Matrix

As a secondary method for evaluating lymphatic tubulogenesis *in vitro*, we used a three-dimensional matrigel matrix to elicit tube formation. In the wells of a 96-well plate, 55 μl of Growth Factor Reduced Matrigel Basement Membrane Matrix (Corning) was allowed to gelatinize for 30 minutes at 37^{o} C in a humidified incubator. After gel formation, $1.2x10^4$ hLECs were plated in designated wells. After 6 hours, hLECs formed tube-like networks and phase contrast images were collected. Tubulogenesis was quantified by counting the number of tubes per image. For inhibitor studies, increasing doses of GMI-1271 and GMI-1359 were incubated with hLECs for 30 minutes, after which, hLECs were added to the matrigel matrix. Each treatment was performed in triplicate.

VIII. Live Cell Imaging of Co-cultures

i. Co-culture Invasion Imaging Assay

To characterize PDAC cell and pancreatic fibroblast interactions with a lymphatic endothelium, hLECs were plated in the wells of a 24-well plate and grown to confluence. Once confluence was achieved, $4x10^4$ S2-013, Colo357, or 13.34 cells were overlaid atop the hLEC monolayer. In studies examining the effects of E-selectin and CXCR4 blockade on this invasion process, GMI-1271 or GMI-1359 was added to hLEC monolayers 30 minutes prior to the addition of PDAC cells or fibroblasts. Phase contrast images at 10X or 20X magnification were collected

every 10 minutes using an IX81 Spinning Disk Upright Confocal Olympus Microscope. During image collection, cells were stored in a 37° C humidified (48%) chamber with 5% CO_2. Live cell movies were made from the images using Slikebook 5.5 software for image acquiring and processing. Cell types were distinguished by cell morphology. Each co-culture and/or treatment conditions were performed in triplicate and multiple cells per well analyzed.

ii. Co-culture Migration Imaging Assay

To characterize the migration properties of a distinct cell population to another distinct cell population, 2-well silicone adhesive cell culture inserts were added to the wells of a 24-well plate. Cells were plated into designated wells at a density of $2x10^4$/insert and allowed to adhere overnight. Inserts were removed once cells had adhered and washed twice to remove non-adherent cells and cell debris. Phase contrast images at 10X magnification were collected every 10 minutes. Each cell combination was performed in triplicate and assay was repeated thrice. Image analysis and front migration rate was performed using NIH open source Image J program.

iii. Co-culture Lymphangiogenesis Assay

To evaluate how pancreatic tumor cells and fibroblasts influenced lymphangiogenesis *in vitro*, we did live cell imaging of these cells in co-cultures with LECs during collagen-I induced tubulogenesis. Human LECs were plated into the wells of a 48-well plate and grown to confluence. Once a confluent monolayer was established, $5x10^4$ S2-013, Colo357, 13.34 cells were overlaid atop the hLEC monolayer along with 100 μg/ml of rat tail collagen-I. Phase contrast images (10X magnification) were collected every 10 minutes. Each cell combination was performed in triplicate and assay was repeated thrice. Image analysis was performed using NIH open source Image J program.

IX. Immunohistochemical Staining

To identify metastatic lesions, formalin-fixed (24 hours) paraffin-embedded (FFPE) mouse tissues were cut into 5 µm sections and deparaffinized and rehydrated using standard procedures. Standard hematoxylin and eosin staining was performed.

Staining for specific proteins, FFPE tissue sections were deparaffinized and rehydrated. Heat-induced antigen retrieval was performed using 10 mM citrate buffer (pH 6.0) containing 0.05% Tween-20 for 10 minutes. Endogenous peroxidases were blocked using DAKO peroxidase block for 5 minutes followed by a 1% BSA protein block for 1 hour. Primary antibodies were incubated overnight at 4º C. For secondary staining identification, DAKO polymer-labelled secondary was used followed by DAB substrate and a hematoxylin counterstain. Primary antibodies included mouse anti-mouse α-smooth muscle actin (Sigma; 1:400), rabbit polyclonal anti-CD31 (Abcam; 1:100) and rabbit polyclonal anti-CD45 (Abcam; 1:100) antibodies.

X. Immunofluorescence Staining

For immunofluorescence staining, deparaffinization, antigen retrieval and blocking were all performed in the same manner as the immunohistochemical staining for FFPE tissue sections. Rabbit polyclonal anti-LYVE-1 (Abcam; 1:100) was incubated with tissues overnight at 4º C. After washing, appropriate Alexa Fluor secondary (1:500) antibodies were applied for 1 hour at room temperature. Sections were mounted with DAPI-containing mounting media (Vector Labs).

For staining of cells *in vitro*, cells were fixed with 10% neutral buffered formalin for 15 minutes. Protein blocking and permeabilization were performed simultaneously with PBS containing 5% FBS and 0.1% Triton X-100 for 30 minutes. Primary antibodies were incubated at 4º C overnight. After washing, appropriate Alexa Fluor secondary antibodies were applied for 1 hour at room temperature. Again, sections were mounted with DAPI-containing mounting media. Primary antibodies used included: mouse anti-human E-selectin (R&D Systems, 1:100); mouse

anti-human VE-cadherin (BioLegend; 1:400); mouse anti-human CA19-9 (1:100); and mouse IgG (Jackson Labs; 1:1000).

XI. Boyden Chamber Migration Assays

For a quantifiable measure of cell migration, Boyden chamber control insert migration plates were used (24 well; 8 μm pore; PET membrane). In the upper chamber, cells were diluted in serum free media at plated at a density of $2.5x10^4$ cells/insert (500 μl/insert). In the lower wells, 750 μl of chemoattractant-containing media was added. After 24 hours of migration, membranes were washed with PBS, and non-migratory PDAC cells were mechanically removed using a Q-tip. Migratory cells were fixed and stained with Diff-Quick staining kit. Membranes were mounted on slides and divided into quadrants. Representative 10X images were collected from each quadrant and the numbers of cells quantified. Each experiment was performed in triplicate.

Several types of chemoattractants were used for various studies: undiluted PDAC conditioned media, undiluted fibroblast conditioned media, EGM-2MV growth media for hLECs, RPMI containing 7% FBS for PDAC cells and fibroblasts, or 200 ng/ml CXCL12 diluted in serum free media. When studies employ GMI-1271 or GMI-1359, inhibitors were added to the upper chamber and lower well at designated concentrations.

XII. Live Cell Fluorescent Labeling

To help identify disparate cell types in co-culture assays, cells were fluorescently labeled with either 5 μM Vybrant CFDA-SE Cell Tracer or 10 μM Cell Tracker Orange CMRA (Invitrogen, Carlsbad, CA). Briefly, cells were incubated with designated concentrations of the fluorescent labels diluted in serum free media at 37° C for 15-30 minutes. After labeling, cells were washed with prewarmed, serum containing media for 30 minutes at 37° C. Washing media was removed and cells were prepped and counted for co-culture assays.

XIII. PDAC Adhesion Assays

For evaluation of the role of E-selectin and CXCR4 in PDAC cell adhesion, hLECs were plated in 8-well chamber slides (BD Biosciences) and grown to confluence. After establishing a confluent monolayer, hLECs were pretreated with increasing doses of GMI-1271 or GMI-1359 for 1 hour. After hLEC pretreatment, $2.5x10^4$ CFDA-SE-labeled PDAC cells were overlaid on top of the hLEC monolayers. Non-adhered tumor cells were washed away with PBS and adhered cells were fixed with a 10% neutral buffered formalin. Slides were mounted with DAPI-containing mounting media and images collected and quantified. Four representative fields were imaged at a 4X magnification. Three replicate wells were analyzed per experiment, and each experiment was also performed in triplicate.

XIV. Transendothelial Migration Assays

Using a modified Boyden chamber system (24 well; 8.0 μm pore), $3x10^4$ hLECs were plated on the underside of PET membrane insert and allowed to grow to confluence. In some experiments, hLEC monolayers were pre-treated with 2 ng/ml recombinant human TNFα (R&D Systems) for 7 hours to induce inflammatory E-selectin expression. In experiments with CXCL12, hLECs were pretreated with 200 ng/ml recombinant human CXCL12 for 8 hours. Additionally, hLECs were pretreated with increasing doses of GMI-1271 or GMI-1359 or mouse anti-human CXCR4 neutralizing antibody (10 μg/ml) for 1 hour. After pretreatment, $5x10^4$ CFDA-SE-labeled PDAC cells were diluted into serum free RPMI and added to the upper insert of the Boyden chamber. In the lower wells, EGM-2MV was added as a chemoattractant. PDAC cells were allowed to transendothelial migrate for 24 hours. Following TEM, membranes were washed with PBS, and non-migratory PDAC cells were mechanically removed using a Q-tip. Membranes were then fixed with methanol and mounted on slides using DAPI-containing mounting medium. Five representative images at 10X magnification were taken of every membrane and the CFDA-SE

fluorescent pancreatic tumor cells were quantified. Three replicate wells were analyzed per experiment, and each experiment was also performed in triplicate.

XV. Transwell Co-culture and qRT-PCR

$4x10^5$ hLECs were plated on the underside of PET membrane inserts (0.4 μm pore; 24 mm diameter; BD Biosciences) and incubated overnight. The next day, $6x10^5$ PDAC cells or pancreatic fibroblasts were added to upper side of the membrane and co-cultured with the hLECs for designated times. After co-culturing, mRNA was isolated from hLECs using RNAqueous Micro Isolation kit (Invitrogen). 200 ng RNA was reverse transcribed using Verso cDNA Synthesis kit (Thermo Scientific). Triplicate qRT-PCR reactions were performed using SYBR Green Master Mix (Applied Biosystems) per manufacturer's specifications. Relative fold changes were calculated based on normalization to GAPDH using cycle threshold values. E-selectin forward primer: 5'-TGTGGGTCTGGGTAGGAACC-3'; reverse primer: 5'-AGCTGTGTAGCATAGGGCAAG-3'; GAPDH forward primer: 5'-GAAGGTGAAGGTCGGAGTC-3'; reverse primers 5'-CAAGCTTCCCGTTCTCAGCC-3'.

XVI. Orthotopic Implantation Models

i. S2-013 Orthotopic Implantation

S2-013 ($2x10^6$ cells) were orthotopically implanted into the pancreases of female athymic nude mice (4-6 weeks old; Jackson Labs). Tumors were allowed to establish over the course of two weeks prior to the start of treatment. Following tumor development, mice were divided into treatment groups. For metastasis studies, mice were treated for 4 weeks then sacrificed. For survival studies, mice were treated until end stage disease. The criteria for end stage disease included severe weight loss, excessive ascites accumulation, or extreme weakness/inactivity. Primary pancreatic tumors and metastatic organ sites (lymph nodes, lungs, diaphragm, liver, kidneys and spleen) were collected at the end of each study and evaluated for tumor microenvironment composition and metastatic lesion presence.

ii. KPC8060 Orthotopic Implantation

For evaluation of GMI-1271 and GMI-1359 effectiveness in immunocompetent mice, $9x10^4$ KPC8060 mouse PDAC cells were implanted into the pancreas of syngeneic C57BL/6 mice. In some studies, treatments were initiated two weeks post-orthotopic implantation; in other studies, treatments were initiated the day after orthotopic implantation. Similar to experiments with S2-013, both survival and metastatic studies (2-week duration), were performed.

iii. Inhibitor Treatment Schedules

All injections were administered by intraperitoneal injections. **Table 2.2** describes the various drugs and treatment schedules performed in the *in vivo* tumor studies. PD-L1 was administered on days following gemcitabine treatment as it has been previously demonstrated that immunotherapy results in better responses after cytotoxic tumor killing (244).

iv. Immune Cell Isolation from Mouse Tumors

For analysis of immune cell populations within KPC8060 tumors, primary tumors were collected and minced into small pieces. Tissue was then digested in RPMI containing 10% FBS, 2 mg/ml Collagenase A and 0.25 units/ml DNase I for 45 minutes at 37^{o} C with shaking. Cells were washed twice then resuspended in PBS and prepped for flow cytometry.

Table 2.2 Drug schedule for *in vivo* treatment of mice.

Drug	Dose	Frequency
Vehicle Control (PBS)	---	Daily
GMI-1271 (low dose)	40 mg/kg	Daily
GMI-1271 (high dose)	40 mg/kg	Twice daily
GMI-1359	40 mg/kg	Daily
Gemcitabine*	60 mg/kg	Every 4 days
Gemcitabine	100 mg/kg	Every 4 days
Anti-PD-L1 antibody	160 μg/mouse	Every 4 days following gemcitabine

Table 2.2 lists the small molecule inhibitors and chemotherapy used in the metastasis and survival *in vivo* studies of orthotopically challenged mice as well the KPC drug enrollment study. Drugs were administered by intraperitoneal injection.

* For initial evaluation of GMI-1271 efficacy *in vivo*, gemcitabine was used at 60 mg/kg. However, for all other subsequent *in vivo* studies, it was used at 100 mg/kg (165, 245).

XVII. *In Vivo* Drug Enrollment Studies

To evaluate GMI-1359 efficacy in a spontaneous mouse model of pancreatic cancer, *LSL-Kras$^{G12D/+}$;LSL-Trp53$^{R172H/+}$;Pdx-1-Cre* (KPC) mice were monitored by ultrasound imaging for the development of pancreas tumors. Enrollment eligibility was determined by the mean of the shortest and longest tumor diameters of the largest tumor cross section being 4 to 7 mm in diameter. Upon attainment of the enrollment eligibility, mice were randomized into 4 treatment groups: 1) Vehicle (PBS) control; 2) 40 mg/kg GMI-1359 daily; 3) 160 µg/mouse anti-PD-L1 antibody; 4) combination GMI-1359 and anti-PD-L1. Tumors growth was monitored weekly by ultrasound imaging. Mice were treated until they displayed signs of end stage disease (extreme lethargy, excessive ascites accumulation, and/or severe cachexia).

XVIII. Statistical Analysis

Statistical analyses were performed using GraphPad Prism 5 software. Student t test was used for tubulogenesis assays, binding assays and transendothelial migration assays. Student t test was also used to evaluate statistical significance in tumor volume, weight, desmoplasia, and lymphatic and blood vascular densities in the *in vivo* studies. One-way ANOVA was used for proliferation assays. Statistical significance for survival studies was determined using log-rank tests. Significance level was set at $p<0.05$ and error bars represent standard deviations.

CHAPTER 3:

Characterization of Lymphatic Endothelial Communications and Interactions with Pancreatic Tumor Cells and Pancreatic Fibroblasts

Excerpts from this chapter have been edited from:

Steele, MM and Hollingsworth, MA. Regulation of cellular lymphatic biology by pancreatic tumor cells and fibroblasts. (In submission to Oncotarget)

I. Introduction

Pancreatic ductal adenocarcinoma (PDAC), the fourth leading cause of cancer-related deaths in the United States, is lethal with a median survival of 6 months and a 5-year survival rate of 7% (1). Very little progress has been made in improving overall patient survival (4). One of the factors impeding development of successful therapies for this deadly disease is the complexity of the PDAC microenvironment. A dense desmoplastic response is one of the defining characteristics of this disease and can comprise up to 80% of the tumor mass (159). Although there is debate about the role of fibroblasts in tumor progression, some fibroblast components of the desmoplastic response are significant contributors to PDAC progression through promotion of tumor growth and survival, immune suppression, and metastasis. These tumor-supporting fibroblasts provide paracrine support to tumor cells as well as other tumor-supporting cell types within the PDAC microenvironment including immune cells and vascular and lymphatic endothelial cells [reviewed in (246-248).

Lymphatic vessel invasion and subsequent metastasis to the lymph nodes are frequently observed events during pancreatic cancer progression (5, 28, 33). At the time of diagnosis, more than 70% of pancreatic cancer patients present with lymph node involvement (56, 249-251), and this lymph node involvement strongly correlates with poor patient prognosis (34-37). Additionally, lymph node status is a significant factor in staging patients and selecting appropriate therapy (39, 40, 111). Although clinicians and researchers recognize the importance of lymph node involvement for patient prognosis and therapy selection, the biological mechanisms governing lymphatic vessel invasion and lymph node metastasis remain poorly understood.

Due to their prevalence within the PDAC microenvironments, pancreatic fibroblasts are probable effectors of lymphatic biology and function within PDAC tumors and likely promote PDAC invasion of lymphatic vessels. However, the mechanisms by which fibroblasts impact lymphatic endothelial cells, the main cell type comprising lymphatic vessels, have not been widely

investigated. In this paper, we describe, for the first time, evidence for intercellular communications and interactions between fibroblasts and lymphatic endothelial cells. We demonstrate that fibroblasts promote lymphatic recruitment, accelerate lymphangiogenesis, and invasion. Using a combination of live cell imaging and endpoint co-culture techniques, we compare the effects of fibroblasts or pancreatic tumor cells on lymphatic endothelial cells to elucidate the contributions by each cell type to the biology of lymphatic endothelial cells within the PDAC microenvironment.

II. Results

Lymphatic endothelial cells strongly migrate toward pancreatic fibroblasts *in vitro*.

We evaluated the capacity of pancreatic fibroblast and PDAC cells to recruit hLECs through secreted paracrine factors. Conditioned media (CM) was collected from a panel of pancreatic tumor cells (Colo357, S2-013, BxPC-3, T3M4, Hs766T, HPAF-II) and pancreatic fibroblasts derived from normal pancreas (13.34) and used as chemoattractants for hLECs in a Boyden chamber migration system. 13.34 pancreatic fibroblasts were determined to be of an activated phenotype (αSMA^{+}) suggesting they are capable of producing abundant growth factors and cytokines necessary to induce cellular migration (**Supplementary Figure 3.1A-D**) (167). Data in **Figure 3.1A** show that CM from Colo357, S2-013, and T3M4 PDAC cells induced modest levels of directional hLEC migration compared to unconditioned media. Hs766T, BxPC-3, or HPAF-II CM did not induce significant hLEC migration compared to unconditioned control media. In contrast, 13.34 pancreatic fibroblast CM induced high levels of hLEC migration. In our hands, 13.34 CM was a stronger chemoattractant for hLECs than standard endothelial growth media EGM-2MV (positive control), which contains necessary growth factors and serum for hLEC maintenance.

To determine if the chemotactic effect was specific to the 13.34 line, hLEC migration toward CM collected from other pancreatic fibroblast lines was also evaluated. CM from three separate lines of normal pancreatic fibroblasts - 13.7, 13.8, and 13.9, strongly induced directional hLEC migration compared to unconditioned media (**Figure 3.1B**). We also evaluated CM from a

Figure 3.1

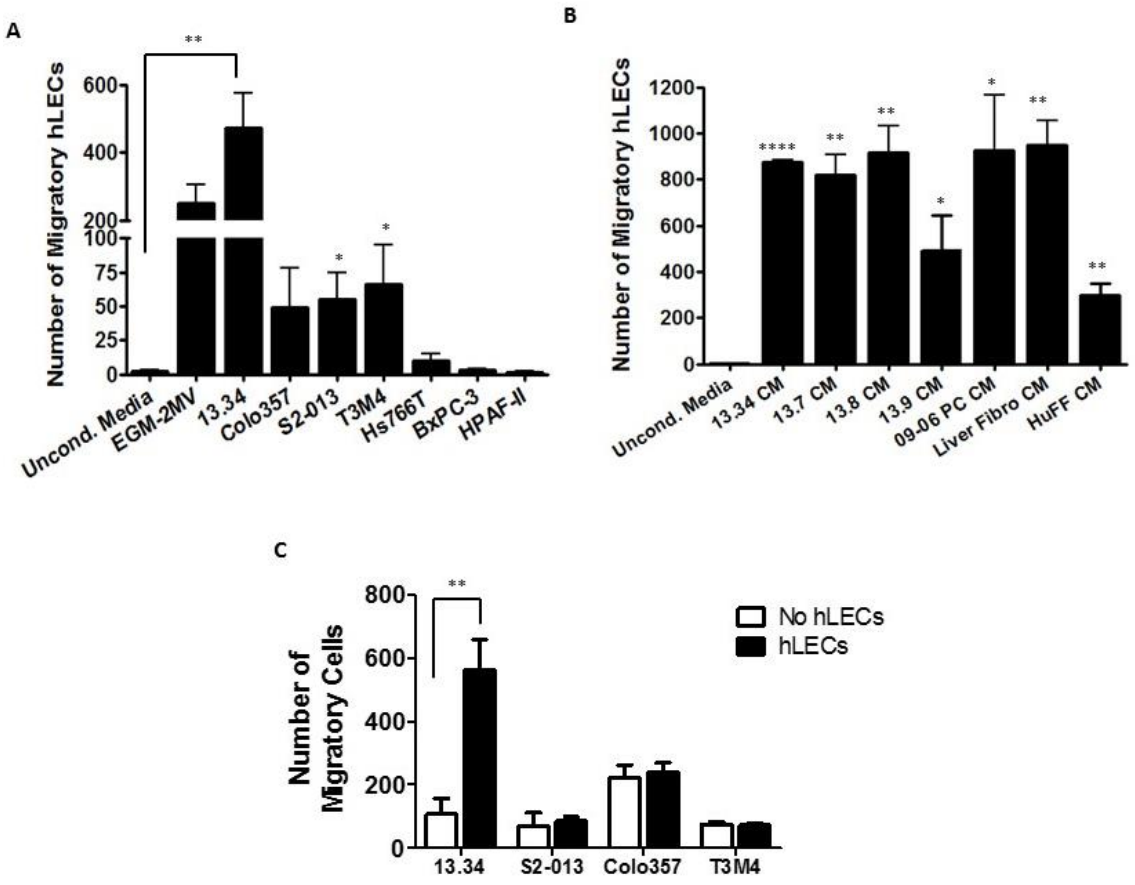

Figure 3.1 Pancreatic fibroblasts strongly induce hLEC migration while PDAC cells only induce moderate hLEC migration.

A) Conditioned media (CM) from pancreatic fibroblasts (13.34) or PDAC lines (Colo357, S2-013, T3M4, Hs766T, BxPC-3, HPAF-II) was evaluated as a potential chemoattractant for hLECs using a Boyden chamber migration system. EGM-2MV with 5% FBS was used as a positive control for hLEC migration. Graphical representation is the mean of 3 replicate membranes; experiment was repeated 3 times. *p<0.05, **p<0.01; error bars = s.d.

B) Conditioned media from a panel of human non-transformed pancreatic fibroblasts (13.34, 13.7, 13.8, 13.9), PDAC-associated fibroblasts (09-06 PC), PDAC liver metastasis-associated fibroblasts (liver fibro), or dermal foreskin fibroblasts (HuFF) was used as a chemoattractant to induce hLEC migration. Graphical representation is the mean of 3 replicate membranes; experiment was repeated 3 times. *p<0.05, **p<0.01, ****p<0.0001; error bars = s.d.

C) hLECs were plated in the lower well of a Boyden chamber to act as a chemoattractant for 13.34 fibroblasts or S2-013, Colo357, or T3M4 cells. Graphical representation is the mean of 3 replicate membranes; experiment was repeated 3 times. **p<0.01; error bars = s.d.

tumor-associated fibroblast line, 09-06 PC, which also strongly attracted hLEC populations. Comparable results were obtained for CM from fibroblasts isolated from a liver metastasis of PDAC patient sample (liver fibroblast CM). CM from neonatal dermal foreskin fibroblasts (HuFF) consistently displayed a weaker ability to attract hLECs compared to CM from the other fibroblast lines; however, CM from this line consistently attracted enhanced numbers of hLECs compared to unconditioned media. These data demonstrate that pancreatic fibroblasts are strong inducers of hLEC migration, and suggest that their presence strongly supports lymphatic recruitment to primary PDAC tumor sites.

As the ability of PDAC cells and fibroblasts to migrate toward lymphatic vessels is also key for key for successful lymphatic-directed dissemination, we evaluated the ability of hLEC paracrine factors to induce migration of PDAC cells and pancreatic fibroblasts. Across multiple replicate experiments, 13.34 fibroblasts consistently showed strong migration toward hLECs as compared to control wells without hLECs present (**Figure 3.1C**). PDAC cells did not demonstrate an increased ability to migrate toward hLECs compared to control wells that lacked hLECs.

Chemotactic communication between pancreatic fibroblasts and PDAC cells is highly variable across PDAC lines.

To more fully understand cell-cell communications within the pancreatic tumor microenvironment, we also examined the ability of PDAC tumor cell lines to induce pancreatic fibroblast migration as well as the ability of pancreatic fibroblasts to induce PDAC migration. **Figure 3.2A** shows that conditioned media from BxPC-3 and Colo357 PDAC lines significantly increased pancreatic fibroblast migration compared to unconditioned media. HPAF-II PDAC cells were unresponsive to 13.34 conditioned media. Unexpectedly, the conditioned media from S2-013 cells consistently inhibited 13.34 fibroblast migration compared to unconditioned media.

Figure 3.2

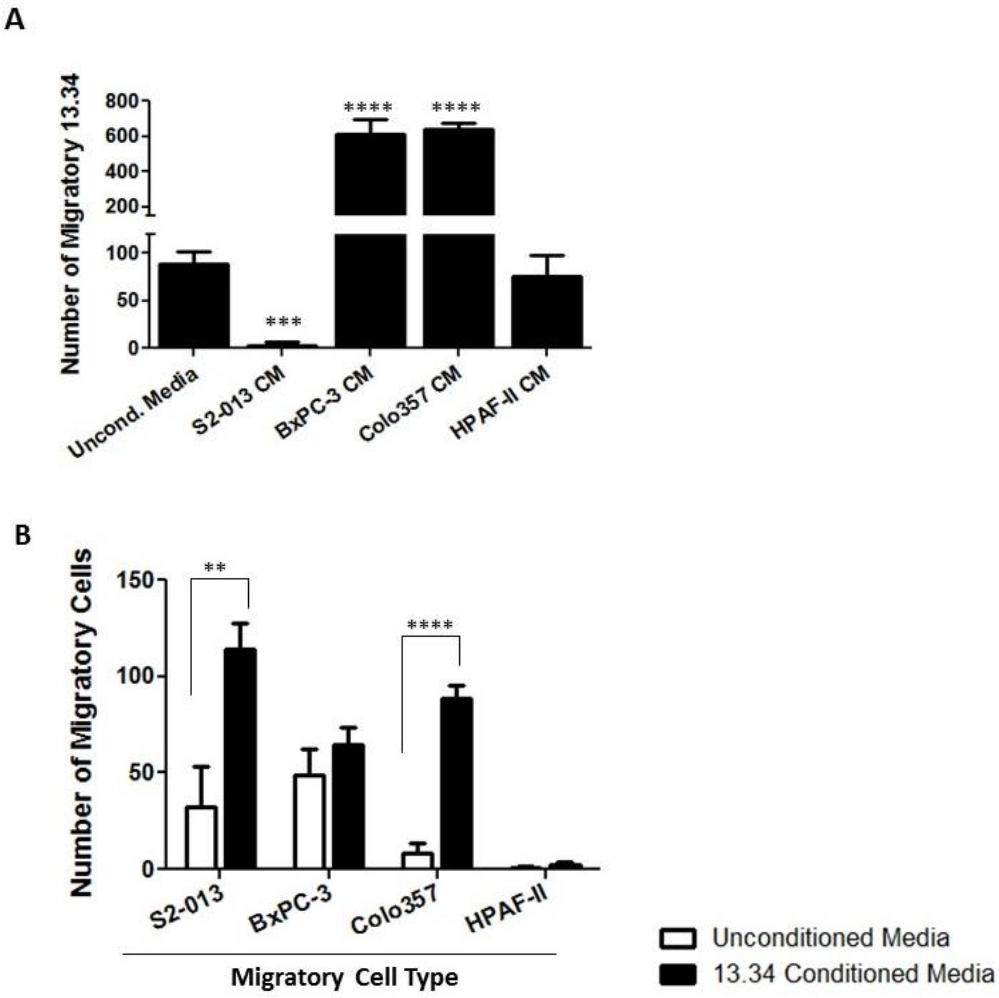

Figure 3.2 Chemotactic communication between pancreatic fibroblasts and PDAC cells is highly variable across PDAC lines.

A) Boyden migration plates were used to evaluate the ability of S2-013, BxPC-3, Colo357, and HPAF-II CM to induce 13.34 fibroblast migration. Graph represents the mean of 3 membranes per conditioned media type; experiment was repeated 3 times. ***$p<0.001$, ****$p<0.0001$; error bars = s.d.

B) CM from 13.34 pancreatic fibroblasts was loaded into the lower wells of a migration plate to act as a potential chemoattractant for S2-013, Bx-PC-3, Colo357, and HPAF-II PDAC cells. 13.34 CM strongly induced S2-013 and Colo357 migration but did not alter on BxPC-3 or HPAF-II migration compared to unconditioned media. Graphical representation is the mean of 3 membranes/treatment; experiment was repeated 3 times. **$p<0.01$, ****$p<0.0001$; error bars = s.d.

We also examined whether factors secreted from 13.34 pancreatic fibroblasts were capable of inducing PDAC cell migration. Although S2-013 cells do not induce pancreatic fibroblast migration, these cells are strongly attracted to the secreted factors found in pancreatic fibroblast conditioned media (**Figure 3.2B**). Colo357 PDAC cells were also strongly attracted to 13.34 conditioned media compared to unconditioned media. BxPC-3 and HPAF-II PDAC cells demonstrated no difference in migration to 13.34 conditioned media compared to unconditioned media.

Live cell imaging characterization of homogenous cell populations.

Boyden chamber migration systems allow for easy quantification of cell migration; however, these assays only capture migration of a single cell type at a fixed endpoint. Using live cell imaging, we examined real-time migration of PDAC cells, pancreatic fibroblasts, and/or hLECs in co-culture. Various cell types were plated into the wells of a 2-well silicone insert. Once the cells within the wells of the inserts had adhered to the bottom of the well, the insert was removed, creating a 500 μm gap-exclusion zone between the two cell populations. Images of cell migration into the gap were captured every 10 minutes for 24 hours and then the frames were stitched together. The use of a barrier, rather than a scratch, to create a gap between two cell populations is important for multiple reasons: a) it permits migration analysis of disparate cell types; b) it minimizes cell damage which can influence migration results, and c) it creates a uniform gap in all multiple experimental wells. Using live cell imaging, we followed the migration pattern and morphology changes of two cell types as they migrated toward one another. **Figure 3.3** diagrams some of the terminology used to describe these assays.

For controls, we initially characterized the migration of identical cell populations (13.34 to 13.34; hLEC to hLEC; S2.013 to S2.013; and Colo357 to Colo357; **Figure 3.4A-D**). Numerous similarities were seen when cells of the same type migrate toward one another. The migration fronts of each home population move at uniform rates, and the cells at the leading edge of the migration front remain associated with the home population; individual cells did not escape the home

Figure 3.3

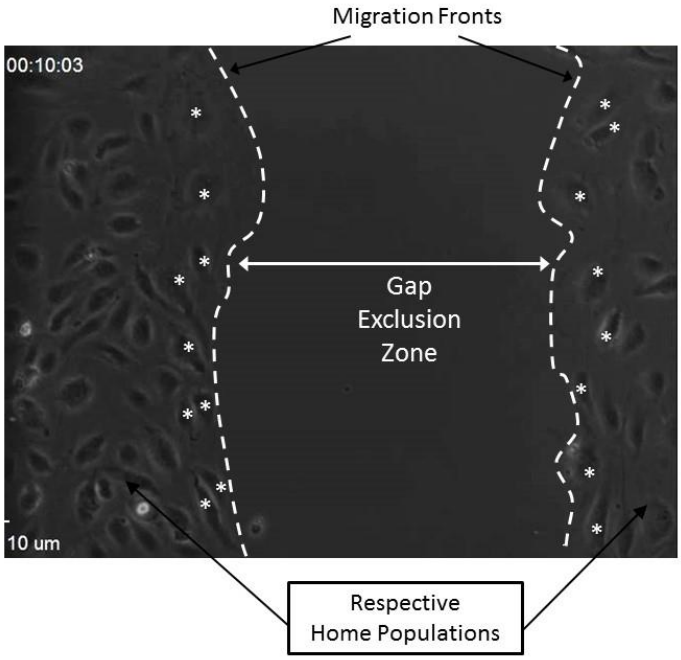

Figure 3.3 Co-culture migration illustration and terminology.

Two-well silicone removeable inserts were adhered to the bottom of the wells of 24-well plate. Disparate or similar cell types were seeded into each of the wells. Following cell adhesion to the bottom of the well, the silicone insert was removed creating a uniform 500 µm gap between the two cell populations. The population where a cell type was plated prior to the start of the experiment is referred to as its "home" population. The "migration front" refers the edge of the population migrating into the gap (dashed line). The individual cells at the boundary of the migration front are referred to as "leading edge" cells (asterisks).

population to traverse the gap and interact with the opposing population of cells. When migration fronts met at gap closure, the forward migration of each cell population stopped and the cells at the edge of each front integrated to form a homogenous monolayer. No cells were observed crawling atop the approaching cell population nor did one population drive the opposing front backward.

Some dissimilarities were noted among the different cell types during homogeneous cell migration. Human LECs populations moved as a single, connected group. The cells at the leading edge of the migration flattened out and formed obvious lamellipodia on the side of the cell facing the gap (**Figure 3.4A**). The cells behind the leading edge appeared to pulled along by the leading cells and did not form obvious lamellipodia themselves. All the cells retained a round cell shape. No proliferation was undergone by the hLECs at the leading front while the cells behind the front were observed regularly dividing. Upon gap closure, hLECs at the leading edge integrated to form a single cohesive population.

Unlike hLECs, pancreatic fibroblasts at the leading edge of the migration front significantly elongated toward the oncoming fibroblast population (**Figure 3.4B**). Fibroblasts both at the leading edge and behind the leading edge formed filipodia in the direction of the opposing fibroblasts. Each population migrated as a loosely connected group with all the cells remaining in close proximity. As the leading edges closed the gap, individual fibroblasts intermixed but retained their elongated shape in the direction of the opposite cell population.

Figure 3.4

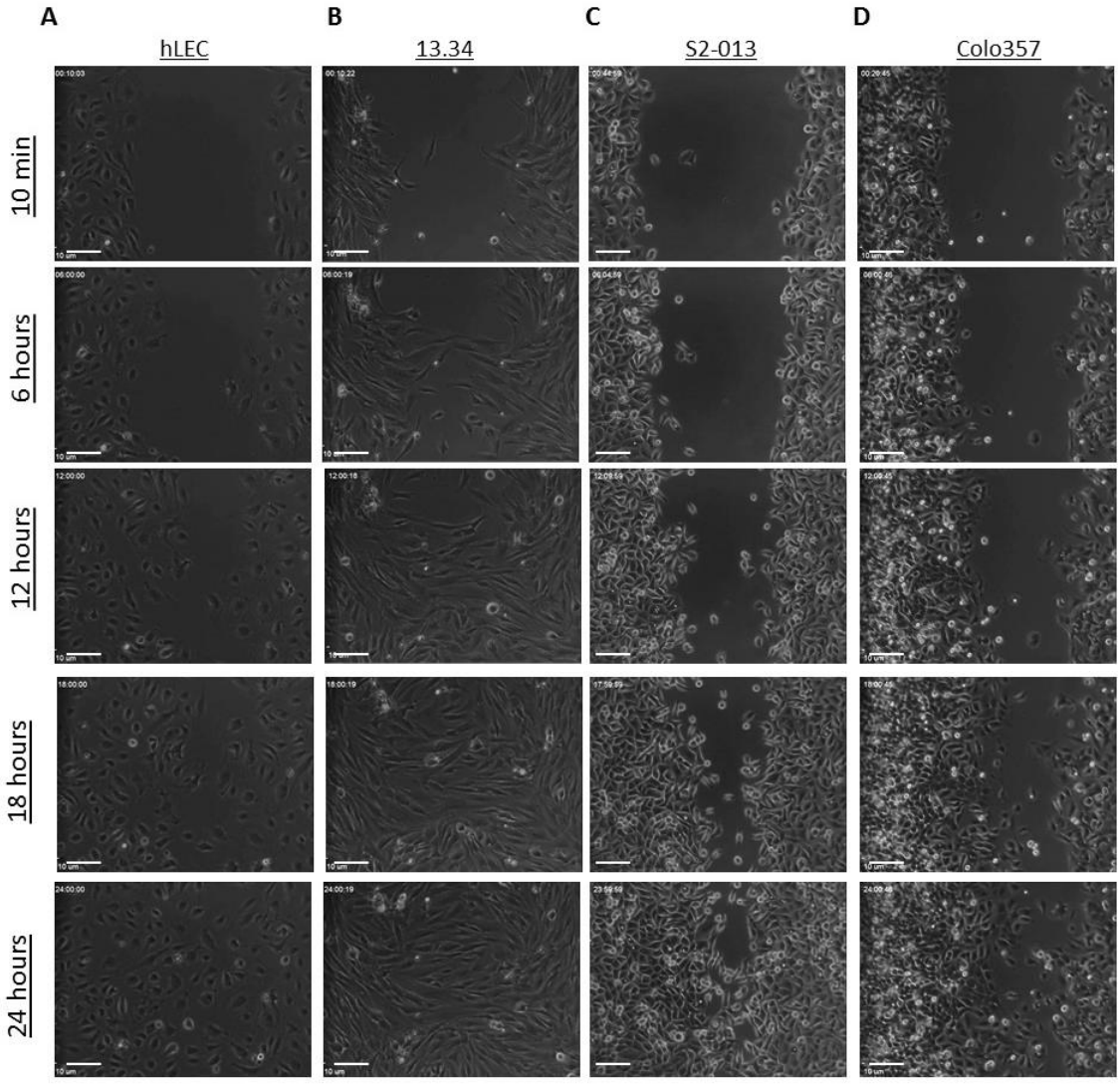

Figure 3.4 Live cell imaging characterization of the migration patterns of identical cell populations.

A-D) Live cell imaging of two cell populations of the same type migrating across a gap toward one another. Images were collected at 10X magnification every 10 minutes for 24 hours. Figures A-D contain representative steady state images collected at 10 minute, 6 hour, 12 hour, 18 hour, and 24 hour timepoints at the same location. Scale bar = 100 µm

S2-013 cells displayed much more individual movements among cells within the home population but the movement did not appear to be directed toward the opposing S2-013 population (**Figure 3.4C**). S2-013 cells both at the migration front and behind it formed lamellipodia; however, the lamellipodia were not always orientated in the direction of the other S2-013 population. Similar to the fibroblasts, S2-013 populations migrated as a loosely connected group while closing the gap. Cells at both the leading edge and behind the leading edge underwent significant amounts of proliferation. Once the gap closed individual cell movements slowed and cells formed a single cohesive monolayer.

Colo357 gap closure was much slower compared to that of the other cell types as the gap did not completely close by 24 hours (**Figure 3.4D**). Much like the hLECs, Colo357 populations migrated as a single connected population with very little movement among the individual cells. Cell division was frequently observed behind the migration front. A significant accumulation of cells behind the migration front suggested that proliferation may have contributed to gap closure. Additionally, lamellipodia formation was not orientated in the direction of the oncoming Colo357 population.

Characterization of migration of disparate cell types in co-culture using live cell imaging.

Next, we characterized the migration patterns of cells toward a disparate cell type initially focusing on co-cultures of hLECs with 13.34 pancreatic fibroblasts or PDAC cells (S2-013, Colo357; **Figure 3.5A-D**). **Figure 3.5A** displays the migration of hLECs to hLECs as a reference for control migration. Assessment of migration patterns between pancreatic fibroblasts and hLECs revealed that, similar to homogenous migration, 13.34 elongated and formed filipodia in the direction of the approaching hLEC population (**Figure 3.5B**). Unlike migration toward an identical cell population, individual 13.34 cells were observed exiting the home population and migrating

Figure 3.5

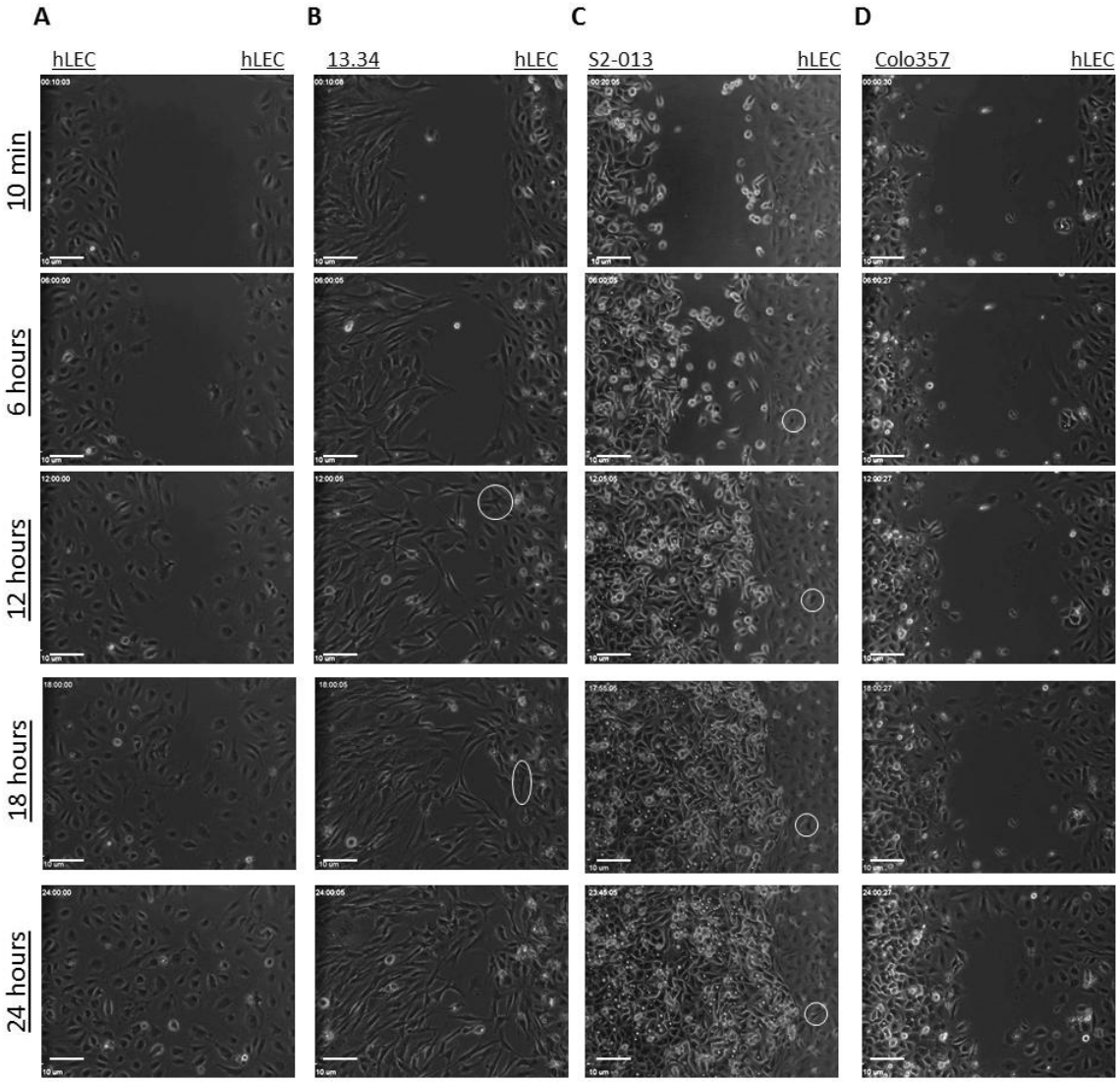

Figure 3.5 Live cell imaging characterization of the migration patterns of hLECs in co-culture with pancreatic fibroblasts or PDAC cells.

A-D) Live cell imaging of the migration patterns of hLECs in **A)** monoculture or in co-culture with **B)** 13.34 fibroblasts, **C)** S2-013, or **D)** Colo357 PDAC cells. Images were collected at 10X magnification every 10 minutes for 24 hours at the exact same location. Figures A-D contain representative steady state images collected at the 10 minute, 6 hour, 12 hour, 18 hour, and 24 hour timepoints. Circles indicate examples of cells crawling atop by not invading the hLEC population. Scale bar = 100 μm

across the gap toward the hLEC population. 13.34 fibroblasts demonstrated a greater migration potential by closing more of the gap than the hLEC population. Migration of hLECs toward 13.34 fibroblasts was relatively similar to migration toward another hLEC population: hLECs moved as a cohesive unit with leading edge cells forming lamellipodia in the direction of the oncoming fibroblasts. As the migration fronts converged, 13.34 fibroblasts and hLECs did not intermix. Rather, the two populations remained abutted against one another. The only exception to this was the occasionally observed fibroblast crawling atop the hLEC population (white circles).

Examination of S2-013 and hLEC migration in co-cultures revealed that leading edge hLECs elongated perpendicularly to the approaching S2-013 population (**Figure 3.5C**). These cells did not form lamellipodia nor did the hLEC migration front progress very far into the gap. Individual S2-013 cells at the leading edge of the migration front were observed very early to exit the home population and migrate across the gap to the opposing hLEC population. After physical contact was made with hLEC cells, S2-013 cells often returned to the home population. As the S2-013 migration front got closer to the hLEC population, the hLEC front was observed to recede backward. Eventually the S2-013 front closed the gap between the two populations and then physically forced the hLEC population backward. There was no intermixing of two cell types upon gap closure although a handful of S2-013 were observed crawling atop the hLEC monolayer.

Examination of Colo357, another PDAC line, migration toward hLECs revealed that a small number of hLEC migrate across the gap early toward the Colo357 population (**Figure 3.5D**). However, these hLECs never fully lost contact with their home population. Unlike S2-013 migration toward hLECs, individual Colo357 cells did not exit their home population and migrate across the gap toward the hLEC population. The Colo357 population moved as a single cohesive unit as did the majority of the hLEC population. Colo357 cells did not induce hLEC recession like the S2-013 cells did. Since both Colo357 and hLEC migration is relatively slow, the gap never fully closed between the two cell types in 24 hours.

Lastly, we characterized the migration patterns of pancreatic fibroblasts and pancreatic tumor cells toward one another (**Figure 3.6A-C**). Unlike migration toward hLEC cells, migrating S2-013 cells remained with the home population moving as a loosely connected group (**Figure 3.6B**). Individual S2-013 cells were not observed to escape the home population and migrate across the gap toward the fibroblasts. S2-013 lamellipodia formation was not orientated in the direction of the approaching fibroblasts, but rather formation occurred on all sides of the cell. Similar to other experimental setups, 13.34 fibroblasts at the leading edge elongated and formed filipodia in the direction of the approaching S2-013 population. Although elongated, leading edge 13.34 cells remained associated with the home population. Once the two fronts met to close the gaps, progress forward stopped and both migration fronts remained stationary. Cells of opposing type did not intermix nor were they observed to crawl atop the opposing monolayer.

Examination of 13.34 and Colo357 migration in co-culture again demonstrated 13.34 elongation toward the approaching Colo357 cells (**Figure 3.6C**). However, unlike migration toward S2-013 cells, numerous individual 13.34 fibroblasts exited the home population and migrated toward the approaching Colo357 population making multiple physical contacts with the PDAC cells. The Colo357 cells maintained tight contact with the home population and do not migrate cross the gap. When the two fronts closed the gap, front progression stopped and neither population regressed nor intermixed with the opposing cell population.

Analysis of the rate of gap closure and cellular migration front progression from live cell imaging.

Using the live cell images, we calculated the rates of gap closure as well as the migration rates of each cell front under the examined co-culture settings. The rate of gap closure was relatively consistent across the groups, with migration between two S2-013 populations being the fastest and migration between two Colo357 populations being the slowest (**Figure 3.7A**). As gap closure rate is the average velocity of two migration fronts, we also calculated the rate of migration for each front in each of the co-culture conditions (**Figure 3.7B-E**). The migration rate of hLECs

Figure 3.6

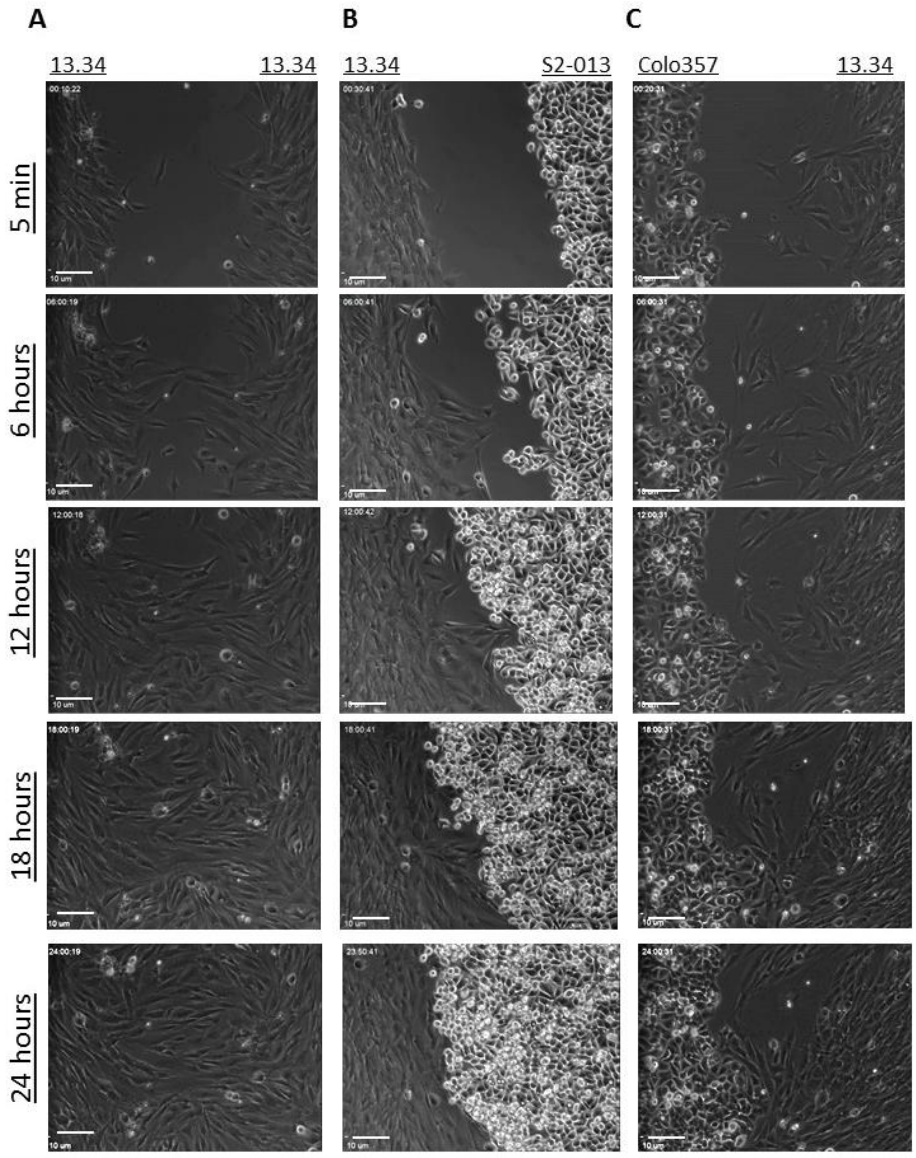

Figure 3.6 Live cell imaging characterization of the migration patterns of pancreatic fibroblasts in co-culture with PDAC cells.

A-C) Live cell imaging of the migration patterns of pancreatic fibroblasts in **A)** monoculture or in co-culture with **B)** S2-013 or **C)** Colo357 PDAC cells. Images were collected at 10X magnification every 10 minutes for 24 hours. Figures A-D contain representative steady state images collected at the 10 minute, 6 hour, 12 hour, 18 hour, and 24 hour timepoints at the same location. Scale bar = 100 µm

Figure 3.7

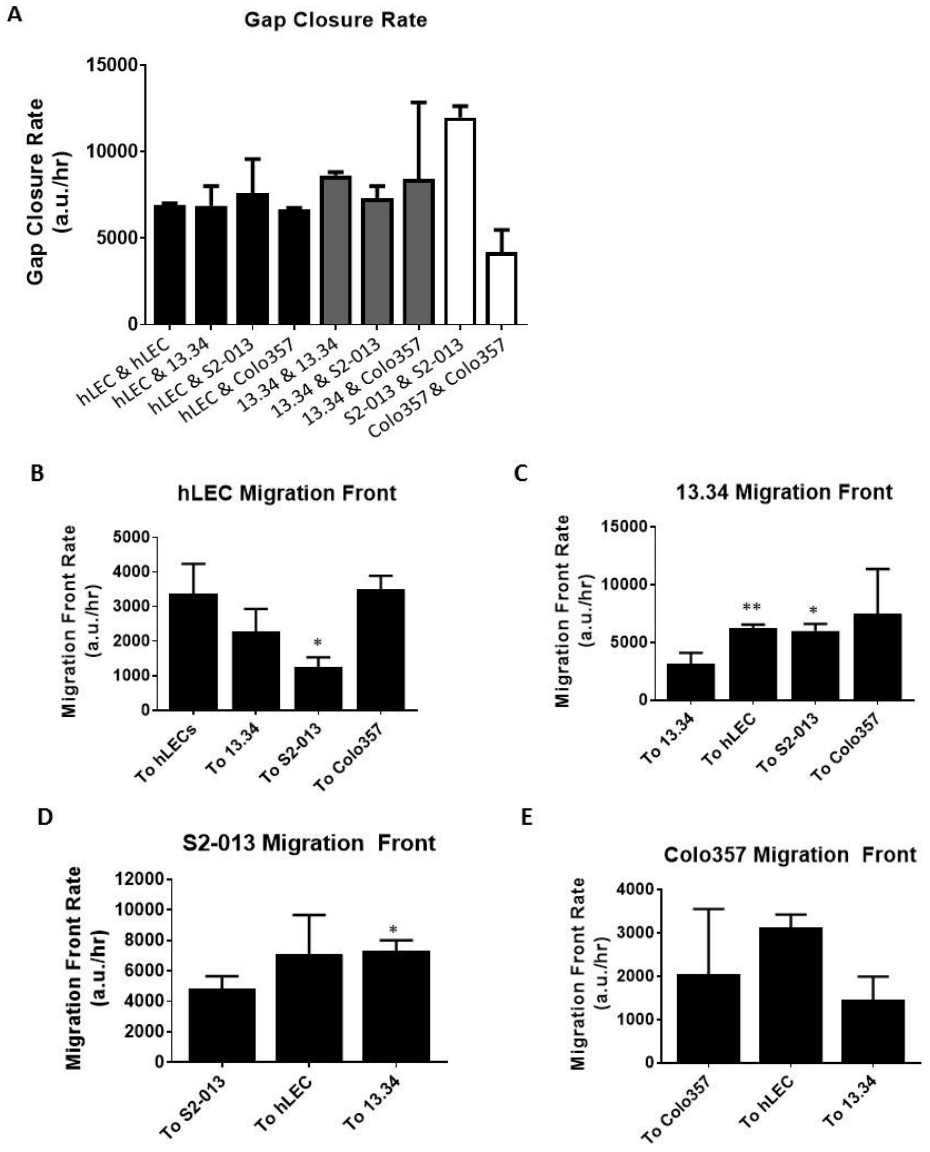

Figure 3.7 Rate of front progression during co-culture migration.

A) Graphical representation of the mean rate of gap closure in a series of co-culture migration assays. Rate = d/t, where d = length of the gap and t = total time to gap closure. If the gap did not completely close, t = 24 hours. This is a measure of the average rate of both population fronts. n=6 gap closure studies per co-culture setup. a.u.= arbitrary units; error bars = s.d.

B-E) Graphical representation of the mean rate of the migration front for **B)** hLECs, **C)** 13.34 fibroblasts, **D)** S2-013 or **E)** Colo357 PDAC cells in a series of co-culture migration assays. Rate = $(x_1-x_0)/t$, where x_1 = area covered by a cell population at gap closure, x_0 = area covered at t = 0, and t = time of gap closure. If the gap did not close, t = 24 hours. n=6 gap closure studies per co-culture setup. Asterisks indicate a statistically significant change in the migration rate of a cell type when in co-culture with a disparate cell type compared to the migration rate when in co-culture with the same cell type. *$p<0.05$, **$p<0.01$; a.u.= arbitrary units; error bars = s.d.

was relatively similar when migration was toward other hLECs, 13.34 fibroblasts, or Colo357 cells (**Figure 3.7B**). However, the hLEC rate significantly slowed when migration was toward S2-013 cells. The 13.34 fibroblast migration rate was slowest toward another 13.34 population, but it significantly increased during migration toward an hLEC or an S2-013 population (**Figure 3.7C**). The rate of S2-013 migration was fastest toward hLECs and 13.34 fibroblasts compared to migration toward another S2-013 population (**Figure 3.7D**). Lastly, Colo357 migration was slowest toward pancreatic fibroblasts and fastest toward hLECs (**Figure 3.7E**). Asterisks indicate statistical significance of co-culture migration compared to monoculture migration.

Pancreatic tumor cells and fibroblasts accelerate *in vitro* lymphatic tubulogenesis and disrupt normal tube network organization.

Lymphangiogenesis is a crucial physiological function of lymphatic endothelial cells, particularly during times of wound healing, inflammation, and malignancy. To evaluate the effects of PDAC cells and pancreatic fibroblasts on lymphangiogenesis, we performed live cell imaging of collagen-I-induced hLEC tubulogenesis when co-cultured with PDAC cells or pancreatic fibroblasts. **Figure 3.8A** shows fixed timepoints of normal tubulogenesis when hLECs are in monoculture. At 4 hours, hLECs lost their smooth cell boundaries and developed a more dendritic appearance with many cellular protrusions. By 8 hours, several individual hLEC cells started to coalesce into an immature tube-like configuration, and by 12 hours, a network of interconnected tubes began to form. Tube formation was completed by 20 hours when nearly all individual hLECs incorporated into the network.

The addition of 13.34 pancreatic fibroblasts or PDAC cells (S2-013, Colo357) to hLECs during collagen-I-induced tubulogenesis resulted in significant changes to the tubulogenesis process (**Figure 3.8B-D**). For three different co-culture experimental designs, tube formation began much earlier than was observed for hLECs in monoculture. Thirty minutes following initiation, tube-like structures were initiated in the co-culture system; this was not seen until 8 hours in the monoculture model. Also unlike the monoculture system where every hLEC cell coalesced into the

Figure 3.8 Characterization of lymphatic tubulogenesis in the presence of PDAC cells or pancreatic fibroblasts.

A-E) Live cell imaging of *in vitro* collagen-I-induced hLEC tubulogenesis in **A)** monoculture or in co-culture with **B)** 13.34 fibroblasts, **C)** S2-013, **D)** Colo357, or **E)** additional hLECs. Images were collected at 10X magnification every 10 minutes for 24 hours at the exact same location. Figures A-E contain representative steady state images collected at the 30 minute, 4 hour, 12 hour, 18 hour, and 20 hour timepoints. Scale bars = 100 μm

F) Quantitative analysis of the mean number of hLECs tubes formed when in monoculture or in co-culture with 13.34, S2-013, or Colo357 cells at t=20 hours. 3 replicate wells were analyzed per experiment; experiment was performed 3 times. *$p<0.05$, **$p<0.01$, ****$p<0.0001$; error bars = s.d.

G) Quantitative analysis of the mean number of disconnected or broken hLEC tubes under monoculture and co-culture conditions at t=20 hours. 3 replicate wells were analyzed per experiment; experiment was performed 3 times. **$p<0.01$, ****$p<0.0001$; error bars = s.d.

H) Graphical representation the percentage of co-culture cell types 13.34, S2-013, or Colo357 either associated (physical contact) or not associated (no physical contact) with hLEC tubes at t=20 hours. *$p<0.05$, ***$p<0.001$; error bars = s.d.

I) Representative images of 13.34, S2-013, or Colo357 cells in culture with hLECs during collagen-I-induced tubulogenesis. 13.34, S2-013, or Colo357 were labeled with green CFDA-SE cell tracer and hLECs were labeled with orange CMRA cell tracer. Scale bar = 25 μm

Figure 3.8

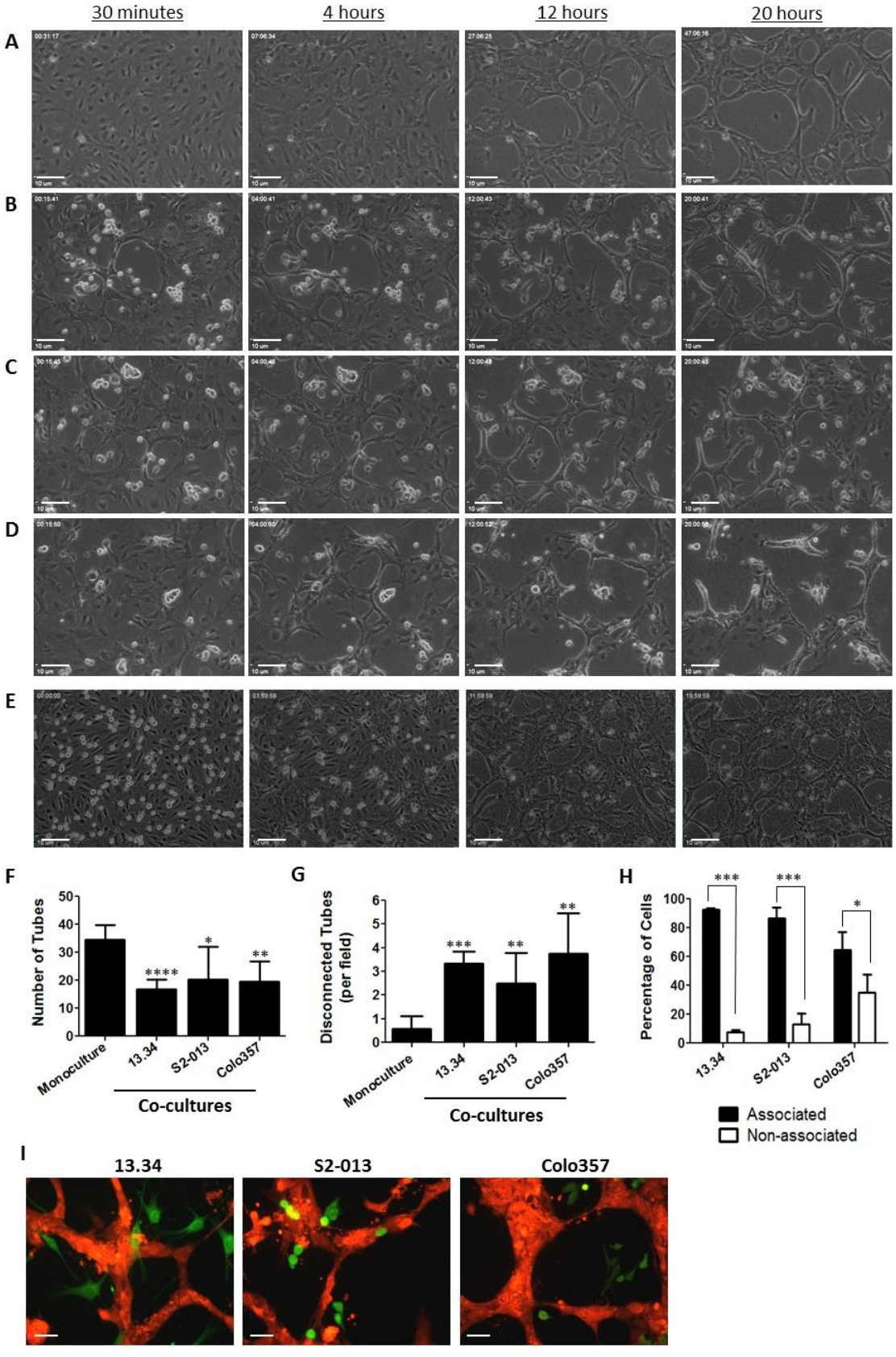
30 minutes
4 hours
12 hours
20 hours
A
B
C
D
E
F
Number of Tubes
Monoculture
13.34
S2-013
Colo357
Co-cultures
G
Disconnected Tubes (per field)
H
Percentage of Cells
Associated
Non-associated
I
13.34
S2-013
Colo357

tube network, many individual hLEC cells remained unincorporated at the time of tube network completion. Pancreatic tumor cells and fibroblasts significantly reduced the number of hLEC tubes formed (**Figure 3.8F**). Furthermore, the tubes formed in the co-culture settings had thin diameters and were disconnected from branch points or nodal clusters (**Figure 3.8G**). Examination of the tumor cell and fibroblast position revealed that most of these cells closely associated with hLEC tubes or hLEC nodes (**Figure 3.8H**). However, the tumor cells and fibroblasts did not incorporate into the tube network themselves (**Figure 3.8I**). To ensure that the acceleration in tubulogenesis by PDAC cells or pancreatic fibroblasts was not simply due to increases in total cell number during induction, the assay was performed with the addition hLECs commensurate with the addition of collagen-I. Similar to the monoculture studies described above, hLEC tube formation started around 8 hours and was complete at 20 hours; there was no acceleration of tuber formation with the addition of hLECs to the culture (**Figure 3.8E**). Nearly all hLECs, including those added at the time of induction, incorporated into the tube network. Moreover, the tubes had thick diameters and all were connected to network branch points or nodal clusters. Altogether these data suggest that pancreatic fibroblasts and tumor cells are capable of accelerating lymphatic tube formation through a process that leads to poorly formed lymphatic networks with decreased diameters and disjointed tubes *in vitro*.

Characterization of pancreatic tumor cell invasion of simulated lymphatic endothelia.

The ability of PDAC cells to invade lymphatic endothelia is a critical step for dissemination to lymph nodes. We evaluated this this function *in vitro* through transendothelial migration (TEM) assays as diagramed in **Figure 3.9A**. Briefly, a confluent hLEC monolayer was established on the underside of the porous membrane of a Boyden chamber insert (**Figure 3.9B**). Plating the hLECs on the underside of the membrane orientates the basal side of the LECs toward the invading PDAC cells similarly to lymphatic invasion *in vivo*. Following monolayer formation, a chemoattractant was added to the lower well and PDAC cells diluted in serum free media were added to the upper insert. PDAC cells underwent TEM for 20-24 hours. The TEM capacity of a panel of PDAC lines

Figure 3.9

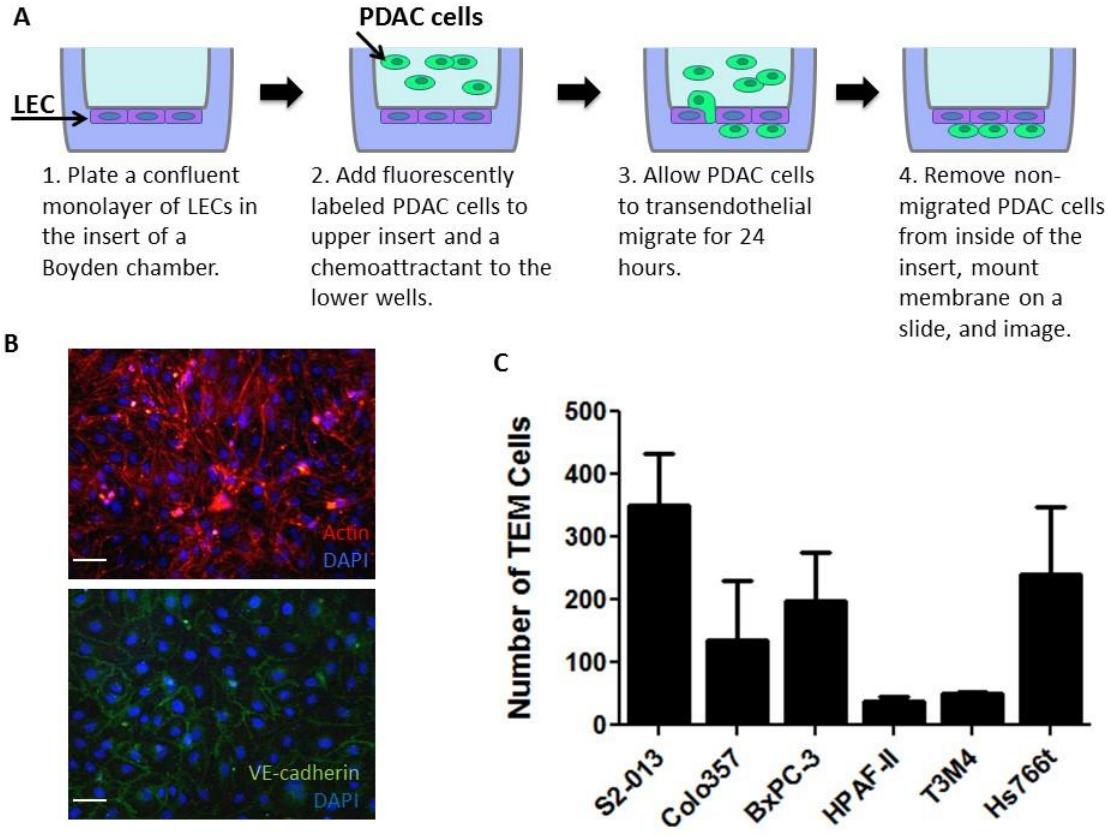

Figure 3.9 Evaluation of the TEM capacity of PDAC cells *in vitro*.

A) Diagram illustrating the setup of an *in vitro* transendothelial migration assay. Human LEC monolayers were established on the bottom of the membrane to position the basal cell surface of hLECs toward the invading PDAC cells; this is analogous to lymphatic invasion *in vivo*.

B) Representative immunofluorescent images of hLEC monolayers plated on the underside of a Boyden chamber membrane. Actin (red; top) and VE-cadherin (green; bottom) labeling was used to demonstrate that the hLECs formed a confluent monolayer on the underside of the membrane and there were no gaps between hLEC cells. Potential gaps would have allowed PDAC cells to cross the endothelial barrier without undergoing invasion. Cell nuclei were stained with DAPI (blue). Scale bar = 50 µm

C) Graphical representation of TEM through a lymphatic endothelium by a panel of PDAC cell lines: S2-013, Colo357, BxPC-3, HPAF-II, T3M4, and HS766T. 3 replicate membranes/cell type; experiment was repeated 3 times. Error bars = s.d.

is shown in **Figure 3.9C**. Not all PDAC lines displayed the same propensity to invade a lymphatic endothelium: S2-013 cells demonstrated a high rate of TEM; Hs766t, BxPC-3, and Colo357 cells demonstrated a moderate rate; and HPAF-II and T3M4 demonstrated a low rate.

We collected steady state images of fluorescently labeled PDAC cells (BxPC-3, Colo357, HPAF-II, and S2-013) and pancreatic fibroblasts (13.34) invading a lymphatic monolayer. To evaluate the position of invasion within the monolayer, we used immunofluorescence staining of endothelial-specific adherens junction protein VE-cadherin to visualize hLEC cell boundaries (**Figure 3.10A-F**). There were three possible positions of PDAC cell invasion of a lymphatic monolayer: 1) where two endothelial cells came together (bicellular junction); 2) where three endothelial cells came together (tricellular junction); or 3) on the cell body of an endothelial cell. The majority of PDAC cells invaded at tricellular endothelial junctions (**Figure 3.10G**). Occasionally, PDAC cells would invade at bicellular junctions and even less often transcellularly through an endothelial cell body. PDAC cells caused a loss of VE-cadherin at the site of invasion; however, occasionally, VE-cadherin loss also occurred at sites away from invasion (arrowhead, **Figure 3.10D**). Comparable to the invasion pattern of PDAC cells, 13.34 pancreatic fibroblasts also preferred to invade at tricellular junctions (**Figure 3.10F, G**). However, 13.34 cells also demonstrated the unique ability to elongate across the top of the monolayer without invading into it (no disruption of VE-cadherin staining). This was not seen in any of the co-cultures with PDAC cells. We compared the invasion pattern of PDAC cells and the 13.34 pancreatic fibroblasts to that of freshly isolated leukocytes (**Figure 3.10H-I**). Leukocytes displayed no preference for an endothelial junction type during adhesion or invasion of the lymphatic monolayer.

Live cell imaging was also used to fully characterize PDAC invasion of a simulated lymphatic endothelium. Examination of S2-013 PDAC invasion revealed that S2-013 cells invade a monolayer in clusters; single cells were rarely successful at invading the monolayer (**Figure**

Figure 3.10 Characterization of PDAC invasion of an hLEC endothelium.

A) Representative image of an hLEC monolayer prior to addition of PDAC cells. Immunofluorescent staining with VE-cadherin (red) antibody indicates fully-matured cell junctions between adjacent hLEC cells. Nuclei are labeled with DAPI (blue). Asterisks represent potential cellular invasion sites on the hLEC monolayer: the white asterisk is an example of a tricellular junction; the yellow asterisk is an example of a bicellular junction; and the pink asterisks is an example of an endothelial cell body location. Scale bars = 50 μm

B-E) Representative images of **B)** BxPC-3, **C)** Colo357, **D)** HPAF-II, and **E)** S2-013 invasion of an hLEC monolayer. PDAC cells were labeled with a CFDA-SE (green) cell tracer and hLEC adherens junctions were labeled with VE-cadherin (red) antibody. Nuclei were labeled with DAPI (blue). **D)** Arrowhead indicates an example of VE-cadherin loss in hLECs distant from sites of invasion. Scale bars = 50 μm

F) Representative image of 13.34 fibroblasts invading an hLEC monolayer. 13.34 cells were labeled with CMRA cell tracer (orange) and hLEC adherens junctions were labeled with VE-cadherin (green). Nuclei were labeled with DAPI (blue). Scale bar = 50 μm

G) Graphical representation of the locations within an hLEC monolayer invaded by PDAC cells and fibroblasts: tricellular junctions, bicellular junctions, or atop endothelial cell body. ****$p<0.0001$; error bars = s.d.

H) Representative image of leukocyte entering an hLEC monolayer. Freshly isolated leukocytes were labeled with CMRA cell tracer (orange) and hLEC adherens junctions were labeled with VE-cadherin (green). Nuclei were labeled with DAPI (blue). Scale bar = 50 μm

I) Graphical representation of the locations on an hLEC monolayer where leukocytes preferred to enter: tricellular junctions, bicellular junctions, or atop endothelial cell body. Error bars = s.d.

Figure 3.10

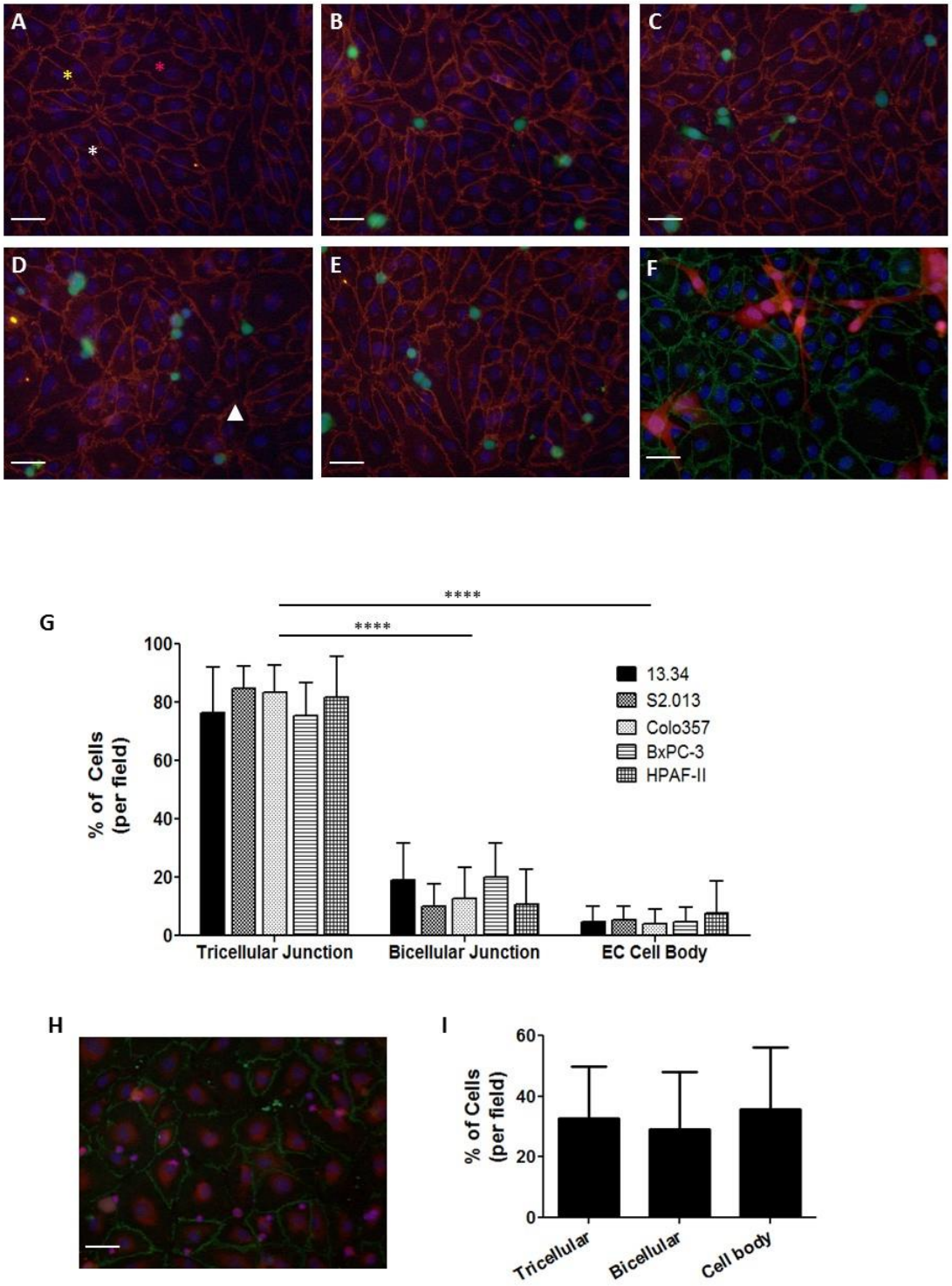
A
B
C
D
E
F
G
****
****
100
80
60
40
20
0
% of Cells
(per field)
13.34
S2.013
Colo357
BxPC-3
HPAF-II
Tricellular Junction
Bicellular Junction
EC Cell Body
H
I
60
40
20
0
% of Cells
(per field)
Tricellular
Bicellular
Cell body

Figure 3.11

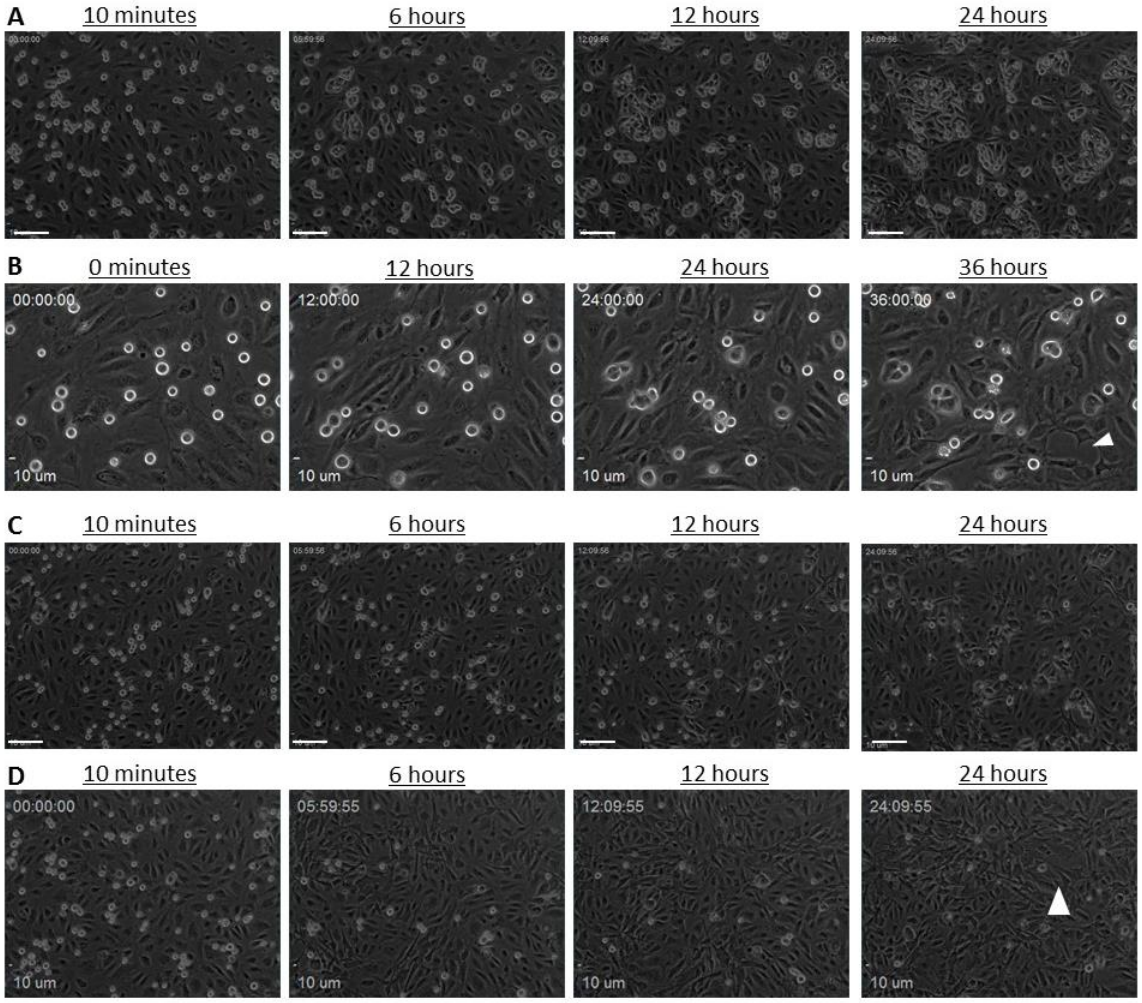

Figure 3.11 Live cell imaging evaluation of PDAC invasion of an hLEC endothelium

A) Representative live cell imaging photographs of S2-013 invasion of a lymphatic endothelium at 10 minutes, 6 hours, 12 hours, and 24 hours. Individual images were collected at 10X magnification every 10 minutes for 24 hours at the exact same location. Scale bar = 100 µm

B) Representative live cell imaging photographs of S2-013 invasion of a lymphatic endothelium at 10 minutes, 12 hours, 24 hours, and 36 hours. Individual images were collected at 20X magnification every 10 minutes for 36 hours at the exact same location. Scale bar = 10 µm

C) Representative live cell imaging photographs of Colo357 invasion of a lymphatic endothelium at 10 minutes, 6 hours, 12 hours, and 24 hours. Individual images were collected at 10X magnification every 10 minutes for 24 hours at the exact same location. Scale bar = 100 µm

D) Representative live cell imaging photographs of 13.34 fibroblast invasion of a lymphatic endothelium at 10 minutes, 6 hours, 12 hours, and 24 hours. Individual images were collected at 10X magnification every 10 minutes for 24 hours at the exact same location. Scale bar = 100 µm

3.11A). Rather individual S2-013 cells actively migrated to clusters to augment invasion through collective cell migration. Following successful invasion, S2-013 clusters expanded the opening in the monolayer by physically forced extension of tumor cells and endothelial retraction. Expanding S2-013 islands physically pushed against the surrounding endothelial cells to further open the monolayer. Additionally, hLECs actively retracted from the invaded S2-013 cells, creating larger holes in the monolayer; this retraction often occurred in the absence of contact between the two cell types. Human LECs at the invasive boundary displayed an elongated morphology. Non-invaded S2-013 cells migrated across the top of the monolayer to sites of successful invasion; this migration to invaded sites appeared to be directed and non-random. These newly recruited S2-013 cells then rapidly incorporated into the invaded S2-013 population. **Figure 3.11B** illustrates this process at a greater magnification and decreased S2-013 density. As seen in the steady-state immunofluorescence images, S2-013 cells were also able to induce gaps in the monolayer at sites distant to invasion (**Figure 3.11B** arrowhead).

Colo357 invasion was also evaluated to determine if all PDAC cells invade in the same manner (**Figure 3.11C**). Like S2-013 cells, Colo357 also invaded the monolayer as clusters (albeit smaller clusters compared to S2-013 cells), and single Colo357 cells migrated toward clusters to augment collective cell migration and invasion. Colo357 cells did not invade the monolayer as rapidly as S2-013 cells: by 6 hours numerous S2-013 cells had invaded the monolayer while very few Colo357 cells had invaded the monolayer at this same time point. Like S2-013 cells, Colo357 formed islands within the hLEC monolayer and recruited other Colo357 cells to sites of successful invasion. Colo357 cells invasion was principally physical pressure to enlarge openings in the hLEC monolayer openings; there was less endothelial retraction induced by Colo357 cells compared to S2-013 cells.

Evaluation of fibroblast entry into an hLEC monolayer revealed that 13.34 cells are much less invasive in this system compared to PDAC cells (**Figure 3.11D)**. Many of the 13.34 cells

remained atop the endothelial layer and did not invade into it, although a small invaded cluster can be seen within the monolayer by 24 hours (**Figure 3.11D**; arrowhead). These pancreatic fibroblasts did not induce endothelial retraction, suggesting accompanying PDAC cells may be required to enhance fibroblast migration across an endothelium.

III. Conclusions

Very few studies have evaluated how pancreatic tumor cells interact with lymphatic endothelia, and even fewer studies have examined how pancreatic fibroblasts interact with lymphatic endothelia. We demonstrated that pancreatic fibroblasts are strong recruiters of LECs, while PDAC cells only moderately recruited LECs. Pancreatic fibroblasts also strongly induce PDAC migration, but this induction is very dependent on the PDAC cell line, as is the ability of a PDAC line to induce fibroblast migration. Co-culture analysis of the effects of fibroblasts and PDAC cells on lymphangiogenesis revealed that all these cell types accelerated lymphangiogenesis and led to poorly developed lymphatic networks with thin, broken vessels and defective LEC incorporation. Finally, evaluating PDAC invasion revealed that different PDAC lines have varying abilities to invade a lymphatic endothelium, but all PDAC cells preferred to invade at tricellular endothelial junctions. Live cell imaging uncovered many of the minute differences that allow different PDAC lines to invade a lymphatic endothelium. Understanding the role of LECs in the PDAC tumor microenvironment is still in its infancy. The work presented here lays the groundwork for understanding the impacts that pancreatic tumor cells and fibroblasts have on lymphatic biology.

Supplementary Figure 3.1

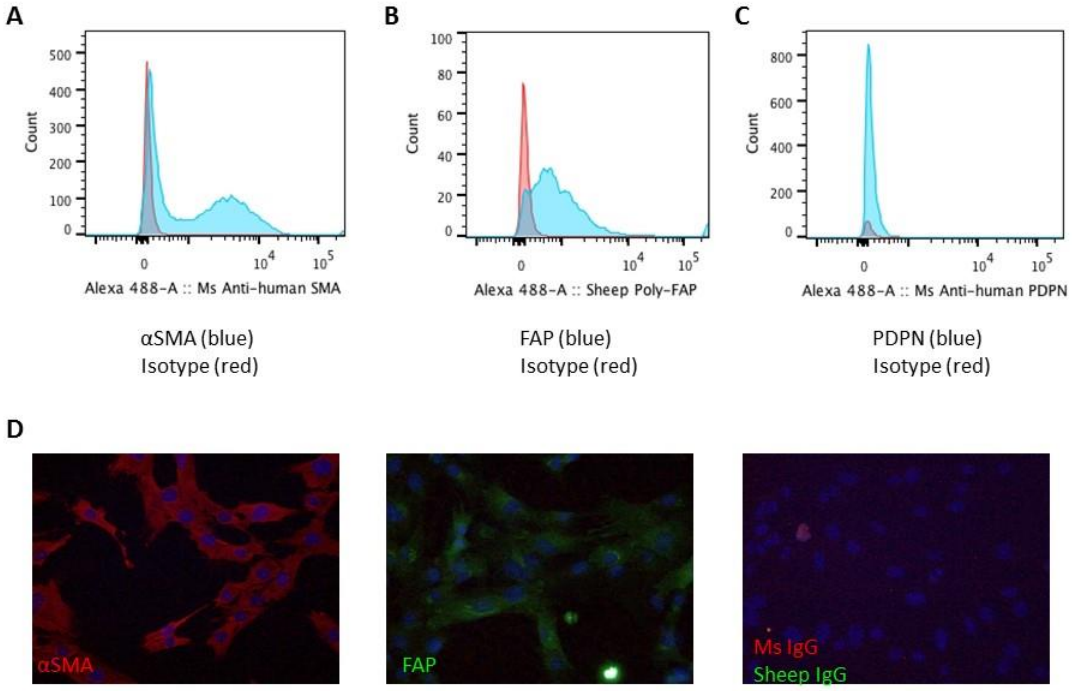

Supplementary Figure 3.1 Characterization of 13.34 pancreatic fibroblasts.

A-C) Flow cytometry evaluating αSMA, FAP, and podoplanin fibroblast markers in 13.34 pancreatic fibroblasts. Red histograms represent isotype control; blue histograms indicate **A)** αSMA (activation marker) **B)** FAP, and **C)** podoplanin expression. 13.34 fibroblasts demonstrated positive expression for αSMA and FAP and were negative for podoplanin.

D) Immunofluorescence staining for αSMA (red) and FAP (green) in 13.34 fibroblasts. Mouse IgG_1 isotype antibodies (red; far right) and sheep polyclonal IgG antibodies (green; far right) were used as negative controls. Cell nuclei were labeled with DAPI.

CHAPTER 4:

A novel glycomimetic inhibitor reveals the role of E-selectin in lymphatic invasion and dissemination of pancreatic cancer

Excerpts from this chapter have been edited from:

Steele, MM, Radhakrishnan, P, O'Connell, K., Mohr, AM, Caffrey, T, Grandgenett, PM, Grunkemeyer, JA, Mehla, K, Patil, P, Fink, DM, Hanson, RL, Fogler, WE, Magnani, JL, and Hollingsworth, MA. A novel glycomimetic inhibitor reveals the role of E-selectin in lymphatic invasion and dissemination of pancreatic cancer. (In final preparation)

I. Introduction

Pancreatic ductal adenocarcinoma (PDAC) is the fourth leading cause of cancer-related deaths in the United States and has a dismal 7% 5-year survival rate (1). One of earliest and most frequently observed sites of PDAC metastasis is the draining lymph nodes, which also correlates with poor prognosis (34-36). The process of lymph node metastasis requires interactions between tumor cells and lymphatic endothelial cells, the primary cell type comprising lymphatic vasculature. The specific mechanisms that regulate PDAC invasion of lymphatic vessels are poorly understood. One hypothesis is that tumor cells invade lymphatic vasculature by utilizing molecular processes similar to those used by immune cells during lymphatic intravasation. Although not fully understood, it is known that leukocyte entry into lymphatics is regulated by several adhesion proteins including E-selectin, intercellular adhesion molecule-1 (ICAM-1), and vascular adhesion molecule-1 (VCAM-1) (146). Many of these same adhesion proteins have also been implicated as regulators of tumor-endothelial interactions and vasculature invasion for many cancer types (252).

Adhesion protein E-selectin belongs to the selectin family of proteins, which are single-pass transmembrane glycoproteins that encode a lectin-like domain which forms an adhesive receptor capable of binding to carbohydrate ligands including sialyl Lewis$^{A/X}$ (sLe$^{A/X}$) motifs (253). E-selectin expression is restricted to endothelial cells and is known to facilitate endothelial-leukocyte interactions during immune cell extravasation across the blood vasculature (254, 255). Recently, it has been determined that E-selectin plays a similar role in the lymphatic vasculature for leukocyte intravasation during inflammation (256). Many types of tumors, including PDAC, have been shown to appropriate leukocyte intra- and extravasation mechanisms for invasion of blood vessels during dissemination (146, 257). However, the role E-selectin in tumor invasion of lymphatic vessels has not been investigated.

The investigation reported here was to determine the role of E-selectin in PDAC metastasis through the lymphatic vasculature. Using a novel glycomimetic, small molecule antagonist of E-

selectin ligand binding to $sLe^{A/X}$, GMI-1271, in combination with chemotherapy, we demonstrate that E-selectin blockade decreases metastasis to lymphatic vasculature-dependent sites in orthotopic models of spontaneous PDAC metastasis. Additionally, combinatorial treatment with GMI-1271 and gemcitabine extended survival in an immune competent model of pancreatic cancer. We report for the first time that inhibition of E-selectin ligand binding resulted in a significant reduction in metastasis to lymph nodes. Immunohistochemical staining revealed that the reduction in metastasis by GMI-1271 was not due to decreased lymphatic and blood vessel densities at the tumor site. Rather, E-selectin blockade through GMI-1217 impaired the ability of PDAC cells to adhere to and migrate across an endothelial barrier *in vitro*. Interestingly, co-culture of PDAC cells with lymphatic endothelial cells induced E-selectin expression in lymphatics to facilitate this invasion. Together, our data demonstrate that PDAC cells use E-selectin-dependent mechanisms to gain access to the lymphatic vasculature for dissemination to lymph nodes.

II. Results

PDAC cells express the E-selectin ligand sialyl Lewis^{A}.

We examined the expression of E-selectin ligands, $sLe^{A/X}$, on a panel of human PDAC cell lines to select lines for studies of interactions with E-selectin on lymphatic endothelial cells. Western blot analyses demonstrated that several PDAC lines express the sLe^{A} including S2-013, Capan-2, and BxPC-3 cells (**Figure 4.1A**). The polydispersed migration of glycoproteins containing sLe^{A} is consistent with the known expression of this glycan on multiple proteins in these cells. These same cell lines also had detectable levels of sLe^{A} on proteins secreted into conditioned media (**Figure 4.1B**). PDAC lines T3M4, Colo357, Hs766t, and HPAF-II and pancreatic fibroblasts (13.34) showed no expression of sLe^{A} (**Figure 4.1A-B**). Expression of sLe^{A} was also confirmed by immunofluorescence staining (**Figure 4.1C**). E-selectin ligand sLe^{X} was not detected in any of the

Figure 4.1 PDAC cells express E-selectin ligand sialyl Lewis ^{A}.

A) Immunoblot (50 µg protein/lane) analysis of sLe^A expression in pancreatic fibroblasts (13.34) and a panel of human PDAC cell line lysates (T3M4, Colo357, Capan-2, Hs766T, BxPC-3, HPAF-II, and S2-013). β-actin expression was used as a loading control for all cell lines. Capan-2, BxPC-3, and S2-013 demonstrate expression of sLe^A. The smeared pattern indicates that sLe^A is expressed on a multitude of PDAC proteins.

B) Immunoblot (30 µl/lane) analysis of sLe^A expression in pancreatic fibroblasts (13.34) and a panel of human PDAC cell line conditioned media. Secreted proteins from Capan-2, BxPC-3, and S2-013 display sLe^A expression.

C) Immunofluorescence staining indicating sLe^A expression in S2-013, Capan-2, and BxPC-3 PDAC cells. SLe^A (green) is expressed by several individual PDAC cells, but not all cells within a population. Cell nuclei are stained with DAPI (blue). Scale bars = 25 µm

D) Immunofluorescence staining indicating sLe^A expression in non-implanted S2-013 (left) and *in vivo* implanted S2-013 (right) cells. *In vivo* implantation of S2-013 increases the number of cells expressing sLe^A (green) as compared to S2-013 cells not implanted. Cell nuclei are stained with DAPI (blue). Scale bars = 50 µm

Figure 4.1

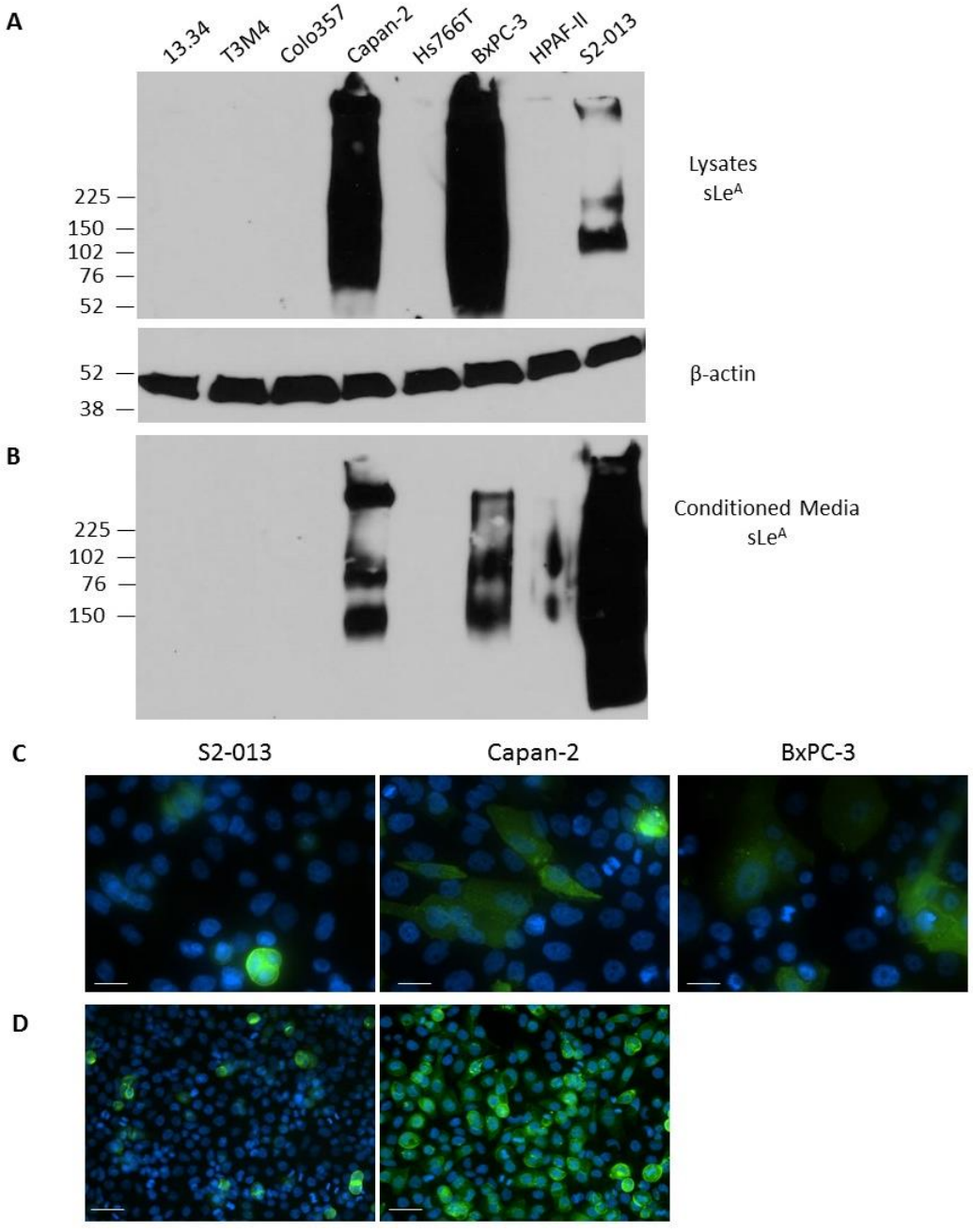
A
13.34
T3M4
Colo357
Capan-2
Hs766T
BxPC-3
HPAF-II
S2-013
225
150
102
76
52
Lysates
sLe^A
52
38
β-actin
B
225
102
76
150
Conditioned Media
sLe^A
C
S2-013
Capan-2
BxPC-3
D

PDAC lines (data not shown). To ensure that PDAC cells retained sLe^A expression following *in vivo* implantation, S2-013 PDAC cells were orthotopically implanted into the pancreases of athymic mice for 3 weeks and then isolated from the tumors. Immunofluorescence staining revealed that *in vivo* implantation increased the incidence of sLe^A expression in S2-013 cells (**Figure 4.1D**).

GMI-1271 in combination with gemcitabine reduces vasculature-dependent metastasis of PDAC.

We evaluated the effects of blocking the binding of E-selectin to ligands (using GMI-1271) on PDAC metastasis *in vivo* with a specific focus on metastasis to the lymph nodes. S2-013 PDAC cells, which express sLe^A and frequently metastasize to lymph nodes (258, 259) were orthotopically implanted into the pancreas of athymic mice. Treatment with GMI-1271 was initiated two weeks after tumor implantation. Mice were randomized to 6 different treatment groups: vehicle, low dose GMI-1271, high dose GMI-1271, gemcitabine, low dose GMI-1271 with gemcitabine, and high dose GMI-1271 with gemcitabine. Treatment with GMI-1271 alone (low or high dose) had no impact on *in vivo* tumor growth compared to control mice (**Figure 4.2A**). This result was verified *in vitro* by examining the effects of GMI-1271 on PDAC proliferation (**Supplementary Figure 4.1**). As expected, mice treated with gemcitabine showed a significant reduction in tumor size compared to mice treated with the vehicle control; however, addition of GMI-1271 (low and high dose) to gemcitabine treatment did not further decrease tumor size (**Figure 4.2A**). Gross histological examination of representative sections revealed that GMI-1271 had no effect on the overall morphology of primary tumors or the metastatic lesions (**Figure 4.2B)**. None of the GMI-1271-treated mice displayed any drug-induced toxicities.

Since E-selectin has been previously implicated in promoting tumor dissemination, we evaluated several candidate organs for the presence of metastases following treatment with GMI-1271. **Figure 4.3A** illustrates observed lesions found in representative sections of lungs, lymph nodes, and liver. Untreated control mice demonstrated a high incidence of PDAC metastasis to the

Figure 4.2

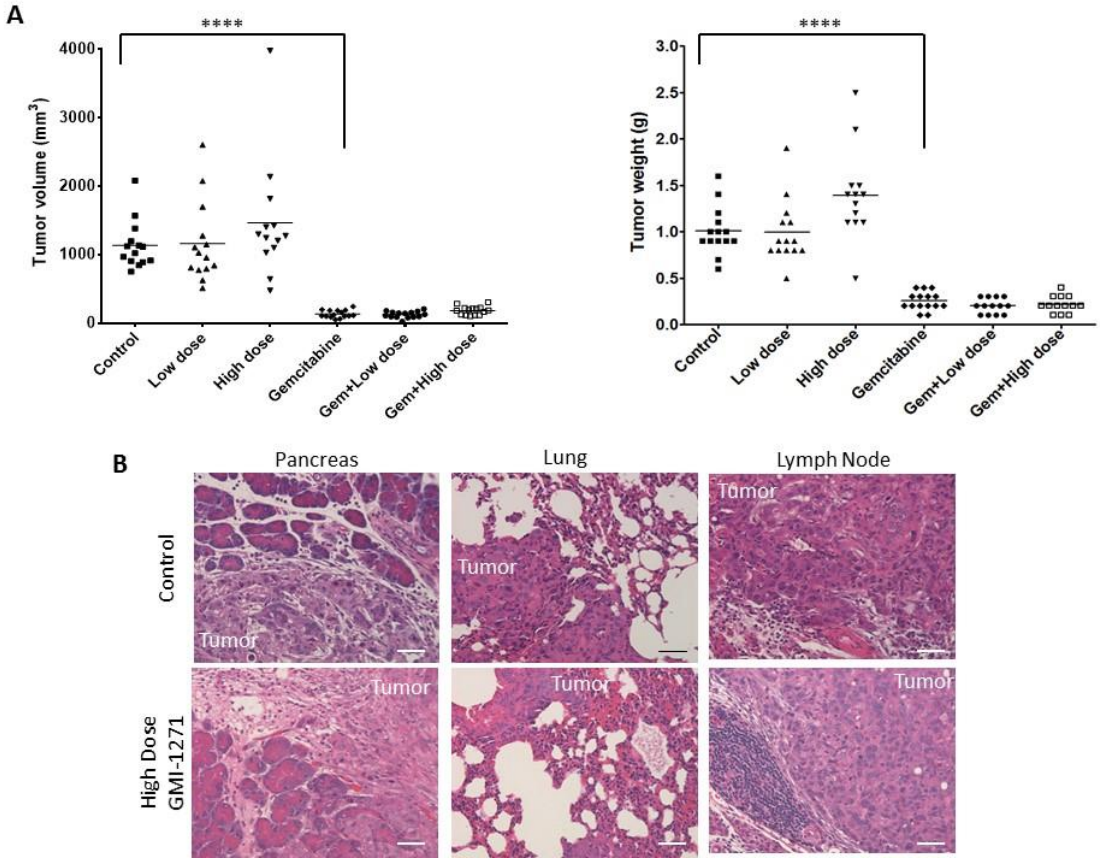

Figure 4.2 E-selectin blockade has no impact on PDAC growth or morphology *in vivo.*

Human S2-013 PDAC cells were orthotopically implanted into the pancreases of athymic female mice and allowed to establish for 2 weeks. GMI-1271 and gemcitabine treatments were administered for 4 weeks, after which tumors and metastatic organs were collected. n = 15 mice/treatment group.

A) Graphical representation of tumor volume and weight for each treatment group. E-selectin blockade (high or low dose) had no impact on tumor size. As expected, gemcitabine significantly reduced tumor size, but combinatorial treatment GMI-1271 and gemcitabine did not further decrease tumor size. ****$p<0.0001$

B) Representative histological sections of S2-013 primary tumors, lung lesions, and lymph node lesions from mice treated with vehicle control (PBS) or GMI-1271. High dose GMI-1271 did not alter primary tumor morphology. Scale bars = 50 µm.

Figure 4.3

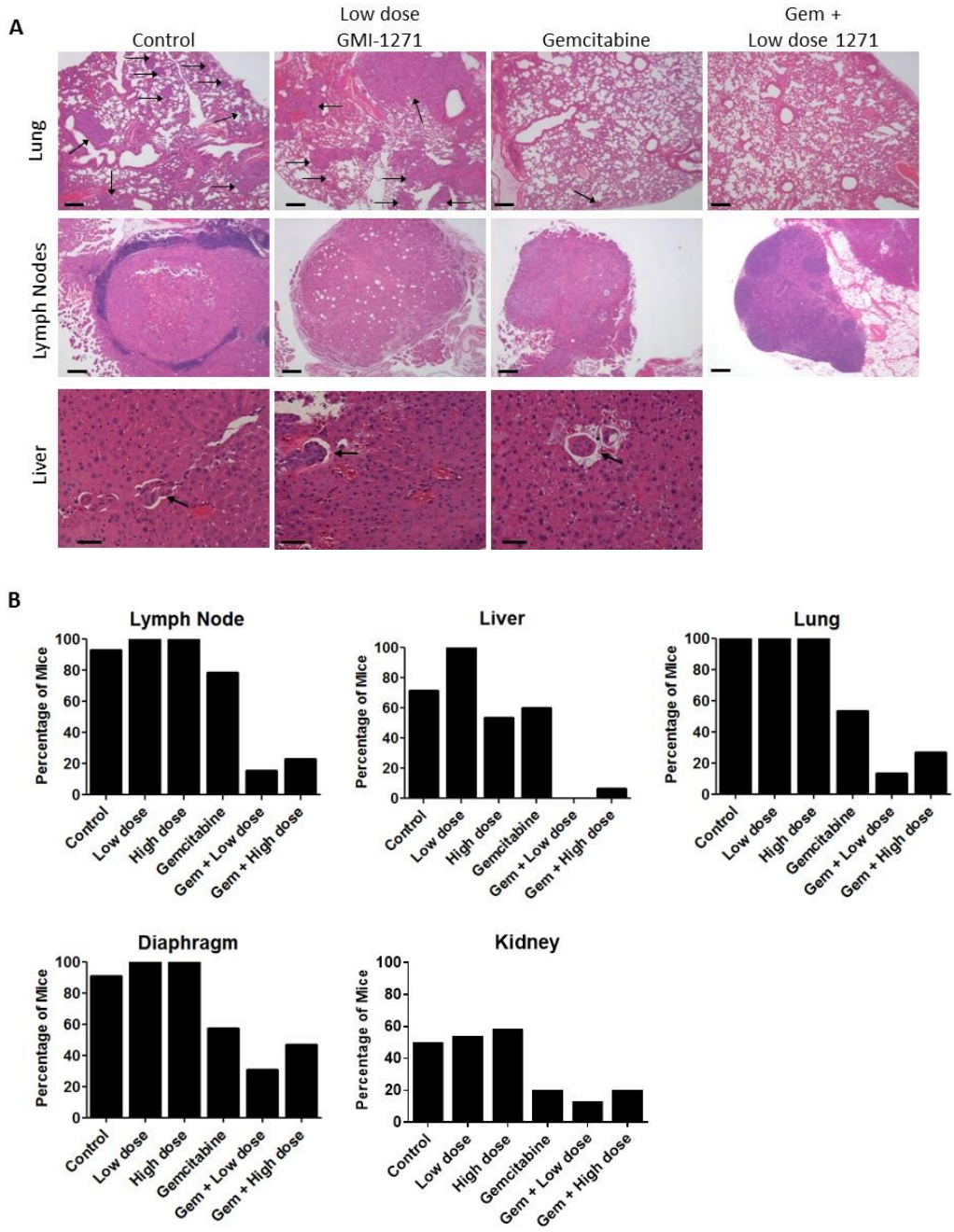

Figure 4.3. E-selectin blockade reduces pancreatic cancer metastasis *in vivo.*

A) Representative histological sections of spontaneous lung, lymph node, and liver lesions from GMI-1271-treated mice. Arrows indicate metastatic lesions. Scale bars = 200 µm for lung and lymph node. Scale bar = 50 um for liver. n=15 mice/treatment group.

B) The presence of spontaneous metastatic lesions was identified in lymph nodes, liver, lungs, diaphragm, kidney, spleen, and peritoneum using histological staining of multiple representative sections. Graphs represent the absolute percentage of mice per group exhibiting spontaneous metastases in the indicated organs. n= 15 mice/group

lymph nodes, lungs, liver, diaphragm, spleen, and peritoneum (**Figure 4.3B**). We observed a reduction in metastatic incidence to the liver in mice treated with high dose GMI-1271. Treatment with GMI-1271 alone (low or high dose) did not significantly affect the incidence of metastasis to other organs.

Gemcitabine monotherapy moderately decreased metastatic incidence to all organs examined when compared to vehicle-treated mice (**Figure 4.3B**). Interestingly, combinatorial treatment with gemcitabine and low dose GMI-1271 resulted in a significant reduction in metastatic incidence within all examined organs, except spleen, compared to mice treated with gemcitabine only (**Figure 4.3B**). In groups receiving gemcitabine and high dose GMI-1271, metastatic incidence to most organs was also reduced compared to the gemcitabine only treatment group, though not to levels greater than that observed with low dose GMI-1271. Examination of lesion size revealed that GMI-1271, alone or in combination with gemcitabine, had no impact on lesion growth if tumor cells reached a distant site (**Supplementary Figure 4.2**).

As E-selectin regulates immune cell trafficking, we sought to determine if E-selectin blockade was impeded immune cell trafficking to tumors. Immunohistochemical staining revealed total numbers of $CD45^+$ leukocytes within the tumors remained relatively similar across all treatment groups (**Figure 4.4A-B**). Also, there was no effect of the treatments on the presence of tertiary lymphoid aggregates within primary tumors (**Figure 4.4C-D**).

GMI-1271 significantly prolongs survival in an immune competent model of PDAC.

We evaluated survival of immune deficient mice challenged with S2-013 following treatments with PBS, low dose GMI-1271, gemcitabine (100 mg/kg) or a combination of gemcitabine and GMI-1271. There was no difference in survival of animals treated with GMI-1271 either as a monotherapy or in combination with gemcitabine (**Figure 4.5A**). Histological examination of organs at end stage revealed that GMI-1271 in combination with gemcitabine

Figure 4.4

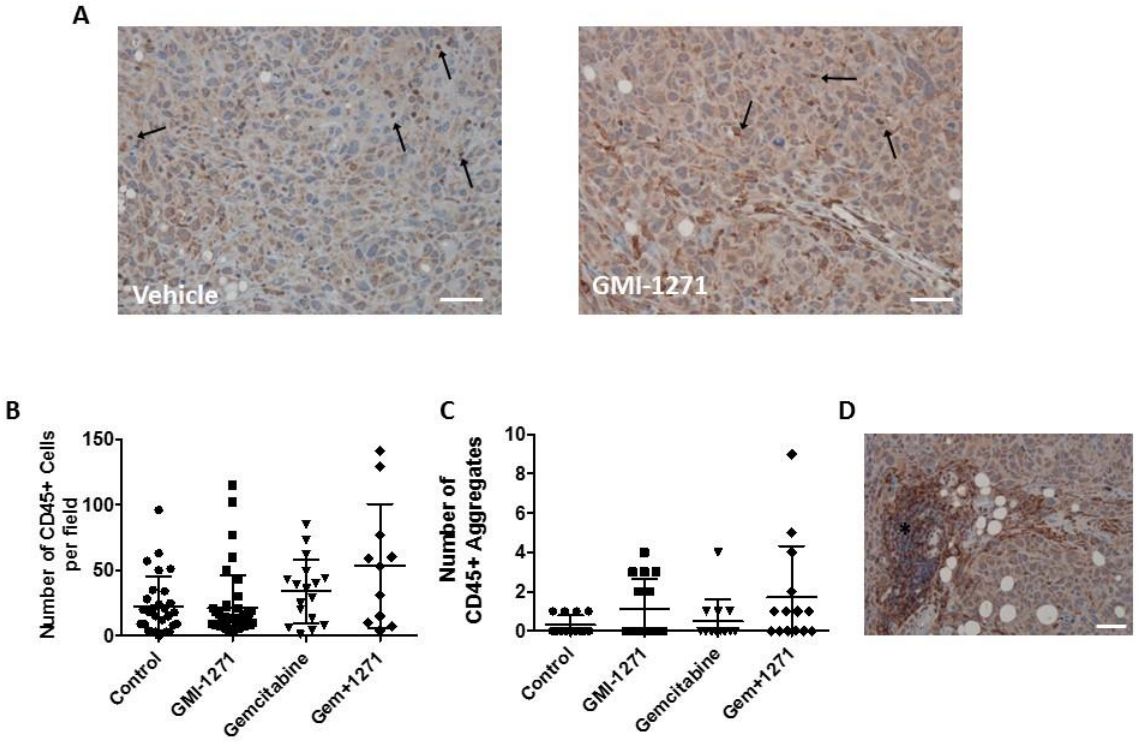

Figure 4.4 GMI-1271 does not affect total numbers of CD45+ leukocytes within orthotopic PDAC tumors.

A) Representative immunohistochemical staining of CD45+ (brown) immune cells within PDAC primary tumor sections. Arrows indicate CD45+ immune cells. Sections were counterstained with hematoxylin (blue). Scale bar = 50 µm

B) Quantification of the number of CD45+ leukocytes per field within the tumors. Four sections from four different mice were examined; at least 4 fields at 20X magnification were collected per section. GMI-1271 did not affect total numbers of CD45+ immune cells within the primary tumor. Error bars = s.d.

C) Quantification of the number of CD45+ tertiary lymphoid aggregates (TLAs) per tumor section. 15 sections examined/treatment group. Error bars = s.d.

D) Representative staining of a CD45+ (brown) TLAs. Asterisk indicates a TLA. Sections were counterstained with hematoxylin (blue). Scale bar = 100 µm

Figure 4.5

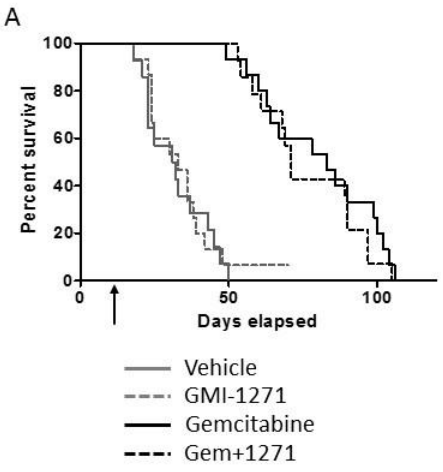

Treatment	Median Survival (days)
Vehicle	31.5
GMI-1271	33
Gemcitabine	83
Gem + 1271	71

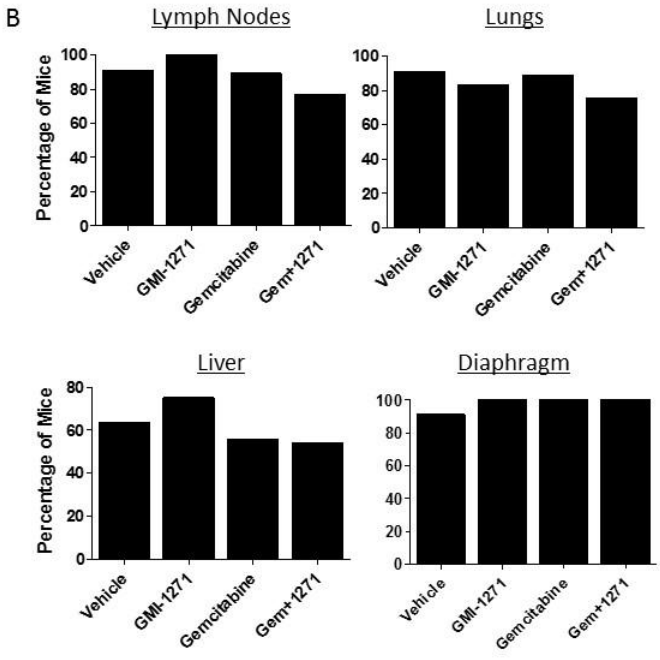

Figure 4.5 GMI-1271 does not improve animal survival in an immune incompetent model of PDAC.

A) Kaplan-Meier survival curve for S2-013-challenged athymic mice treated with PBS, GMI-1271, gemcitabine, or Gem+1271. Arrow indicates treatment start day. n = 10 mice/group. Log-rank tests determined no statistical significance between the GMI-1271 treatment groups.

B) Graphical representation of the absolute metastatic incidence in KPC-challenged mice at end stage disease. n = 10 mice/group

resulted in decreased metastasis to the lymph nodes, lungs, and liver at end stage disease compared to the gemcitabine treated group (**Figure 4.5B**).

We also evaluated the effects of GMI-1271 on survival in immune competent mice using transplanted KPC tumors. A tumor line isolated from the *KPC* pancreatic cancer mouse model was implanted into the pancreases of C57BL/6 mice. After two weeks to establish tumors, mice were treated with GMI-1271, gemcitabine, or both. The GMI-1271 monotherapy did not prolong survival compared to untreated mice (**Figure 4.6A**). Interestingly, in this immune competent model, GMI-1271, when used in combination with gemcitabine, significantly improved animal survival compared to mice treated with gemcitabine only ($p=0.0302$). All mice were evaluated at end stage disease, and mice treated with both GMI-1271 and gemcitabine demonstrated a slightly lower incidence of metastasis to the lungs, diaphragm, kidney and spleen compared to mice treated with only gemcitabine (**Figure 4.6B**).

GMI-1271 does not decrease PDAC metastasis to the lymph nodes by reducing lymphatic vascular density *in vivo*.

Our results demonstrated that E-selectin blockade significantly reduced PDAC metastasis to the lymph nodes. We next evaluated the lymphatic vessel density (LVD) within primary tumors to determine if changes in LVD following gemcitabine and GMI-1271 treatment might explain the reduction in metastatic incidence within the lymph nodes. Immunofluorescent staining revealed that GMI-1271-treated mice had similar numbers of LYVE-1^+ lymphatic vessels within primary tumors compared to tumors from control mice (**Figure 4.7A-B**). Moreover, gemcitabine and combinatorial treatment with GMI-1271 did not alter LVD within primary tumors.

We further verified that E-selectin blockade did not impact lymphatic growth by examining the effects of GMI-1271 on hLEC proliferation and tubulogenesis *in vitro*. Treatment with increasing concentrations of GMI-1271 did not impair hLEC proliferation in culture over the course of 96 hours (**Figure 4.7C**). In collagen-I-induced tubulogenesis studies, low concentrations (10-50

Figure 4.6

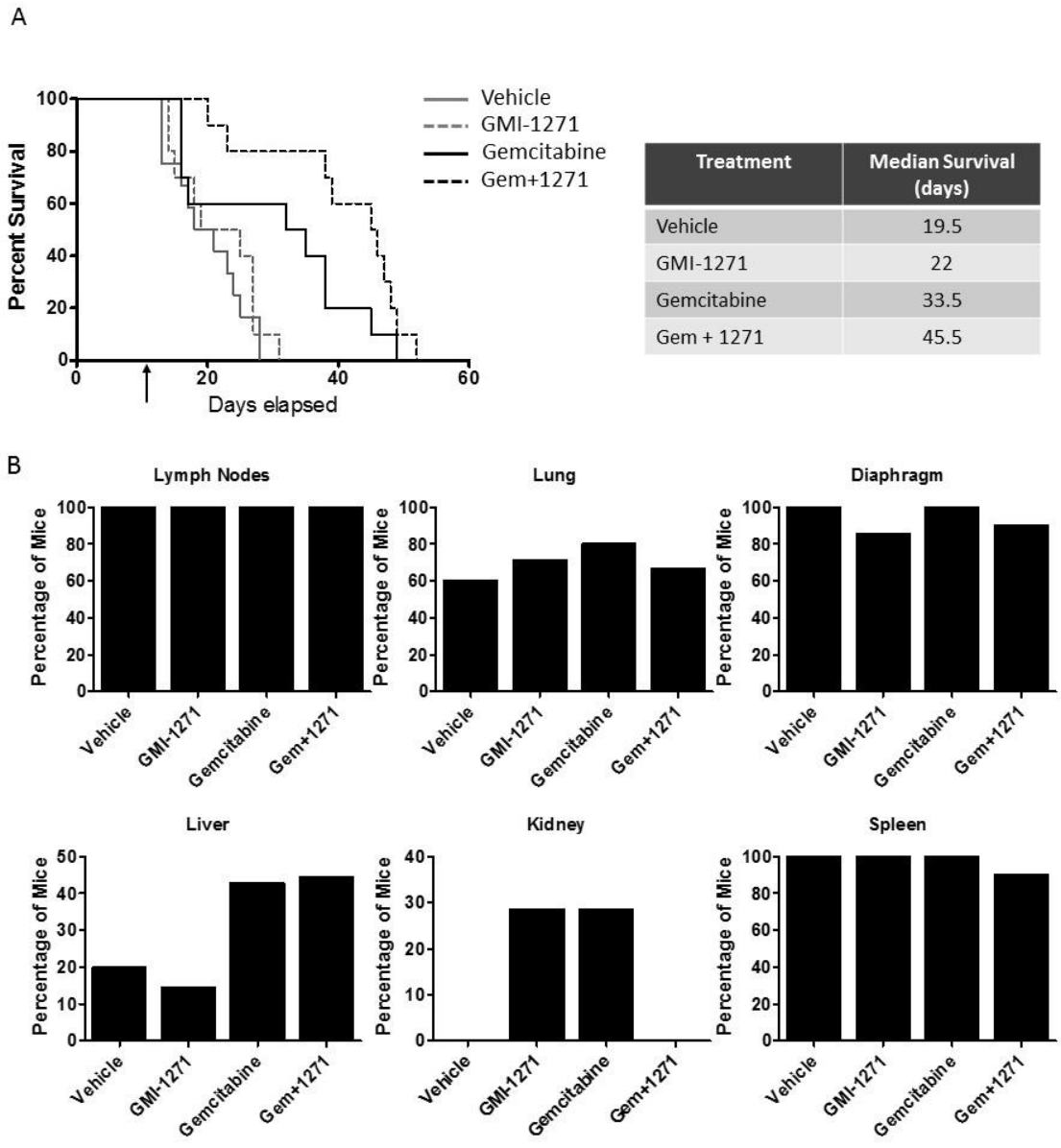

Treatment	Median Survival (days)
Vehicle	19.5
GMI-1271	22
Gemcitabine	33.5
Gem + 1271	45.5

Figure 4.6 GMI-1271 improves survival when used in combination with gemcitabine in an immune competent model of PDAC.

A) Kaplan-Meier survival curve for KPC-challenged C57BL/6 mice treated with PBS, GMI-1271, gemcitabine, or Gem+1271. Arrow indicates treatment start day. n = 10 mice/group. Log-rank test: p = 0.0302 between gemcitabine vs gem+1271.

B) Graphical representation of the absolute metastatic incidence in KPC-challenged mice at end stage disease. n = 10 mice/group

Figure 4.7 GMI-1271 does not decrease lymphatic vascular density within the primary site nor does it impact LEC growth.

A) Representative immunofluorescent staining of LYVE-1^+ (red) lymphatic vessels within the primary tumor. Nuclei are stained with blue DAPI. Arrows indicate LYVE-1+ lymphatic vessels. Scale bars = 50 μm

B) Quantification of the number of LYVE-1^+ lymphatic vessels within the primary tumor site. n=4 mice/treatment group; 4 images (20X magnification) were collected per tumor section. Error bars = s.d.

C) hLECs were treated with increasing concentrations of GMI-1271 and proliferation monitored for 96 hours. n=6 technical replicates/treatment and per timepoint; experiments were repeated 3 times. GMI-1271 did not affect hLEC proliferation *in vitro*. Error bars = s.d.

D) Quantification of the number of hLEC tubes formed in a three-dimensional (3D) collagen-I matrix following treatment with GMI-1271. n=3 replicate wells; 3 separate experiments performed. *$p<0.05$; **$p<0.01$; error bars = s.d.

E) Representative images of hLEC tube networks in a 3D collagen-I matrix following GMI-1271 treatments. Scale bars = 100 μm

F) Quantification of the number of hLEC tubes formed in a 3D matrigel matrix following treatment with GMI-1271. n=3 replicate wells; 3 separate experiments performed. *$p<0.05$; error bars = s.d.

G) Representative images of hLEC tube networks in a 3D matrigel matrix following GMI-1271 treatments. Scale bar = 250 μm

Figure 4.7

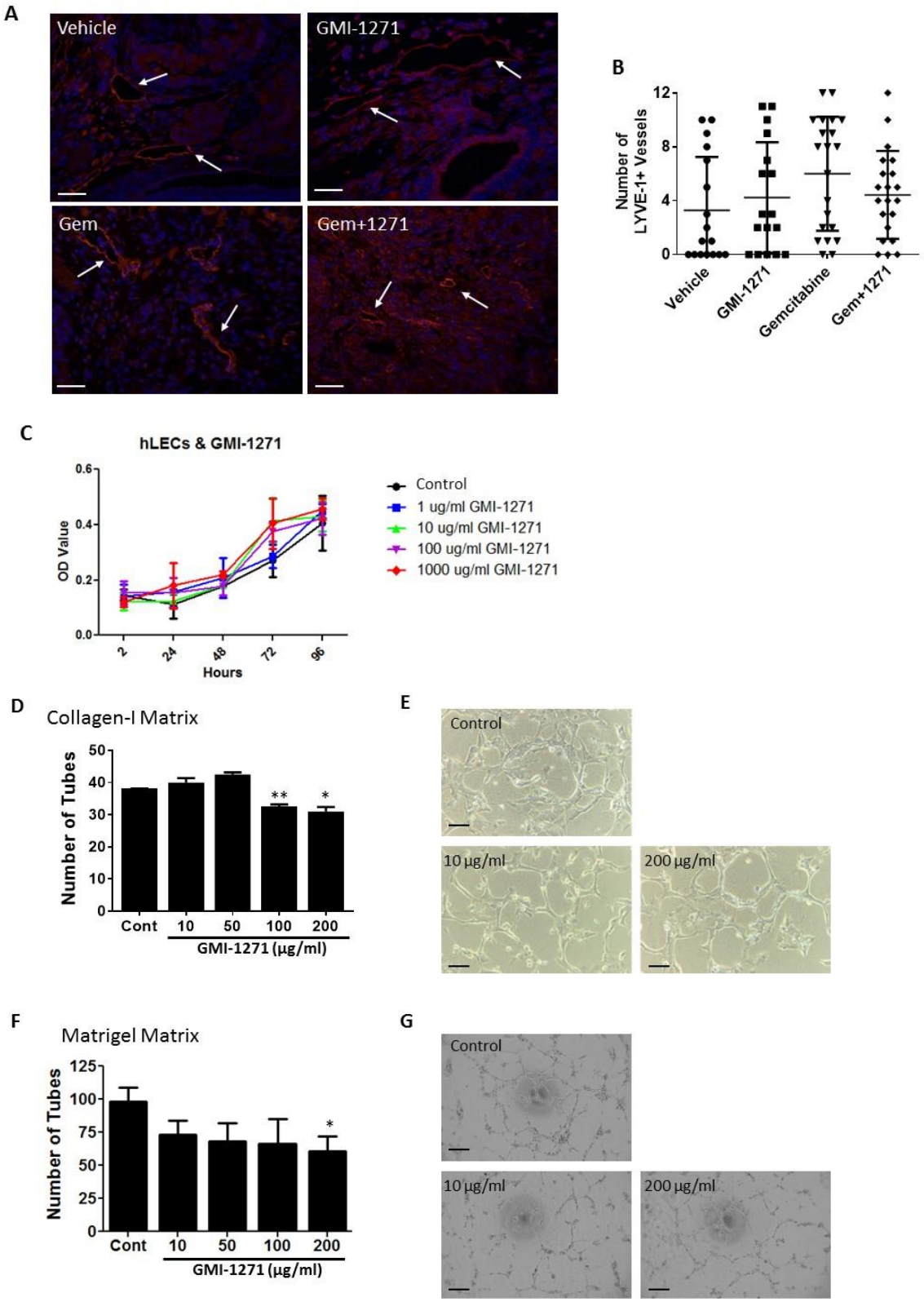
A
Vehicle
GMI-1271
Gem
Gem+1271
B
Number of LYVE-1+ Vessels
12
8
4
0
Vehicle
GMI-1271
Gemcitabine
Gem+1271
C
hLECs & GMI-1271
OD Value
0.6
0.4
0.2
0.0
2
24
48
72
96
Hours
Control
1 ug/ml GMI-1271
10 ug/ml GMI-1271
100 ug/ml GMI-1271
1000 ug/ml GMI-1271
D
Collagen-I Matrix
Number of Tubes
50
40
30
20
10
0
**
*
Cont
10
50
100
200
GMI-1271 (µg/ml)
E
Control
10 µg/ml
200 µg/ml
F
Matrigel Matrix
Number of Tubes
125
100
75
50
25
0
*
Cont
10
50
100
200
GMI-1271 (µg/ml)
G
Control
10 µg/ml
200 µg/ml

µg/ml) had no impact on hLEC tube formation (**Figure 4.7D-E**). However, high concentrations of GMI-1271 (100-200 µg/ml) slightly decreased hLEC tubulogenesis but did not completely block the process. High levels of GMI-1271 reduced hLEC tube formation by approximately 15%. This study was repeated using another extracellular matrix to induce hLEC tubulogenesis, matrigel. Again, high concentrations GMI-1271 slightly decreased Matrigel-induced hLEC tubulogenesis (approximately 38%); however, it did not completely block the process (**Figure 4.7F-G**). Taken altogether, these results suggest that E-selectin blockade by GMI-1271 does not reduce lymph node metastasis by inhibiting lymphangiogenesis or lymphatic endothelial proliferation.

Lymphatic vessels are not the only escape route for tumor dissemination and many tumors are known to invade blood vessels; thus, we also evaluated blood vessel densities in primary PDAC tumors. Immunohistochemical staining for CD31 revealed no difference in vascular densities among control and GMI-1271-treated tumors and no difference among gemcitabine and combinatorial gemcitabine and GMI-1271 treated tumors (**Figure 4.8A-B**). We confirmed this finding by demonstrating GMI-1271 has no impact on vascular endothelial cell proliferation *in vitro* (**Figure 4.8C**).

GMI-1271 inhibits the ability of E-selectin ligand -expressing PDAC cells to adhere to and transendothelial migrate across a lymphatic endothelium.

Since decreased PDAC metastasis to lymph nodes was not attributed to a diminished presence of lymphatics in the primary tumor, we examined whether E-selectin blockade impaired tumor-lymphatic interactions. We performed a series of *in vitro* experiments to evaluate PDAC adhesion to and migration across a lymphatic endothelium in the presence of GMI-1271. We examined the response to E-selectin blockade of both E-selectin ligand expressing (S2-013, BxPC-3) and non-expressing (Colo357, HPAF-II) PDAC lines.

Treatment of hLECs with GMI-1271 significantly inhibited the adhesion of sLe^A-expressing S2-013 and BxPC-3 PDAC cells to a lymphatic monolayer in a concentration-dependent

Figure 4.8

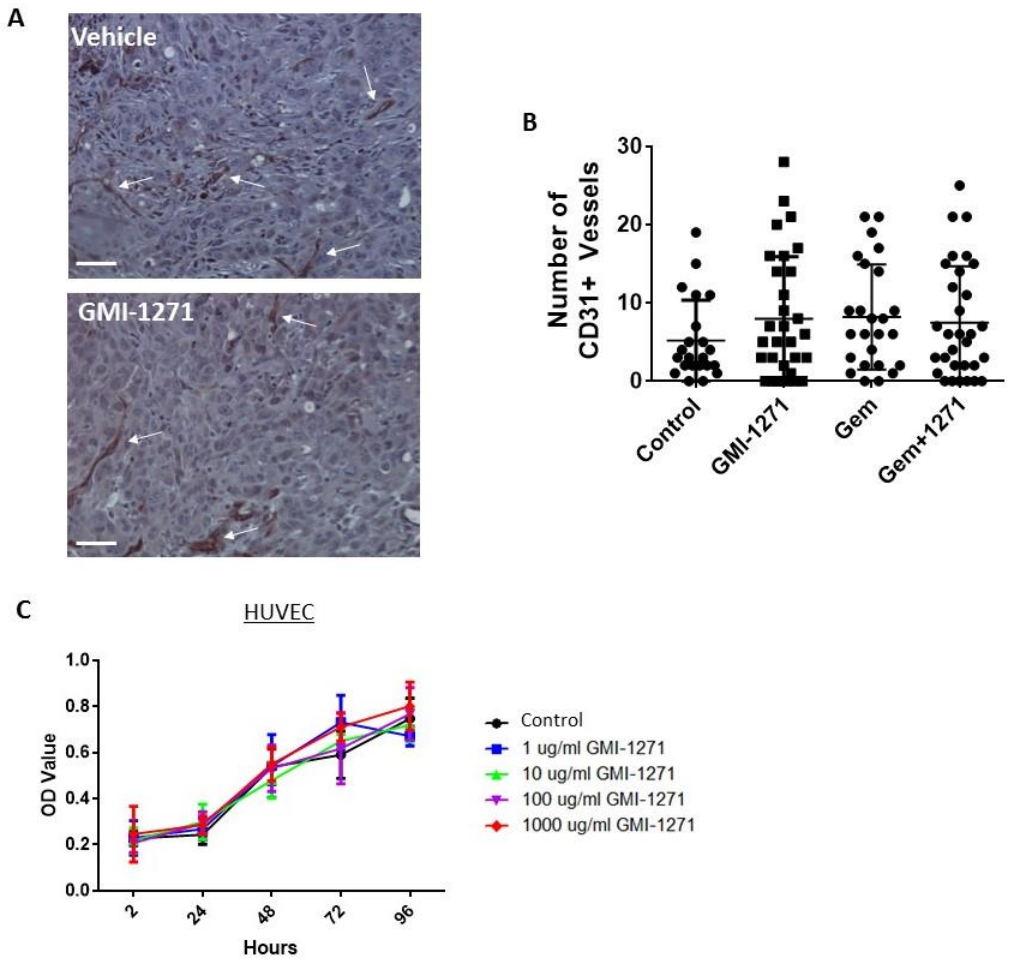

Figure 4.8 GMI-1271 does not decrease the number of blood vessels at the primary tumor site.

A) Representative immunohistochemical staining of $CD31^+$ (brown) blood vessels within primary tumors of mice orthotopically challenged with S2-013 PDAC cells and treated with GMI-1271 for 4 weeks. Sections were counterstained with hematoxylin (blue). Arrows indicate CD31+ blood vessels. Scale bars = 50 µm.

B) Quantification of the number of $CD31^+$ blood vessels per field within the primary tumor. Five (20X magnification) representative images were collected per tumor section from 4 mice within each treatment group. Error bars = s.d.

C) Vascular endothelial cells (HUVECs) were treated with increasing concentrations of GMI-1271 and proliferation monitored for 96 hours using a methylene blue assay. n=6 technical replicates/treatment and per timepoint; experiments were repeated three times. Error bars = s.d.

manner (**Figure 4.9A**). However, blocking E-selectin had no impact on the ability of non-sLe^A-expressing Colo357 or HPAF-II PDAC cells to adhere to a lymphatic endothelium (**Figure 4.9B**).

We also evaluated whether E-selectin blockade impaired PDAC transendothelial migration (TEM) across a lymphatic endothelium using an *in vitro* model of TEM. **Figure 4.10A** shows that GMI-1271 significantly decreased the TEM of sLe^A-expressing PDAC cells (S2-013, BxPC-3) in a dose dependent manner. However, GMI-1271 had no significant impact on the TEM of PDAC cells not expressing the E-selectin ligands (Colo357, HPAF-II; **Figure 4.10B**). It is of note that the sLe^A-expressing PDAC cells had a stronger capacity to undergo lymphatic TEM compared to PDAC cells not expressing sLe^A.

We sought to determine if E-selectin blockade also inhibited PDAC TEM across a lymphatic endothelium under inflammatory conditions. Human LECs were stimulated with inflammatory cytokine TNF-α, a known inducer of E-selectin expression in endothelial cells, and this significantly increased the TEM of E-selectin ligand-expressing PDAC S2-013 cells (**Figure 4.10C**). Additional treatment with GMI-1271 restored TNFα-induced PDAC TEM rates to control levels. TNFα did not increase the TEM rate of PDAC cells not expressing E-selectin ligands (Colo357) and GMI-1271 was ineffective at inhibiting TEM for this cell line (**Figure 4.10D**).

PDAC cells are capable of inducing expression of E-selectin in hLECs.

Uninflamed hLECs are reported to express very little to no E-selectin (5), yet E-selectin blockade inhibited PDAC TEM. We therefore investigated the hypothesis that PDAC cells were capable of inducing E-selectin expression in hLECs in co-culture. Using a transwell system, we co-cultured hLECs with PDAC cells S2-013 and Colo357 for varying lengths of time and then evaluated E-selectin mRNA expression in hLECs. TNFα-treated hLECs were used as a positive control for induction of E-selectin expression. After only 1 hour of co-culturing S2-013, E-selectin mRNA was substantially increased in hLECs compared to hLECs in monoculture (**Figure 4.11A**). E-selectin mRNA levels began to decrease following 6 hours of co-culturing. Interestingly,

Figure 4.9

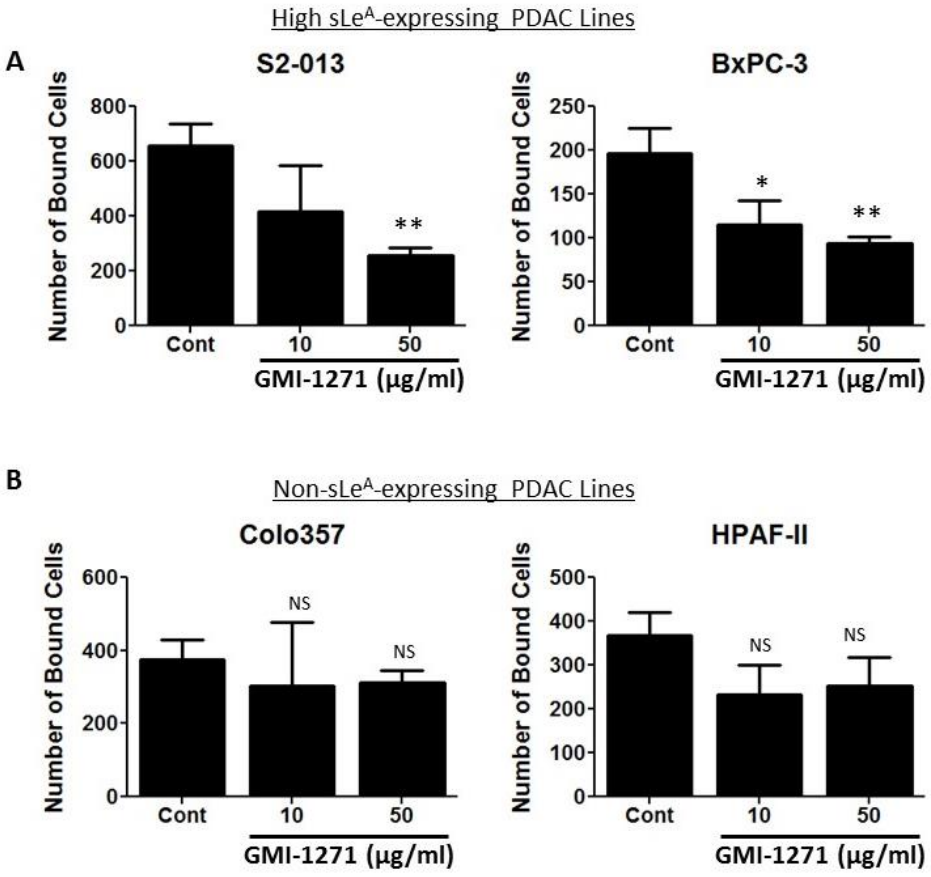

Figure 4.9 GMI-1271 inhibits the binding of sLe^A-expressing pancreatic tumor cells to lymphatic endothelia under steady state conditions.

A) Human LEC monolayers were pretreated with increasing concentrations of GMI-1271. Fluorescently-labeled sLe^A-expressing (S2-013, BxPC-3) PDAC cells were overlaid atop the monolayer and allowed to adhere to the LEC monolayer for 1 hour in the presence of GMI-1271. n=3 replicate wells; 4 images/well were collected for quantification. *p<0.05; **p<0.01; error bars=s.d.

B) Human LEC monolayers were pretreated with increasing concentrations of GMI-1271. Fluorescently-labeled non-sLe^A-expressing (Colo357, HPAF-II) PDAC cells were overlaid atop the monolayer and allowed to adhere to the LEC monolayer for 1 hour in the presence of GMI-1271. n=3 replicate wells; 4 images/well were collected for quantification. Error bars=s.d.

Figure 4.10

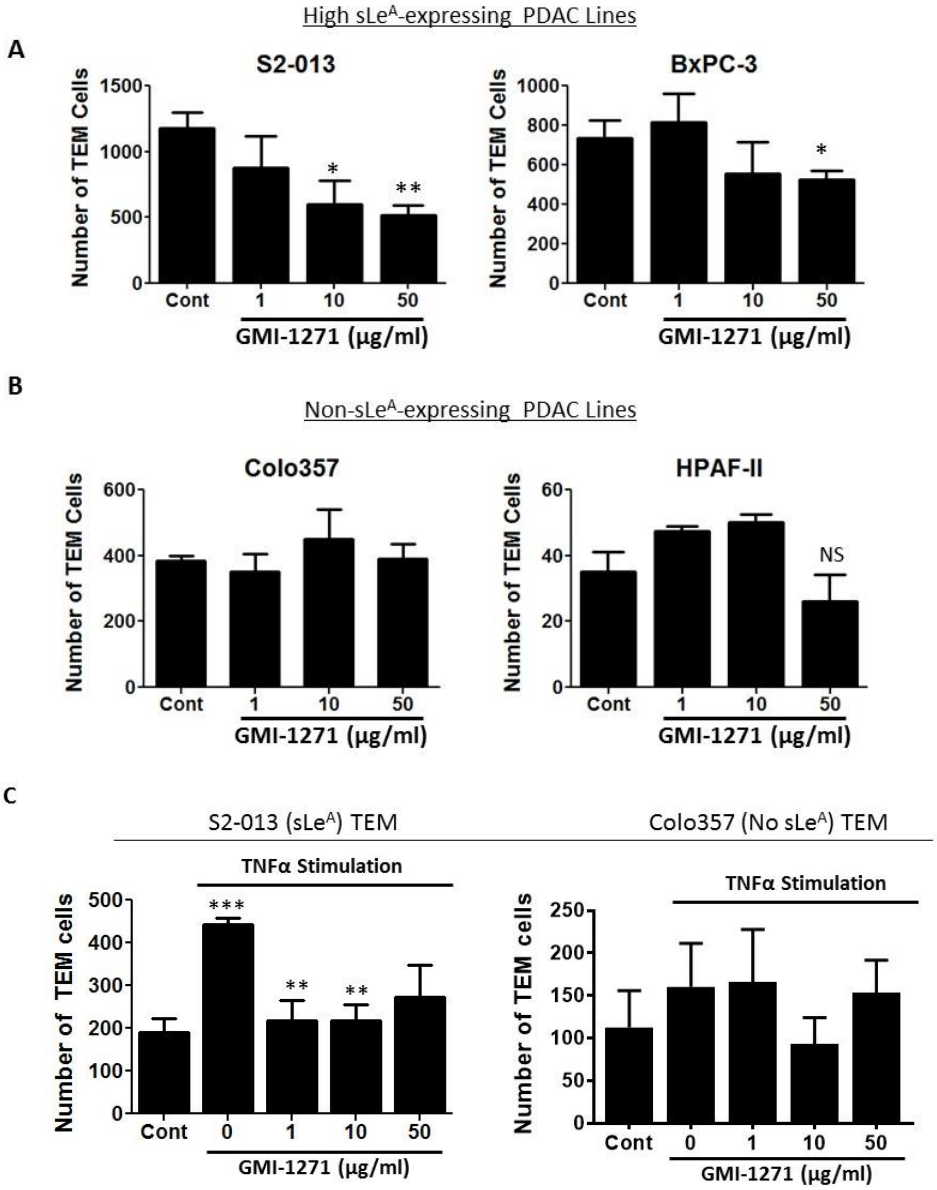

Figure 4.10 GMI-1271 inhibits the ability of sLe^A-expressing PDAC cells to transendothelial migrate across a lymphatic endothelium both under uninflamed and inflamed conditions.

A-B) Human LEC monolayers were established on the underside of Boyden chamber membranes and then pretreated with increasing concentrations of GMI-1271. Fluorescently labeled **A**) sLe^A-expressing (S2-013, BxPC-3) or **B**) non-sLe^A-expressing (Colo357, HPAF-II) PDAC cells were plated in the upper insert and allowed to undergo TEM for 20-24 hours in the presence of GMI-1271. n=3 replicate wells; 5 image collected/well for quantification. *p<0.05; **p<0.01; error bars=s.d.

C) hLEC monolayers were pretreated with TNFα to induce inflammatory E-selectin expression and TEM experiments repeated. n=3 replicate wells; 5 image collected/well for quantification. *p<0.05; **p<0.01; ***p<0.001; error bars=s.d.

Colo357 cells, which are not dependent on E-selectin for invasion of lymphatic endothelia, also upregulated E-selectin mRNA in hLECs. (**Figure 4.11A**), but E-selectin mRNA levels began to decrease following just 1 hour of co-culturing. Pancreatic fibroblasts also induced E-selectin mRNA expression in hLECs but to a lesser extent as the PDAC lines (**Figure 4.11B**). Normalization based on TNFα-induced E-selectin expression revealed that S2-013 and Colo357 induce E-selectin mRNA expression in hLECs at similar levels for the first hour (**Figure 4.11C**). However, after the first hour Colo357 and 13.34-induced E-selectin rapidly declined, while S2-013-induced E-selectin expression levels remained substantially elevated for longer periods of time.

Induction of E-selectin expression in hLECs by S2-013 and pancreatic fibroblasts was also evaluated at the protein level. Flow cytometry indicated a slight increase in the extracellular expression of E-selectin in hLECs following 6 hours of co-culture with S2-013 cells (**Figure 4.11D**). Pancreatic fibroblasts showed no induction of E-selectin protein in hLECs. Immunofluorescence staining of hLEC and S2-013 co-cultures confirmed upregulation of E-selectin expression at the protein level (**Figure 4.11E-I**). Unstimulated monocultures of hLECs displayed very low E-selectin expression (**Figure 4.11E**), while TNFα stimulation markedly increased E-selectin expression in hLECs (**Figure 4.11F**). Co-culturing with S2-013 cells for 2 hours produced a slight increase in hLEC expression of E-selectin (**Figure 4.11G**). As co-culturing time was increased to 4 (**Figure 4.11H**) and 6 hours (**Figure 4.11I**), hLEC expression of E-selectin significantly increased. Taken altogether, these results indicate that PDAC cells are capable of inducing E-selectin expression in hLECs and this E-selectin expression facilitates PDAC cell invasion.

Figure 4.11 PDAC cells induce E-selectin expression in lymphatic endothelial cells.

A-B) Human LECs were plated on the underside of a transwell system membrane (pore: 0.4µm) and human PDAC lines **A**) S2-013 or Colo357 or **B**) pancreatic fibroblasts (13.34) were plated on the upper side. At the designated timepoints, mRNA was collected from hLECs and analyzed for E-selectin expression by qRT-PCR. E-selectin mRNA expression was normalized to GAPDH. Controls included E-selectin expression in hLECs in monoculture and hLECs treated with 2 ng/ml TNFα-treated for 6 hours. Monoculture hLEC expression of E-selectin mRNA was set equal to 1. n=3 technical replicates and each experiment co-culture performed thrice. ***p<0.001; ****p<0.0001; error bars=s.d.

C) TNFα-induced E-selectin mRNA expression was normalized across plates to compare E-selectin induction in hLECs by PDAC tumor cells and fibroblasts.

D) Flow cytometry analysis examining the expression of E-selectin in non-permeabilized hLECs following co-culturing with S2-013 (left) or pancreatic fibroblasts (right). Red histogram indicates E-selectin expression in monoculture hLECs (negative control); green histograms indicate TNFα-induced E-selectin expression in hLECs (positive control); blue histograms indicate E-selectin expression in hLEC following 2.5 hours of co-culturing; and orange histograms indicate E-selectin expression in hLEC following 6 hours of co-culturing.

E-I) Immunofluorescence staining indicating E-selectin (red) expression in permeabilized hLECs following co-culture with S2-013 PDAC cells. **E)** Control hLECs display very low to no expression of E-selectin while **F)** TNFα stimulation significantly increased E-selectin expression. Coculturing with S2-013 cells increased E-selectin expression in hLECs at **G)** 2 hours, **H)** 4 hours, and **I)** 6 hours with 6 hours of co-culturing displaying the highest level of expression. Cell nuclei are stained with DAPI (blue). Scale bars = 50 µm

Figure 4.11

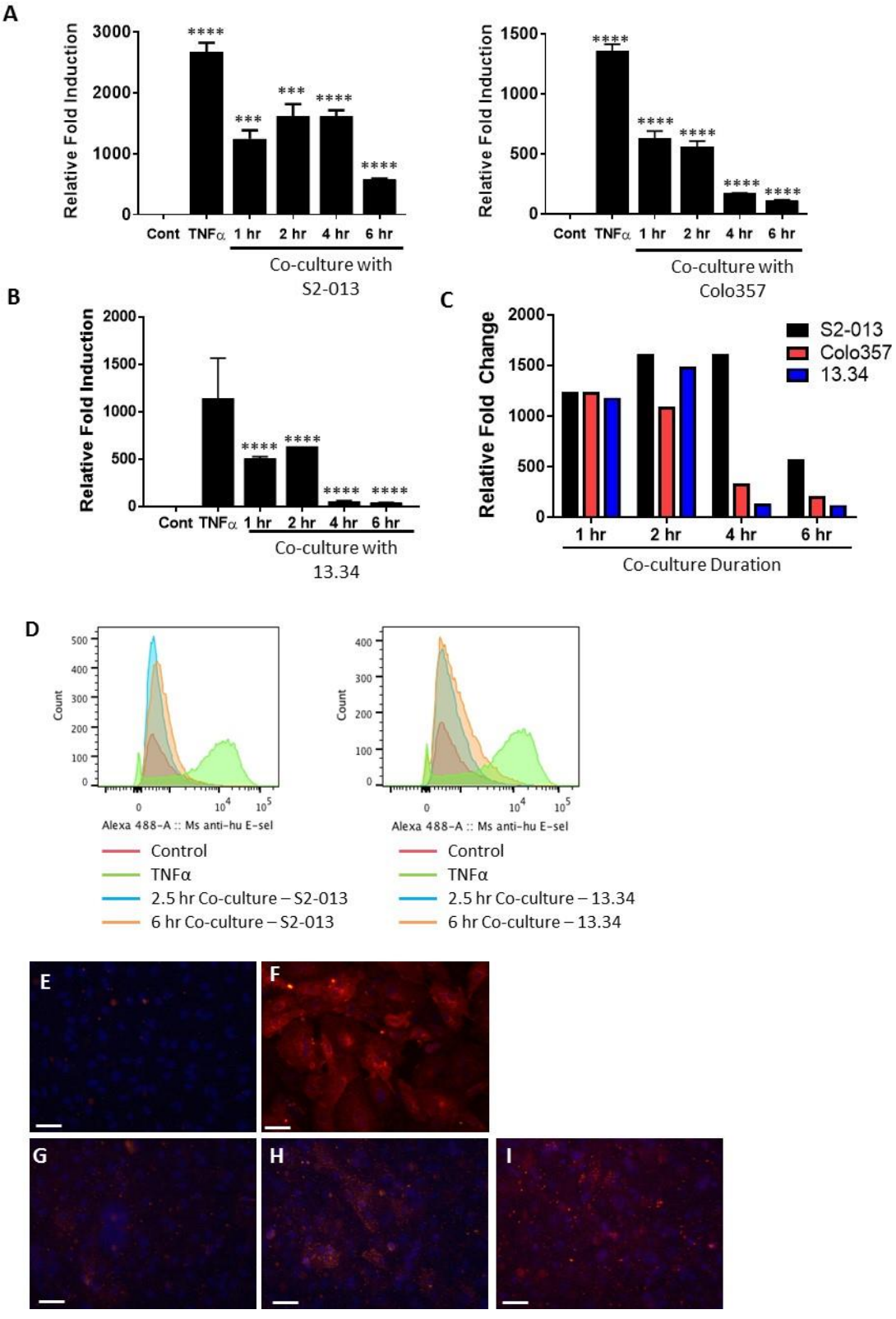
A
Relative Fold Induction
3000
2000
1000
0
****
***
***
****
****
Cont
TNFα
1 hr
2 hr
4 hr
6 hr
Co-culture with S2-013
1500
1000
500
0
****
****
****
****
****
Co-culture with Colo357
B
Relative Fold Induction
2000
1500
1000
500
0
****
****
****
****
Co-culture with 13.34
C
Relative Fold Change
2000
1500
1000
500
0
S2-013
Colo357
13.34
1 hr
2 hr
4 hr
6 hr
Co-culture Duration
D
Count
500
400
300
200
100
0
0
10^4
10^5
Alexa 488-A :: Ms anti-hu E-sel
Control
TNFα
2.5 hr Co-culture – S2-013
6 hr Co-culture – S2-013
400
300
200
100
0
Control
TNFα
2.5 hr Co-culture – 13.34
6 hr Co-culture – 13.34
E
F
G
H
I

III. Conclusions

Adhesion protein E-selectin has been shown to regulate metastasis in a variety of cancers (146, 257, 260). However, its direct role in the metastasis of pancreatic cancer *in vivo* has not been fully evaluated. Using a novel glycomimetic small molecule antagonist of E-selectin, we demonstrated that E-selectin influences PDAC dissemination *via* the vasculature systems, and that blocking its ligand binding function decreased PDAC metastasis. Although it is known that E-selectin plays a role in vascular invasion of tumor cells, we demonstrated for the first time a role for E-selectin in facilitating tumor cell invasion of the lymph nodes *via* the lymphatic vasculature. Using GMI-1271, we showed that blockade of E-selectin significantly impairs PDAC adhesion to a simulated lymphatic endothelium and subsequent transendothelial invasion. *In vivo*, this blockade led to a significant decrease in lymph node metastasis. This inhibition of transendothelial invasion was contingent upon the expression of E-selectin ligands on PDAC cells. Lastly, we showed that PDAC cells can directly regulate the expression of E-selectin in order to undergo TEM. Novel E-selectin antagonist GMI-1271 holds promise as a potential treatment for PDAC and other metastatic malignancies as well.

Supplementary Figure 4.1

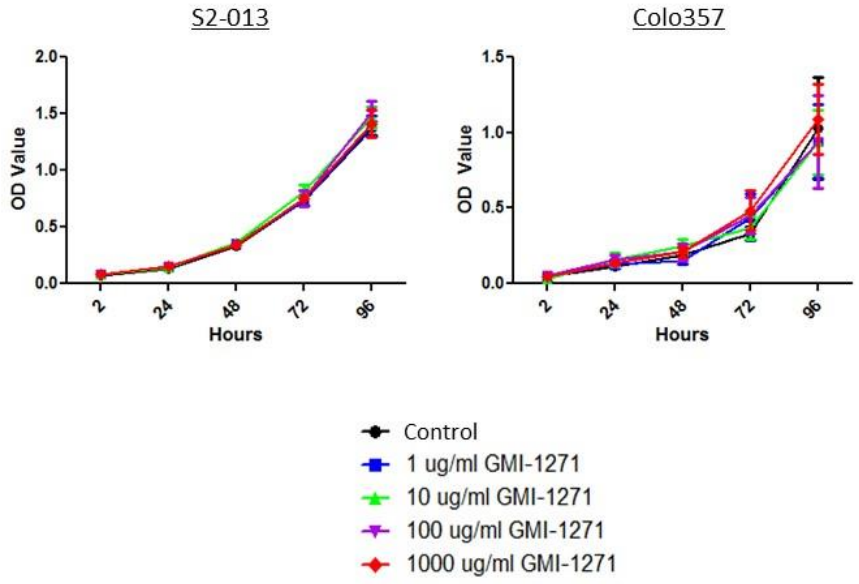

Supplementary Figure 4.1 GMI-1271 does not alter PDAC proliferation *in vitro*.

S2-013 and Colo357 PDAC cells were treated with increasing concentrations of GMI-1271 and proliferation monitored for 96 hours using a methylene blue assay. n=6 technical replicates/treatment and per timepoint; experiments were repeated three times. Error bars = s.d.

Supplementary Figure 4.2

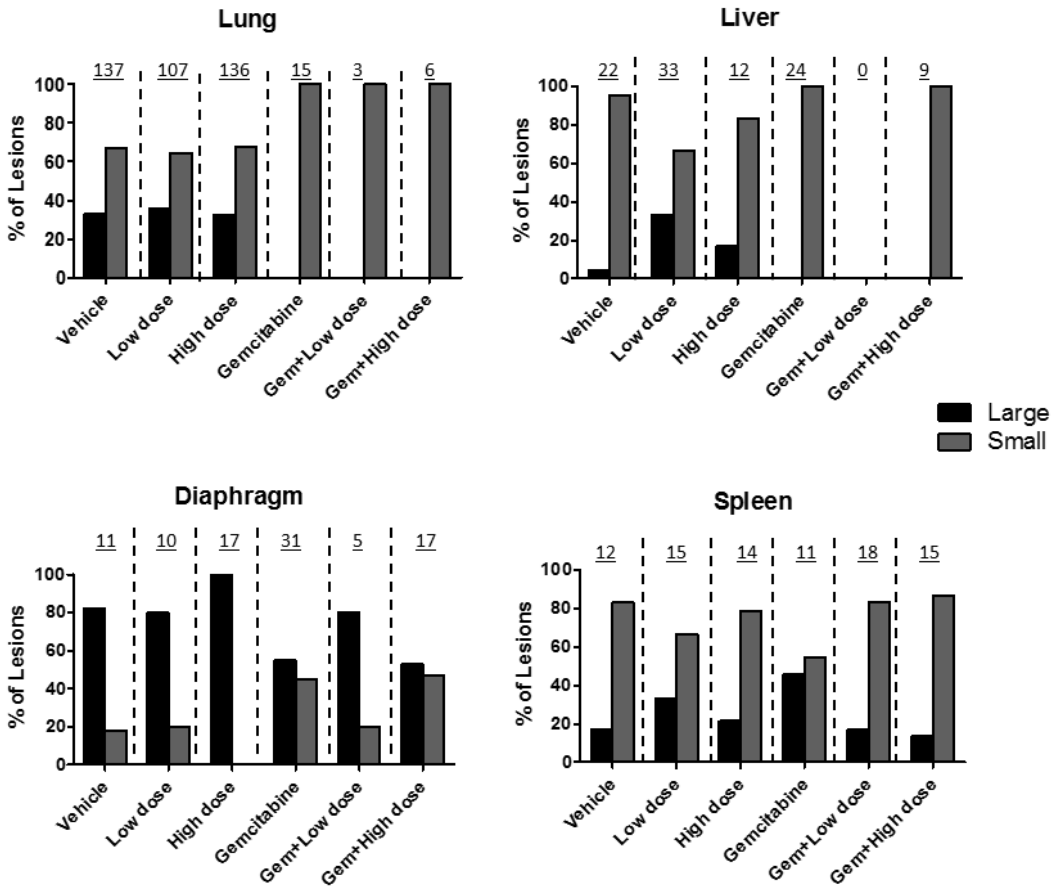

Supplementary Figure 4.2 E-selectin blockade does not impair lesion growth following colonization at a distant site.

Evaluation of the size distribution of metastatic lesions. Numbers above bar indicate total number of lesions quantified per treatment group. Large lesions > 100 cells/lesion; small lesions < 100 cells/lesion.

CHAPTER 5:

Effects of E-selectin and CXCR4 Dual Inhibition by Novel Inhibitor, GMI-1359, on Pancreatic Cancer and the Tumor Microenvironment

I. Introduction

CXCR4 is the most frequently overexpressed chemokine receptor in malignancy (261, 262). High expression of CXCR4 and its predominant ligand, CXCL12, frequently correlates with advanced tumor stage and poor patient prognosis in many types of cancer including pancreatic (140, 263, 264), breast (128, 265-267), lung (268-270), renal (271), melanoma (101), colorectal (272), brain (273), and prostate cancers (274). In the setting of PDAC, CXCR4 first becomes upregulated in early stage precursor PanINs and expression continues to increase as PanINs progress to malignancy (264). Pancreatic tumor cells themselves express high levels of CXCR4 but very low levels of its ligand. CXCL12 is mainly secreted by the cellular components of the tumor microenvironment such as activated fibroblasts and endothelial cells (275, 276). CXCL12-CXCR4 signaling within the primary tumor has been shown support PDAC progression by promoting tumor cells proliferation (277), invasion (278), angiogenesis (137, 279, 280), chemoresistance (281), and immune evasion (171).

Studies have also indicated that CXCR4 and CXCL12 are significant players in the regulation of tumor metastasis. CXCR4-expressing tumor cells often follow CXCL12 gradients to distant organs sites during dissemination. Organs that most highly express CXCL12, the lungs, liver, and bone marrow, are frequent sites for tumor dissemination (128, 282-284). CXCL12-CXCR4 has also been shown to promote angio- and lymphangiogenesis which increases the number of potential routes tumor cells can use to escape the primary site (280, 285). CXCL12 expression by lymphatic and vascular endothelial cells attracts CXCR4+ tumor cells to the lymphovascular niche where CXCR4 enables transendothelial invasion (101, 286-288). Additionally, this CXCL12+ lymphovascular niche within the primary and metastatic tumor sites provides chemoprotection to CXCR4+ tumor cells and inhibits therapy-induced cell death (101). The role of CXCR4 in promoting metastasis as well as other pro-tumor mechanisms makes it an interesting target for cancer therapy.

Our studies examine the role of CXCL12-CXCR4 in facilitating intercellular communications and interactions among cells of the PDAC microenvironment: tumor cells, fibroblasts, and lymphatic endothelial cells. Specifically, we focus on potential roles it may have in lymphatic-directed metastasis. Using a novel small molecule antagonist of both CXCR4 and E-selectin, GMI-1359, our results demonstrate that GMI-1359 is an effective inhibitor of previously described CXCR4-dependent mechanisms *in vitro*. Additionally, we performed side-by-side studies with GMI-1359 and GMI-1271, an E-selectin only antagonist, to elucidate the CXCR4-dependent effects from the E-selectin-dependent effects of this dual inhibitor. Our results indicate that CXCL12 secretion from pancreatic fibroblasts facilitates the recruitment of LECs, and blockade of CXCR4 abrogates this recruitment. Moreover, CXCR4 expression facilitates the ability of hLECs to support PDAC adhesion and transendothelial migration across a lymphatic barrier. These *in vitro* studies demonstrate an essential role for CXCR4 in supporting lymphatic recruitment and invasion for PDAC invasion and metastasis. Examination of *in vivo* antagonism of CXCR4 in PDAC orthotopic mouse models resulted in delayed metastasis of PDAC and a significant reorganization of the PDAC microenvironment. Unfortunately, *in vivo* treatment with GMI-1359 did not result in prolonged animal survival when used alone or in combination with chemo- and immunotherapies in both immune incompetent and immune competent mice. However, alterations to the dosage and treatment schedule of GMI-1359 in combination with other PDAC therapies may improve survival in future studies.

II. Results

Characterization of CXCR4 and CXCL12 expression in cellular components of the PDAC tumor microenvironment.

To understand the potential effects of GMI-1259 on PDAC tumor cells, we examined the expression of CXCR4 in a panel of human PDAC cell lines. Western blot analysis demonstrated that all examined PDAC cell lines expressed CXCR4, albeit at varying levels (**Figure 5.1A**). Flow cytometry analysis on non-permeabilized PDAC cells confirmed this expression and showed that

Figure 5.1 Pancreatic tumor cell express CXCR4 in culture.

A) Western blot (50 µg protein/lane) analysis demonstrating CXCR4 expression in a panel of human PDAC cell line lysates: HPAF-II, S2-013, Hs766t, T3M4, Capan-2, BxPC-3, MiaPaca-2, and Colo357. β-actin expression was used as a loading control for all cell lines.

B) Flow cytometry confirming expression of CXCR4 in a panel of non-permeabilized human PDAC cell lines: S2-013, Colo357, BxPC-3, Capan-2, MiaPaca-2. Rabbit polyclonal IgG was used as an isotype control. Blue histograms represent the IgG isotype control and red histograms represent CXCR4 labeling.

C) Immunofluorescence staining indicating CXCR4 expression in human PDAC cell lines. CXCR4 (red) is diffusely expressed across the cell surface. Cell nuclei are stained with DAPI (blue). Rabbit polyclonal isotype control was used as a negative control (red; bottom row, far right image). Scale bars = 25 µm

Figure 5.1

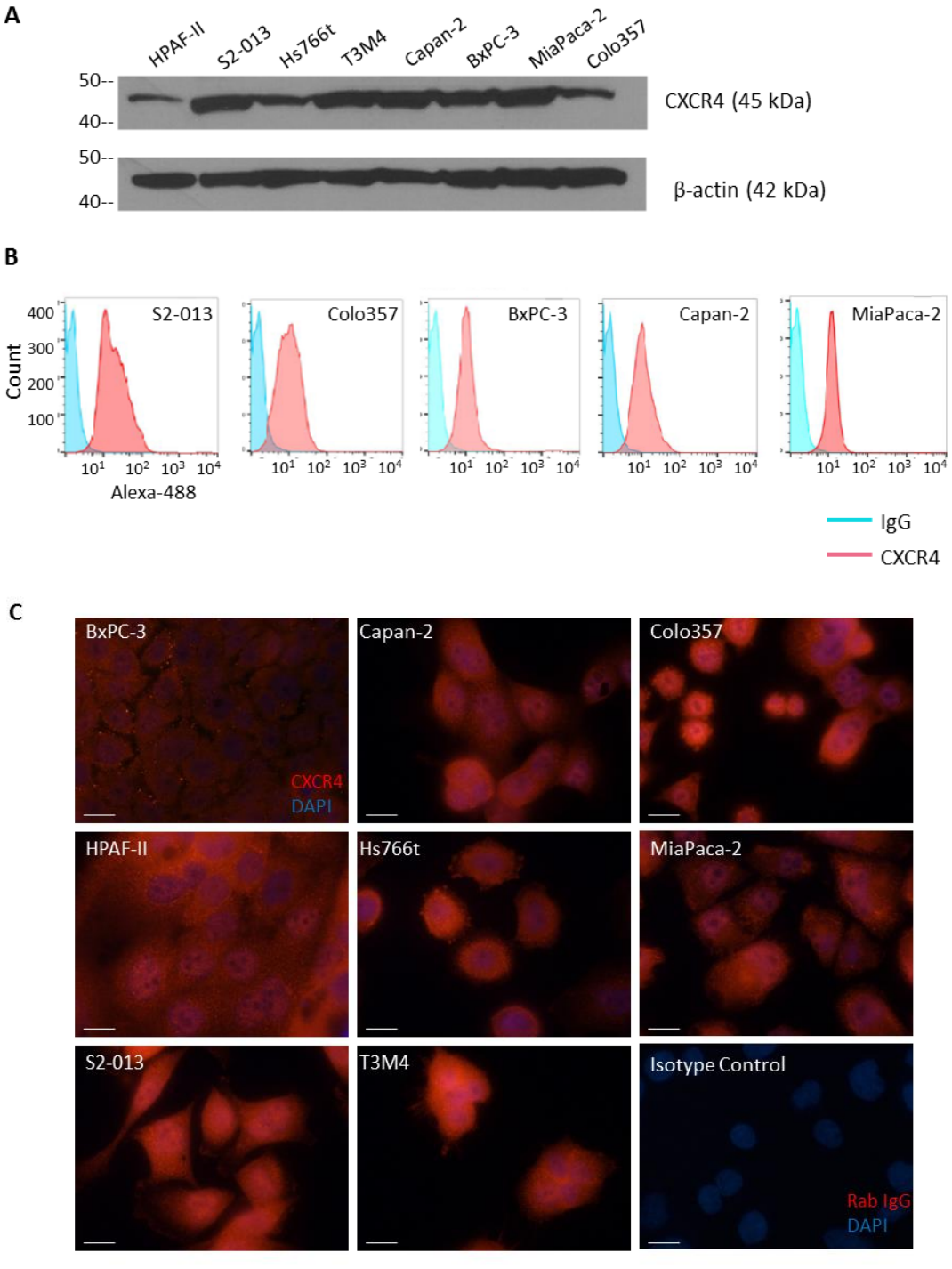
A
HPAF-II
S2-013
Hs766t
T3M4
Capan-2
BxPC-3
MiaPaca-2
Colo357
50--
40--
CXCR4 (45 kDa)
β-actin (42 kDa)
B
Count
S2-013
Colo357
BxPC-3
Capan-2
MiaPaca-2
Alexa-488
IgG
CXCR4
C
BxPC-3
CXCR4
DAPI
Capan-2
Colo357
HPAF-II
Hs766t
MiaPaca-2
S2-013
T3M4
Isotype Control
Rab IgG
DAPI

CXCR4 is expressed on the PDAC cell surface (**Figure 5.1B**). Lastly, immunofluorescence staining revealed that CXCR4 is distributed uniformly across the cell surface of PDAC cells (**Figure 5.1C**).

Cell types of the PDAC tumor microenvironment were also evaluated for CXCR4 expression. Western blot analysis revealed that pancreatic fibroblasts (13.34) and lymphatic (hLECs) and vascular (HUVECs) endothelial cells express measurable levels of CXCR4 (**Figure 5.2A**). Human neonatal foreskin fibroblasts (HuFF) were used a negative control for CXCR4. Flow cytometry confirmed expression of CXCR4 in the pancreatic fibroblasts and hLECs (**Figure 5.2B**). Immunofluorescence staining revealed that pancreatic fibroblasts express CXCR4 across the cell surface while hLECs and HUVECs have more nuclear expression of CXCR4 (**Figure 5.2C**). LECs also demonstrated low levels of CXCR4 across the cell surface.

To characterize the expression of the CXCR4 ligand, CXCL12, ELISA analysis was performed on both conditioned media (secreted CXCL12) and whole cell lysates (cell-bound CXCL12) from PDAC cells, pancreatic fibroblasts (13.34), and hLECs. In culture, only pancreatic fibroblasts constitutively secrete CXCL12 into conditioned media (**Figure 5.3A**). CXCL12 was not detected by ELISA in the conditioned media of PDAC cells S2-013 and Colo357 nor was it detected in hLEC conditioned media. ELISA analysis on whole cell lysates revealed expression of CXCL12 in PDAC cells, pancreatic fibroblasts, and hLECs suggesting that CXCL12 may be bound to the cell surface or sequestered within intracellular compartments (**Figure 5.3B**). Flow cytometry on permeabilized samples confirmed the intracellular expression of CXCL12 within these same cell types (**Figure 5.3C**).

GMI-1359 effects on PDAC tumor cell, fibroblast, and endothelial cell proliferation.

We evaluated the effects of GMI-1359 on PDAC cells, fibroblasts, and endothelial cell proliferation. Both of the examined PDAC lines, S2-013 and Colo357, showed little response to treatment with 10 µg/ml GMI-1359 over the course of 96 hours (**Figure 5.4A**). At higher

Figure 5.2

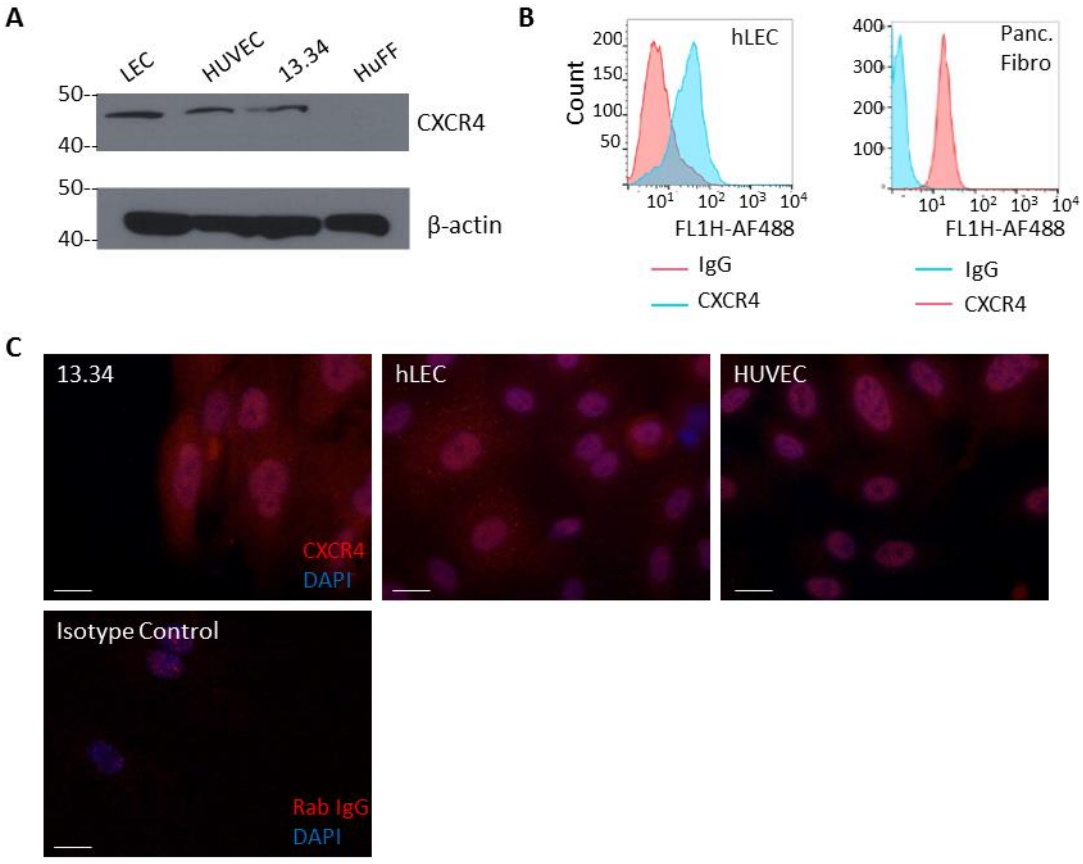

Figure 5.2 Expression of CXCR4 in cell types of the PDAC microenvironment.

A) Western blot (30 µg protein/lane) analysis demonstrating CXCR4 expression in human lymphatic endothelial cells (LECs), vascular endothelial cells (HUVECs), and pancreatic fibroblasts (13.34) lysates. Human neonatal foreskin fibroblasts (HuFF) lysates were used as a negative control for CXCR4 expression. β-actin expression was used as a loading control for all cell lines.

B) Flow cytometry confirming expression of CXCR4 in human lymphatic endothelial cells (hLECs), and pancreatic fibroblasts (13.34). For hLECs, the red histogram indicates IgG isotype control labeling and the blue histogram indicates CXCR4 labeling. For pancreatic fibroblast, the blue histogram indicates IgG isotype control labeling and the red histogram represents CXCR4 labeling.

C) Immunofluorescence staining indicating CXCR4 expression in 13.34 pancreatic fibroblasts, hLECs, and HUVECs. CXCR4 (red) is diffusely expressed across the cell surface of 13.34 cells while mainly nuclear staining is seen in the hLECs and HUVECs. Cell nuclei are stained with DAPI (blue). Rabbit polyclonal isotype control was used as a negative control (lower left image). Scale bars = 25 µm

Figure 5.3

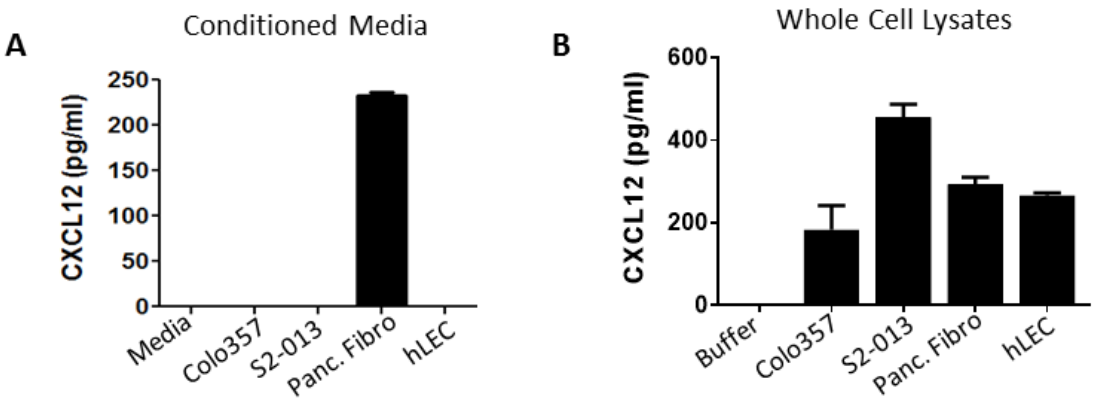

Figure 5.3 CXCL12 secretion and expression in PDAC cells and tumor microenvironment cell types.

A) ELISA-based quantification of CXCL12 within conditioned media of PDAC cells (Colo357, S2-013), pancreatic fibroblasts (13.34), or hLECs. Media was conditioned for 24 hours by equal numbers of cells in equal volumes of serum free media. Unconditioned serum free media was used as a control. 3 replicate wells were analyzed per experiment and experiments were performed thrice. Error bars = s.d.

B) ELISA-based quantification of CXCL12 within whole cell lysates (2000 µg/ml) of PDAC cells (Colo357, S2-013), pancreatic fibroblasts (13.34), or hLECs. Lysis buffer was used as a control. 3 replicate wells were analyzed per experiment and experiments were performed thrice. Error bars = s.d.

Figure 5.4 Effect of GMI-1359 on PDAC, fibroblast, and endothelial cell proliferation and morphology.

Methylene blue assay measuring the proliferation of **A)** S2-013, **B)** Colo357, **C)** 13.34 pancreatic fibroblasts, **D)** hLECs, or **E)** HUVECs treated with increasing concentrations of GMI-1359 or GMI-1271 (0, 10, 100, 1000 µg/ml). Line graphs represent cell numbers collected at 2, 24, 48, 72, or 96 hours. OD values were read at 650 nm. 5 replicate wells were performed at each inhibitor concentration and each time point. Experiment was repeated 3 times. Error bars = s.d. Phase contrast images (10X magnification) are of S2-013, Colo357, 13.34, and hLEC treated with 100 µg/ml GMI-1359 for 72 hours. Scale bars = 100 µm

Figure 5.4

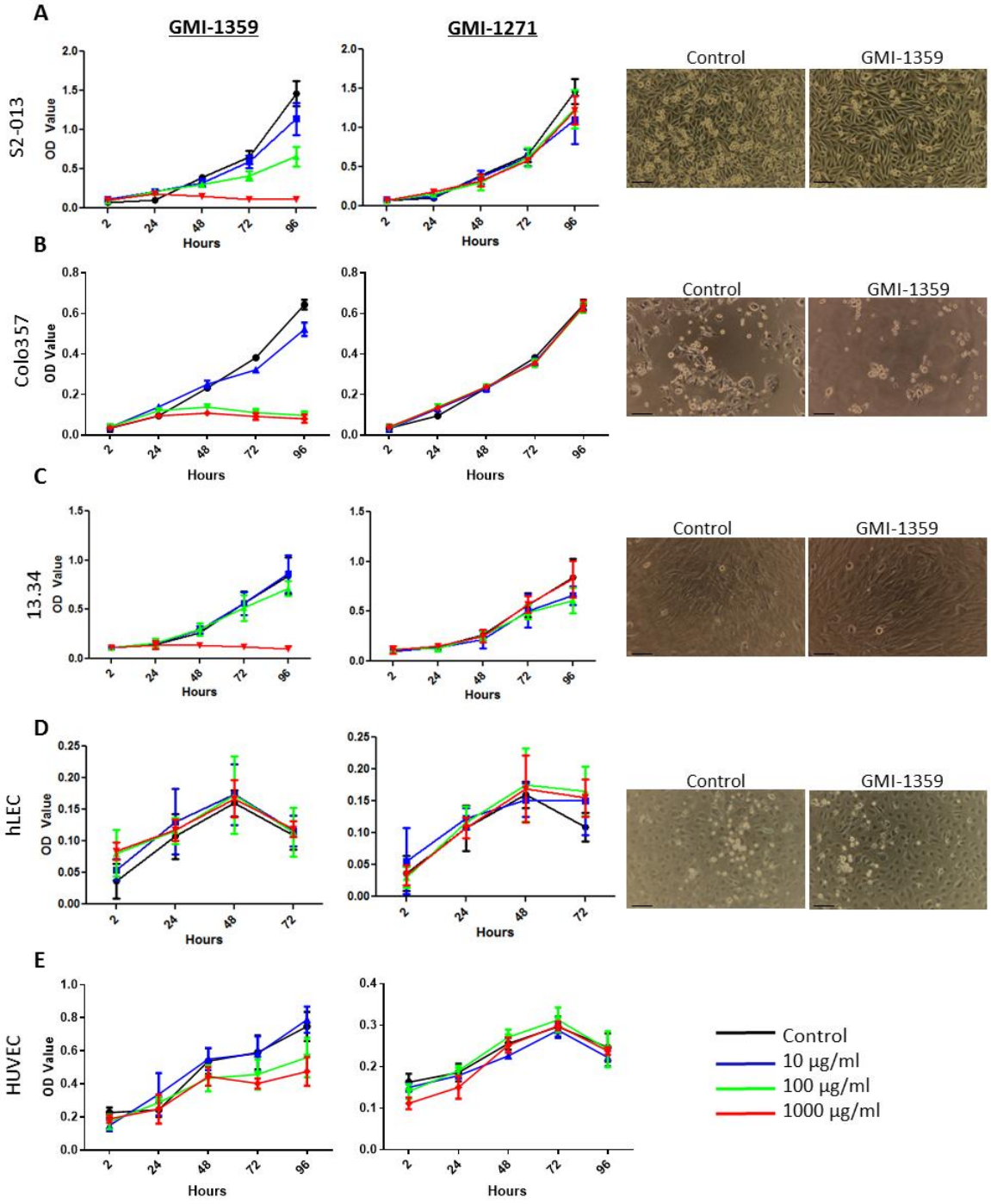
A
GMI-1359
GMI-1271
S2-013
OD Value
Hours
Control
GMI-1359
B
Colo357
C
13.34
D
hLEC
E
HUVEC
Control
10 µg/ml
100 µg/ml
1000 µg/ml

concentrations, proliferation appeared normal for the first 24 hours for S2-013 cells. However, by 72-96 hours, S2-013 proliferation significantly decreased with increasing concentrations of GMI-1359. Examination of cell morphology revealed that GMI-1359-treated S2-013 PDAC cells had an elongated morphology compared to untreated cells. Similar to S2-013 cells, 10 µg/ml GMI-1359 had little effect on Colo357 proliferation (**Figure 5.4B**). However, at 100 and 1000 µg/ml, GMI-1359 completely impaired Colo357 proliferation after 24 hours. GMI-1271 did not affect Colo357 at any of the examined concentrations. Examination of cell morphology revealed the Colo357 cells were undergoing cell death after 72 hours of treatment with 100 µg/ml GMI-1359. GMI-1271 had no impact on S2-013 or Colo357 proliferation at any of the tested concentrations (**Figure 5.4A-B**).

The effects of GMI-1359 on pancreatic fibroblast and endothelial cell proliferation were also evaluated. Treatment with 10 µg/ml GMI-1359 had no effect on 13.34 proliferation (**Figure 5.4C**). At 100 µg/ml, GMI-1359 slightly reduced pancreatic fibroblast proliferation, but not significantly. By 1000 µg/ml GMI-1359, 13.34 proliferation was completely inhibited. GMI-1271 had no significant impact on 13.34 proliferation. Morphologic examination revealed that treatment with 100 µg/ml GMI-1359 for 72 hours had no impact on 13.34 morphology. LEC proliferation was unaffected by GMI-1359 or GMI-1271 treatment even at high concentrations (**Figure 5.4D**). Increasing concentrations of GMI-1359 moderately inhibited HUVEC proliferation (**Figure 5.4E**). Even at high concentrations of GMI-1359 (1000 µg/ml), HUVEC still proliferated but at a reduced rate. GMI-1271 had no impact on HUVEC proliferation.

GMI-1359 inhibits CXLC12-induced signaling and CXCL12-directed migration by blocking CXCR4.

To verify that GMI-1359 blocks CXCR4 function, we examined its ability to inhibit CXCL12-induced ERK1/2 phosphorylation and CXCL12-induced migration. We used hLECs as a model cell type as it has been previously reported that CXCL12 induces these effects in hLECs (285). In agreement with these reports, CXCL12 induced phosphorylation of ERK 1/2 within 5 minutes of stimulation (**Figure 5.5A**). By 30 minutes, phospho-ERK1/2 levels returned to steady

state levels. Total ERK1/2 levels remained unchanged during CXCL12 stimulation. CXCR4 blockade with GMI-1359 significantly decreased, but did not completely inhibit, CXCL12-induced ERK1/2 activation in hLECs. Blockade of E-selectin alone with GMI-1271 had no effect on ERK1/2 activation during CXCL12 simulation. These data suggest that GMI-1359 blocks CXCR4 function resulting in inhibition of CXCL12-induced ERK1/2 phosphorylation (**Figure 5.5B**).

The impact of GMI-1359 on CXCL12-induced migration of hLECs was also examined. When present in the lower wells of a Boyden chamber system, increasing concentrations of recombinant CXCL12 induced a strong upregulation of hLEC migration (**Figure 5.6A**). Pretreatment of hLECs with GMI-1359 significantly impaired hLEC migration toward CXCL12. Regardless of CXCL12 concentration, 10 μg/ml GMI-1359 was sufficient to return hLEC migration to control levels. To verify that GMI-1359 impaired only CXCL12-induced migration and was not a general inhibitor of migration process, we evaluated its effects on hLEC migration using endothelial growth media EGM-2MV containing FBS and growth factors as the chemoattractant. GMI-1359 had no impact on hLEC migration toward FBS/growth factor-containing media (**Figure 5.6B**). Combined these results demonstrate that GMI-1359 inhibits CXCL12-induced migration and is not a general inhibitor of the hLEC migration process.

We also evaluated the ability of GMI-1359 to impair CXCL12-induced migration of another CXCR4-expressing cell type, S2-013 PDAC cells. At 100 ng/ml, CXCL12 moderately increased S2-013 directional migration; however, increasing the concentration to 500 ng/ml did not further increase in S2-013 migration (**Figure 5.6C**). Pretreatment with GMI-1359 reduced S2-013 migration toward CXCL12 but did not return migration to control levels. Similar to hLECs, GMI-1359 did not affect S2-013 migration toward FBS-containing media (**Figure 5.6D**), again, demonstrating that GMI-1359 specifically inhibits the CXCL12-directed migration and is not a general inhibitor of migration.

Figure 5.5

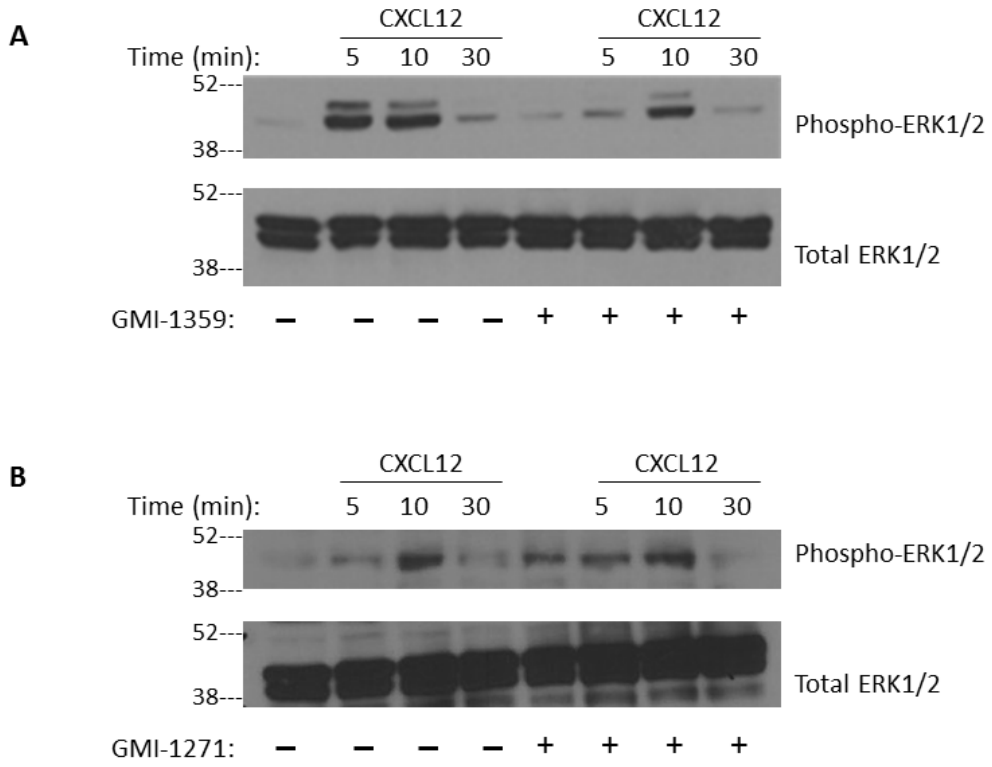

Figure 5.5 Blockade of CXCR4 by GMI-1359 reduced ERK1/2 activation in hLECs.

A) Western blot analysis of phopho-ERK1/2 activation in hLECs following stimulation with 200 ng/ml human recombinant CXCL12 for 5, 10, or 30 minutes. Designated hLECs were pretreated with 10 µg/ml GMI-1359 30 minutes prior to CXCL12 stimulation.

B) Western blot analysis of phopho-ERK1/2 activation in hLECs following stimulation with 200 ng/ml human recombinant CXCL12 for 5, 10, or 30 minutes. Designated hLECs were pretreated with 10 µg/ml GMI-1271 for 30 minutes prior to CXCL12 stimulation.

Figure 5.6

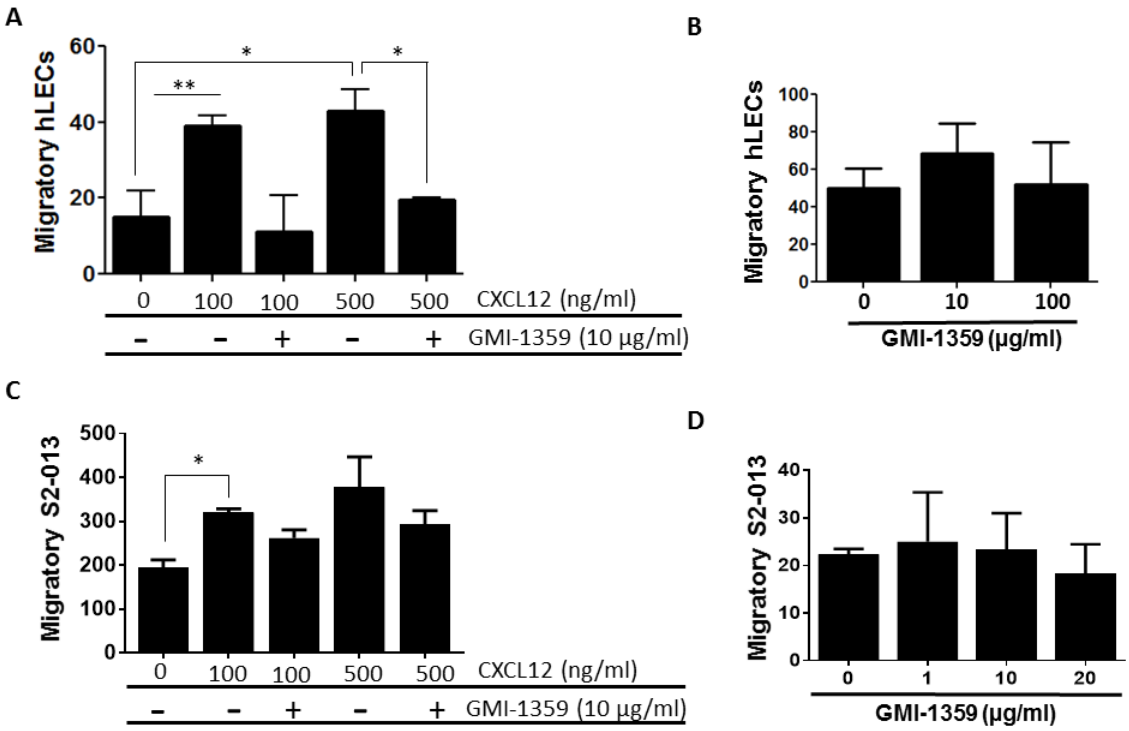

Figure 5.6 CXCR4 blockade by GMI-1359 inhibits CXCL12-induce migration of hLECs and S2-013.

A) The lower wells of a Boyden chamber plates were loaded with serum free media containing either 0, 100 or 500 ng/ml CXCL12. Human LECs were diluted in serum free media and added to the upper inserts. Designated hLECs were pretreated with 10 µg/ml GMI-1359 for 30 minutes prior to plating in the upper inserts. Migration was stopped after 16 hours and quantified. CXCL12 induced hLEC migration. Treatment with GMI-1359 significantly inhibited CXCL12-induced hLEC migration. Quantification is the average of 3 replicate membranes; experiment was repeated 3 times. *$p<0.05$, **$p<0.01$, error bars = s.d.

B) The lower wells of a Boyden chamber plates were loaded FBS/growth factor-containing EGM-2MV. Human LECs or were diluted in serum free media and added to the upper inserts. Designated hLECs were pretreated with 10 µg/ml GMI-1359 for 30 minutes prior to plating in the upper inserts. Migration was stopped after 16 hours and quantified. Quantification is the average of 3 replicate membranes; experiment was repeated 3 times. Error bars = s.d.

C) Migration plates were set up as described in Figure 5.6A except with S2-013 cells. CXCL12 moderately increased S2-013 migration. Quantification is the average of 3 replicate membranes; experiment was repeated 3 times. *$p<0.05$, error bars = s.d.

D) The lower wells of a Boyden chamber plates were loaded FBS-containing RPMI. S2-013 cells were diluted in serum free media and added to the upper inserts. Designated S2-013 cells were pretreated with 10 µg/ml GMI-1359 for 30 minutes prior to plating in the upper inserts. Migration was stopped after 16 hours and quantified. Quantification is the average of 3 replicate membranes; experiment was repeated 3 times. Error bars = s.d.

CXCR4 blockade through GMI-1359 completely inhibited CXCL12-induced hLEC migration but did not completely suppress CXCL12-stimulated ERK1/2 activation. The other known receptor for CXCL12, CXCR7, has been shown to induce ERK1/2 signaling, but has no known role in migration (289, 290). Therefore, we hypothesized that hLECs may express CXCR7. Flow cytometry revealed that hLECs do, in fact, express CXCR7 and that may explain why GMI-1359 did not completely suppress ERK1/2 activation following CXCL12 stimulation (**Supplementary Figure 5.1**).

Pancreatic fibroblasts induce hLEC migration via the CXCL12-CXCR4 chemokine axis.

Previously, we demonstrated that pancreatic fibroblasts strongly induced hLEC migration and also secrete abundant amounts of CXCL12. We evaluated whether fibroblast-induced hLEC migration was dependent on a CXCL12 gradient secreted by the fibroblasts. Using 13.34 conditioned media as a chemoattractant in a Boyden migration assay, hLECs were pretreated with either dual E-selectin/CXCR4 antagonist GMI-1359 or E-selectin only antagonist GMI-1271. Treatment with GMI-1359 completely abrogated fibroblast- induced hLEC migration (**Figure 5.7A**). In the presence of 10 µg/ml GMI-1359, hLEC migration to pancreatic fibroblast conditioned media returned to the same level as that induced by unconditioned media. Blockade of E-selectin alone through GMI-1271 had no significant impact on hLEC migration to fibroblast conditioned media. These results demonstrate that pancreatic fibroblasts strongly induce hLEC migration through secretion of CXCL12 and blockade of the CXCL12 receptor, CXCR4, complete abolishes this fibroblast-induced hLEC migration.

We also hypothesized that S2-013 and Colo357 PDAC cell migration toward pancreatic fibroblast conditioned media may also be dependent on the CXCL12-CXCR4 axis. Pretreatment with GMI-1359 moderately reduced (38.7%) S2-013 migration toward pancreatic fibroblast conditioned media (**Figure 5.7B)**. However, fibroblast-induced S2-013 migration did not return to

Figure 5.7

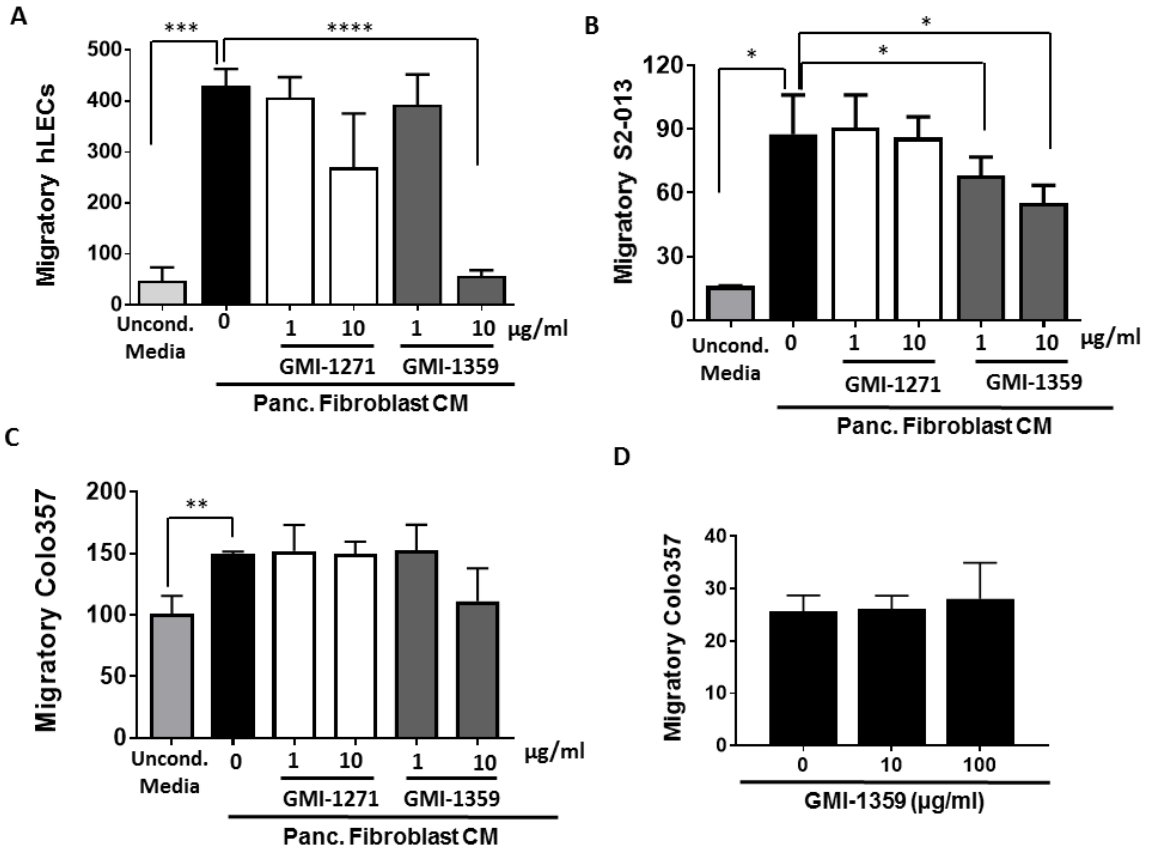

Figure 5.7 Pancreatic fibroblast strongly induce hLEC, but not pancreatic tumor cell, migration through CXCL12 secretion and this migration can be inhibited by GMI-1359.

A-C) 13.34 pancreatic fibroblasts conditioned media (CM) was loaded into the lower wells of a Boyden chamber plate. 2.5 x 10^4 **A)** hLECs, **B)** S2-013, or **C)** Colo357 cells were diluted in serum free media and added to the upper inserts. Designated cells were pretreated with 10 µg/ml GMI-1359 for 30 minutes prior to plating in the upper inserts. Migration was stopped after 16 hours and quantified. Graphical representation is the mean of 3 replicate membranes; experiment was repeated 3 times. *p<0.05, **p<0.01, ***p<0.001, ****p<0.0001 error bars = s.d.

D) Lower wells of Boyden chamber plates were loaded with FBS-containing media to induce cellular migration. 2.5 x 10^4 Colo357 cells were diluted in serum free media and added to the upper inserts. Designated cells were pretreated with 0, 10, 100 µg/ml GMI-1359 for 30 minutes prior to plating in upper inserts. Migration was stopped after 16 hours and quantified. Graphical representation is the mean of 3 replicate membranes; experiment was repeated 3 times. Error bars = s.d.

the same levels as migration induced by unconditioned media. Blockade of CXCR4 had even less of impact on Colo357 migration to pancreatic fibroblast conditioned media (**Figure 5.7C**). Blockade of E-selectin with GMI-1371 had no impact on S2-013 or Colo357 migration toward pancreatic fibroblast conditioned media. Similar to previously described experiments with S2-013 cells, Colo357 migration toward FBS-containing growth media was not impacted by CXCR4 inhibition (**Figure 5.7D**) These data suggest that PDAC migration toward pancreatic fibroblasts is only partially dependent on CXCL12 and that other factors contribute to this migration.

CXCR4 faciliates PDAC adhesion to and transendothelial migration across lymphatic endothelial barriers.

CXCR4 has been shown to play a role in promoting lymphatic-leukocyte interactions during intravasation (276). We hypothesized that CXCR4 may also facilitate PDAC-lymphatic interactions during tumor cell invasion. To examine the role of CXCR4 in facilitating PDAC adhesion to a lymphatic endothelium, a confluent monolayer of hLECs was established and pretreated with increasing concentrations of GMI-1359. Following pretreatment, either S2-013 or Colo357 PDAC cells were overlaid atop the monolayer and allowed to adhere for one hour. Treatment with GMI-1359 significantly impaired S2-013 adhesion to an hLEC endothelium (**Figure 5.8A**). Since S2-013 cells express E-selectin ligands, the ability of GMI-1359 to inhibit S2-013 adhesion may have been due to E-selectin blockade by this dual inhibitor. Therefore, to determine if CXCR4 may also contribute to endothelial adhesion, we examined the ability of GMI-1359 to suppress adhesion of a PDAC cell line that does not express E-selectin ligands, Colo357. Interestingly, blockade of CXCR4 through GMI-1359 significantly inhibited the ability of Colo357 to adhere to a lymphatic endothelium in a dose-dependent manner (**Figure 5.8A**). We performed similar PDAC adhesion assays using vascular endothelial cells (HUVECs) in place of hLECs. GMI-1359 moderately inhibited the adhesion of both E-selectin ligand-expressing and non-expressing PDAC cells to a vascular endothelium, though these studies with HUVECs never achieved statistical significance (**Figure 5.8B**).

Figure 5.8 Blockade of CXCR4 by GMI-1359 inhibits PDAC adhesion and transendothelial migration across a lymphatic endothelium.

A) Human LEC monolayers were pretreated with increasing concentrations of GMI-1359 for 1 hour. Fluorescently-labeled S2-013 or Colo357 PDAC cells were overlaid atop the monolayer and allowed to adhere to the LEC monolayer for 1 hour in the presence of GMI-1359. Non-adherent PDAC cells were washed away and adherent cells were quantified. Graphical representation is the mean of 3 replicate wells. Four representative images (4X magnification) were collected per well. *$p<0.05$; **$p<0.01$; error bars = s.d.

B) HUVEC monolayers were pretreated with increasing concentrations of GMI-1359 for 1 hour. Fluorescently-labeled S2-013 or Colo357 PDAC cells were overlaid atop the monolayer and allowed to adhere to the HUVEC monolayer for 1 hour in the presence of GMI-1359. Non-adherent PDAC cells were washed away and adherent cells were quantified. Graphical representation is the mean of 3 replicate wells. Four representative images (4X magnification) were collected per well. Error bars=s.d.

C) Human LEC monolayers were established on the underside of Boyden chamber membranes and then pretreated with increasing concentrations of GMI-1359 for 1 hour. Fluorescently-labeled S2-013 or Colo357 PDAC cells were plated in the upper insert and allowed to undergo TEM for 20-24 hours in the presence of GMI-1359. Non-transmigrated PDAC cells were mechanically removed and transmigrated cells were quantified. Graphs represent the mean of 3 replicate membranes; experiment was repeated 3 times. *$p<0.05$; **$p<0.01$; error bars = s.d.

D) Human LEC monolayers were established on the underside of Boyden chamber membranes and then pretreated with 10 μg/ml anti-CXCR4 blocking antibody for 1 hour. Fluorescently-labeled S2-013 cells were plated in the upper insert and allowed to undergo TEM for 20-24 hours in the presence of GMI-1359. Non-transmigrated PDAC cells were mechanically removed and transmigrated cells were quantified. Graphs represent the mean of 3 replicate membranes; experiment was repeated 3 times. *$p<0.05$; **$p<0.01$; error bars = s.d.

Figure 5.8

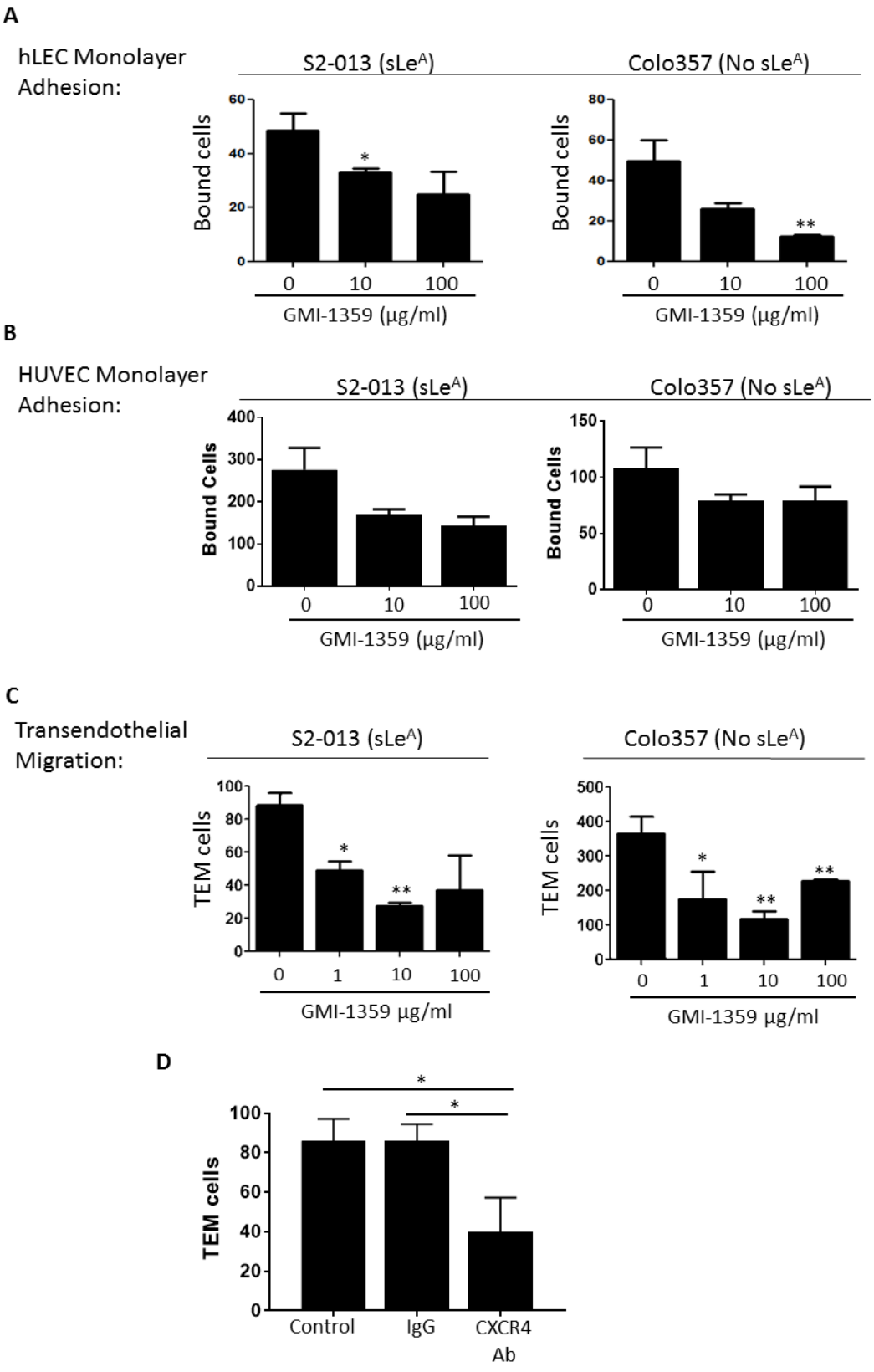
A
hLEC Monolayer Adhesion:
S2-013 (sLeA)
Colo357 (No sLeA)
Bound cells
GMI-1359 (µg/ml)
B
HUVEC Monolayer Adhesion:
S2-013 (sLeA)
Colo357 (No sLeA)
Bound Cells
GMI-1359 (µg/ml)
C
Transendothelial Migration:
S2-013 (sLeA)
Colo357 (No sLeA)
TEM cells
GMI-1359 µg/ml
D
TEM cells
Control
IgG
CXCR4 Ab

As tumor cell adhesion to an endothelium does not directly translate to invasion, we set up a series of PDAC transendothelial migration (TEM) assays to determine if CXCR4 blockade could inhibit tumor invasion of an endothelium. LEC monolayers were established on the underside of Boyden chamber membranes and pretreated with increasing concentrations of GMI-1359. Following pretreatment, CFDA-SE-labeled S2-013 were added to the upper insert and allowed to undergo TEM for 20-24 hours. S2-013 TEM across a lymphatic endothelium was markedly reduced in the presence of GMI-1359 (**Figure 5.8C**). To determine if this inhibition was due to E-selectin, CXCR4, or both, we again evaluated the effects of GMI-1359 on the TEM of PDAC cells not expressing E-selectin ligands. Similar to S2-013 TEM, TEM across a lymphatic endothelium by Colo357 cells was significantly reduced in the presence of GMI-1359 (**Figure 5.8C**). As further verification of the role of CXCR4 in PDAC TEM, we also performed TEM assays in the presence of a CXCR4 blocking antibody. Similar to GMI-1359, the CXCR4 blocking antibody significantly reduced the TEM of S2-013 cells across a lymphatic endothelium (**Figure 5.8D**). The data from these experiments demonstrate that CXCR4 plays a considerable role in the interactions between PDAC cells and lymphatic endothelium and that blockade of this receptor significantly impairs the adhesion and TEM of PDAC cells across a lymphatic endothelium.

CXCR4 ligand CXCL12 promotes the ability of hLECs to facilitate PDAC TEM.

To evaluate the role for the CXCR4 ligand, CXCL12, on PDAC TEM, we stimulated hLEC monolayers with 200 ng/ml human recombinant CXCL12 for 8 hours, washed the monolayer, and then added PDAC cells. In some experiments, hLEC monolayers were pretreated with GMI-1271 or 1359 for 1 hour and then washed prior to the addition of S2-013 PDAC cells. Neither GMI-1271 nor 1359 was present during the TEM process to elucidate the effects of blocking E-selectin and CXCR4 only on the hLEC monolayers during PDAC TEM. In inhibitor-only-treated hLECs, pretreatment of monolayers with GMI-1271 or 1359 significantly impaired the ability of hLECs to

facilitate S2-013 TEM (**Figure 5.9A**). Since neither GMI-1271 nor 1359 was present during the TEM process, these results suggest that expression of E-selectin and CXCR4 by hLECs facilitates PDAC cell TEM. This was not unexpected for E-selectin as E-selectin expression is restricted to endothelial cells. However, CXCR4 is expressed by both PDAC cells and hLECs and blockade of CXCR4 in only the hLECs significantly impaired PDAC TEM.

We also evaluated the role of CXCL12 in hLEC-facilitated TEM. CXCL12 stimulation of hLECs resulted in a significant increase in the ability of hLECs to facilitate S2-013 TEM (**Figure 5.9A**). As expected, blockade of CXCR4 in hLECs through GMI-1359 abrogated this CXCL12-enhanced TEM of S2-013 cells. Unexpectedly, GMI-1271 pretreatment of hLECs also suppressed CXCL12-enhanced S2-013 TEM. Under E-selectin blockade only, the ability of CXCL12-stimulated hLEC to facilitate S2-013 TEM was returned to control levels. This suggests a link between CXCL12 stimulation and E-selectin. Similar results with CXCL12 and GMI-1359 were seen using Colo357 cells (**Figure 5.9B**). Lastly, we evaluated whether a cellular of source of CXCL12 could stimulate hLEC-facilitated TEM similarly to recombinant CXCL12. Lymphatic monolayers were pretreated with conditioned media from 13.34 pancreatic fibroblasts. Some monolayers were also pretreated with GMI-1271 or 1359. Pancreatic fibroblast conditioned media moderately increased the ability of hLECs to facilitate PDAC TEM (**Figure 5.9C**). The fold increase in TEM was similar to treatment with recombinant CXCL12 (1.5 times control levels). Pretreatment with GMI-1271 or 1359 again returned S2-013 TEM to control levels.

GMI-1359 delays metastasis in an *in vivo* orthotopic model of pancreatic cancer.

Our *in vitro* studies demonstrated that the CXCL12-CXCR4 axis plays a significant role in facilitating PDAC-endothelial interactions during invasion, and that blockade of both E-selectin and CXCR4 through GMI-1359 significantly impairs TEM of PDAC cells. We next evaluated whether GMI-1359 could impair this invasion *in vivo* and prevent spontaneous PDAC metastasis. We orthotopically challenged athymic mice with S2-013 PDAC cells for 2 weeks and then

Figure 5.9

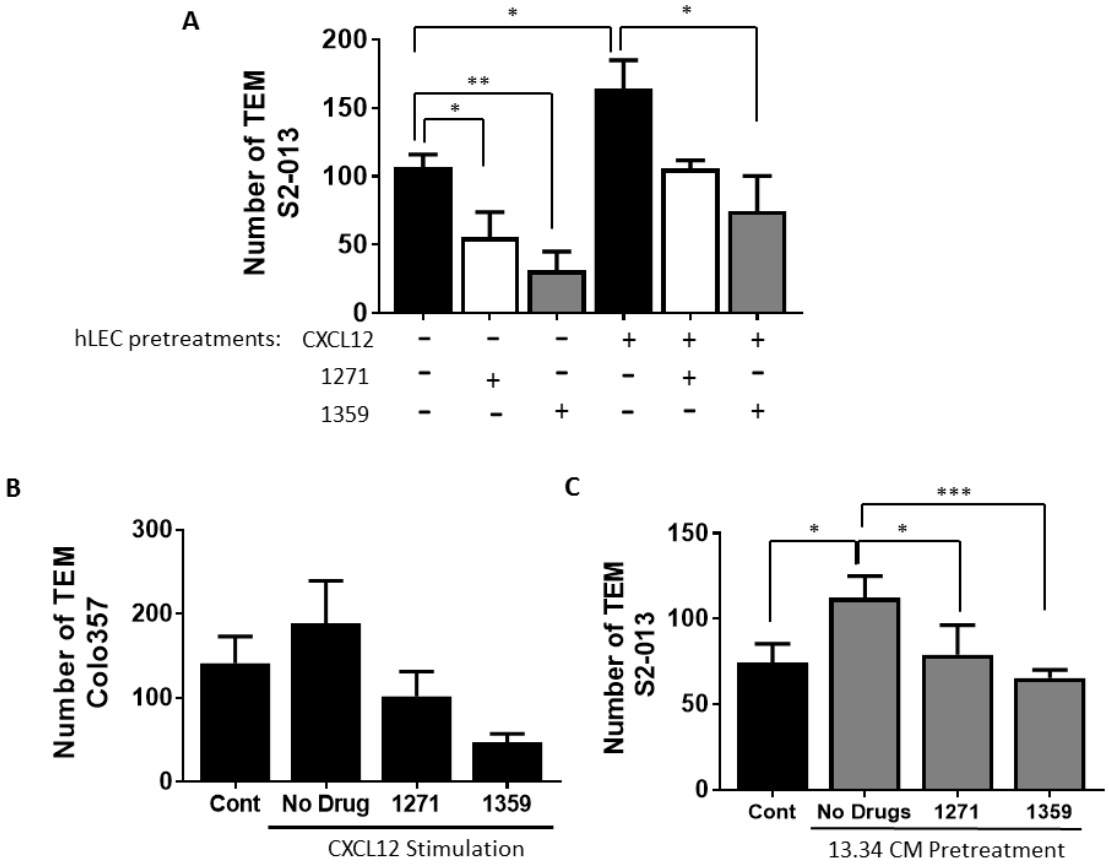

Figure 5.9 CXCL12 stimulation of lymphatic endothelial cells enhances pancreatic tumor transendothelial migration.

A-B) Human LEC monolayers were stimulated with 200 ng/ml CXCL12 for 8 hours and either 10 µg/ml GMI-1271 or GMI-1359 for 1 hour. Monolayers were washed three times prior to the addition of migratory cells so that only hLECs would be affected by CXCL12 and inhibitors. Fluorescently-labeled **A)** S2-013 of **B)** Colo357 cells were plated in the upper insert and allowed to undergo TEM for 20-24 hours. Non-transmigrated PDAC cells were mechanically removed and transmigrated cells were quantified. Graphs represent the mean of 3 replicate membranes; experiment was repeated 3 times. *p<0.05; **p<0.01; error bars = s.d.

C) Human LEC monolayers were stimulated with pancreatic fibroblast conditioned media (CM) for 8 hours and either 10 µg/ml GMI-1271 or GMI-1359 for 1 hour. Monolayers were washed three times prior to the addition of migratory cells so that only hLECs would be affected by CM and inhibitors. Fluorescently labeled S2-013 cells were plated in the upper insert and allowed to undergo TEM for 20-24 hours. Number of transmigrated cells were quantified. Graphs represent the mean of 3 replicate membranes; experiment was repeated 3 times. *p<0.05; ***p<0.001; error bars = s.d.

distributed the mice among 6 treatment groups with 15 mice per group: 1) vehicle control (PBS), 2) GMI-1271, 3) GMI-1359, 4) gemcitabine (Gem), 5) Gem+1271, or 6) Gem+1359. We chose to investigate the effects of using GMI-1359 in combination with gemcitabine because CXCR4 has been implicated in promoting gemcitabine resistance in pancreatic tumor cells (291). GMI-1271 was used in this study to elucidate E-selectin-dependent and CXCR4-dependent effects. Mice were treated for 4 weeks after which they were sacrificed and organs collected for metastatic analysis.

Analysis of tumor size among the treatment groups revealed that monotherapy with GMI-1359 had no impact on PDAC tumor size in these mice (**Figure 5.10A-B**). In accordance with our previous studies, GMI-1271 monotherapy also did not reduce tumor size, but gemcitabine did significantly reduce tumor size. When used in combination with gemcitabine, GMI-1359 treatment did not further reduce tumor size compared to mice treated with gemcitabine monotherapy (**Figure 5.10A-B)**. Histological examination of the tumors both at the primary site and metastatic sites revealed that neither GMI-1271 nor 1359 treatment affected the morphology of the tumor cells (**Figure 5.10C**). None of the mice displayed any drug-induced toxicities when treated with GMI-1359.

Next, we surveyed several representative organ sections from spleen, lymph nodes, liver, lung, kidney, and diaphragm for presence of metastatic lesions by gross microscopic analysis. Results from this metastatic study are displayed in **Figure 5.11A**. In accordance with our previous studies, GMI-1271 monotherapy did not significantly reduce the incidence of metastasis to any of the organs sites examined when compared to the vehicle control treatment group. Gemcitabine monotherapy reduced metastasis to all examined sites compared to control mice. This reduction in metastasis by gemcitabine is likely due to inhibition of primary tumor growth. The combination of gemcitabine and GMI-1271 further reduced the incidence of metastasis to all organ sites except lungs when compared to mice receiving gemcitabine only. Assessment of metastatic sites also revealed that GMI-1359 monotherapy decreased metastatic incidence within the spleen and slightly

Figure 5.10

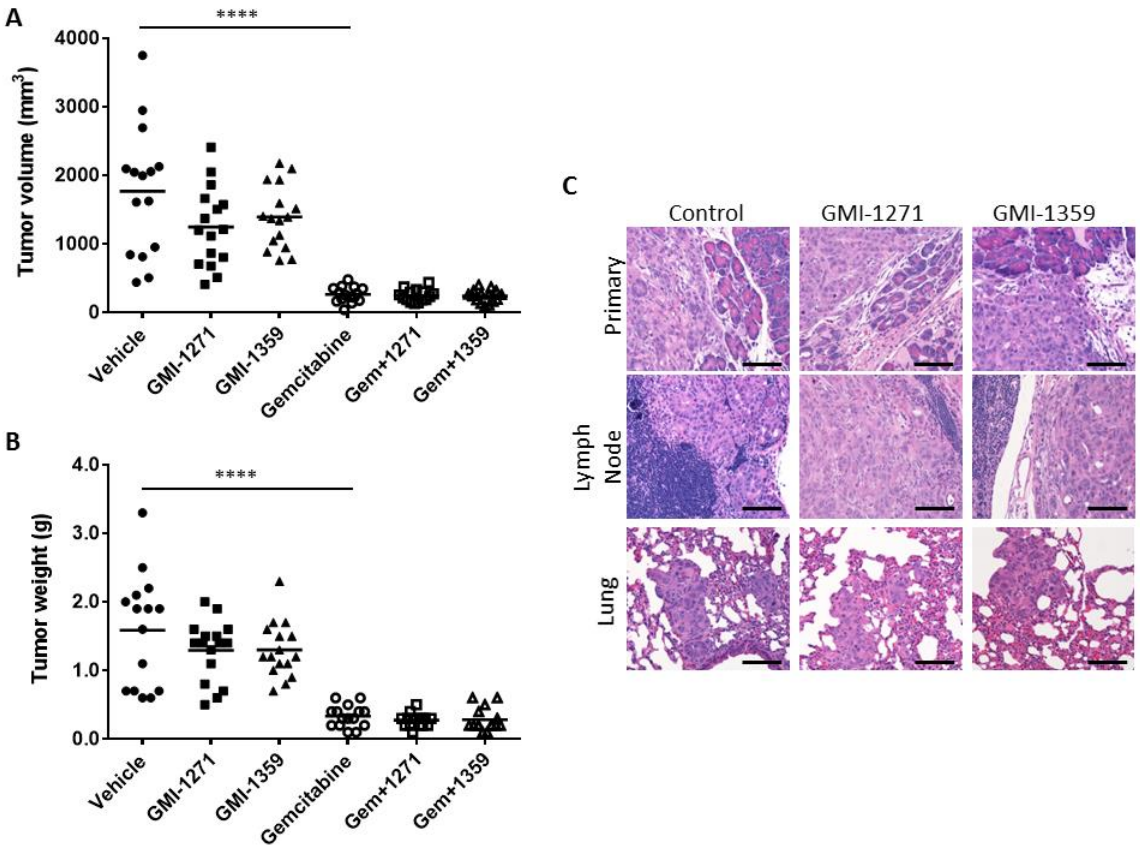

Figure 5.10 GMI-1359 does not affect *in vivo* tumor growth or morphology in an immune incompetent orthotopic model of pancreatic cancer.

Human S2-013 PDAC cells were orthotopically implanted into the pancreases of athymic female mice and allowed to establish for 2 weeks. Treatments were given for 4 weeks, after which tumors and metastatic organs were collected. n = 15 mice/treatment group.

A-B) Graphical representation of **A)** tumor volume (based on length, width, height measurements) and **B)** weight for each treatment group. ****$p<0.0001$

C) Representative histological sections of S2-013 PDAC tumors, lung lesions, and lymph node lesions from mice treated with vehicle control (PBS), GMI-1271, or GMI-1359. Scale bars = 200 µm.

Figure 5.11

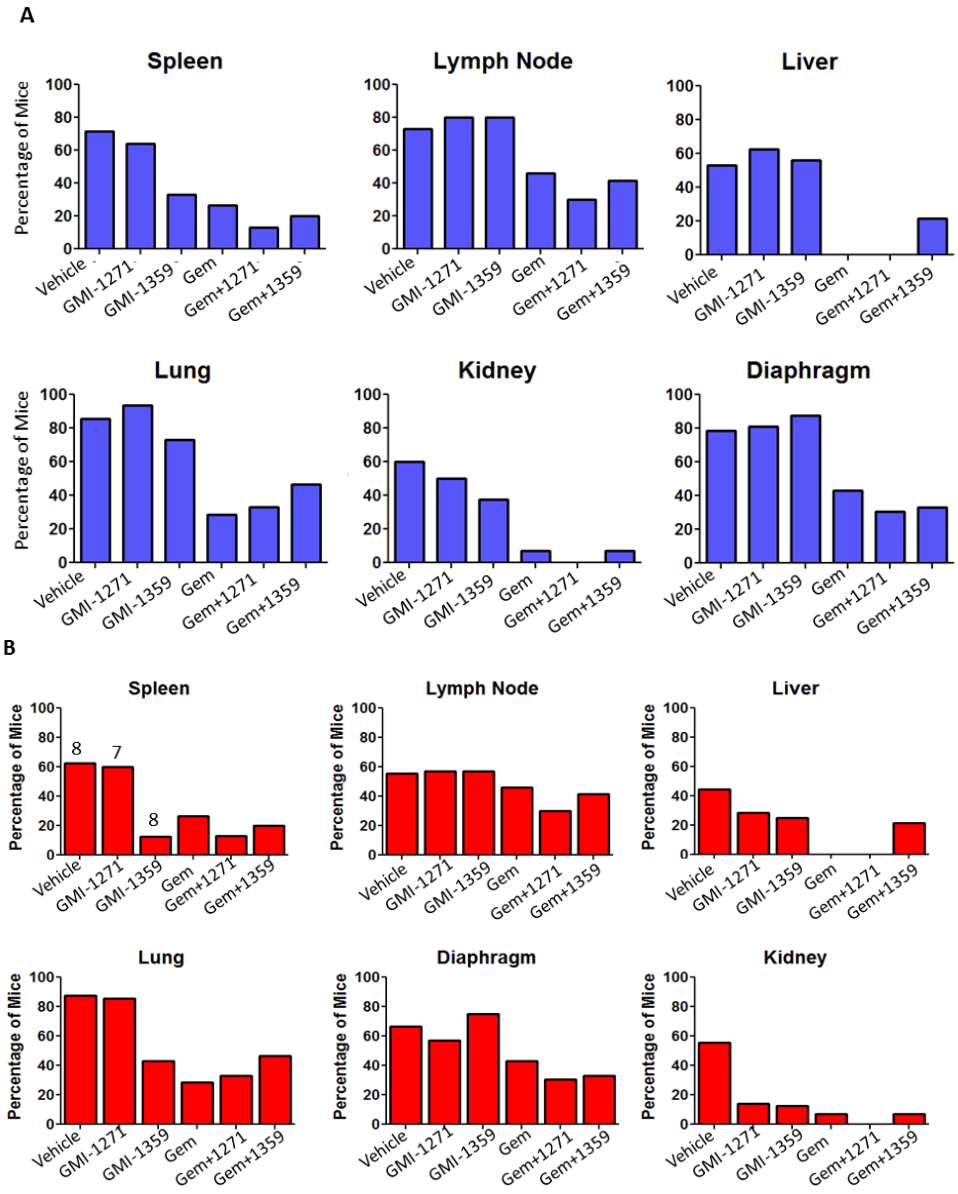

Figure 5.11 GMI-1359 delays metastasis in an immune incompetent orthotopic model of pancreatic cancer.

A) The presence of spontaneous metastatic lesions was identified in spleen, lymph nodes, liver, lungs, kidney, and diaphragm of all mice using histological staining of representative sections. Graphs represent the absolute percentage of mice per treatment group exhibiting spontaneous metastases in the indicated organs. n = 15 mice/group

B) The presence of spontaneous metastatic lesions was identified in spleen, lymph nodes, liver, lungs, kidney, and diaphragm of only mice completing the study. Graphs represent the absolute percentage of mice per treatment group exhibiting spontaneous metastases in the indicated organs. Vehicle n = 8; GMI-1271 n = 7; GMI-1359 n = 8; Gemcitabine, Gem + 1271 and Gem + 1359: n = 15.

within the lungs and kidneys compared to control mice. Surprisingly, the addition of gemcitabine to GMI-1359 therapy had no impact on the incidence of metastasis when compared to mice receiving gemcitabine only. A couple of sites (liver and lung) even demonstrated a slightly increased percentage of mice having metastases when treated with GMI-1359 and gemcitabine.

Approximately half of the mice in the vehicle control, GMI-1271, and GMI-1359 monotherapy groups succumbed to disease prior to the end of the 4-week study. Since these mice most likely would have had advanced disease at death, their results may have obscured any small effect or delay GMI-1359 may have had on S2-013 metastasis. Excluding the mice that died prior to treatment completion, **Figure 5.11B** displays the absolute incidence of metastasis in only the mice surviving to the end of the study. Mice treated with GMI-1359 monotherapy demonstrated significantly reduced metastasis to the spleen, lung, kidney, and liver as compared to vehicle control mice. GMI-1271 had no impact on the incidence of metastasis when only examining the mice that completed the study. This suggests that at the tested dose and treatment schedule, GMI-1359 may delay PDAC metastasis but it does not completely inhibit metastasis *in vivo*.

Blockade of CXCR4 significantly alters the cellular organization of the PDAC tumor microenvironment.

As several cell types comprising the PDAC tumor microenvironment express CXCR4 and use this receptor to facilitate intercellular communications, we evaluated how CXCR4 blockade alters the cellular organization of the tumor microenvironment. Staining for αSMA, a marker for activated fibroblasts, revealed that treatment with GMI-1359 significantly reduced the amount of desmoplasia within the primary tumor (**Figure 5.12A**). Quantification revealed that GMI-1359 resulted in a 2.8-fold reduction in desmoplasia within the primary tumors compared to control tumors (**Figure 5.12B**). This same result was also found among the gemcitabine and GMI-1359 combinatorial treated group: tumors treated with gemcitabine and GMI-1359 had significantly reduced levels of desmoplasia (2.2-fold) compared to tumors treated with gemcitabine alone. Neither gemcitabine nor GMI-1271 had any impact on desmoplasia. These data suggest that the

Figure 5.12

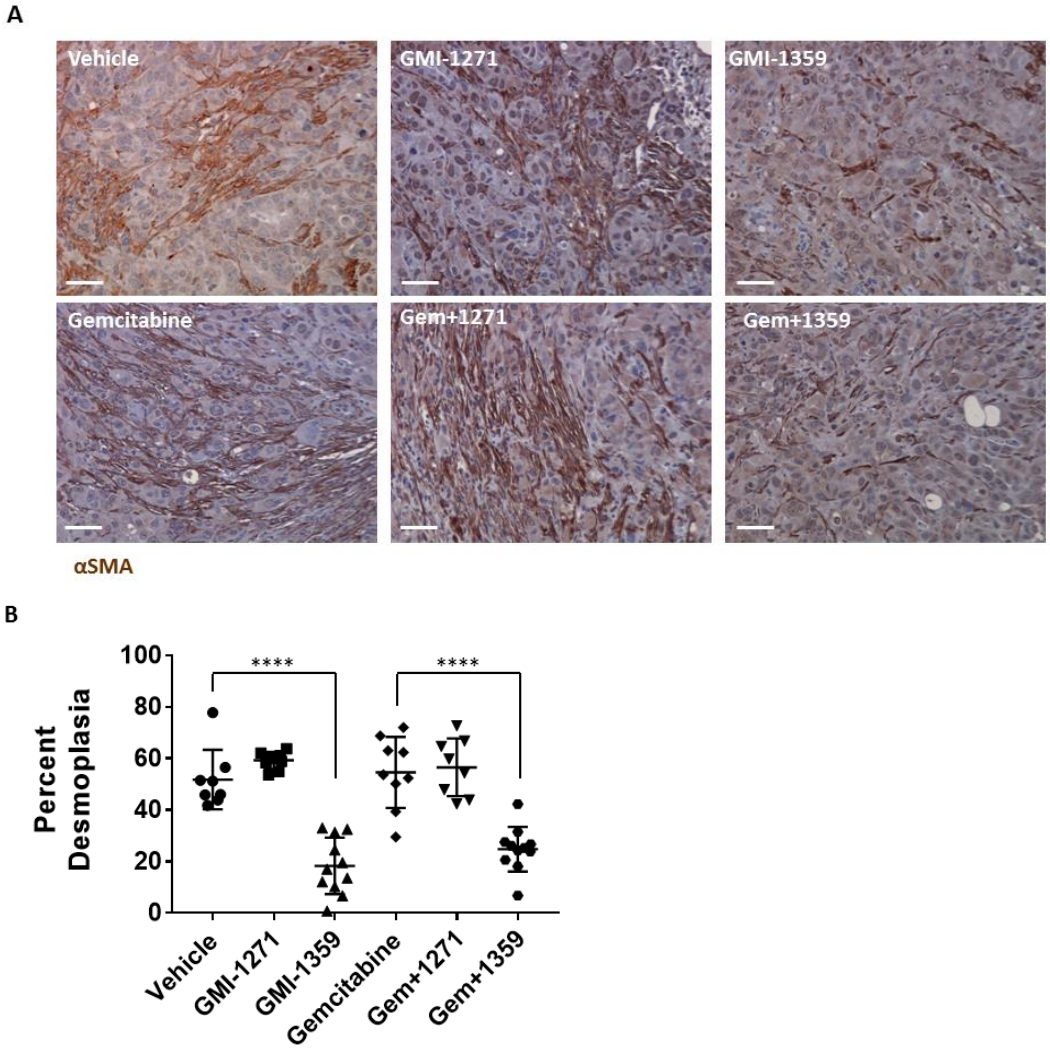

Figure 5.12 *In vivo* treatment with GMI-1359 significantly reduces tumor desmoplasia in an S2-013 orthotopic model of pancreatic cancer.

A) Representative immunohistochemical staining of αSMA (brown) in primary tumors of mice orthotopically challenged with S2-013 PDAC cells and treated with either, PBS, GMI-1271, GMI-1359, and/or gemcitabine for 4 weeks. Counterstaining was performed with hematoxylin (blue). Scale bars = 50 μm.

B) Graphical representation of morphometric quantification of desmoplasia within primary orthotopic tumors following treatment. Grids (1400 pixel^2/box; total of 825 grid boxes/field) were superimposed over 20X images of representative tumor sections. Number boxes containing +αSMA staining was divided by the total number of grid boxes and multiplied by 100 to calculate percent desmoplasia/field. Two to three representative images were collected per section from 4 mice/treatment group. Primary tumors from mice treated with GMI-1359 had a marked reduction in desmoplasia. ****$p<0.0001$; error bars = s.d.

CXCL12-CXCR4 axis plays a significant role in the recruitment and/or activation of fibroblasts within PDAC primary tumors.

Next, lymphatic (LVD) and blood (BVD) vessel densities within the primary tumor site were evaluated. Immunofluorescence staining of LYVE-1, a marker of LECs, in primary tumor sections revealed that neither gemcitabine nor GMI-1271 affected LVD (**Figure 5.13A-B**). However, tumors from mice treated with GMI-1359 had drastically fewer lymphatic vessels within the primary tumor site. Reduced LVD was also found in mice treated with both gemcitabine and GMI-1359. Unexpectedly, immunohistochemical staining for CD31, an endothelial marker, revealed no difference in BVD among any of the treatment groups (**Figure 5.14A-B**). These data suggest that the CXCL12-CXCR4 chemokine axis may be a critical player in the recruitment of lymphatic vessels to tumor sites through either direct or indirect mechanisms. Additionally, these data demonstrate that blood vessel recruitment is not necessarily regulated by the same mechanisms as lymphatic vessel recruitment.

Lastly, we evaluated the presence of $CD45^+$ leukocytes within the primary tumors of the various treatment groups. Immunohistochemical staining and quantification revealed no difference in the total number of immune cells present within the primary tumors (**Figure 5.15A-B**). Intratumoral tertiary lymphoid aggregates (TLAs) were also quantified (**Figure 5.15C-D**), and analysis revealed there was no difference in the total number of TLAs present per tumor section among the 6 treatment groups.

GMI-1359 does not prolong survival of orthotopically-challenged athymic mice.

Although GMI-1359 demonstrated only a slight delay in PDAC metastasis, it resulted in a significant reorganization of the PDAC tumor microenvironment. We next investigated whether GMI-1359 treatment and the reduction in desmoplasia may extend animal survival. We performed similar *in vivo* experiments as described earlier, but rather than stopping the study at 4 weeks, we treated mice until they reached end stage disease. When used as monotherapies, neither GMI-1271

Figure 5.13

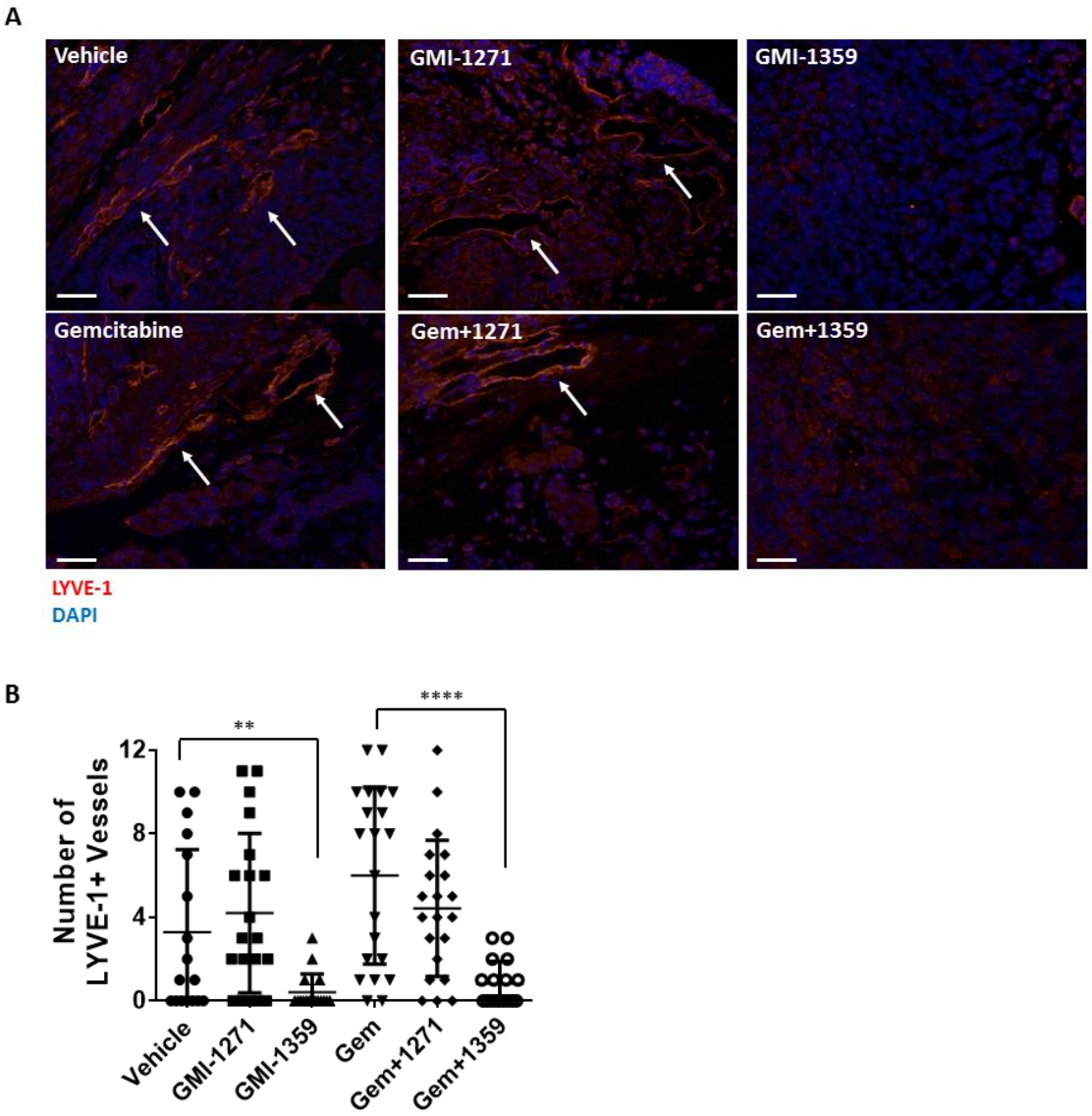

Figure 5.13 Orthotopically challenged mice treated with GMI-1359 demonstrate a marked reduction in lymphatic vessel densities.

A) Representative immunofluorescent staining of LYVE-1^{+} (red) lymphatic vessels within primary tumors of mice orthotopically challenged with S2-013 PDAC cells and treated with either, PBS, GMI-1271, GMI-1359, and/or gemcitabine for 4 weeks. Nuclei are stained with DAPI (blue). Arrows indicate LYVE-1+ lymphatic vessels. Scale bars = 50 µm.

B) Quantification of the number of LYVE-1^{+} lymphatic vessels per field within the primary tumor. Five (20X magnification) representative images were collected per tumor section from 4 mice within each treatment group. GMI-1359-treated tumors displayed a significant reduction in lymphatic vascular densities. **p<0.01; ****p<0.0001; Error bars = s.d.

Figure 5.14

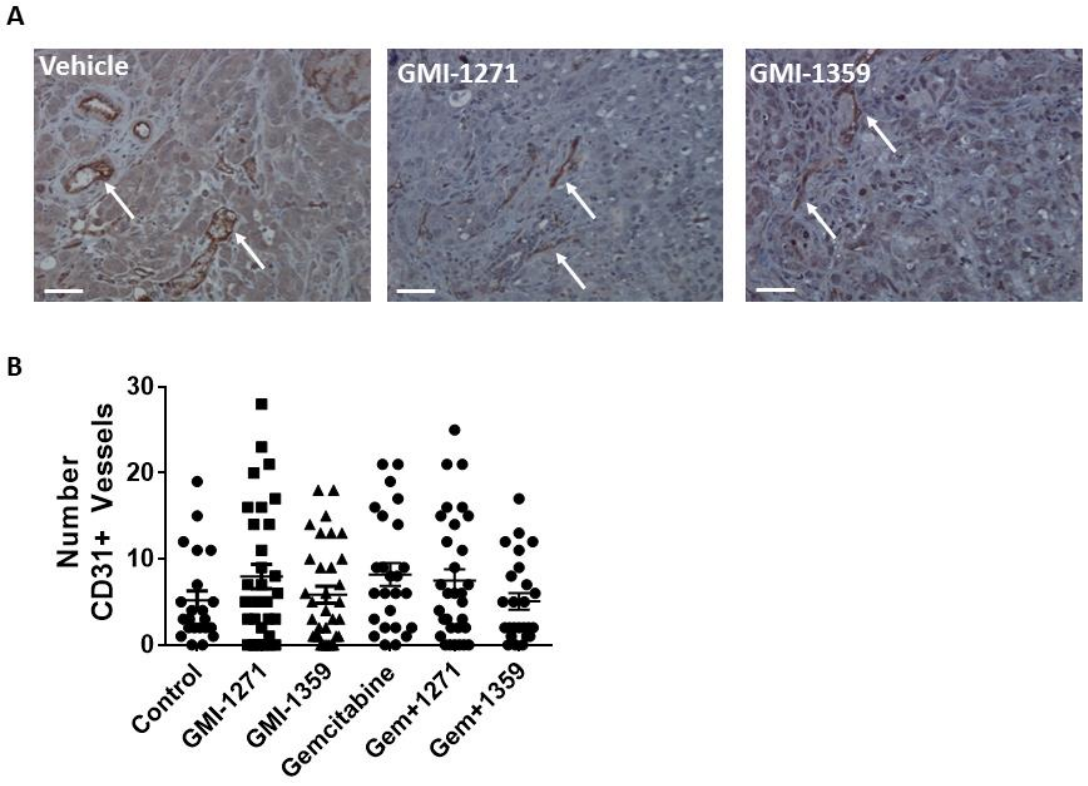

Figure 5.14 Orthotopically challenged mice treated with GMI-1359 demonstrate no change in blood vessel densities.

A) Representative immunohistochemical staining of $CD31^+$ (brown) blood vessels within primary tumors of mice orthotopically challenged with S2-013 PDAC cells and treated with either, PBS, GMI-1271, or GMI-1359 for 4 weeks. Sections were counterstained with hematoxylin (blue). Arrows indicate CD31+ blood vessels. Scale bars = 50 µm.

B) Quantification of the number of $CD31^+$ blood vessels per field within the primary tumor. Five (20X magnification) representative images were collected per tumor section from 4 mice within each treatment group. GMI-1359 treatment had no impact on blood vessel densities within the primary tumor. Error bars = s.d.

Figure 5.15 Orthotopic tumors treated with GMI-1359 demonstrate no change in immune infiltration compared to control mice.

A) Representative immunohistochemical staining of $CD45^+$ (brown) leukocytes within primary tumors of mice orthotopically challenged with S2-013 PDAC cells and treated with either, PBS, GMI-1271, GMI-1359, and/or gemcitabine for 4 weeks. Sections were counterstained with hematoxylin (blue). Scale bars = 50 μm.

B) Quantification of the number of $CD45^+$ leukocytes per field within the primary tumors. Five (20X magnification) representative images were collected per tumor section from 4 mice within each treatment group. GMI-1359 treatment had no impact on immune cell infiltration within the primary tumor. Error bars = s.d.

C) Representative immunohistochemical staining of $CD45^+$ (brown) tertiary lymphoid aggregates (TLAs) within primary tumors of mice orthotopically challenged with S2-013 PDAC cells and treated with either, PBS, GMI-1271, GMI-1359, and/or gemcitabine for 4 weeks. Arrow indicates a TLA. Sections were counterstained with hematoxylin (blue). Scale bars = 100 μm

D) Quantification of the number of $CD45^+$ TLAs per primary tumor section for all orthotopically-challenged mice. GMI-1359 treatment had no impact on immune cell infiltration within the primary tumor. Error bars = s.d.

Figure 5.15

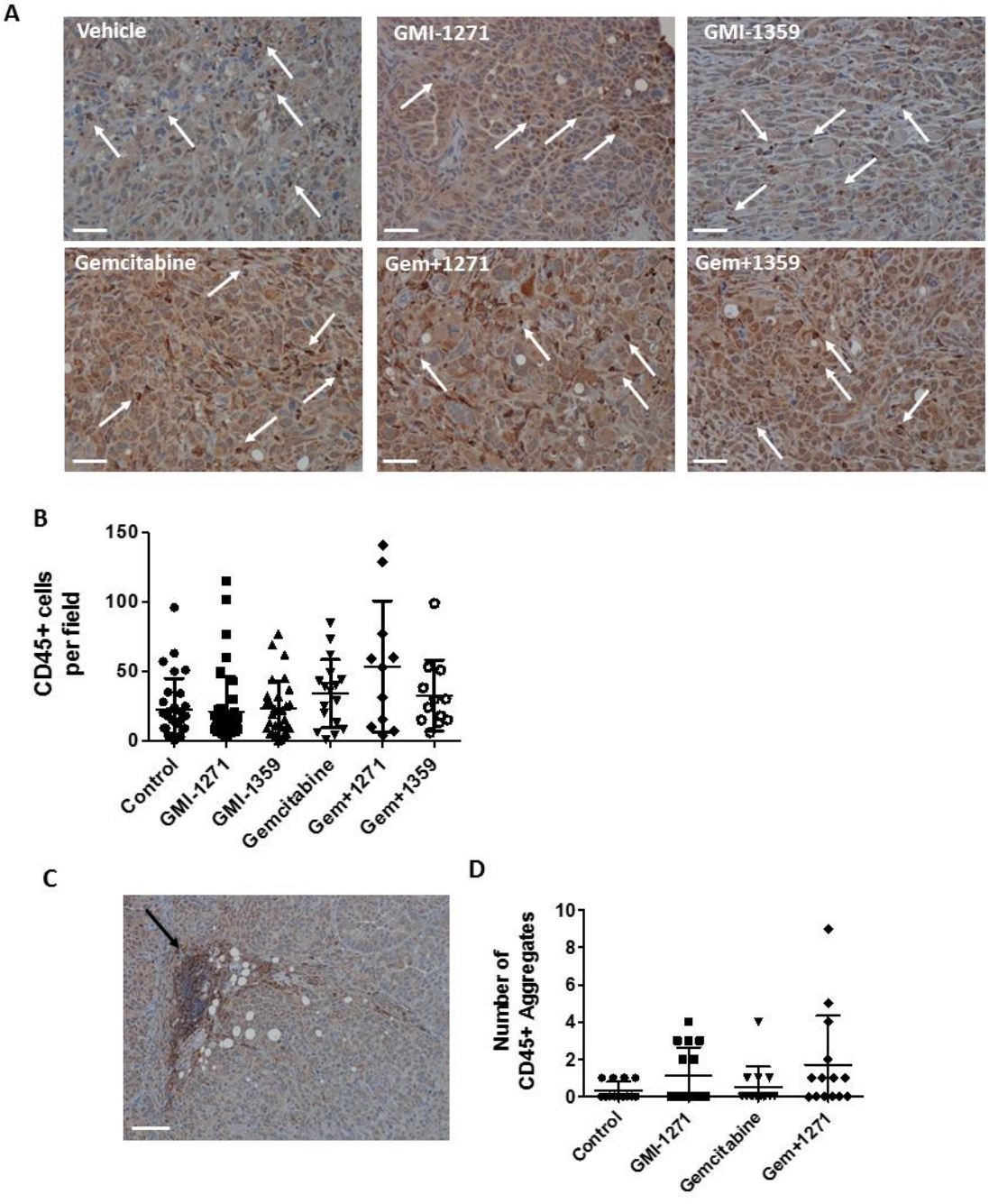
A
Vehicle
GMI-1271
GMI-1359
Gemcitabine
Gem+1271
Gem+1359
B
CD45+ cells per field
150
100
50
0
Control
GMI-1271
GMI-1359
Gemcitabine
Gem+1271
Gem+1359
C
D
Number of CD45+ Aggregates
10
8
6
4
2
0
Control
GMI-1271
Gemcitabine
Gem+1271

nor 1359 prolonged animal survival as compared to the control group (**Figure 5.16A**). We also performed these same treatments in combination with gemcitabine since GMI-1359 reduced desmoplasia in the tumors and that might result in improved chemotherapy to the tumor. Unfortunately, combinatorial treatment of GMI-1271 or 1359 with gemcitabine also did not prolong survival when compared to mice receiving gemcitabine only (**Figure 5.16B**). Comparison of tumor weight and volume revealed no significant difference in tumor size among the mice treated with GMI-1271 or GMI-1359 compared to vehicle-treated mice (**Figure 5.16C**). Mice treated with gemcitabine had significantly smaller tumors at end stage disease compared to vehicle control-treated mice. Combinatorial treatment of GMI-1271 or GMI-1359 with gemcitabine did not further reduce tumor size.

GMI-1359 does not prolong survival of orthotopically-challenged immune competent mice.

CXCR4 signaling has been shown to inhibit T cell responses in pancreatic cancer (171). We next evaluated if GMI-1359 may prolong survival in immune competent mice where T cell responses may be impacted by CXCR4 blockade. For initial studies, we chose to orthotopically implant PDAC cells isolated from primary tumors of *LSL-Kras$^{G12D/+}$;LSL-Trp53$^{R172H/+}$;Pdx-1-Cre* (KPC) mice into syngeneic immune competent C57BL/6 mice. To determine if isolated KPC PDAC cells would respond to GMI-1271 or 1359 treatments, we evaluated two lines, KPC8060 and KPC8069 for CXCR4 expression and E-selectin binding. Flow cytometry (**Figure 5.17A**), immunofluorescence staining (**Figure 5.17B**), and immunoblotting (**Figure 5.17C**) all confirmed that these KPC lines express CXCR4. GlycoMimetics, Inc. assessed the ability of KPC8060 and KPC8069 to interact with E-selectin using mouse E-selectin-Fc chimeric proteins. Employing flow cytometry as a readout, they demonstrated that both KPC lines had an enhanced ability to bind to the E-selectin chimeras as compared to IgG-Fc negative control chimeras (data not shown).

Initial in vivo studies with the KPC 8060 mouse PDAC line were performed in a similar manner as the S2-013 studies. Briefly, 9 x 10^4 KPC 8060 cells were implanted into the pancreases

Figure 5.16

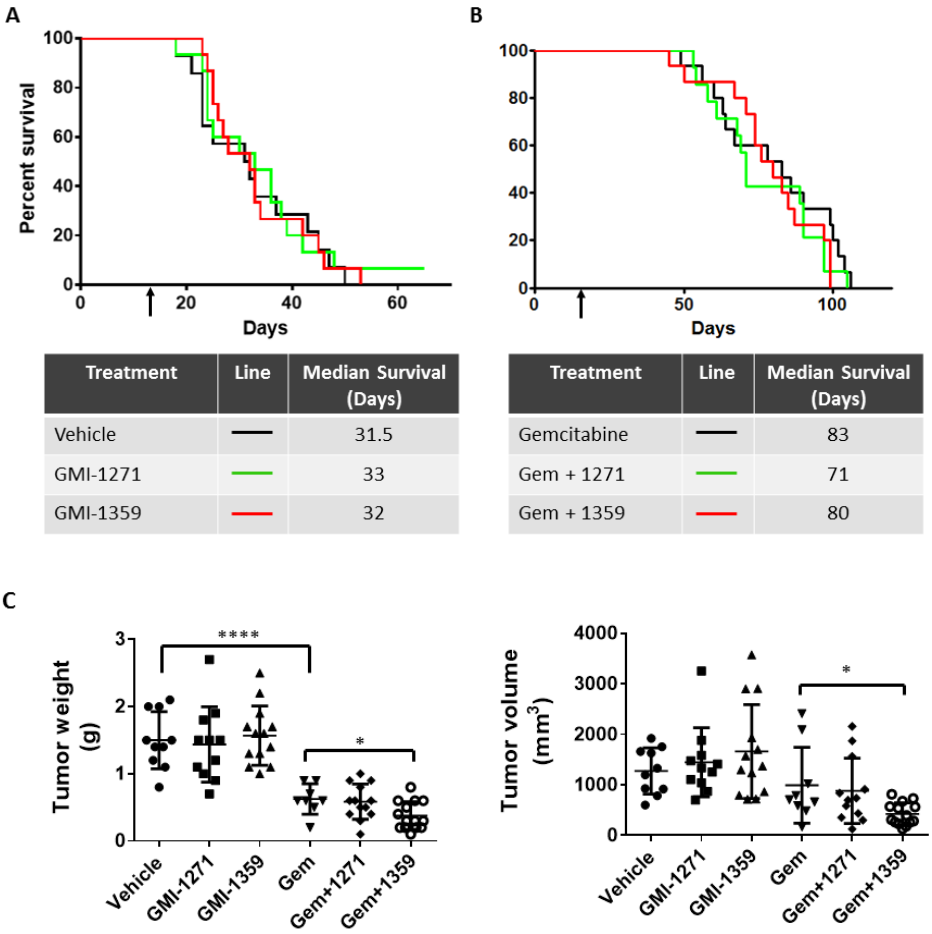

Treatment	Line	Median Survival (Days)
Vehicle		31.5
GMI-1271		33
GMI-1359		32

Treatment	Line	Median Survival (Days)
Gemcitabine		83
Gem + 1271		71
Gem + 1359		80

Figure 5.16 GMI-1359 does not prolong survival of orthotopically challenged immune incompetent mice whether administered as a monotherapy or in combination with chemotherapy.

A) Kaplan-Meier survival curve of immune incompetent mice orthotopically challenged with S2-013 PDAC cells. Following tumor establishment, mice were treated with vehicle control (PBS), GMI-1271, or GMI-1359 until end stage disease. Arrows specify treatment start day. Tables denote median survival (in days) for each treatment group. Log-rank tests indicate no survival benefit for mice treated with GMI-1271 or GMI-1359 compared to vehicle control. n = 15 mice/treatment group

B) Kaplan-Meier survival curve of immune incompetent mice orthotopically challenged with S2-013 PDAC cells. Following tumor establishment, mice were treated with vehicle control gemcitabine (Gem), Gem+1271, or Gem+1359 until end stage disease. Arrows specify treatment start day. Tables denote median survival (in days) for each treatment group. Gemcitabine significantly extended survival compared to vehicle control mice ($p<0.0001$). Log-rank tests indicated no survival benefit for mice treated with Gem+1271 or Gem+1359 compared to mice receiving only gemcitabine. n = 15 mice/treatment group.

C) Graphical representation of tumor weight and tumor volume for each treatment group. *$p<0.05$, ****$p<0.0001$; error bars = s.d.

Figure 5.17

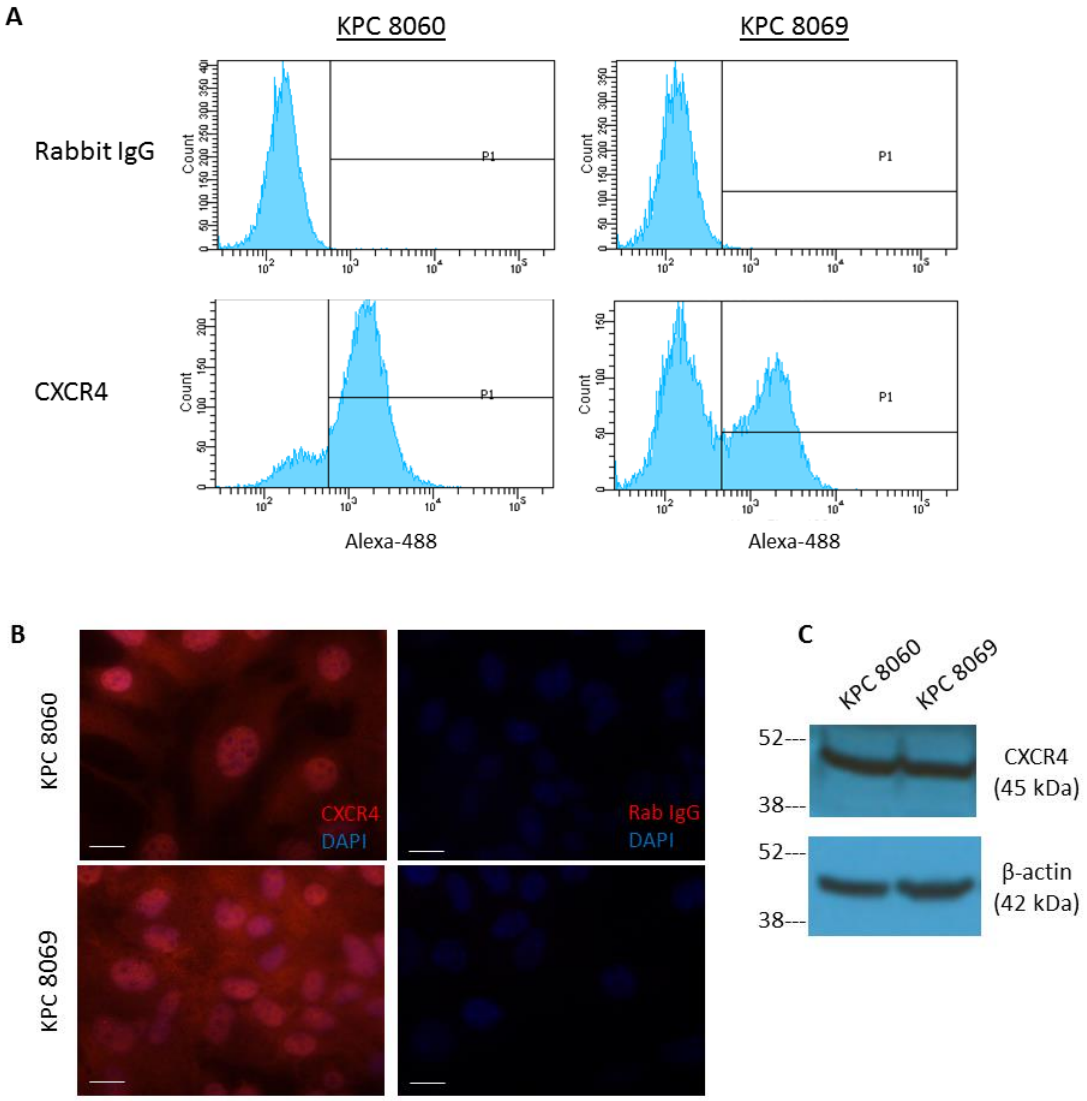

Figure 5.17 PDAC cells isolated from KPC mice express CXCR4.

A) Flow cytometry confirming expression of CXCR4 in mouse PDAC cell lines KPC8060 and KPC8069. The upper histograms indicate IgG isotype control labeling and the lower histograms indicate CXCR4 labeling. Both KPC cell lines demonstrate CXCR4 expression.

B) Immunofluorescence staining indicating CXCR4 expression in mouse PDAC cell lines KPC8060 and KPC8069. CXCR4 (red) is diffusely expressed across the cell surface. Cell nuclei are stained with DAPI (blue). Rabbit polyclonal isotype control was used as a negative control (red; far right images). Scale bars = 25 µm

C) Western blot (50 µg protein/lane) analysis demonstrating CXCR4 expression in a panel of mouse KPC8060 and KPC8069 lysates. β-actin expression was used as a loading control for all cell lines.

of syngeneic C57BL/6 mice. Tumors were allowed to establish for 2 weeks prior to the initiation of treatment. Unexpectedly, KPC 8060 cells demonstrated very rapid and aggressive growth in vivo. By the treatment start day, some mice were already showing signs of advanced disease such as cachexia or death. Neither GMI-1271 nor 1359 monotherapies prolonged animal survival (**Figure 5.18A**). Treatment with gemcitabine alone nearly doubled animal survival compared to control mice (p=0.0124; **Figure 5.18B**). Unexpectedly, combinatorial treatment with gemcitabine and GMI-1271 resulted in a statistical increase in animal survival compared to mice receiving gemcitabine only (p=0.0302). Combinatorial treatment with gemcitabine and GMI-1359 had no impact on animal survival when compared to the gemcitabine group. Histological staining revealed no significant difference in tumor morphology among the treatment groups (**Figure 5.18C**), and all mice had similarly sized primary tumors at death regardless of treatment (**Figure 5.18D**).

Due to the aggressive growth of KPC8060 tumors in vivo, we repeated the survival study but with treatments beginning the day following orthotopic challenge. Similar to the previously described study, GMI-1271 and GMI-1359 monotherapies failed to prolong animal survival even when treatments were administered during early stage disease (**Figure 5.19A**). Additionally, combinatorial treatment of GMI-1271 or GMI-1359 with gemcitabine also failed to prolong animal survival compared to mice receiving gemcitabine alone (**Figure 5.19B**). Analysis of tumor size revealed that mice treated with gemcitabine either alone or in combination with GMI-1271 or 1359 succumb to PDAC with statistically larger tumors than their control or monotherapy counterparts (**Figure 5.19C**).

Incidence of metastasis in the KPC8060 orthotopic model with GMI-1271 or GMI-1359 treatment.

To determine the effects of GMI-1271 and 1359 on metastasis in immune competent mice, a pilot study was performed in the KPC8060 orthotopic model. KPC8060 cells were implanted into the pancreases of C57BL/6 mice. Treatments were initiated the day after implantation. After 2 weeks of treatment, mice were sacrificed and tissues collected and processed for microscopic

Figure 5.18 GMI-1359 does not prolong survival of orthotopically challenged immune competent mice with aggressive late stage disease, but GMI-1271 does when used in combination with gemcitabine.

A) Kaplan-Meier survival curve of immune competent mice orthotopically challenged with KPC8060 PDAC cells. Following tumor establishment, mice were treated with vehicle control (PBS), GMI-1271, or GMI-1359 until end stage disease. Arrows specify treatment start day. Tables denote median survival (in days) for each treatment group. Log-rank tests indicate no survival benefit for mice treated with GMI-1271 or GMI-1359 monotherapies compared to vehicle control. n = 10 mice/treatment group

B) Kaplan-Meier survival curve of immune competent mice orthotopically challenged with KPC8060 PDAC cells. Following tumor establishment, mice were treated with vehicle control gemcitabine (Gem), Gem+1271, or Gem+1359 until end stage disease. Arrows specify treatment start day. Tables denote median survival (in days) for each treatment group. Gemcitabine significantly extended survival compared to vehicle control mice ($p=0.0124$). Log-rank tests indicate a survival benefit for mice treated with Gem+1271 compared to mice treated with gemcitabine only ($p=0.0302$). There was no survival benefit for mice treated with Gem+1359 compared to mice receiving only gemcitabine. n = 10 mice/treatment group.

C) Representative histological sections of KPC8060 orthotopic tumors treated with vehicle control (PBS), GMI-1271, or GMI-1359. Scale bars = 50 μm.

D) Graphical representation of tumor volume and weight for each treatment group. Error bars = s.d.

Figure 5.18

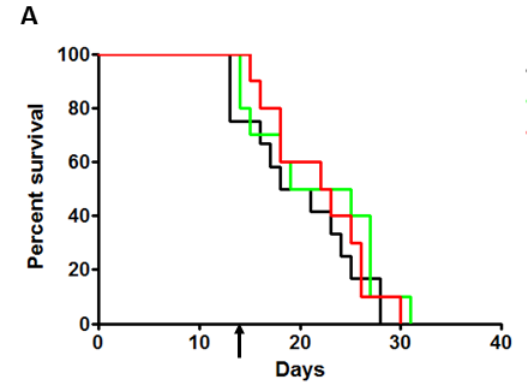

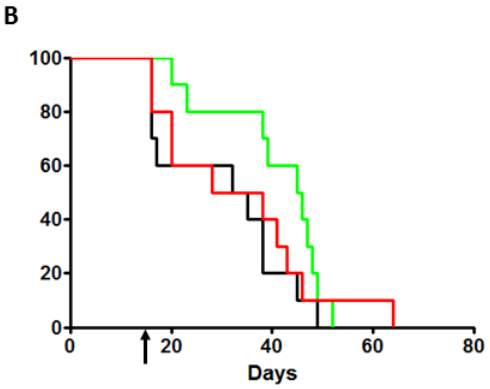

Treatment	Line	Median Survival (Days)
Vehicle		19.5
GMI-1271		22
GMI-1359		22.5

Treatment	Line	Median Survival (Days)
Gemcitabine		33.5
Gem + 1271		45.5
Gem + 1359		33

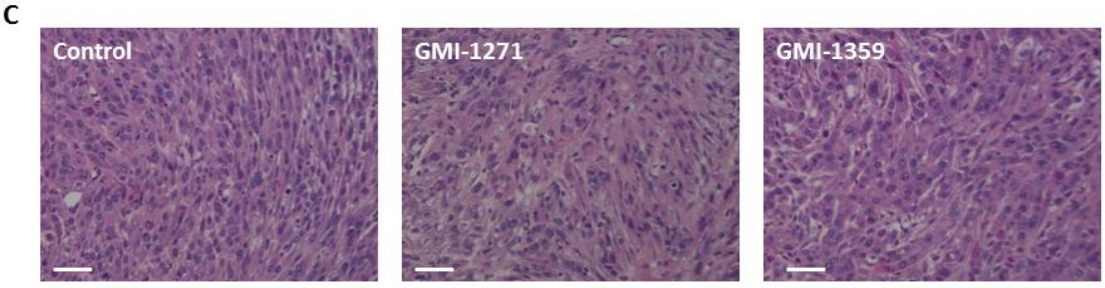

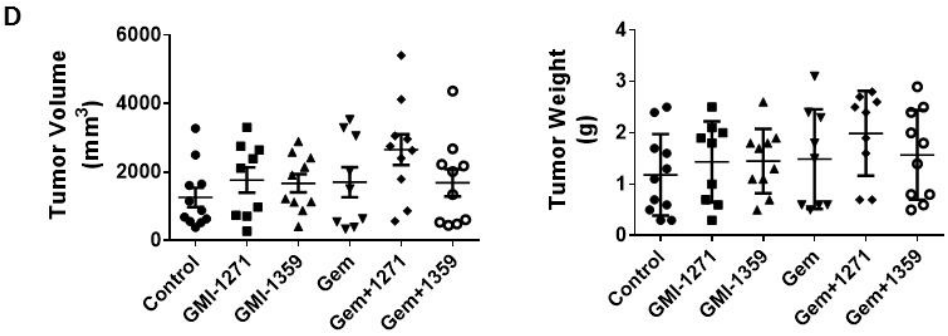

Figure 5.19 GMI-1359 does not prolong survival of orthotopically challenged immune competent mice with early stage disease.

A) Kaplan-Meier survival curve of immune competent mice orthotopically challenged with KPC8060 PDAC cells. Treatments began the day after PDAC cell implantation and continued until mice reach end stage disease. Tables indicate median survival (in days) for each treatment group. Log-rank tests indicate no survival benefit for mice treated with GMI-1271 or GMI-1359 compared to vehicle control. n = 10 mice/treatment group

B) Kaplan-Meier survival curve of immune competent mice orthotopically challenged with KPC8060 PDAC cells Treatments began the day after PDAC cell implantation and continued until mice reach end stage disease. Tables indicate median survival (in days) for each treatment group. As expected, gemcitabine significantly extended survival compared to vehicle control mice (*$p<0.0001$*). Log-rank tests indicate no survival benefit for mice treated with Gem+1271 or Gem+1359 compared to mice receiving only gemcitabine. n = 10 mice/treatment group.

C) Graphical representation of tumor weight and tumor volume for each treatment group. KPC8060 orthotopically challenged mice treated with gemcitabine, Gem+1271, or Gem+1359 had statistically larger tumors than their non-gemcitabine treated counterparts (GMI-1271 vs Gem+ 1271: $p<0.0001$; GMI-1359 vs Gem+1359 $p =0.0189$). *$p<0.05$; **$p<0.01$; $p<0.001$; error bars = s.d.

Figure 5.19

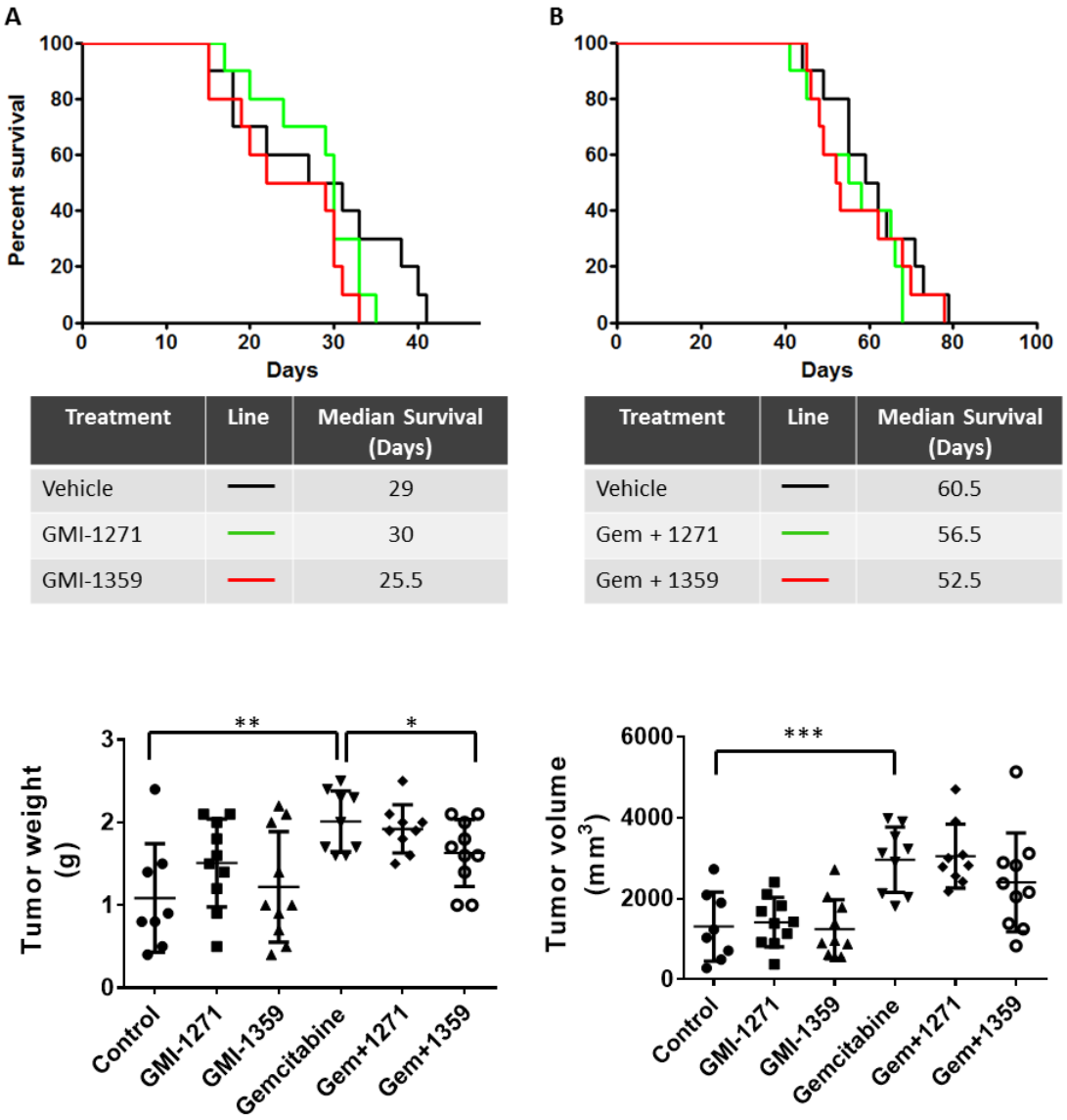

Treatment	Line	Median Survival (Days)
Vehicle		29
GMI-1271		30
GMI-1359		25.5

Treatment	Line	Median Survival (Days)
Vehicle		60.5
Gem + 1271		56.5
Gem + 1359		52.5

identification of metastases. All mice survived to the end of the 2-week treatment period; however, many of the mice were demonstrating signs of advanced disease such as lethargy and significant weight loss. Similar to previous studies, *in vivo* treatment with GMI-1271 or 1359 had no impact on tumor size (**Figure 5.20A**). Examination of organs for metastatic lesions revealed that very few organs contained metastatic lesions after 2 weeks of tumor progression in the KPC8060 orthotopic model even though the animals demonstrated symptoms of advanced stage disease (**Figure 5.20B**). This suggests that KPC8060 orthotopic challenge may not be a good model for metastatic studies. Treatment with either GMI-1271 or 1359 had no significant impact on the incidence of metastasis in these mice. Flow cytometry revealed that treatment with GMI-1271 or 1359 had no impact on the immune cell subtypes (T cells, B cells, NK cells, macrophages, MDSCs, or dendritic cells) present within the primary tumors (**Figure 5.20C**).

***In vivo* efficacy of GMI-1271 and 1359 in combination with chemo- and immunotherapies.**

Ozdemir et al. demonstrated that although loss of αSMA+ CAFs in PDAC tumors resulted in more aggressive tumors, it also made these tumors susceptible to immunotherapy (175). Additionally, another recent study demonstrated that ablation of FAP+ CAFs in KPC mice also improved checkpoint antagonist immunotherapy (171). To go along with this, they also demonstrated that treatment with AMD3100, a CXCR4 antagonist, also improved immunotherapy efficacy, resulting in significant tumor regression in KPC mice. This study examined tumor regression for only a short period (6 days) and did not examine the results of chronic inhibition of CXCR4. Therefore, we evaluated whether CXCR4 blockade with GMI-1359 could improve immunotherapy efficacy and impair PDAC progression over an extended period of time. For initial studies that could be done rapidly, we evaluated the efficacy of GMI-1359 and anti-PD-L1 combinatorial therapy in our orthotopic model with KPC8060 PDAC cells. Seven treatment groups were set up with 10 mice per group: 1) Vehicle, 2) anti-PD-L1, 3) anti-PD-L1 + 1271, 4) anti-PD-L1 + 1359, 5) anti-PD-L1 + Gem, 6) anti-PD-L1 + Gem + 1271, and 7) PD-L1 + Gem + 1359.

Mice were treated until end stage disease and then necropsies performed. The survival curves indicate that the addition of GMI-1271 or 1359 to anti-PD-L1 immunotherapy did not result in extended survival compared to PD-L1 treatment alone (**Figure 5.21A**). Treatment with both gemcitabine and anti-PD-L1 significantly improved survival compared to anti-PD-L1 therapy alone ($p<0.0001$; **Figure 5.21B**). However, the addition of GMI-1271 or GMI-1359 did not result in significantly improved survival compared to mice receiving the PD-L1/gemcitabine combination (**Figure 5.21B**). Analysis of tumor size revealed no major difference across the 7 treatment groups (**Figure 5.21C**).

Figure 5.20 GMI-1359 does not impact metastasis of KPC cells orthotopically implanted into immune competent mice.

A) Graphical representation of tumor volume and tumor weight for mice treated with vehicle control, GMI-1271 or GMI-1359 for 2 weeks following KPC8060 tumor implantation in C57BL/6 mice. Treatment began the day after implantation and continued for 14 days. n = 5 mice/group; error bars = s.d.

B) The presence of spontaneous metastatic lesions was identified in lungs, lymph nodes, spleen, kidney, diaphragm, and liver of all mice using histological staining of representative sections. Graphs represent the absolute percentage of mice per treatment group exhibiting spontaneous metastases in the indicated organs. n = 5 mice/group

C) Flow cytometry analysis of immune cell subtypes within KPC8060 primary tumors of mice treated with vehicle control, GMI-1271, or GMI-1359 for 2 weeks. n = 5 mice/group; error bars = s.d.

Figure 5.20

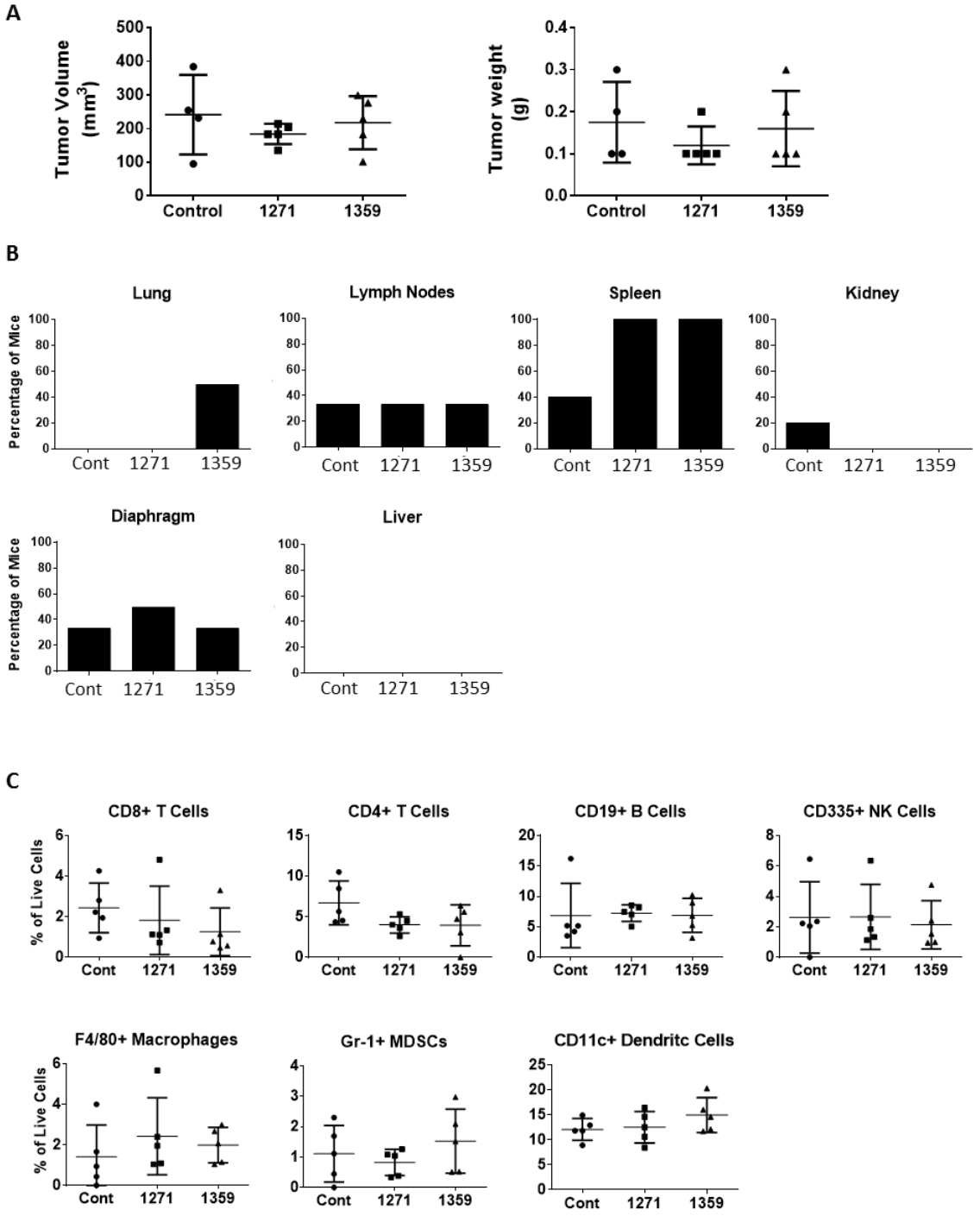
A
Tumor Volume (mm3)
500
400
300
200
100
0
Control
1271
1359
Tumor weight (g)
0.4
0.3
0.2
0.1
0.0
Control
1271
1359
B
Lung
Lymph Nodes
Spleen
Kidney
Percentage of Mice
100
80
60
40
20
0
Cont
1271
1359
Diaphragm
Liver
C
CD8+ T Cells
CD4+ T Cells
CD19+ B Cells
CD335+ NK Cells
% of Live Cells
F4/80+ Macrophages
Gr-1+ MDSCs
CD11c+ Dendritc Cells

Figure 5.21 GMI-1359 does not prolong survival of orthotopically challenged immune competent mice whether administered in combination with chemotherapy or immunotherapy.

A) Kaplan-Meier survival curve of immune competent mice orthotopically challenged with KPC8060 PDAC cells and treated with GMI-1271 or GMI-1359 and immunotherapy anti-PD-L1. Treatments began the day after PDAC cell implantation and continued until mice reach end stage disease. Tables denote median survival (in days) for each treatment group. Log-rank tests indicate no survival benefit for mice treated with a combination of PD-L1 and GMI-1271 or GMI-1359 compared to receiving the vehicle control or anti-PD-L1 only. n = 10 mice/treatment group.

B) Kaplan-Meier survival curve of immune competent mice orthotopically challenged with KPC8060 PDAC cells and treated with GMI-1271 or GMI-1359 and immunotherapy anti-PD-L1. Treatments began the day after PDAC cell implantation and continued until mice reach end stage disease. Tables denote median survival (in days) for each treatment group. Log-rank tests indicate no survival benefit for mice treated with a combination of PD-L1 and gemcitabine with GMI-1271 or GMI-1359 compared to receiving PD-L1 and gemcitabine only. Addition of gemcitabine to PD-L1 treatment significantly improved survival in this KPC orthotopic model ($p<0.0001$). n = 10 mice/treatment group.

C) Graphical representation of tumor volume and tumor weight for mice treated with GMI-1271 or GMI-1359 in combination with chemotherapy (gemcitabine) and/or immunotherapy (anti-PD-L1). Error bars = s.d.

Figure 5.21

A

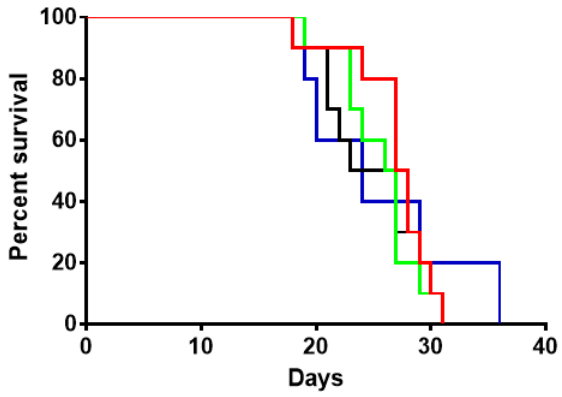

Treatment	Line	Median Survival (Days)
Vehicle		24
PD-L1		25
PD-L1 + 1271		26.5
PD-L1 + 1359		27.5

B

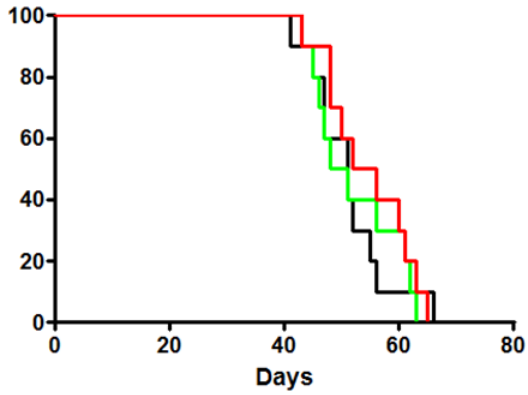

Treatment	Line	Median Survival (Days)
PD-L1 + Gem		51
PD-L1 + Gem +1271		49.5
PD-L1 + Gem+ 1359		54

C

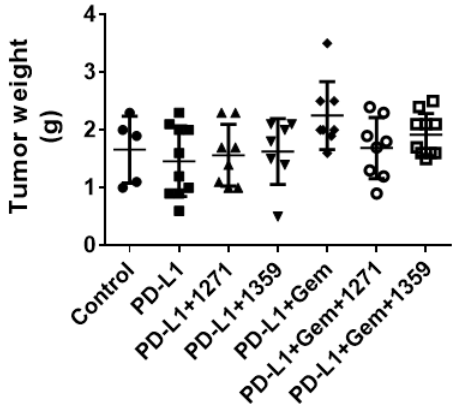

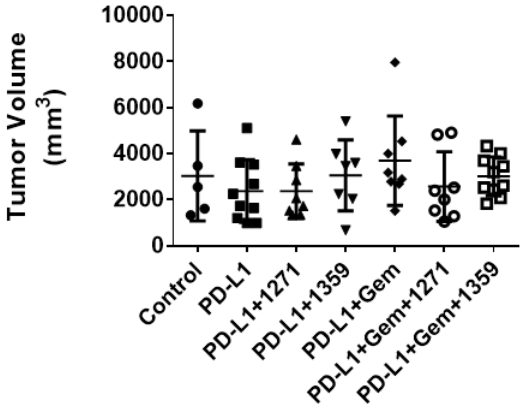

III. Conclusions

Our results indicate that the CXCL12-CXCR4 chemokine axis mediates interactions between cellular components of the PDAC microenvironment including tumor cells, fibroblasts and endothelial cells. Using a novel dual inhibitor of E-selectin and CXCR4, GMI-1359, we demonstrate that pancreatic fibroblast secretion of CXCL12 strongly induces hLEC migration and that when CXCR4 is blocked through GMI-1359 treatment, this migration is completely abrogated. Additionally, we show for the first time that CXCR4 on lymphatic endothelial is capable of mediating pancreatic tumor cell adhesion and transendothelial migration during invasion of a lymphatic endothelium. GMI-1359 treatment blocked both these processes regardless of E-selectin ligand expression on the PDAC cells demonstrating a role for CXCR4 during endothelia invasion.

In vivo studies in athymic mice using an S2-013 pancreas orthotopic model demonstrated that blockade of CXCR4 with GMI-1359 moderately delays PDAC metastasis. However, this GMI-1359 delay in metastasis did not result in prolonged animal survival. Animals treated with GMI-1359 demonstrated significant reorganization of the primary tumor microenvironment: drastically decreased desmoplasia and reduced lymphatic vascular densities. Interestingly, blood vascular density and immune cell infiltration remained unaffected by GMI-1359 and CXCR4 blockade. As CXCR4 is a negative regulator of T cell function in PDAC tumors (171), we investigated the efficacy of GMI-1359 in an immune competent model by orthotopically implanting KPC8060 PDAC cells into the pancreases of C57BL/6 mice. Unfortunately, GMI-1359 did not prolong animal survival even when in used in combination with chemotherapy and/or immunotherapy under the tested treatment schedule. GMI-1359 holds promise as a tool for investigating the role of CXCR4 in *in vitro* studies; however, more work needs to be done to improve its *in vivo* efficacy in combination with other approved pancreatic cancer therapies.

Supplementary Figure 5.1

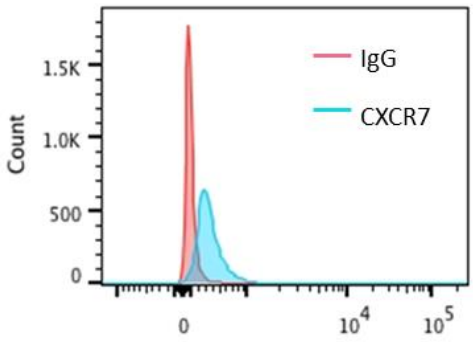

Supplementary Figure 5.1 CXCR7 expression in lymphatic endothelial cells

Flow cytometry showing positive CXCR7 expression in hLECs. The red histogram indicates IgG isotype control labeling and the blue histogram indicates CXCR7 labeling.

CHAPTER 6:

Discussion and Future Directions

Excerpts from this chapter have been edited from:

a) Fink, DM[1], Steele, MM[1], and Hollingsworth, MA (2015). The lymphatic system and pancreatic cancer. Cancer Lett; ePublished.

[1]Authors contributed equally to this publication

Selected sections from this chapter authored by Maria Steele (in "The lymphatic system and pancreatic cancer" review) were also previously used (with the permission of Maria Steele) in the dissertation of Darci Fink (entitled "Inflammation- and cancer-associated neurolymphatic remodeling and cachexia in pancreatic ductal adenocarcinoma). These sections are indicated in this chapter by quotation marks.

b) Steele, MM, Radhakrishnan, P, O'Connell, K, Mohr, AM, Caffrey, T, Grandgenett, PM, Grunkemeyer, JA, Mehla, K, Patil, P, Fink, DM, Hanson, RL, Fogler, WE, Magnani, JL, and Hollingsworth, MA. A novel glycomimetic inhibitor reveals the role of E-selectin in lymphatic invasion and dissemination of pancreatic cancer. (In final preparation)

c) Steele, MM and Hollingsworth, MA. Regulation of cellular lymphatic biology by pancreatic tumor cells and fibroblasts. (In submission to Oncotarget)

I. Overview

Cancer metastasis into and through the lymphatic vasculature and lymph nodes occurs early and frequently during PDAC development and progression (5, 28, 33) and is strongly correlated with poor patient prognosis (34-37). This suggests the lymphatic system is likely a substantial contributor to PDAC progression and metastasis. Although clinicians and researchers recognize the importance of lymph node involvement as a determinant of PDAC prognosis and therapy selection, the mechanisms governing lymphatic-directed metastasis are almost completely unknown. Furthermore, very few studies have examined the contributions of the PDAC microenvironment in promoting lymphatic invasion and metastasis. In this dissertation, we set out to characterize how PDAC cells and pancreatic fibroblasts, major cellular components of the PDAC microenvironment, communicate and interact with lymphatic endothelial cells, the main cell type comprising lymphatic vessels. Our studies went on to explore the roles of adhesion protein E-selectin and chemokine receptor CXCR4 in lymphatic invasion *in vitro* and how targeting these proteins impacts metastasis and survival in mice orthotopically challenged with PDAC.

II. Characterization of PDAC Cells and Pancreatic Fibroblasts Impact Lymphatic Biology

The pancreatic tumor microenvironment is arguably one of the most complex of any malignancy. Due to their prevalence in pancreatic tumor tissues, pancreatic fibroblasts exert a prominent influence over many cell types of the PDAC microenvironment including lymphatic endothelial cells, the cells responsible for facilitating PDAC dissemination to the lymph nodes. Through work presented in this chapter, we demonstrate for the first time the cell biology of *in vitro* interactions between pancreatic tumor cells, pancreatic fibroblasts, and lymphatic endothelial cells during processes that included cellular recruitment and tubulogenesis.

We showed that several PDAC cell lines display a moderate ability to induce directional hLEC migration; however, pancreatic fibroblasts, through the secretion of soluble paracrine factors, strongly induce hLEC migration (we would later identify one of these paracrine factors to be

CXCL12). Additionally, pancreatic fibroblasts co-cultured with hLECs accelerated lymphatic tubulogenesis resulting in poorly formed tube networks. The ability of fibroblasts to facilitate hLEC recruitment and tubulogenesis at the cellular level was anticipated as studies have demonstrated that fibroblasts secrete a number of pro-lymphangiogenic factors such as VEGF-C, VEGF-D, VEGF-A, PDGF, EGF, and FGF (75, 78-81). Immunohistochemical studies have demonstrated that lymphatic vessel densities are highest in the stromal compartment of tumors and lowest in the intratumoral compartments, suggesting that there is an intimate association between fibroblasts and lymphatics within tumors (79). Specific to PDAC, Bailey et al., demonstrated that depletion of activated fibroblasts within the PDAC tumors of orthotopically challenged mice led to a significant reduction in lymphatic vessel density and metastasis to lymph nodes (163). This groups findings were corroborated by our *in vivo* studies demonstrating that elimination of αSMA^{+} fibroblasts from PDAC tumors (through CXCR4 blockaded) correlated with significantly reduced lymphatic vessel density within pancreatic tumors.

Our studies suggest that pancreatic fibroblasts are key to the recruitment and formation of new of lymphatic vessels within PDAC tumors. Other non-tumor cell types of the tumor microenvironment have also been implicated as contributors of lymphatic recruitment and lymphangiogenesis within tumors, such as tumor associated macrophages (202-205, 232), mast cells (292-294), and dendritic cells (83, 295). The studies reported here as well as others support the hypothesis that malignancies exploit the pro-lymphangiogenic mechanisms of tumor microenvironment cells to augment tumor invasion of lymphatic vessels and subsequent dissemination to lymph nodes, a common site of metastasis for many tumors including PDAC. Further research is needed to define the specific molecules that mediate the influence of tumor-associated fibroblasts on lymphatic biology and function.

Our studies also demonstrate that paracrine factors secreted from several PDAC lines induce moderate hLEC migration, albeit not as strongly as pancreatic fibroblasts. Furthermore,

these same PDAC lines (S2-013, Colo357) also accelerated tubulogenesis in co-culture with hLECs. This accelerated tubulogenesis resulted in poorly formed lymphatic networks replete broken tubes and dissociated LECs. These poorly structured lymphatic networks support previous studies that described intratumoral lymphatic vessels from both clinical and *in vivo* samples as being disorganized, collapsed, and non-functional (118, 119, 296) and suggest that tumor cells are a significant contributor to malformed lymphatics within overall tumor structure. Studies have demonstrated that PDAC cells secrete a number of pro-lymphangiogenic factors and therefore are capable of influencing tumor-associated lymphangiogenesis (107, 116, 297, 298). In support of this conclusion, numerous studies have correlated the expression of pro-lymphangiogenic within primary tumors (both tumor-secreted and stromal-secreted) with LVD and lymph node metastasis including in the setting of PDAC (107, 116, 137, 297-300). However, many previous studies relied on immunohistochemical staining to correlate the expression of pro-lymphangiogenic factors with LVD and lymph node metastasis rather than studies showing direct effects by specific cell types, which are demonstrated by the results presented in this manuscript. Further work is needed to elucidate the specific paracrine signaling mechanism induced by PDAC cells use to promote tumor-associated lymphangiogenesis.

We also for the first time report on PDAC and pancreatic fibroblast invasion of a simulated lymphatic endothelium. Chemotactic-directed TEM assays demonstrated that both PDAC cells and pancreatic fibroblasts are capable of crossing a lymphatic endothelial barrier albeit at differing rates. Steady state images of invasion revealed that PDAC cells primarily invade a lymphatic monolayer at tricellular junctions between LECs suggesting that PDAC cells mainly undergo paracellular routes during endothelial invasion as opposed to transcellular invasion. These results coincide with previous studies demonstrating that PDAC cells also invade vascular endothelia at tricellular junctions (301). Additionally, the preference of PDAC cells to invade tricellular junctions indicates invasion is not a random process in which PDAC cells invade the most proximal

lymphatic location. Rather PDAC cells showed preference for specific sites to attach to and invade the lymphatic vasculature. It was also notable that tumor cells preferred a pattern of collective migration during invasion, suggesting that the formation of invasive sites produces a local chemotactic environment that recruits other cells to the invading cell mass. Definition of the molecular factors that produce this effect requires further investigation, but is likely important given emerging reports in the literature of the potential importance of collective migration of cells during invasion and metastasis (302, 303). Only a handful of studies have examined the mechanisms regulating transmigration at tricellular junctions, and these studies evaluated vascular endothelial junctions. It has been proposed that tricellular junctions express a discontinuous pattern of adherens junctions that enables greater cell TEM (304, 305). Another study demonstrated that vascular endothelial tricellular junctions have enriched expression of adhesion proteins (306). Further investigation will be needed to determine if these same mechanisms enable PDAC invasion of lymphatic tricellular junctions.

Pancreatic fibroblasts also interacted with hLECs at tricellular junctions. However, unlike PDAC cells, pancreatic fibroblasts demonstrated the ability to remain atop the hLEC monolayer without invading, as seen in steady state images and live cell imaging. This implies that the fibroblasts seek to establish a stable interaction with and along the LECs, in contrast to tumor cells. TEM assays demonstrated that fibroblasts are capable of invading lymphatic endothelia; however, the capacity of these to form higher order structures (e.g. tubes surrounded by fibroblasts) were not addressed in the studies presented here. Although tumor-associated fibroblasts have been shown to accompany tumor cells to distant metastatic sites (161, 307), our results raise the possibility that pancreatic fibroblasts' interactions with tumor cells facilitate fibroblast invasion of endothelial layers during dissemination, a process that may also contribute to the disorganization of lymphatics that is observed in tumors.

Few studies have evaluated the paracrine mechanisms by which pancreatic tumor cells communicate and interact with lymphatic endothelial cells, and even fewer studies have evaluated the paracrine mechanisms by which pancreatic fibroblasts influence the biology of LEC and lymphatics. The work presented here lays the groundwork for understanding the biological impact of interactions between pancreatic tumor cells, fibroblasts lymphatic endothelial cells. A better understanding of the processes of lymphatic invasion and lymph node metastasis in PDAC will significantly contribute to our overall understanding of this deadly disease and provide insights for the development of novel efficacious therapies for pancreatic cancer.

III. Blockade of E-selectin and Implications for PDAC Therapy

Adhesion protein E-selectin has been shown to regulate metastasis in a variety of cancers (146, 252, 257, 260). However, its direct role in the metastasis of pancreatic cancer *in vivo* has not been fully evaluated. Using a novel glycomimetic small molecule antagonist of E-selectin, we demonstrated that E-selectin influences PDAC dissemination *via* the vasculature systems, and that blocking its ligand binding function decreased PDAC metastasis. Although it is known that E-selectin plays a role in vascular invasion of tumor cells, we demonstrated for the first time a role for E-selectin in facilitating tumor cell invasion of the lymph nodes *via* the lymphatic vasculature.

The normal role of E-selectin is to initiate the tethering of circulating leukocytes to vascular endothelia during extravasation (254, 255, 308). Previous studies demonstrated that tumor cells expressing the E-selectin ligands $sLe^{A/X}$ exploit the function of E-selectin for dissemination (146, 252, 257, 260, 309). However, very few studies have examined the functional role of E-selectin in lymphatics especially in regards to tumor invasion. It has been demonstrated that activated LECs upregulate E-selectin expression (146, 310) which enables leukocyte TEM and trafficking to the lymph nodes (131, 256). Using GMI-1271, we demonstrated for the first time that blockade of E-selectin significantly impairs PDAC adhesion to a simulated lymphatic endothelium and subsequent transendothelial invasion. *In vivo*, this blockade led to a significant decrease in lymph

node metastasis. These results are consistent with studies showing PDAC cells and other tumor cells use E-selectin to facilitate invasion of blood vessels for dissemination (311-313).

Corresponding to our *in vitro* results, blockade of E-selectin *in vivo* reduced PDAC metastasis to lymph nodes in an orthotopic model of pancreatic cancer. No prior reported *in vivo* studies have examined tumor metastasis specifically to the lymph nodes during E-selectin blockade. We demonstrated that this reduction in lymph node metastasis by E-selectin blockade was not due to inhibition of tumor growth nor decreased LVD at the primary tumor site. In patient samples from several cancer types, it has been noted that there is a potential correlation between high expression of E-selectin/E-selectin ligands and presence of lymph node metastases (314-319). In the setting of PDAC, only one study has examined this relationship, and they found no correlation between the expression of E-selectin/E-selectin ligands and lymph node metastases (320). Thus, further investigation is warranted to determine if there is a correlation between the expression of E-selectin/E-selectin ligands and lymph node metastasis in clinical samples of pancreatic cancer and whether E-selectin a major contributor to lymph node metastasis.

Our *in vivo* results demonstrated that E-selectin blockade by GMI-1271 resulted in decreased metastasis to the lymph nodes and other organs: liver, lungs, diaphragm, and kidney. Metastasis to these sites would be dependent on PDAC cell trafficking through the vasculature systems and necessitate interactions between E-selectin on endothelial cells and E-selectin ligands on tumor cells. Confirming the posited role of E-selectin in vasculature-dependent metastasis, previous studies demonstrated a strong correlation between high expression of E-selectin/E-selectin ligands and increased metastatic burden and poor prognosis in patient tumor samples (321-323). Additionally, prior studies have demonstrated that metastasis specifically to the liver and lungs is often regulated by E-selectin, suggesting that E-selectin may influence organ selectivity during tumor dissemination (324-327). However, other studies presented contrasting results that found E-selectin dispensable for tumor homing to the liver and lungs (328). Our results support the

hypothesis that E-selectin regulates organ selectivity during PDAC dissemination, as PDAC metastasis to the liver and lung were the sites most highly impacted by E-selectin blockade. It is unknown but possible that E-selectin influences tumor selectivity to other sites (i.e. lymph nodes, diaphragm, kidneys) as well.

Not all PDAC cell lines examined in our study used E-selectin-dependent mechanisms for invasion of lymphatic endothelia *in vitro* and these were predictably resistant to GMI-1271 treatment. Additionally, E-selectin blockade did not completely prevent PDAC dissemination *in vivo.* These suggest that additional mechanisms contribute to PDAC invasion of endothelial barriers. Other proteins have been implicated in tumor invasion of endothelia including ICAM-1, VCAM-1, platelet endothelial cell adhesion molecule-1, chemokine receptors CXCR4 and CXCR7, integrins, and others (reviewed in (260)). Additionally, immune cells can act as an intermediate linker cell type between tumor cells and endothelial cells to facilitate endothelial invasion (329, 330). This multicellular process could render non-E-selectin ligand-expressing tumors susceptible to E-selectin blockade *in vivo,* as immune cells are known to use E-selectin for intra- and extravasation across endothelia. Colo357 cells, which were shown to use E-selectin-independent mechanisms for TEM, were capable of upregulating E-selectin expression in hLECs. Investigation as to whether PDAC cells upregulate E-selectin to promote leukocyte-assisted TEM or for an alternative mechanism, would provide additional insight into the mechanisms driving tumor cell transendothelial invasion. It was interesting that PDAC cell lines using E-selectin-independent mechanisms directly for TEM had reduced capacities to invade a lymphatic endothelial barrier compared to E-selectin ligand-expressing PDAC cell lines. This suggests that direct E-selectin-independent mechanisms of invasion may be less efficient compared to E-selectin-dependent mechanisms. More work needs to be done to fully elucidate the mechanisms that underlie the process of lymphatic invasion by tumor cells.

GMI-1271 was particularly effective at reducing metastasis and extending survival when used in combination with chemotherapy. The improved efficacy of combination therapy with gemcitabine is of biological interest and clinical importance. As an anti-proliferative agent, gemcitabine significantly reduces the number of potentially metastatic PDAC cells within the tumor. Additional treatment with GMI-1271 effectively inhibited the dissemination of the remaining metastatic-capable tumor cells. Alternatively, E-selectin has been shown to promote chemoresistance by facilitating tumor interactions with a protective vascular niche (331). Following GMI-1271 administration, it is possible that PDAC cells were forced to exit the vascular niche and enter blood and lymphatic vessels where gemcitabine effectively destroyed more of these transiting tumor cells. It is also possible that inhibition of E-selecting ligand binding disrupted other cell-cell interactions in the tumor microenvironment which thereby improved the delivery of gemcitabine. As E-selectin has other biological functions, it is possible that unknown mechanisms contributed to the enhanced efficacy of GMI-1271 and gemcitabine when administered together.

E-selectin is crucial for leukocyte trafficking to inflamed tissues including tumor sites. Immune cells within tumor microenvironments are often significant contributors to tumor cell killing, survival, proliferation, immune suppression, and metastasis (180, 212, 332). Although our results showed no change in the total numbers of immune cells present within the primary tumor following GMI-1271 treatment, it is possible that GMI-1271 modified the composition of specific immune cell subtypes within the PDAC microenvironment and that this contributed to decreased metastasis. Concordant with this possibility, we showed that GMI-1271 (in combination chemotherapy) improved survival of immunocompetent mice (but not immune compromised mice) following orthotopic challenge. This suggests a link between E-selectin and immune cell-dependent mechanisms that modulate tumor progression. Further analysis is warranted to elucidate the effects of E-selectin blockade on immune cell recruitment to tumors and how GMI-1271 may work in combination with immunotherapies.

Our studies demonstrate for the first time the effectiveness of using a glycomimetic small molecule antagonist of E-selectin, GMI-1271, in the setting of solid tumors. Until now, GMI-1271 has mainly been evaluated in hematological malignancies specifically acute myeloid leukemia (AML) (333, 334). These AML studies demonstrated that GMI-1271 enhanced leukemic stem cell mobilization, resulting in improved efficacy of chemotherapy and prolonged animal survival *in vivo*. Similar to our findings, successful treatment of AML *in vivo* was dependent on combinatorial treatment with an anti-tumor therapy and GMI-1271. Currently, this E-selectin antagonist is in phase 1/2 clinical trials for AML (NCT02306291). Additional studies should evaluate the effectiveness of GMI-1271 in other solid tumors and as well as its ability to inhibit metastasis in early diagnosed tumors.

In the clinic, PDAC patients are most often diagnosed with advanced metastatic disease. However, approximately 15-20% of patients are diagnosed with localized resectable disease (1, 6). For these patients, GMI-1271 may be an effective therapy for slowing or reducing PDAC dissemination prior to surgical resection. Moreover, unclean resection margins pose a substantial risk for disease recurrence (15). GMI-1271 treatment along with chemotherapy may prevent this recurrence and improve patient survival.

In summary, we demonstrate E-selectin is important regulator of lymphatic-directed metastasis of pancreatic cancer. The novel glycomimetic E-selectin antagonist GMI-1271 impairs PDAC interactions with endothelial cells resulting in decreased tumor dissemination. GMI-1271 is a promising agent for inhibiting metastasis in solid tumors. Further work needs to be done to determine the effectiveness of GMI-1271 in other solid tumors, its effects on immunity, and its ability to improve chemotherapy efficacy.

IV. Dual Blockade of CXCR4 and E-selectin and Implications for PDAC Therapy

i. CXCR4 contributes to invasion of a lymphatic endothelium by PDAC cells

Very few studies have investigated the role of the CXCL12-CXCR4 chemokine axis in lymphatic endothelial cells. The studies that have examined this axis demonstrated it contributes to lymphatic migration and lymphangiogenesis (285, 335). We confirmed the finding that hLEC migration is stimulated by recombinant CXCL12 as well as CXCL12 secreted from pancreatic fibroblasts. Blockade of CXCR4 on hLECs through treatment with GMI-1359 completely abrogated CXCL12-induce migration. As GMI-1359 is a dual inhibitor of both CXCR4 and E-selectin, we demonstrated that the effects were due to CXCR4 antagonism, as E-selectin only antagonism did not abrogate CXCL12-induced hLEC migration.

The CXCL12-CXCR4 axis has also been implicated in facilitating vascular extravasation by immune cells and vascular invasion by tumor cells including those of PDAC (277, 286-288, 336-339). However, a role for CXCR4 in lymphatic invasion has not been fully elucidated. Our *in vitro* results demonstrated that the CXCL12-CXCR4 chemokine axis supports PDAC adhesion to and TEM across a lymphatic endothelium and that blockade of CXCR4 significantly impairs these processes. Since GMI-1359 antagonizes both CXCR4 and E-selectin, a protein we previously showed regulated PDAC TEM, we evaluated the effects of GMI-1359 on two types of PDAC cells: ones that express E-selectin ligands (S2-013) and ones that do not express E-selectin ligands (Colo357). Not only did GMI-1359 inhibit the TEM of E-selectin ligand-expressing PDAC cells (S2-013) but also inhibited the TEM of PDAC cells that do not express E-selectin ligands (Colo357). These results were also confirmed using neutralizing antibody specific to CXCR4. Our findings are consistent with one other study that demonstrated the CXCL12-CXCR4 axis contributes to the TEM of DCs across an inflamed lymphatic endothelium (276). Altogether, our results demonstrated that CXCR4 plays a role in the invasion of lymphatic endothelia by PDAC cells and by blocking its function we can inhibit PDAC TEM.

To further dissect the role of CXCL12-CXCR4 in lymphatic invasion, we pretreated only the hLEC monolayer with GMI-1359 and demonstrated that blocking hLEC CXCR4 significantly impaired PDAC TEM. Furthermore, pretreatment of the hLEC monolayer with CXCL12 significantly enhanced the ability of hLECs to facilitate PDAC TEM. Additional pretreatment with GMI-1359 returned CXCL12-enhanced TEM to below unstimulated levels. This is the first study demonstrating that endothelial expression of CXCR4 plays a role in enabling PDAC TEM. Previous studies have focused on the role of CXCR4 in the invading cell type (i.e. immune cells or tumor cells) enabling TEM (277, 286-288, 336, 340). If CXCR4 on hLECs regulates PDAC TEM, then PDAC cells would need to express the ligand, CXCL12. Indeed, ELISA of whole cell lysates indicated PDAC cells express CXCL12; however, it is not constitutively secreted from PDAC cells as we did not detect it in PDAC conditioned media. Non-secreted, immobilized CXCL12 has been shown to contribute to immune cell TEM across a vascular endothelium (340). To solidify our findings, cell-specific knockdown of CXCR4 in hLECs, PDAC cells, or both cell types is needed to accurately determine which CXCR4-expressing cell type is regulating PDAC invasion. It would not be surprising if CXCR4 in both the endothelial cells and the PDAC cells was contributing to lymphatic invasion. Similar studies should also be performed using CXCL12 knockdown strategies. It would also be interesting to determine if the other receptor for CXCL12, CXCR7, also contributes to lymphatic invasion of PDAC cells. CXCR7 expression in pancreatic tumors correlates with lymph node metastasis (341) and has been shown to accelerate tumor invasion *in vivo* (342).

Unexpectedly, our *in vitro* results also revealed that E-selectin antagonism (using GMI-1271) returned CXCL12-enhanced hLEC facilitation of PDAC TEM to control levels. This suggests that CXCL12 may upregulate E-selectin expression in lymphatic endothelial cells. A previous set of studies did demonstrate that CXCL12 could induce E-selectin expression in vascular endothelial cells to facilitate diabetic wound healing (343). More studies are needed to verify the

ability of CXCL12 to induce E-selectin expression in hLECs and what mechanisms regulate this induction.

ii. *In vivo* blockade of CXCR4 and E-selectin in PDAC challenged mice

Based on our in vitro results, we decided to evaluate whether dual inhibition of CXCR4 and E-selectin reduced PDAC metastasis and improved overall survival. Similar to our GMI-1271 studies, we performed our *in vivo* studies with athymic mice that were orthotopically challenged with the human PDAC line S2-013. Our findings demonstrated GMI-1359 monotherapy decreased metastatic incidence within the spleen, liver, lungs, and kidneys compared to treatment with the vehicle control. However, this was only apparent when we excluded the mice that did not complete the 4-week treatment regimen. When used in combination with gemcitabine, GMI-1359 failed to reduce PDAC metastasis when compared to mice treated with gemcitabine alone. Consistent with our previous *in vivo* studies, GMI-1271 in combination with gemcitabine was the most effective at reducing PDAC metastasis. Although the reduction in metastasis with GMI-1359 was not substantial, it is consistent with studies showing CXCR4 expression in pancreatic cancer patient samples correlates with metastatic burden (137, 140).

Due to its efficacy in reducing metastatic incidence, we anticipated that GMI-1359 would prolong animal survival. However, GMI-1359 failed to improve overall animal survival when used as either a single agent or in combination with gemcitabine in our immunocompromised orthotopic model. Obfuscating our results is the gemcitabine treatment. We suspect that prolonged treatment with gemcitabine contributed to animal death as all mice treated with gemcitabine were severely cachexic at end stage and died with much smaller tumors compared to mice not treated with gemcitabine. For future studies requiring extended treatment, we recommend treating athymic mice with a lower dose of gemcitabine.

Being a chemokine receptor, CXCR4 regulates the recruitment of various cell types to the PDAC microenvironment. We, therefore, evaluated the effects GMI-1359 had on the cellular

composition of the PDAC microenvironment. Unexpectedly, immunohistochemical staining revealed that GMI-1359 treatment significantly decreased the desmoplastic reaction within primary tumors as determined by loss of activated (αSMA^{+}) fibroblasts. This was the result of blocking CXCR4 as blockade of E-selectin alone had no impact on activated fibroblast presence. In the past, researchers hypothesized that reducing the desmoplastic barrier would result in improved drug perfusion into the tumor (165). However, more recent studies suggest that pancreatic fibroblasts may constrain tumor growth and progression as depletion of tumoral fibroblasts led to the development of both highly aggressive and highly proliferative undifferentiated tumors (175-177). This may explain why GMI-1359 did not prolong overall animal survival as we may have inadvertently promoted tumor growth and aggressiveness by eliminating fibroblasts from the PDAC microenvironment.

For future studies, we would like to determine the mechanism by which blockade of CXCR4 decreases the presence of αSMA+ fibroblasts in PDAC tumors. The most obvious hypothesis would be that blocking the CXCL12 chemokine gradient impairs recruitment of fibroblasts to the tumor. However, an alternative hypothesis would be that CXCR4 regulates the activation status of fibroblasts and that antagonism of this receptors reverts fibroblasts to a quiescent state (αSMA^{-}). Currently, there are no specific markers for identifying quiescent fibroblasts in tumor sections. Most studies rely upon *in vitro* stimulation to evaluate the ability of protein or drug to induce or inhibit fibroblast activation (167). A third hypothesis pertains to the regulation of Shh. This morphogen is one of the major drivers of desmoplasia in pancreatic cancer (166). PDAC-secreted Shh promotes desmoplasia through paracrine signaling in pancreatic fibroblasts. It was recently uncovered that Shh expression in PDAC cells is regulated by the CXCL12-CXCR4 axis (344). GMI-1359 may indirectly suppresses desmoplasia by inhibiting PDAC cell secretion of Shh thus preventing its paracrine signaling in pancreatic fibroblasts which is necessary to drive desmoplasia.

We also noted a reduction in LVD within the primary tumors of mice treated with GMI-1359. There are a handful of explanations for this finding. CXCL12 is a known lymphangiogenic factor (285, 335) and blockade of its receptor, CXCR4, would inhibit lymphangiogenesis and reduce tumor LVDs. In agreement with this hypothesis, we demonstrated that CXCL12 is a strong chemoattractant for lymphatic endothelial cells and blockade of CXCR4 potentially impairs recruitment of lymphatic vessels to the primary tumor. Alternatively, CXCL12 is a chemoattractant for many cell types within the PDAC microenvironment. Blockade of CXCR4 may have impaired the recruitment of cells known to secrete pro-lymphangiogenic factors such as CAFs and TAMs, and, this, in turn, reduced lymphatic vessel numbers within the tumor. In line with this, GMI-1359 drastically reduced the number of αSMA^{+} fibroblasts within primary tumors, and without these fibroblasts to induce lymphatic migration and stimulate lymphangiogenesis, LVD remained low in GMI-1359-treated tumors. Further research is needed to determine the mechanisms by which GMI-1359 reduces lymphatic vessel densities, although one can predict it is likely a combination of direct and indirect mechanisms.

GMI-1359 significantly reduced LVD within primary tumor sites, but it did not suppress PDAC metastasis to the lymph nodes. This finding is likely due to disruption of the PDAC microenvironment including the reduction in desmoplasia following GMI-1359 treatment. Although we did not see a change in the total number of immune infiltrates, it is likely GMI-1359 altered the immune cell composition of the tumor as well. By disrupting the "normal" PDAC microenvironment, it is possible that tumors acquired a more aggressive phenotype enabling successful metastasis the lymph nodes despite decreased lymphatic densities. The mechanisms contributing to tumor aggressiveness following GMI-1359 treatment and stromal disruption are likely to be complex and dependent upon the functions of multiple cell types.

Although GMI-1359 significantly reduced the presence of lymphatic vessels within the primary tumor, we saw no change in blood vessel densities. This is surprising considering the

overlap of mechanisms that contribute to both lymphangiogenesis and angiogenesis. The discrepancy in lymphatic vessel and blood vessel densities suggests that the mechanisms promoting lymphatic vessel growth within PDAC tumors are not necessarily the same as those promoting blood vessel growth. This idea of differential mechanisms regulating lymphatic and vascular growth is supported by studies examining lymphangiogenesis within tumor draining lymph nodes. These lymph nodes undergo massive lymphangiogenic remodeling prior to the arrival of tumor cells but the blood vasculature remains unchanged (95, 345-347). Adding to the complexity is that these lymph nodes contain an abundance of both pro-lymphangiogenic and pro-angiogenic factors, yet only lymphangiogenesis occurs. More work needs to be done to determine the differential factors regulating lymphatic and vascular growth within PDAC tumors.

The CXCL12-CXCR4 axis has been shown to be a negative regulator of anti-tumor T cell responses within PDAC tumors (171). Therefore, we investigated CXCR4 blockade in an immune competent mouse model. To accelerate our studies, we orthotopically challenged C57BL/6 mice with a KPC cell line (KPC8060) derived by our laboratory. In our first set of studies, tumors were allowed to establish for two weeks after which treatments were initiated. Unexpectedly, KPC cells display a very aggressive phenotype following orthotopic implantation: just two weeks after implantation, mice began to show signs of end stage disease (lethargy, extreme cachexia, and/or significant accumulation of ascites). We consulted with Dr. David Tuveson whose laboratory developed the KPC mouse and they have observed a similar aggressiveness when orthotopically implanting KPC cell lines into syngeneic mice. Despite demonstrating late stage disease, we proceeded with the survival study. Unfortunately, GMI-1359 treatment failed to improve the survival of mice with advanced disease. These studies were repeated except treatment regimens began the day following KPC cell implantation. Even in animals with early stage disease, GMI-1359 failed to prolong overall animal survival. In future studies, we would like to profile the tumor microenvironments of GMI-1359-treated immune competent mice just as we did with the

immunocompromised mice. In these mice, we will also evaluate changes to the immune cell compartment. We expect that the tumors from GMI-1359-treated immunocompetent mice will similarly display a significant reduction in desmoplasia and LVD. We also expect that GMI-1359 will significantly alter the immune cell subtypes found within the tumor.

Ozdemir et al. demonstrated that depleting the fibroblasts from the PDAC tumor microenvironment makes these tumors susceptible to immunotherapy (175). Additionally, Feig et al. demonstrated that CXCR4 blockade (with AMD3100) significantly improved immunotherapy efficacy resulting in tumor regression in KPC mice (171). We evaluated if blockade of CXCR4 and the ensuing depletion of pancreatic fibroblasts improves the efficacy of anti-PD-L1 immunotherapy in KPC-challenged C57BL/6 mice. Unfortunately, in our study GMI-1359 did not improve survival when used in combination with gemcitabine and/or anti-PD-L1 immunotherapy. Feig et al. observed approximately a 15% reduction in tumor size after only 6 days of treatment with CXCR4 inhibitor AMD3100 and anti-PD-L1 antibodies. Although not investigated in their study, one would suspect that tumor regression would translate to improved overall survival. Contrarily, our studies demonstrated that chronic blockade of CXCR4 failed to improve anti-PD-L1 efficacy and did not prolong overall animal survival.

iii. Ongoing future studies: Combinatorial treatment of KPC mice with GMI-1359 and anti-PD-L1 immunotherapy

Our results demonstrated that CXCR4 blockade improved neither the efficacy of immunotherapy nor overall survival in orthotopically challenged mice. However, orthotopic tumor models often do not recapitulate the human disease nor do these tumors respond appropriately to therapies. Therefore, we are currently evaluating GMI-1359 efficacy in combination with immunotherapy for the treatment of pancreatic cancer in KPC mice. We have designed a drug enrollment study that uses ultrasound imaging to identify PDAC tumors and track their growth *in vivo.* Pancreatic tumors are typically identifiable by ultrasound at 4 mm in diameter. Enrollment eligibility is determined by the mean of the shortest and longest tumor diameters of the largest

tumor cross section being 4 to 7 mm in diameter. Upon attainment of the enrollment eligibility, mice are randomized into 4 treatment groups: 1) Vehicle (PBS) control; 2) 40 mg/kg GMI-1359 daily; 3) 160 µg/mouse anti-PD-L1 antibody; 4) combination GMI-1359 and anti-PD-L1. Tumors growth is monitored weekly by ultrasound imaging. Mice are treated until they display signs of end stage disease.

Although this investigation is still ongoing, we have some preliminary data. **Figure 6.1A** illustrates the relative change in tumor size across the various treatment groups. For effective evaluation of tumor growth, a minimum of three images are needed: an image at the time of enrollment; an image following 1 week of treatment; and an image following 2 weeks of treatment. At this point in the trial, we see no significant effect of GMI-1359 inhibiting KPC tumor growth. The same is true for combinatorial treatment with GMI-1359 and anti-PD-L1. Treatment with PD-L1 alone appears to be slightly increasing PDAC tumor growth. By plotting the tumor growth for each enrolled mouse, we can see that individual mice respond to therapy relatively similarly within a treatment group (**Figure 6.1B**). Plotting the relative change in tumor size as a waterfall plot, we can evaluate the relative change in tumor size for individual mice after 2, 3, or 4 weeks of treatment (**Figure 6.1C**). Mice treated with GMI-1359 alone or in combination with anti-PD-L1 demonstrate similar tumor growth rates as control mice, while anti-PD-L1-treated mice demonstrate slightly elevated tumor growth rates. With only 2-4 total mice enrolled per group, significantly more mice will need to be enrolled before any accurate conclusions can be made regarding the effects of GMI-1359 and immunotherapy in KPC mice.

In this trial, we are also evaluating post-enrollment animal survival. Based on median survival time, GMI-1359 may be prolonging animal survival compared to vehicle-treated mice (**Figure 6.1D**). Mice treated with anti-PD-L1 alone demonstrate the longest post-enrollment survival time while mice treated with both GMI-1359 and anti-PD-L1 demonstrate a slightly shorter survival time. **Table 6.1** indicates the post-enrollment survival time for each individual mouse and

Figure 6.1 Tumor growth and post-enrollment survival time for KPC mice treated with GMI-1359 and/or immunotherapy.

A) Line graph showing the relative average change in KPC tumor size (diameter) following enrollment into the GMI-1359 drug study. Upon attainment of enrollment criteria, mice are randomized into four treatment groups: 1) vehicle control (black line), 2) 40 mg/kg GMI-1359 daily (blue line), 3) 160 μg/mouse anti-PD-L1 every 4 days (green line), or 4) GMI-1359 + PD-L1 (red line). Tumors are image every week by ultrasound to follow tumor growth. Initial tumor size was normalized to 1 to account for starting size variations. Error bars = s.d.

B) Line graph demonstrating change in tumor growth for each KPC mouse. Tumors are image every week by ultrasound to follow tumor growth. Initial tumor size was normalized to 1 to account for starting size variations. Asterisks indicates mice is still enrolled in the trial. Error bars = s.d.

C) Waterfall plots demonstrating final tumor volume changes after 2 weeks of treatment (left) or 3 weeks of treatment (right). Each bar represents a single mouse.

D) Kaplan-Meier survival curve demonstrating survival post-enrollment (days) for KPC mice enrolled in the GMI-1359/PD-L1 drug study. Median survival listed to the right.

Figure 6.1

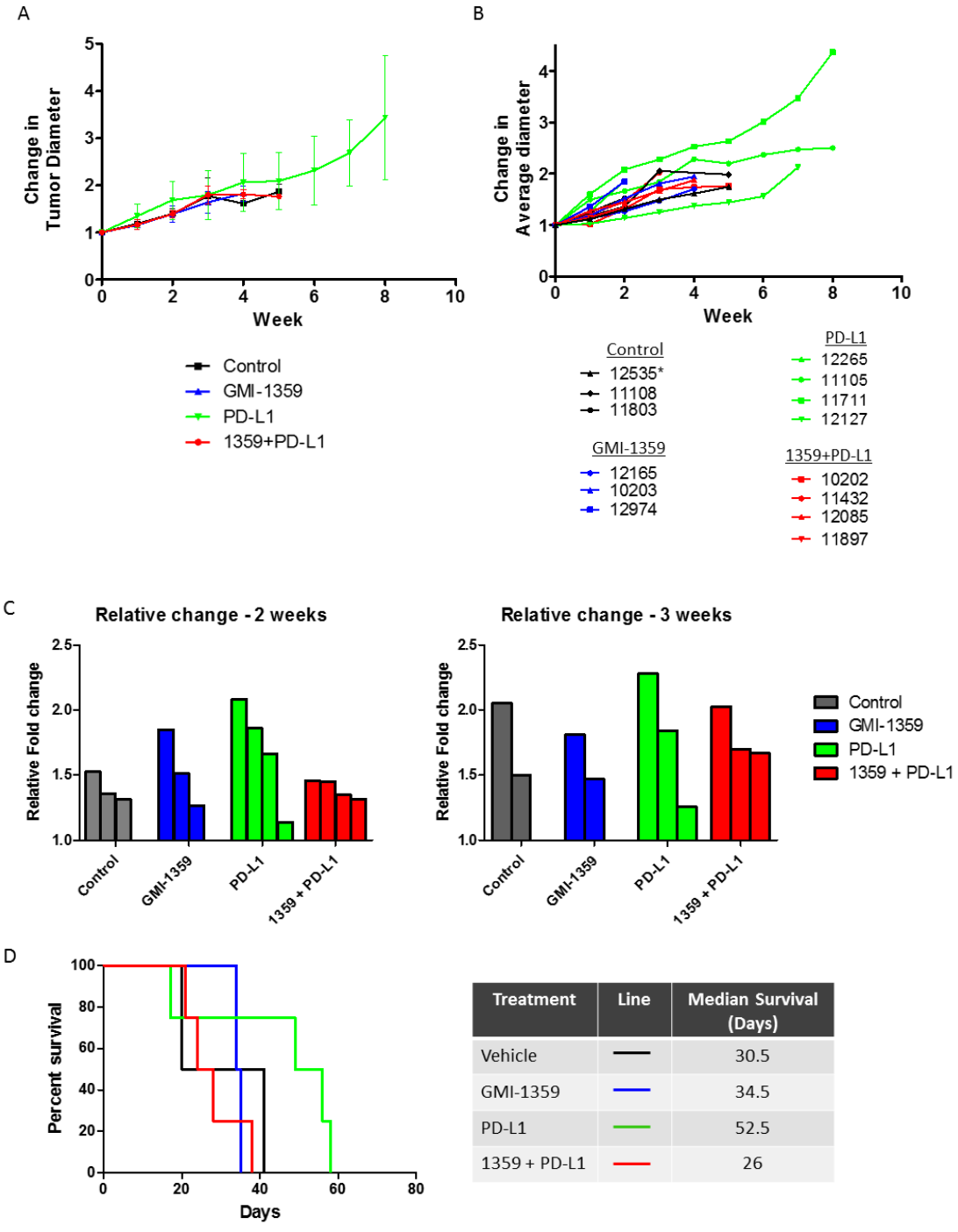

Treatment	Line	Median Survival (Days)
Vehicle		30.5
GMI-1359		34.5
PD-L1		52.5
1359 + PD-L1		26

Table 6.1 KPC Drug Enrollment Mouse Identification List

Mouse	Gender	Treatment Group	Survival Length (Days)	Notes
11803	F	Control	20	
11108	F	Control	41	
12535*	M	Control	42	Still Enrolled
12658*	M	Control	20	Still Enrolled
10203	F	1359	38	
12165	M	1359	35	
12080*	M	1359	14	Still Enrolled
12265	M	PD-L1	17	
11105	M	PD-L1	56	
11711	M	PD-L1	58	
12127	F	PD-L1	49	
12121*	F	PD-L1	20	Still Enrolled
11432	F	1359 + PD-L1	24	
10202	F	1359 + PD-L1	38	
12085	M	1359 + PD-L1	28	
11897	M	1359 + PD-L1	21	

Table 6.1 lists all the KPC mice that have been enrolled in the drug study along with the treatment group, total number of survival days post-enrollment, and the current status of the mouse. Asterisks indicates mice currently enrolled in the trial.

illustrates the variability in survival times within each treatment group. Again, too few animals have been enrolled in the study, and, therefore, no accurate conclusions can be made at this time.

V. Targeting the Lymphatic System as Treatment for PDAC

i. Potential lymphatic-targeted therapies

"Due to advanced stage at diagnosis and its complex microenvironmental organization, pancreatic ductal adenocarcinoma has proven to be very difficult to treat. Surgical removal of the tumor is the most effective option, but only approximately 15% of cases are considered resectable (348, 349). Of those cases in which resection is an option, incomplete removal of microscopic disease (R1 residual margin status) only slightly improves patient survival over those cases presenting with unresectable metastatic disease (350, 351). Non-surgical options for pancreatic cancer include radiation, chemotherapy, or a combination of both. Some approved chemotherapies for the treatment of pancreatic cancer are the use of FOLFIRINOX, gemcitabine, albumin-bound paclitaxel, cisplatin, and oxaliplatin (as well as others) (352, 353). However, these drugs have had limited success in prolonging patient survival. Development of targeted therapies that specialize in blocking crucial molecular pathways of the pancreatic tumor and its microenvironment is becoming an increasingly attractive therapeutic option."

"Anti-angiogenic therapies were originally developed to starve tumors of important nutrients and oxygen and to reduce the number of potential routes for dissemination. However, clinical trials demonstrated that, when used alone, anti-angiogenic therapy was not sufficient to improve patient survival. Unexpectedly though, the results indicated that anti-angiogenic therapy significantly improved survival of patients with solid tumors when used in combination with conventional chemotherapies (354-356). These findings led to the evolution of the current vascular normalization theory: the use of anti-angiogenic therapy to block aberrant tumor angiogenesis and alleviate vessel dysfunction (357). By restoring the balance between pro- and anti-angiogenic factors, anti-angiogenic therapies improved vessel organization, stabilized cell-to-cell junctions,

increased pericyte coverage, and, consequently, reduced fluid leakage. All these factors, in turn, relieved blood flow irregularities resulting in improved delivery of chemotherapy to all parts of the tumor (358). Unfortunately, in the setting of pancreatic cancer, anti-angiogenic therapies have had either no effect or only transient effects on improving patient survival even when used in combination with standard chemotherapies (359-363). PDAC tumors are unusually hypovascular and desmoplastic negating the ability of even normalized vessels to deliver therapy (364). The failure of anti-angiogenic therapy in PDAC may also be the result of tumor cells circumventing the VEGF-A/VEGFR-1 blockade through autocrine or paracrine secretion of alternative angiogenic factors, such as the prototypical lymphangiogenic factors which have overlapping angiogenic functions (363, 365-367)."

"Targeting the tumor lymphatic vasculature as a treatment for cancer is beginning to gain interest among both basic and clinical research groups with the primary focus on anti-lymphangiogenic therapies. Lymphangiogenic growth factors are not critical for the maintenance of adult lymphatic vessels in homeostasis. This allows for extended treatment with anti-lymphangiogenic therapies in tumor settings without disruption of pre-existing vessels and with minimal drug-induced toxicities (368, 369). Numerous pre-clinical *in vivo* studies have demonstrated that blocking pro-lymphangiogenic factors VEGF-C and VEGF-D and their receptor VEGFR-3 significantly reduces tumor lymphangiogenesis and lymph node metastases in many tumor types including pancreatic (108), breast (370-373), melanoma (369), renal (374), lung (156, 375), gastric (376, 377), prostate (378), hepatocellular (379), and bladder (380). Other protein targets of lymphangiogenesis that have shown promise in inhibiting lymphatic metastasis *in vivo* include the VEGFR-3 co-receptor Nrp-2 (381, 382) and the angiopoietins Ang-1 and -2 (383, 384). Currently, two humanized neutralizing antibodies are in clinical trials for patients with solid tumors: VGX-100, which inhibits VEGF-C (NCT01514123) and IMC-3C5, which inhibits VEGFR-3 (NCT01288989)."

"The blockade of a single VEGF/VEGFR pathway will likely be insufficient to inhibit tumor lymphangiogenesis and lymph node metastasis due to the multiple compensatory and overlapping roles of the VEGF ligands and receptors (52, 66, 366, 385). Other growth mechanisms outside of VEGF/VEGFR signaling may also regulate lymphangiogenesis in the tumor setting, such as PDGF-BB/PDGFR (76) and FGF/FGFR (386). Receptor tyrosine kinase inhibitors (RTKIs) often target multiple receptors allowing them to inhibit several signaling pathways simultaneously—including the VEGFR pathways. Both pre-clinical comparative studies and clinical trials have determined the safety and efficacy of numerous anti-angiogenic/-lymphangiogenic RTKIs for the treatment of cancer including foretinib (387), cediranib (388, 389), and axitinib (390-392). Some of these RTK inhibitors have also been approved for clinical use. Sorafenib, which inhibits VEGFR-1 and -3, PDGFR-β, FGFR-1, and Raf proteins, has been approved for renal cell (RCC) and hepatocellular carcinomas (393-395); sunitinib, which inhibits VEGFR-1 and -3, and PDGFR-α and -β, has been approved to treat pancreatic neuroendocrine tumors, RCC, and gastrointestinal stromal tumors (396-399); and pazopanib, which inhibits VEGFR-1 and -3, PDGFR-α and -β, and FGFR, has been approved to treat RCC and soft tissue sarcoma (400-402) (RTKIs further reviewed in (42)). Vatalanib, which inhibits VEGFR-1, -2, and -3, and PDGFR-β, is currently in clinical trials for the treatment of various solid tumors including pancreatic, ovarian, and breast cancers. This RTKI has been shown to directly inhibit angiogenesis, lymphangiogenesis, and tumor growth in pre-clinical models of pancreatic cancer as well as other cancer models (403-407). In a recent clinical trial, vatalanib resulted in a partial or stable response for some metastatic pancreatic cancer patients who had initially failed gemcitabine treatment (408). Many of these lymphangiogenic receptor-targeting RTKIs hold promise for the treatment of early-diagnosed and resectable cancers (52). Unfortunately, these are not typical characteristics of pancreatic cancer, and, consequently, many of these drugs have failed to significantly improve pancreatic cancer patient survival (391, 409-411)."

"Lymphangiogenesis is not the only manner by which the lymphatic vasculature may promote tumor progression. As discussed previously, pre-existing lymphatic vessels can directly facilitate metastasis by transporting tumor cells to distant sites, and our studies with GMI-1271 and GMI-1359 indicate that is possible to target mechanisms of lymphatic invasion by tumor cells during dissemination. Lymphatic endothelia may also contribute to immune suppression by altering DC and T cell responses. However, the processes of lymphatic invasion and lymphatic-directed immune suppression are poorly understood and much more work needs to be done to determine if these functions can be specifically targeted in lymphatic vessels for effective treatment of PDAC as well as other cancers."

ii. Using lymphatic vessels to deliver therapies to lymph nodes

"In pancreatic cancer, metastasis to lymph nodes and distant sites has often already occurred by the time of diagnosis. Anti-lymphangiogenic therapies may inhibit further tumor cell dissemination but will do little to reduce the growth of metastatic tumors that have already colonized distant sites (156, 389, 412). Successful treatment of tumor-invaded lymph nodes has been particularly difficult to achieve. Resection of invaded lymph nodes would intuitively seem to be a promising strategy; however, as discussed above, current clinical imaging technologies cannot reliably detect single cell or microscopic lymph node metastases (413, 414), and excision of an excessive number of lymph nodes is controversial due to conflicting evidence regarding its survival benefits and concerns about post-operative quality-of-life (415, 416). Also, conventional intravenously-administered therapies display poor access to lymphatic vessels and lymph nodes resulting in sub-optimal drug concentrations within lymph nodes (417). This enables tumor cells present within lymph nodes to evade treatment and potentiate future recurrence. Using the lymphatic vasculature as a delivery system for cancer therapies to the lymph nodes has gained increasing interest. For therapies to be effectively taken up by lymphatic vessels and not blood capillaries requires specific characteristics of drug formulations such as being of a particular size and molecular weight, lipophilicity and surface charge of the drug carrier, and concentrations of

the drug and carrier (reviewed in (418, 419)). A few anti-cancer drugs have been formulated to target the lymphatic system and have shown promise *in vivo*: a methyl poly(ethylene glycol)-distearoylphosphatidylethanolamine micelle containing doxorubicin reduced the size of lymph node metastases in a melanoma model (420); a PEGylation of interferon-α2 demonstrated anti-tumor efficacy in the lymph nodes of rats with breast cancer (421); cisplatin conjugated to a copolymer block of poly(ethylene oxide)-block-poly(lysine) successfully treated lymph node metastases in a model of squamous cell carcinoma (422); and gemcitabine loaded onto magnetic multiwalled carbon nanotubes (mMWNTs) resulted in better uptake of gemcitabine in the lymph nodes and regression of lymph node metastases in a subcutaneous model of pancreatic cancer (380). Recently, implantable intralymphatic ports have also been evaluated as a mechanism for delivering drugs and DC vaccines to lymph nodes (423, 424). The field of lymphatic-based drug delivery is still in its infancy and more studies are required to demonstrate efficacy and feasibility in patients."

VI. Conclusions and Perspectives

The lymphatic system almost certainly plays a significant role in PDAC progression, as dissemination is seen early and frequently in PDAC patients. However, the specific mechanisms governing tumor-associated lymphangiogenesis, lymphatic invasion, and lymphatic-directed metastasis are sorely under-researched as are the contributions of the PDAC microenvironment to these processes. In this dissertation, we characterized the effects PDAC cells and pancreatic fibroblasts have on lymphatic endothelial cells in regards to recruitment, lymphangiogenesis, and invasion. Using novel small molecule inhibitors, we specifically focused on the roles of E-selectin and CXCR4 in regulating lymphatic invasion and metastasis. Blockade of E-selectin significantly impaired PDAC interactions with lymphatic endothelia resulting in decreased metastasis to the lymph nodes. Blockade of CXCR4 also impaired PDAC invasion of lymphatic endothelia as well as reshaped the PDAC tumor microenvironment. The work presented in this dissertation uncovers some the mechanisms by which lymphatic endothelial cells support PDAC progression (particularly invasion and metastasis) as well as how both PDAC tumor cells and pancreatic

fibroblasts influence lymphatic biology. Further investigation into the role of the lymphatic vasculature during PDAC progression and metastasis will undoubtedly improve our understanding of PDAC biology and lead to improved pancreatic cancer therapies.

References

1. Siegel RL, Miller KD, Jemal A. Cancer statistics, 2015. CA Cancer J Clin. 2015 Jan-Feb;65(1):5-29.

2. Torre LA, Bray F, Siegel RL, Ferlay J, Lortet-Tieulent J, Jemal A. Global cancer statistics, 2012. CA Cancer J Clin. 2015 Mar;65(2):87-108.

3. Ying H, Dey P, Yao W, Kimmelman AC, Draetta GF, Maitra A, et al. Genetics and biology of pancreatic ductal adenocarcinoma. Genes Dev. 2016 Feb 15;30(4):355-85.

4. Polireddy K, Chen Q. Cancer of the Pancreas: Molecular Pathways and Current Advancement in Treatment. J Cancer. 2016 Jul 7;7(11):1497-514.

5. DiMagno EP, Reber HA, Tempero MA. AGA technical review on the epidemiology, diagnosis, and treatment of pancreatic ductal adenocarcinoma. American Gastroenterological Association. Gastroenterology. 1999 Dec;117(6):1464-84.

6. Vauthey JN, Dixon E. AHPBA/SSO/SSAT Consensus Conference on Resectable and Borderline Resectable Pancreatic Cancer: rationale and overview of the conference. Ann Surg Oncol. 2009 Jul;16(7):1725-6.

7. Burris HA,3rd, Moore MJ, Andersen J, Green MR, Rothenberg ML, Modiano MR, et al. Improvements in survival and clinical benefit with gemcitabine as first-line therapy for patients with advanced pancreas cancer: a randomized trial. J Clin Oncol. 1997 Jun;15(6):2403-13.

8. Hu J, Zhao G, Wang HX, Tang L, Xu YC, Ma Y, et al. A meta-analysis of gemcitabine containing chemotherapy for locally advanced and metastatic pancreatic adenocarcinoma. J Hematol Oncol. 2011 Mar 26;4:11,8722-4-11.

9. Heinemann V, Labianca R, Hinke A, Louvet C. Increased survival using platinum analog combined with gemcitabine as compared to single-agent gemcitabine in advanced pancreatic cancer: pooled analysis of two randomized trials, the GERCOR/GISCAD intergroup study and a German multicenter study. Ann Oncol. 2007 Oct;18(10):1652-9.

10. Cunningham D, Chau I, Stocken DD, Valle JW, Smith D, Steward W, et al. Phase III randomized comparison of gemcitabine versus gemcitabine plus capecitabine in patients with advanced pancreatic cancer. J Clin Oncol. 2009 Nov 20;27(33):5513-8.

11. Von Hoff DD, Ramanathan RK, Borad MJ, Laheru DA, Smith LS, Wood TE, et al. Gemcitabine plus nab-paclitaxel is an active regimen in patients with advanced pancreatic cancer: a phase I/II trial. J Clin Oncol. 2011 Dec 1;29(34):4548-54.

12. Conroy T, Desseigne F, Ychou M, Bouche O, Guimbaud R, Becouarn Y, et al. FOLFIRINOX versus gemcitabine for metastatic pancreatic cancer. N Engl J Med. 2011 May 12;364(19):1817-25.

13. Lee ES, Lee JM. Imaging diagnosis of pancreatic cancer: a state-of-the-art review. World J Gastroenterol. 2014 Jun 28;20(24):7864-77.

14. Herreros-Villanueva M, Bujanda L. Non-invasive biomarkers in pancreatic cancer diagnosis: what we need versus what we have. Ann Transl Med. 2016 Apr;4(7):134.

15. Ujiki MB, Talamonti MS. Surgical management of pancreatic cancer. Semin Radiat Oncol. 2005 Oct;15(4):218-25.

16. Jones S, Zhang X, Parsons DW, Lin JC, Leary RJ, Angenendt P, et al. Core signaling pathways in human pancreatic cancers revealed by global genomic analyses. Science. 2008 Sep 26;321(5897):1801-6.

17. Biankin AV, Waddell N, Kassahn KS, Gingras MC, Muthuswamy LB, Johns AL, et al. Pancreatic cancer genomes reveal aberrations in axon guidance pathway genes. Nature. 2012 Nov 15;491(7424):399-405.

18. Sausen M, Phallen J, Adleff V, Jones S, Leary RJ, Barrett MT, et al. Clinical implications of genomic alterations in the tumour and circulation of pancreatic cancer patients. Nat Commun. 2015 Jul 7;6:7686.

19. Waddell N, Pajic M, Patch AM, Chang DK, Kassahn KS, Bailey P, et al. Whole genomes redefine the mutational landscape of pancreatic cancer. Nature. 2015 Feb 26;518(7540):495-501.

20. Witkiewicz AK, McMillan EA, Balaji U, Baek G, Lin WC, Mansour J, et al. Whole-exome sequencing of pancreatic cancer defines genetic diversity and therapeutic targets. Nat Commun. 2015 Apr 9;6:6744.

21. Klimstra DS, Longnecker DS. K-ras mutations in pancreatic ductal proliferative lesions. Am J Pathol. 1994 Dec;145(6):1547-50.

22. Kanda M, Matthaei H, Wu J, Hong SM, Yu J, Borges M, et al. Presence of somatic mutations in most early-stage pancreatic intraepithelial neoplasia. Gastroenterology. 2012 Apr;142(4):730,733.e9.

23. Murphy SJ, Hart SN, Lima JF, Kipp BR, Klebig M, Winters JL, et al. Genetic alterations associated with progression from pancreatic intraepithelial neoplasia to invasive pancreatic tumor. Gastroenterology. 2013 Nov;145(5):1098,1109.e1.

24. Ryan DP, Hong TS, Bardeesy N. Pancreatic adenocarcinoma. N Engl J Med. 2014 Nov 27;371(22):2140-1.

25. Vincent A, Herman J, Schulick R, Hruban RH, Goggins M. Pancreatic cancer. Lancet. 2011 Aug 13;378(9791):607-20.

26. Rozenblum E, Schutte M, Goggins M, Hahn SA, Panzer S, Zahurak M, et al. Tumor-suppressive pathways in pancreatic carcinoma. Cancer Res. 1997 May 1;57(9):1731-4.

27. Boschman CR, Stryker S, Reddy JK, Rao MS. Expression of p53 protein in precursor lesions and adenocarcinoma of human pancreas. Am J Pathol. 1994 Dec;145(6):1291-5.

28. Hezel AF, Kimmelman AC, Stanger BZ, Bardeesy N, Depinho RA. Genetics and biology of pancreatic ductal adenocarcinoma. Genes Dev. 2006 May 15;20(10):1218-49.

29. Maitra A, Hruban RH. Pancreatic cancer. Annu Rev Pathol. 2008;3:157-88.

30. Hidalgo M. Pancreatic cancer. N Engl J Med. 2010 Apr 29;362(17):1605-17.

31. Aguirre AJ, Bardeesy N, Sinha M, Lopez L, Tuveson DA, Horner J, et al. Activated Kras and Ink4a/Arf deficiency cooperate to produce metastatic pancreatic ductal adenocarcinoma. Genes Dev. 2003 Dec 15;17(24):3112-26.

32. Wilentz RE, Iacobuzio-Donahue CA, Argani P, McCarthy DM, Parsons JL, Yeo CJ, et al. Loss of expression of Dpc4 in pancreatic intraepithelial neoplasia: evidence that DPC4 inactivation occurs late in neoplastic progression. Cancer Res. 2000 Apr 1;60(7):2002-6.

33. Katz MH, Hwang R, Fleming JB, Evans DB. Tumor-node-metastasis staging of pancreatic adenocarcinoma. CA Cancer J Clin. 2008 Mar-Apr;58(2):111-25.

34. Robinson SM, Rahman A, Haugk B, French JJ, Manas DM, Jaques BC, et al. Metastatic lymph node ratio as an important prognostic factor in pancreatic ductal adenocarcinoma. Eur J Surg Oncol. 2012 Apr;38(4):333-9.

35. Kedra B, Popiela T, Sierzega M, Precht A. Prognostic factors of long-term survival after resective procedures for pancreatic cancer. Hepatogastroenterology. 2001 Nov-Dec;48(42):1762-6.

36. Benassai G, Mastrorilli M, Mosella F, Mosella G. Significance of lymph node metastases in the surgical management of pancreatic head carcinoma. J Exp Clin Cancer Res. 1999 Mar;18(1):23-8.

37. Delcore R, Rodriguez FJ, Forster J, Hermreck AS, Thomas JH. Significance of lymph node metastases in patients with pancreatic cancer undergoing curative resection. Am J Surg. 1996 Nov;172(5):463,8; discussion 468-9.

38. Liu QH, Shi ML, Bai J, Zheng JN. Identification of ANXA1 as a lymphatic metastasis and poor prognostic factor in pancreatic ductal adenocarcinoma. Asian Pac J Cancer Prev. 2015;16(7):2719-24.

39. Nathanson SD, Shah R, Rosso K. Sentinel lymph node metastases in cancer: causes, detection and their role in disease progression. Semin Cell Dev Biol. 2015 Feb;38:106-16.

40. Kawada K, Taketo MM. Significance and mechanism of lymph node metastasis in cancer progression. Cancer Res. 2011 Feb 15;71(4):1214-8.

41. Sleeman JP. The lymph node pre-metastatic niche. J Mol Med (Berl). 2015 Nov;93(11):1173-84.

42. Stacker SA, Williams SP, Karnezis T, Shayan R, Fox SB, Achen MG. Lymphangiogenesis and lymphatic vessel remodelling in cancer. Nat Rev Cancer. 2014 Mar;14(3):159-72.

43. Tammela T, Alitalo K. Lymphangiogenesis: Molecular mechanisms and future promise. Cell. 2010 Feb 19;140(4):460-76.

44. Maby-El Hajjami H, Petrova TV. Developmental and pathological lymphangiogenesis: from models to human disease. Histochem Cell Biol. 2008 Dec;130(6):1063-78.

45. Baluk P, Fuxe J, Hashizume H, Romano T, Lashnits E, Butz S, et al. Functionally specialized junctions between endothelial cells of lymphatic vessels. J Exp Med. 2007 Oct 1;204(10):2349-62.

46. Pflicke H, Sixt M. Preformed portals facilitate dendritic cell entry into afferent lymphatic vessels. J Exp Med. 2009 Dec 21;206(13):2925-35.

47. Gerli R, Solito R, Weber E, Agliano M. Specific adhesion molecules bind anchoring filaments and endothelial cells in human skin initial lymphatics. Lymphology. 2000 Dec;33(4):148-57.

48. Solito R, Alessandrini C, Fruschelli M, Pucci AM, Gerli R. An immunological correlation between the anchoring filaments of initial lymph vessels and the neighboring elastic fibers: a unified morphofunctional concept. Lymphology. 1997 Dec;30(4):194-202.

49. Bazigou E, Wilson JT, Moore JE,Jr. Primary and secondary lymphatic valve development: molecular, functional and mechanical insights. Microvasc Res. 2014 Nov;96:38-45.

50. von der Weid PY, Zawieja DC. Lymphatic smooth muscle: the motor unit of lymph drainage. Int J Biochem Cell Biol. 2004 Jul;36(7):1147-53.

51. Leak LV, Burke JF. Fine structure of the lymphatic capillary and the adjoining connective tissue area. Am J Anat. 1966 May;118(3):785-809.

52. Alitalo A, Detmar M. Interaction of tumor cells and lymphatic vessels in cancer progression. Oncogene. 2012 Oct 18;31(42):4499-508.

53. O'Morchoe CC. Lymphatic system of the pancreas. Microsc Res Tech. 1997 Jun 1-15;37(5-6):456-77.

54. Cesmebasi A, Malefant J, Patel SD, Du Plessis M, Renna S, Tubbs RS, et al. The surgical anatomy of the lymphatic system of the pancreas. Clin Anat. 2015 May;28(4):527-37.

55. Isaji S, Kawarada Y, Uemoto S. Classification of pancreatic cancer: comparison of Japanese and UICC classifications. Pancreas. 2004 Apr;28(3):231-4.

56. Kanda M, Fujii T, Nagai S, Kodera Y, Kanzaki A, Sahin TT, et al. Pattern of lymph node metastasis spread in pancreatic cancer. Pancreas. 2011 Aug;40(6):951-5.

57. Sun W, Leong CN, Zhang Z, Lu JJ. Proposing the lymphatic target volume for elective radiation therapy for pancreatic cancer: a pooled analysis of clinical evidence. Radiat Oncol. 2010 Apr 15;5:28,717X-5-28.

58. Fujita T, Nakagohri T, Gotohda N, Takahashi S, Konishi M, Kojima M, et al. Evaluation of the prognostic factors and significance of lymph node status in invasive ductal carcinoma of the body or tail of the pancreas. Pancreas. 2010 Jan;39(1):e48-54.

59. Nagakawa T, Kobayashi H, Ueno K, Ohta T, Kayahara M, Miyazaki I. Clinical study of lymphatic flow to the paraaortic lymph nodes in carcinoma of the head of the pancreas. Cancer. 1994 Feb 15;73(4):1155-62.

60. Zheng W, Aspelund A, Alitalo K. Lymphangiogenic factors, mechanisms, and applications. J Clin Invest. 2014 Mar;124(3):878-87.

61. Veikkola T, Jussila L, Makinen T, Karpanen T, Jeltsch M, Petrova TV, et al. Signalling via vascular endothelial growth factor receptor-3 is sufficient for lymphangiogenesis in transgenic mice. EMBO J. 2001 Mar 15;20(6):1223-31.

62. Joukov V, Pajusola K, Kaipainen A, Chilov D, Lahtinen I, Kukk E, et al. A novel vascular endothelial growth factor, VEGF-C, is a ligand for the Flt4 (VEGFR-3) and KDR (VEGFR-2) receptor tyrosine kinases. EMBO J. 1996 Jan 15;15(2):290-8.

63. Oh SJ, Jeltsch MM, Birkenhager R, McCarthy JE, Weich HA, Christ B, et al. VEGF and VEGF-C: specific induction of angiogenesis and lymphangiogenesis in the differentiated avian chorioallantoic membrane. Dev Biol. 1997 Aug 1;188(1):96-109.

64. Achen MG, Jeltsch M, Kukk E, Makinen T, Vitali A, Wilks AF, et al. Vascular endothelial growth factor D (VEGF-D) is a ligand for the tyrosine kinases VEGF receptor 2 (Flk1) and VEGF receptor 3 (Flt4). Proc Natl Acad Sci U S A. 1998 Jan 20;95(2):548-53.

65. Favier B, Alam A, Barron P, Bonnin J, Laboudie P, Fons P, et al. Neuropilin-2 interacts with VEGFR-2 and VEGFR-3 and promotes human endothelial cell survival and migration. Blood. 2006 Aug 15;108(4):1243-50.

66. Bjorndahl MA, Cao R, Burton JB, Brakenhielm E, Religa P, Galter D, et al. Vascular endothelial growth factor-a promotes peritumoral lymphangiogenesis and lymphatic metastasis. Cancer Res. 2005 Oct 15;65(20):9261-8.

67. Morisada T, Oike Y, Yamada Y, Urano T, Akao M, Kubota Y, et al. Angiopoietin-1 promotes LYVE-1-positive lymphatic vessel formation. Blood. 2005 Jun 15;105(12):4649-56.

68. Yan ZX, Jiang ZH, Liu NF. Angiopoietin-2 promotes inflammatory lymphangiogenesis and its effect can be blocked by the specific inhibitor L1-10. Am J Physiol Heart Circ Physiol. 2012 Jan 1;302(1):H215-23.

69. Kubo H, Cao R, Brakenhielm E, Makinen T, Cao Y, Alitalo K. Blockade of vascular endothelial growth factor receptor-3 signaling inhibits fibroblast growth factor-2-induced lymphangiogenesis in mouse cornea. Proc Natl Acad Sci U S A. 2002 Jun 25;99(13):8868-73.

70. Cao R, Bjorndahl MA, Gallego MI, Chen S, Religa P, Hansen AJ, et al. Hepatocyte growth factor is a lymphangiogenic factor with an indirect mechanism of action. Blood. 2006 May 1;107(9):3531-6.

71. Bjorndahl M, Cao R, Nissen LJ, Clasper S, Johnson LA, Xue Y, et al. Insulin-like growth factors 1 and 2 induce lymphangiogenesis in vivo. Proc Natl Acad Sci U S A. 2005 Oct 25;102(43):15593-8.

72. Fink DM, Connor AL, Kelley PM, Steele MM, Hollingsworth MA, Tempero RM. Nerve growth factor regulates neurolymphatic remodeling during corneal inflammation and resolution. PLoS One. 2014 Nov 10;9(11):e112737.

73. Marino D, Angehrn Y, Klein S, Riccardi S, Baenziger-Tobler N, Otto VI, et al. Activation of the epidermal growth factor receptor promotes lymphangiogenesis in the skin. J Dermatol Sci. 2013 Sep;71(3):184-94.

74. Bracher A, Cardona AS, Tauber S, Fink AM, Steiner A, Pehamberger H, et al. Epidermal growth factor facilitates melanoma lymph node metastasis by influencing tumor lymphangiogenesis. J Invest Dermatol. 2013 Jan;133(1):230-8.

75. Dadras SS. An unexpected role for EGF in lymphangiogenesis-mediated melanoma metastasis to sentinel lymph nodes. J Invest Dermatol. 2013 Jan;133(1):14-6.

76. Cao R, Bjorndahl MA, Religa P, Clasper S, Garvin S, Galter D, et al. PDGF-BB induces intratumoral lymphangiogenesis and promotes lymphatic metastasis. Cancer Cell. 2004 Oct;6(4):333-45.

77. Miyazaki H, Yoshimatsu Y, Akatsu Y, Mishima K, Fukayama M, Watabe T, et al. Expression of platelet-derived growth factor receptor beta is maintained by Prox1 in lymphatic endothelial cells and is required for tumor lymphangiogenesis. Cancer Sci. 2014 Sep;105(9):1116-23.

78. Duong T, Koopman P, Francois M. Tumor lymphangiogenesis as a potential therapeutic target. J Oncol. 2012;2012:204946.

79. Koyama H, Kobayashi N, Harada M, Takeoka M, Kawai Y, Sano K, et al. Significance of tumor-associated stroma in promotion of intratumoral lymphangiogenesis: pivotal role of a hyaluronan-rich tumor microenvironment. Am J Pathol. 2008 Jan;172(1):179-93.

80. Mace TA, Ameen Z, Collins A, Wojcik S, Mair M, Young GS, et al. Pancreatic cancer-associated stellate cells promote differentiation of myeloid-derived suppressor cells in a STAT3-dependent manner. Cancer Res. 2013 May 15;73(10):3007-18.

81. Feig C, Gopinathan A, Neesse A, Chan DS, Cook N, Tuveson DA. The pancreas cancer microenvironment. Clin Cancer Res. 2012 Aug 15;18(16):4266-76.

82. Peppicelli S, Bianchini F, Calorini L. Inflammatory cytokines induce vascular endothelial growth factor-C expression in melanoma-associated macrophages and stimulate melanoma lymph node metastasis. Oncol Lett. 2014 Sep;8(3):1133-8.

83. Huang WC, Nagahashi M, Terracina KP, Takabe K. Emerging Role of Sphingosine-1-phosphate in Inflammation, Cancer, and Lymphangiogenesis. Biomolecules. 2013;3(3):10.3390/biom3030408.

84. Murakami M, Zheng Y, Hirashima M, Suda T, Morita Y, Ooehara J, et al. VEGFR1 tyrosine kinase signaling promotes lymphangiogenesis as well as angiogenesis indirectly via macrophage recruitment. Arterioscler Thromb Vasc Biol. 2008 Apr;28(4):658-64.

85. Cursiefen C, Chen L, Borges LP, Jackson D, Cao J, Radziejewski C, et al. VEGF-A stimulates lymphangiogenesis and hemangiogenesis in inflammatory neovascularization via macrophage recruitment. J Clin Invest. 2004 Apr;113(7):1040-50.

86. Schulz P, Fischer C, Detjen KM, Rieke S, Hilfenhaus G, von Marschall Z, et al. Angiopoietin-2 drives lymphatic metastasis of pancreatic cancer. FASEB J. 2011 Oct;25(10):3325-35.

87. Liu X, Guo XZ, Li HY, Chen J, Ren LN, Wu CY. KAI1 inhibits lymphangiogenesis and lymphatic metastasis of pancreatic cancer in vivo. Hepatobiliary Pancreat Dis Int. 2014 Feb;13(1):87-92.

88. Tang RF, Itakura J, Aikawa T, Matsuda K, Fujii H, Korc M, et al. Overexpression of lymphangiogenic growth factor VEGF-C in human pancreatic cancer. Pancreas. 2001 Apr;22(3):285-92.

89. Morfoisse F, Kuchnio A, Frainay C, Gomez-Brouchet A, Delisle MB, Marzi S, et al. Hypoxia induces VEGF-C expression in metastatic tumor cells via a HIF-1alpha-independent translation-mediated mechanism. Cell Rep. 2014 Jan 16;6(1):155-67.

90. Khromova N, Kopnin P, Rybko V, Kopnin BP. Downregulation of VEGF-C expression in lung and colon cancer cells decelerates tumor growth and inhibits metastasis via multiple mechanisms. Oncogene. 2012 Mar 15;31(11):1389-97.

91. Skobe M, Hawighorst T, Jackson DG, Prevo R, Janes L, Velasco P, et al. Induction of tumor lymphangiogenesis by VEGF-C promotes breast cancer metastasis. Nat Med. 2001 Feb;7(2):192-8.

92. Quagliata L, Klusmeier S, Cremers N, Pytowski B, Harvey A, Pettis RJ, et al. Inhibition of VEGFR-3 activation in tumor-draining lymph nodes suppresses the outgrowth of lymph node metastases in the MT-450 syngeneic rat breast cancer model. Clin Exp Metastasis. 2014 Mar;31(3):351-65.

93. Pereira ER, Jones D, Jung K, Padera TP. The lymph node microenvironment and its role in the progression of metastatic cancer. Semin Cell Dev Biol. 2015 Feb;38:98-105.

94. Kurahara H, Takao S, Shinchi H, Maemura K, Mataki Y, Sakoda M, et al. Significance of lymphangiogenesis in primary tumor and draining lymph nodes during lymphatic metastasis of pancreatic head cancer. J Surg Oncol. 2010 Dec 1;102(7):809-15.

95. Harrell MI, Iritani BM, Ruddell A. Tumor-induced sentinel lymph node lymphangiogenesis and increased lymph flow precede melanoma metastasis. Am J Pathol. 2007 Feb;170(2):774-86.

96. Swartz MA, Lund AW. Lymphatic and interstitial flow in the tumour microenvironment: linking mechanobiology with immunity. Nat Rev Cancer. 2012 Feb 24;12(3):210-9.

97. Munn DH, Mellor AL. The tumor-draining lymph node as an immune-privileged site. Immunol Rev. 2006 Oct;213:146-58.

98. Lund AW, Duraes FV, Hirosue S, Raghavan VR, Nembrini C, Thomas SN, et al. VEGF-C promotes immune tolerance in B16 melanomas and cross-presentation of tumor antigen by lymph node lymphatics. Cell Rep. 2012 Mar 29;1(3):191-9.

99. Hirosue S, Vokali E, Raghavan VR, Rincon-Restrepo M, Lund AW, Corthesy-Henrioud P, et al. Steady-state antigen scavenging, cross-presentation, and CD8+ T cell priming: a new role for lymphatic endothelial cells. J Immunol. 2014 Jun 1;192(11):5002-11.

100. Tewalt EF, Cohen JN, Rouhani SJ, Guidi CJ, Qiao H, Fahl SP, et al. Lymphatic endothelial cells induce tolerance via PD-L1 and lack of costimulation leading to high-level PD-1 expression on CD8 T cells. Blood. 2012 Dec 6;120(24):4772-82.

101. Kim M, Koh YJ, Kim KE, Koh BI, Nam DH, Alitalo K, et al. CXCR4 signaling regulates metastasis of chemoresistant melanoma cells by a lymphatic metastatic niche. Cancer Res. 2010 Dec 15;70(24):10411-21.

102. Lee E, Fertig EJ, Jin K, Sukumar S, Pandey NB, Popel AS. Breast cancer cells condition lymphatic endothelial cells within pre-metastatic niches to promote metastasis. Nat Commun. 2014 Sep 2;5:4715.

103. Garmy-Susini B, Avraamides CJ, Desgrosellier JS, Schmid MC, Foubert P, Ellies LG, et al. PI3Kalpha activates integrin alpha4beta1 to establish a metastatic niche in lymph nodes. Proc Natl Acad Sci U S A. 2013 May 28;110(22):9042-7.

104. Issa A, Le TX, Shoushtari AN, Shields JD, Swartz MA. Vascular endothelial growth factor-C and C-C chemokine receptor 7 in tumor cell-lymphatic cross-talk promote invasive phenotype. Cancer Res. 2009 Jan 1;69(1):349-57.

105. Wang Z, Wu J, Li G, Zhang X, Tong M, Wu Z, et al. Lymphangiogenesis and biological behavior in pancreatic carcinoma and other pancreatic tumors. Mol Med Rep. 2012 Apr;5(4):959-63.

106. Von Marschall Z, Scholz A, Stacker SA, Achen MG, Jackson DG, Alves F, et al. Vascular endothelial growth factor-D induces lymphangiogenesis and lymphatic metastasis in models of ductal pancreatic cancer. Int J Oncol. 2005 Sep;27(3):669-79.

107. Zhang B, Zhao WH, Zhou WY, Yu WS, Yu JM, Li S. Expression of vascular endothelial growth factors-C and -D correlate with evidence of lymphangiogenesis and angiogenesis in pancreatic adenocarcinoma. Cancer Detect Prev. 2007;31(6):436-42.

108. Koch M, Dettori D, Van Nuffelen A, Souffreau J, Marconcini L, Wallays G, et al. VEGF-D deficiency in mice does not affect embryonic or postnatal lymphangiogenesis but reduces lymphatic metastasis. J Pathol. 2009 Nov;219(3):356-64.

109. Shi Y, Tong M, Wu Y, Yang Z, Hoffman RM, Zhang Y, et al. VEGF-C ShRNA inhibits pancreatic cancer growth and lymphangiogenesis in an orthotopic fluorescent nude mouse model. Anticancer Res. 2013 Feb;33(2):409-17.

110. Sipos B, Kojima M, Tiemann K, Klapper W, Kruse ML, Kalthoff H, et al. Lymphatic spread of ductal pancreatic adenocarcinoma is independent of lymphangiogenesis. J Pathol. 2005 Nov;207(3):301-12.

111. Liu Z, Luo G, Guo M, Jin K, Xiao Z, Liu L, et al. Lymph node status predicts the benefit of adjuvant chemoradiotherapy for patients with resected pancreatic cancer. Pancreatology. 2015 May-Jun;15(3):253-8.

112. Konstantinidis IT, Deshpande V, Zheng H, Wargo JA, Fernandez-del Castillo C, Thayer SP, et al. Does the mechanism of lymph node invasion affect survival in patients with pancreatic ductal adenocarcinoma? J Gastrointest Surg. 2010 Feb;14(2):261-7.

113. Buc E, Couvelard A, Kwiatkowski F, Dokmak S, Ruszniewski P, Hammel P, et al. Adenocarcinoma of the pancreas: Does prognosis depend on mode of lymph node invasion? Eur J Surg Oncol. 2014 Nov;40(11):1578-85.

114. Pai RK, Beck AH, Mitchem J, Linehan DC, Chang DT, Norton JA, et al. Pattern of lymph node involvement and prognosis in pancreatic adenocarcinoma: direct lymph node invasion has similar survival to node-negative disease. Am J Surg Pathol. 2011 Feb;35(2):228-34.

115. Zorgetto VA, Silveira GG, Oliveira-Costa JP, Soave DF, Soares FA, Ribeiro-Silva A. The relationship between lymphatic vascular density and vascular endothelial growth factor A (VEGF-A) expression with clinical-pathological features and survival in pancreatic adenocarcinomas. Diagn Pathol. 2013 Oct 18;8:170,1596-8-170.

116. Schneider M, Buchler P, Giese N, Giese T, Wilting J, Buchler MW, et al. Role of lymphangiogenesis and lymphangiogenic factors during pancreatic cancer progression and lymphatic spread. Int J Oncol. 2006 Apr;28(4):883-90.

117. Rubbia-Brandt L, Terris B, Giostra E, Dousset B, Morel P, Pepper MS. Lymphatic vessel density and vascular endothelial growth factor-C expression correlate with malignant behavior in human pancreatic endocrine tumors. Clin Cancer Res. 2004 Oct 15;10(20):6919-28.

118. Olszewski WL, Stanczyk M, Gewartowska M, Domaszewska-Szostek A, Durlik M. Lack of functioning intratumoral lymphatics in colon and pancreas cancer tissue. Lymphat Res Biol. 2012 Sep;10(3):112-7.

119. Padera TP, Kadambi A, di Tomaso E, Carreira CM, Brown EB, Boucher Y, et al. Lymphatic metastasis in the absence of functional intratumor lymphatics. Science. 2002 Jun 7;296(5574):1883-6.

120. Hartveit E. Attenuated cells in breast stroma: the missing lymphatic system of the breast. Histopathology. 1990 Jun;16(6):533-43.

121. Naidoo K, Jones R, Dmitrovic B, Wijesuriya N, Kocher H, Hart IR, et al. Proteome of formalin-fixed paraffin-embedded pancreatic ductal adenocarcinoma and lymph node metastases. J Pathol. 2012 Apr;226(5):756-63.

122. Cui Y, Wu J, Zong M, Song G, Jia Q, Jiang J, et al. Proteomic profiling in pancreatic cancer with and without lymph node metastasis. Int J Cancer. 2009 Apr 1;124(7):1614-21.

123. Vigl B, Aebischer D, Nitschke M, Iolyeva M, Rothlin T, Antsiferova O, et al. Tissue inflammation modulates gene expression of lymphatic endothelial cells and dendritic cell migration in a stimulus-dependent manner. Blood. 2011 Jul 7;118(1):205-15.

124. Tal O, Lim HY, Gurevich I, Milo I, Shipony Z, Ng LG, et al. DC mobilization from the skin requires docking to immobilized CCL21 on lymphatic endothelium and intralymphatic crawling. J Exp Med. 2011 Sep 26;208(10):2141-53.

125. Irino T, Takeuchi H, Matsuda S, Saikawa Y, Kawakubo H, Wada N, et al. CC-Chemokine receptor CCR7: a key molecule for lymph node metastasis in esophageal squamous cell carcinoma. BMC Cancer. 2014 Apr 26;14:291,2407-14-291.

126. Hwang TL, Lee LY, Wang CC, Liang Y, Huang SF, Wu CM. CCL7 and CCL21 overexpression in gastric cancer is associated with lymph node metastasis and poor prognosis. World J Gastroenterol. 2012 Mar 21;18(11):1249-56.

127. Zhao B, Cui K, Wang CL, Wang AL, Zhang B, Zhou WY, et al. The chemotactic interaction between CCL21 and its receptor, CCR7, facilitates the progression of pancreatic cancer via induction of angiogenesis and lymphangiogenesis. J Hepatobiliary Pancreat Sci. 2011 Nov;18(6):821-8.

128. Muller A, Homey B, Soto H, Ge N, Catron D, Buchanan ME, et al. Involvement of chemokine receptors in breast cancer metastasis. Nature. 2001 Mar 1;410(6824):50-6.

129. Guo J, Lou W, Ji Y, Zhang S. Effect of CCR7, CXCR4 and VEGF-C on the lymph node metastasis of human pancreatic ductal adenocarcinoma. Oncol Lett. 2013 May;5(5):1572-8.

130. Sperveslage J, Frank S, Heneweer C, Egberts J, Schniewind B, Buchholz M, et al. Lack of CCR7 expression is rate limiting for lymphatic spread of pancreatic ductal adenocarcinoma. Int J Cancer. 2012 Aug 15;131(4):E371-81.

131. Miteva DO, Rutkowski JM, Dixon JB, Kilarski W, Shields JD, Swartz MA. Transmural flow modulates cell and fluid transport functions of lymphatic endothelium. Circ Res. 2010 Mar 19;106(5):920-31.

132. Emmett MS, Lanati S, Dunn DB, Stone OA, Bates DO. CCR7 mediates directed growth of melanomas towards lymphatics. Microcirculation. 2011 Apr;18(3):172-82.

133. Shields JD, Emmett MS, Dunn DB, Joory KD, Sage LM, Rigby H, et al. Chemokine-mediated migration of melanoma cells towards lymphatics--a mechanism contributing to metastasis. Oncogene. 2007 May 10;26(21):2997-3005.

134. Pang MF, Georgoudaki AM, Lambut L, Johansson J, Tabor V, Hagikura K, et al. TGF-beta1-induced EMT promotes targeted migration of breast cancer cells through the lymphatic system by the activation of CCR7/CCL21-mediated chemotaxis. Oncogene. 2015 May 11.

135. Yu S, Duan J, Zhou Z, Pang Q, Wuyang J, Liu T, et al. A critical role of CCR7 in invasiveness and metastasis of SW620 colon cancer cell in vitro and in vivo. Cancer Biol Ther. 2008 Jul;7(7):1037-43.

136. Wiley HE, Gonzalez EB, Maki W, Wu MT, Hwang ST. Expression of CC chemokine receptor-7 and regional lymph node metastasis of B16 murine melanoma. J Natl Cancer Inst. 2001 Nov 7;93(21):1638-43.

137. Cui K, Zhao W, Wang C, Wang A, Zhang B, Zhou W, et al. The CXCR4-CXCL12 pathway facilitates the progression of pancreatic cancer via induction of angiogenesis and lymphangiogenesis. J Surg Res. 2011 Nov;171(1):143-50.

138. Kaifi JT, Yekebas EF, Schurr P, Obonyo D, Wachowiak R, Busch P, et al. Tumor-cell homing to lymph nodes and bone marrow and CXCR4 expression in esophageal cancer. J Natl Cancer Inst. 2005 Dec 21;97(24):1840-7.

139. Cardones AR, Murakami T, Hwang ST. CXCR4 enhances adhesion of B16 tumor cells to endothelial cells in vitro and in vivo via beta(1) integrin. Cancer Res. 2003 Oct 15;63(20):6751-7.

140. Wehler T, Wolfert F, Schimanski CC, Gockel I, Herr W, Biesterfeld S, et al. Strong expression of chemokine receptor CXCR4 by pancreatic cancer correlates with advanced disease. Oncol Rep. 2006 Dec;16(6):1159-64.

141. Hirakawa S, Detmar M, Kerjaschki D, Nagamatsu S, Matsuo K, Tanemura A, et al. Nodal lymphangiogenesis and metastasis: Role of tumor-induced lymphatic vessel activation in extramammary Paget's disease. Am J Pathol. 2009 Nov;175(5):2235-48.

142. Liu X, Xiao Q, Bai X, Yu Z, Sun M, Zhao H, et al. Activation of STAT3 is involved in malignancy mediated by CXCL12-CXCR4 signaling in human breast cancer. Oncol Rep. 2014 Dec;32(6):2760-8.

143. Uchida D, Onoue T, Kuribayashi N, Tomizuka Y, Tamatani T, Nagai H, et al. Blockade of CXCR4 in oral squamous cell carcinoma inhibits lymph node metastases. Eur J Cancer. 2011 Feb;47(3):452-9.

144. Chu H, Zhou H, Liu Y, Liu X, Hu Y, Zhang J. Functional expression of CXC chemokine recepter-4 mediates the secretion of matrix metalloproteinases from mouse hepatocarcinoma cell lines with different lymphatic metastasis ability. Int J Biochem Cell Biol. 2007;39(1):197-205.

145. Yagi H, Tan W, Dillenburg-Pilla P, Armando S, Amornphimoltham P, Simaan M, et al. A synthetic biology approach reveals a CXCR4-G13-Rho signaling axis driving transendothelial migration of metastatic breast cancer cells. Sci Signal. 2011 Sep 20;4(191):ra60.

146. Johnson LA, Clasper S, Holt AP, Lalor PF, Baban D, Jackson DG. An inflammation-induced mechanism for leukocyte transmigration across lymphatic vessel endothelium. J Exp Med. 2006 Nov 27;203(12):2763-77.

147. Yan J, Jiang Y, Ye M, Liu W, Feng L. The clinical value of lymphatic vessel density, intercellular adhesion molecule 1 and vascular cell adhesion molecule 1 expression in patients with oral tongue squamous cell carcinoma. J Cancer Res Ther. 2014 Nov;10 Suppl:C125-30.

148. Viola K, Kopf S, Huttary N, Vonach C, Kretschy N, Teichmann M, et al. Bay11-7082 inhibits the disintegration of the lymphendothelial barrier triggered by MCF-7 breast cancer spheroids; the role of ICAM-1 and adhesion. Br J Cancer. 2013 Feb 19;108(3):564-9.

149. Kawai Y, Kaidoh M, Ohhashi T. MDA-MB-231 produces ATP-mediated ICAM-1-dependent facilitation of the attachment of carcinoma cells to human lymphatic endothelial cells. Am J Physiol Cell Physiol. 2008 Nov;295(5):C1123-32.

150. Sawa Y, Sugimoto Y, Ueki T, Ishikawa H, Sato A, Nagato T, et al. Effects of TNF-alpha on leukocyte adhesion molecule expressions in cultured human lymphatic endothelium. J Histochem Cytochem. 2007 Jul;55(7):721-33.

151. Kawai Y, Kaidoh M, Yokoyama Y, Sano K, Ohhashi T. Chemokine CCL2 facilitates ICAM-1-mediated interactions of cancer cells and lymphatic endothelial cells in sentinel lymph nodes. Cancer Sci. 2009 Mar;100(3):419-28.

152. Leak LV. The structure of lymphatic capillaries in lymph formation. Fed Proc. 1976 Jun;35(8):1863-71.

153. Dejana E, Orsenigo F, Molendini C, Baluk P, McDonald DM. Organization and signaling of endothelial cell-to-cell junctions in various regions of the blood and lymphatic vascular trees. Cell Tissue Res. 2009 Jan;335(1):17-25.

154. Kerjaschki D, Bago-Horvath Z, Rudas M, Sexl V, Schneckenleithner C, Wolbank S, et al. Lipoxygenase mediates invasion of intrametastatic lymphatic vessels and propagates lymph node metastasis of human mammary carcinoma xenografts in mouse. J Clin Invest. 2011 May;121(5):2000-12.

155. Tacconi C, Correale C, Gandelli A, Spinelli A, Dejana E, D'Alessio S, et al. Vascular endothelial growth factor C disrupts the endothelial lymphatic barrier to promote colorectal cancer invasion. Gastroenterology. 2015 Jun;148(7):1438,51.e8.

156. He Y, Rajantie I, Pajusola K, Jeltsch M, Holopainen T, Yla-Herttuala S, et al. Vascular endothelial cell growth factor receptor 3-mediated activation of lymphatic endothelium is crucial for tumor cell entry and spread via lymphatic vessels. Cancer Res. 2005 Jun 1;65(11):4739-46.

157. Zheng W, Nurmi H, Appak S, Sabine A, Bovay E, Korhonen EA, et al. Angiopoietin 2 regulates the transformation and integrity of lymphatic endothelial cell junctions. Genes Dev. 2014 Jul 15;28(14):1592-603.

158. Neesse A, Michl P, Frese KK, Feig C, Cook N, Jacobetz MA, et al. Stromal biology and therapy in pancreatic cancer. Gut. 2011 Jun;60(6):861-8.

159. Erkan M, Michalski CW, Rieder S, Reiser-Erkan C, Abiatari I, Kolb A, et al. The activated stroma index is a novel and independent prognostic marker in pancreatic ductal adenocarcinoma. Clin Gastroenterol Hepatol. 2008 Oct;6(10):1155-61.

160. Hwang RF, Moore T, Arumugam T, Ramachandran V, Amos KD, Rivera A, et al. Cancer-associated stromal fibroblasts promote pancreatic tumor progression. Cancer Res. 2008 Feb 1;68(3):918-26.

161. Xu Z, Vonlaufen A, Phillips PA, Fiala-Beer E, Zhang X, Yang L, et al. Role of pancreatic stellate cells in pancreatic cancer metastasis. Am J Pathol. 2010 Nov;177(5):2585-96.

162. Apte MV, Park S, Phillips PA, Santucci N, Goldstein D, Kumar RK, et al. Desmoplastic reaction in pancreatic cancer: role of pancreatic stellate cells. Pancreas. 2004 Oct;29(3):179-87.

163. Bailey JM, Mohr AM, Hollingsworth MA. Sonic hedgehog paracrine signaling regulates metastasis and lymphangiogenesis in pancreatic cancer. Oncogene. 2009 Oct 8;28(40):3513-25.

164. Bachem MG, Schunemann M, Ramadani M, Siech M, Beger H, Buck A, et al. Pancreatic carcinoma cells induce fibrosis by stimulating proliferation and matrix synthesis of stellate cells. Gastroenterology. 2005 Apr;128(4):907-21.

165. Olive KP, Jacobetz MA, Davidson CJ, Gopinathan A, McIntyre D, Honess D, et al. Inhibition of Hedgehog signaling enhances delivery of chemotherapy in a mouse model of pancreatic cancer. Science. 2009 Jun 12;324(5933):1457-61.

166. Bailey JM, Swanson BJ, Hamada T, Eggers JP, Singh PK, Caffery T, et al. Sonic hedgehog promotes desmoplasia in pancreatic cancer. Clin Cancer Res. 2008 Oct 1;14(19):5995-6004.

167. Apte MV, Pirola RC, Wilson JS. Pancreatic stellate cells: a starring role in normal and diseased pancreas. Front Physiol. 2012 Aug 28;3:344.

168. Andoh A, Takaya H, Saotome T, Shimada M, Hata K, Araki Y, et al. Cytokine regulation of chemokine (IL-8, MCP-1, and RANTES) gene expression in human pancreatic periacinar myofibroblasts. Gastroenterology. 2000 Jul;119(1):211-9.

169. Shek FW, Benyon RC, Walker FM, McCrudden PR, Pender SL, Williams EJ, et al. Expression of transforming growth factor-beta 1 by pancreatic stellate cells and its implications for matrix secretion and turnover in chronic pancreatitis. Am J Pathol. 2002 May;160(5):1787-98.

170. Bayne LJ, Beatty GL, Jhala N, Clark CE, Rhim AD, Stanger BZ, et al. Tumor-derived granulocyte-macrophage colony-stimulating factor regulates myeloid inflammation and T cell immunity in pancreatic cancer. Cancer Cell. 2012 Jun 12;21(6):822-35.

171. Feig C, Jones JO, Kraman M, Wells RJ, Deonarine A, Chan DS, et al. Targeting CXCL12 from FAP-expressing carcinoma-associated fibroblasts synergizes with anti-PD-L1 immunotherapy in pancreatic cancer. Proc Natl Acad Sci U S A. 2013 Dec 10;110(50):20212-7.

172. Ene-Obong A, Clear AJ, Watt J, Wang J, Fatah R, Riches JC, et al. Activated pancreatic stellate cells sequester CD8+ T cells to reduce their infiltration of the juxtatumoral compartment of pancreatic ductal adenocarcinoma. Gastroenterology. 2013 Nov;145(5):1121-32.

173. Chen R, Pan S, Ottenhof NA, de Wilde RF, Wolfgang CL, Lane Z, et al. Stromal galectin-1 expression is associated with long-term survival in resectable pancreatic ductal adenocarcinoma. Cancer Biol Ther. 2012 Aug;13(10):899-907.

174. Tang D, Yuan Z, Xue X, Lu Z, Zhang Y, Wang H, et al. High expression of Galectin-1 in pancreatic stellate cells plays a role in the development and maintenance of an immunosuppressive microenvironment in pancreatic cancer. Int J Cancer. 2012 May 15;130(10):2337-48.

175. Ozdemir BC, Pentcheva-Hoang T, Carstens JL, Zheng X, Wu CC, Simpson TR, et al. Depletion of carcinoma-associated fibroblasts and fibrosis induces immunosuppression and accelerates pancreas cancer with reduced survival. Cancer Cell. 2014 Jun 16;25(6):719-34.

176. Rhim AD, Oberstein PE, Thomas DH, Mirek ET, Palermo CF, Sastra SA, et al. Stromal elements act to restrain, rather than support, pancreatic ductal adenocarcinoma. Cancer Cell. 2014 Jun 16;25(6):735-47.

177. Lee JJ, Perera RM, Wang H, Wu DC, Liu XS, Han S, et al. Stromal response to Hedgehog signaling restrains pancreatic cancer progression. Proc Natl Acad Sci U S A. 2014 Jul 29;111(30):E3091-100.

178. Ohlund D, Elyada E, Tuveson D. Fibroblast heterogeneity in the cancer wound. J Exp Med. 2014 Jul 28;211(8):1503-23.

179. Sugimoto H, Mundel TM, Kieran MW, Kalluri R. Identification of fibroblast heterogeneity in the tumor microenvironment. Cancer Biol Ther. 2006 Dec;5(12):1640-6.

180. Hanahan D, Coussens LM. Accessories to the crime: functions of cells recruited to the tumor microenvironment. Cancer Cell. 2012 Mar 20;21(3):309-22.

181. Tian H, Callahan CA, DuPree KJ, Darbonne WC, Ahn CP, Scales SJ, et al. Hedgehog signaling is restricted to the stromal compartment during pancreatic carcinogenesis. Proc Natl Acad Sci U S A. 2009 Mar 17;106(11):4254-9.

182. Rasanen K, Vaheri A. Activation of fibroblasts in cancer stroma. Exp Cell Res. 2010 Oct 15;316(17):2713-22.

183. Liao D, Luo Y, Markowitz D, Xiang R, Reisfeld RA. Cancer associated fibroblasts promote tumor growth and metastasis by modulating the tumor immune microenvironment in a 4T1 murine breast cancer model. PLoS One. 2009 Nov 23;4(11):e7965.

184. Kessenbrock K, Plaks V, Werb Z. Matrix metalloproteinases: regulators of the tumor microenvironment. Cell. 2010 Apr 2;141(1):52-67.

185. Shi K, Queiroz KC, Roelofs JJ, van Noesel CJ, Richel DJ, Spek CA. Protease-activated receptor 2 suppresses lymphangiogenesis and subsequent lymph node metastasis in a murine pancreatic cancer model. J Pathol. 2014 Nov;234(3):398-409.

186. Wormann SM, Diakopoulos KN, Lesina M, Algul H. The immune network in pancreatic cancer development and progression. Oncogene. 2014 Jun 5;33(23):2956-67.

187. Grivennikov SI, Greten FR, Karin M. Immunity, inflammation, and cancer. Cell. 2010 Mar 19;140(6):883-99.

188. Mantovani A. The growing diversity and spectrum of action of myeloid-derived suppressor cells. Eur J Immunol. 2010 Dec;40(12):3317-20.

189. Porembka MR, Mitchem JB, Belt BA, Hsieh CS, Lee HM, Herndon J, et al. Pancreatic adenocarcinoma induces bone marrow mobilization of myeloid-derived suppressor cells which promote primary tumor growth. Cancer Immunol Immunother. 2012 Sep;61(9):1373-85.

190. Hiraoka N, Onozato K, Kosuge T, Hirohashi S. Prevalence of FOXP3+ regulatory T cells increases during the progression of pancreatic ductal adenocarcinoma and its premalignant lesions. Clin Cancer Res. 2006 Sep 15;12(18):5423-34.

191. Ikemoto T, Yamaguchi T, Morine Y, Imura S, Soejima Y, Fujii M, et al. Clinical roles of increased populations of Foxp3+CD4+ T cells in peripheral blood from advanced pancreatic cancer patients. Pancreas. 2006 Nov;33(4):386-90.

192. Hermano E, Meirovitz A, Meir K, Nussbaum G, Appelbaum L, Peretz T, et al. Macrophage polarization in pancreatic carcinoma: role of heparanase enzyme. J Natl Cancer Inst. 2014 Oct 18;106(12):10.1093/jnci/dju332. Print 2014 Dec.

193. Gabitass RF, Annels NE, Stocken DD, Pandha HA, Middleton GW. Elevated myeloid-derived suppressor cells in pancreatic, esophageal and gastric cancer are an independent prognostic factor and are associated with significant elevation of the Th2 cytokine interleukin-13. Cancer Immunol Immunother. 2011 Oct;60(10):1419-30.

194. Basso D, Fogar P, Falconi M, Fadi E, Sperti C, Frasson C, et al. Pancreatic tumors and immature immunosuppressive myeloid cells in blood and spleen: role of inhibitory co-stimulatory molecules PDL1 and CTLA4. An in vivo and in vitro study. PLoS One. 2013;8(1):e54824.

195. Bogdan C. Nitric oxide and the immune response. Nat Immunol. 2001 Oct;2(10):907-16.

196. Huang B, Pan PY, Li Q, Sato AI, Levy DE, Bromberg J, et al. Gr-1+CD115+ immature myeloid suppressor cells mediate the development of tumor-induced T regulatory cells and T-cell anergy in tumor-bearing host. Cancer Res. 2006 Jan 15;66(2):1123-31.

197. Rodriguez PC, Ochoa AC. T cell dysfunction in cancer: role of myeloid cells and tumor cells regulating amino acid availability and oxidative stress. Semin Cancer Biol. 2006 Feb;16(1):66-72.

198. Ostrand-Rosenberg S. Myeloid-derived suppressor cells: more mechanisms for inhibiting antitumor immunity. Cancer Immunol Immunother. 2010 Oct;59(10):1593-600.

199. Mundy-Bosse BL, Lesinski GB, Jaime-Ramirez AC, Benninger K, Khan M, Kuppusamy P, et al. Myeloid-derived suppressor cell inhibition of the IFN response in tumor-bearing mice. Cancer Res. 2011 Aug 1;71(15):5101-10.

200. Beyer M, Schultze JL. Regulatory T cells in cancer. Blood. 2006 Aug 1;108(3):804-11.

201. Biswas SK, Mantovani A. Macrophage plasticity and interaction with lymphocyte subsets: cancer as a paradigm. Nat Immunol. 2010 Oct;11(10):889-96.

202. Kurahara H, Takao S, Maemura K, Mataki Y, Kuwahata T, Maeda K, et al. M2-polarized tumor-associated macrophage infiltration of regional lymph nodes is associated with nodal lymphangiogenesis and occult nodal involvement in pN0 pancreatic cancer. Pancreas. 2013 Jan;42(1):155-9.

203. Schoppmann SF, Birner P, Stockl J, Kalt R, Ullrich R, Caucig C, et al. Tumor-associated macrophages express lymphatic endothelial growth factors and are related to peritumoral lymphangiogenesis. Am J Pathol. 2002 Sep;161(3):947-56.

204. Wu H, Xu JB, He YL, Peng JJ, Zhang XH, Chen CQ, et al. Tumor-associated macrophages promote angiogenesis and lymphangiogenesis of gastric cancer. J Surg Oncol. 2012 Sep 15;106(4):462-8.

205. Schoppmann SF, Fenzl A, Nagy K, Unger S, Bayer G, Geleff S, et al. VEGF-C expressing tumor-associated macrophages in lymph node positive breast cancer: impact on lymphangiogenesis and survival. Surgery. 2006 Jun;139(6):839-46.

206. Esposito I, Menicagli M, Funel N, Bergmann F, Boggi U, Mosca F, et al. Inflammatory cells contribute to the generation of an angiogenic phenotype in pancreatic ductal adenocarcinoma. J Clin Pathol. 2004 Jun;57(6):630-6.

207. Rucki AA, Zheng L. Pancreatic cancer stroma: understanding biology leads to new therapeutic strategies. World J Gastroenterol. 2014 Mar 7;20(9):2237-46.

208. Clark CE, Hingorani SR, Mick R, Combs C, Tuveson DA, Vonderheide RH. Dynamics of the immune reaction to pancreatic cancer from inception to invasion. Cancer Res. 2007 Oct 1;67(19):9518-27.

209. Aebischer D, Iolyeva M, Halin C. The inflammatory response of lymphatic endothelium. Angiogenesis. 2014 Apr;17(2):383-93.

210. Liao S, von der Weid PY. Lymphatic system: an active pathway for immune protection. Semin Cell Dev Biol. 2015 Feb;38:83-9.

211. Podgrabinska S, Kamalu O, Mayer L, Shimaoka M, Snoeck H, Randolph GJ, et al. Inflamed lymphatic endothelium suppresses dendritic cell maturation and function via Mac-1/ICAM-1-dependent mechanism. J Immunol. 2009 Aug 1;183(3):1767-79.

212. Inman KS, Francis AA, Murray NR. Complex role for the immune system in initiation and progression of pancreatic cancer. World J Gastroenterol. 2014 Aug 28;20(32):11160-81.

213. Ghiringhelli F, Puig PE, Roux S, Parcellier A, Schmitt E, Solary E, et al. Tumor cells convert immature myeloid dendritic cells into TGF-beta-secreting cells inducing CD4+CD25+ regulatory T cell proliferation. J Exp Med. 2005 Oct 3;202(7):919-29.

214. Seo N, Hayakawa S, Takigawa M, Tokura Y. Interleukin-10 expressed at early tumour sites induces subsequent generation of CD4(+) T-regulatory cells and systemic collapse of antitumour immunity. Immunology. 2001 Aug;103(4):449-57.

215. De Smedt T, Van Mechelen M, De Becker G, Urbain J, Leo O, Moser M. Effect of interleukin-10 on dendritic cell maturation and function. Eur J Immunol. 1997 May;27(5):1229-35.

216. Munn DH, Mellor AL. Indoleamine 2,3-dioxygenase and tumor-induced tolerance. J Clin Invest. 2007 May;117(5):1147-54.

217. Fallarino F, Grohmann U, You S, McGrath BC, Cavener DR, Vacca C, et al. The combined effects of tryptophan starvation and tryptophan catabolites down-regulate T cell receptor zeta-chain and induce a regulatory phenotype in naive T cells. J Immunol. 2006 Jun 1;176(11):6752-61.

218. Munn DH, Sharma MD, Baban B, Harding HP, Zhang Y, Ron D, et al. GCN2 kinase in T cells mediates proliferative arrest and anergy induction in response to indoleamine 2,3-dioxygenase. Immunity. 2005 May;22(5):633-42.

219. Kim R, Emi M, Tanabe K, Arihiro K. Tumor-driven evolution of immunosuppressive networks during malignant progression. Cancer Res. 2006 Jun 1;66(11):5527-36.

220. Rouhani SJ, Eccles JD, Riccardi P, Peske JD, Tewalt EF, Cohen JN, et al. Roles of lymphatic endothelial cells expressing peripheral tissue antigens in CD4 T-cell tolerance induction. Nat Commun. 2015 Apr 10;6:6771.

221. Preynat-Seauve O, Contassot E, Schuler P, Piguet V, French LE, Huard B. Extralymphatic tumors prepare draining lymph nodes to invasion via a T-cell cross-tolerance process. Cancer Res. 2007 May 15;67(10):5009-16.

222. Swartz MA. Immunomodulatory roles of lymphatic vessels in cancer progression. Cancer Immunol Res. 2014 Aug;2(8):701-7.

223. Leek RD, Harris AL. Tumor-associated macrophages in breast cancer. J Mammary Gland Biol Neoplasia. 2002 Apr;7(2):177-89.

224. Condeelis J, Pollard JW. Macrophages: obligate partners for tumor cell migration, invasion, and metastasis. Cell. 2006 Jan 27;124(2):263-6.

225. Kurahara H, Shinchi H, Mataki Y, Maemura K, Noma H, Kubo F, et al. Significance of M2-polarized tumor-associated macrophage in pancreatic cancer. J Surg Res. 2011 May 15;167(2):e211-9.

226. Sugimura K, Miyata H, Tanaka K, Takahashi T, Kurokawa Y, Yamasaki M, et al. High infiltration of tumor-associated macrophages is associated with a poor response to chemotherapy and poor prognosis of patients undergoing neoadjuvant chemotherapy for esophageal cancer. J Surg Oncol. 2015 May;111(6):752-9.

227. Yuan ZY, Luo RZ, Peng RJ, Wang SS, Xue C. High infiltration of tumor-associated macrophages in triple-negative breast cancer is associated with a higher risk of distant metastasis. Onco Targets Ther. 2014 Aug 21;7:1475-80.

228. Ding M, Fu X, Tan H, Wang R, Chen Z, Ding S. The effect of vascular endothelial growth factor C expression in tumor-associated macrophages on lymphangiogenesis and lymphatic metastasis in breast cancer. Mol Med Rep. 2012 Nov;6(5):1023-9.

229. Storr SJ, Safuan S, Mitra A, Elliott F, Walker C, Vasko MJ, et al. Objective assessment of blood and lymphatic vessel invasion and association with macrophage infiltration in cutaneous melanoma. Mod Pathol. 2012 Apr;25(4):493-504.

230. Zhang BC, Gao J, Wang J, Rao ZG, Wang BC, Gao JF. Tumor-associated macrophages infiltration is associated with peritumoral lymphangiogenesis and poor prognosis in lung adenocarcinoma. Med Oncol. 2011 Dec;28(4):1447-52.

231. Yang H, Kim C, Kim MJ, Schwendener RA, Alitalo K, Heston W, et al. Soluble vascular endothelial growth factor receptor-3 suppresses lymphangiogenesis and lymphatic metastasis in bladder cancer. Mol Cancer. 2011 Apr 11;10:36,4598-10-36.

232. Zumsteg A, Baeriswyl V, Imaizumi N, Schwendener R, Ruegg C, Christofori G. Myeloid cells contribute to tumor lymphangiogenesis. PLoS One. 2009 Sep 17;4(9):e7067.

233. Fischer C, Jonckx B, Mazzone M, Zacchigna S, Loges S, Pattarini L, et al. Anti-PlGF inhibits growth of VEGF(R)-inhibitor-resistant tumors without affecting healthy vessels. Cell. 2007 Nov 2;131(3):463-75.

234. Marconi C, Bianchini F, Mannini A, Mugnai G, Ruggieri S, Calorini L. Tumoral and macrophage uPAR and MMP-9 contribute to the invasiveness of B16 murine melanoma cells. Clin Exp Metastasis. 2008;25(3):225-31.

235. Ran S, Montgomery KE. Macrophage-mediated lymphangiogenesis: the emerging role of macrophages as lymphatic endothelial progenitors. Cancers (Basel). 2012 Sep;4(3):618-57.

236. McColl BK, Baldwin ME, Roufail S, Freeman C, Moritz RL, Simpson RJ, et al. Plasmin activates the lymphangiogenic growth factors VEGF-C and VEGF-D. J Exp Med. 2003 Sep 15;198(6):863-8.

237. Hall KL, Volk-Draper LD, Flister MJ, Ran S. New model of macrophage acquisition of the lymphatic endothelial phenotype. PLoS One. 2012;7(3):e31794.

238. Hunter KE, Palermo C, Kester JC, Simpson K, Li JP, Tang LH, et al. Heparanase promotes lymphangiogenesis and tumor invasion in pancreatic neuroendocrine tumors. Oncogene. 2014 Apr 3;33(14):1799-808.

239. Schledzewski K, Falkowski M, Moldenhauer G, Metharom P, Kzhyshkowska J, Ganss R, et al. Lymphatic endothelium-specific hyaluronan receptor LYVE-1 is expressed by stabilin-1+, F4/80+, CD11b+ macrophages in malignant tumours and wound healing tissue in vivo and in bone marrow cultures in vitro: implications for the assessment of lymphangiogenesis. J Pathol. 2006 May;209(1):67-77.

240. Lee JY, Park C, Cho YP, Lee E, Kim H, Kim P, et al. Podoplanin-expressing cells derived from bone marrow play a crucial role in postnatal lymphatic neovascularization. Circulation. 2010 Oct 5;122(14):1413-25.

241. Maruyama K, Ii M, Cursiefen C, Jackson DG, Keino H, Tomita M, et al. Inflammation-induced lymphangiogenesis in the cornea arises from CD11b-positive macrophages. J Clin Invest. 2005 Sep;115(9):2363-72.

242. Hingorani SR, Petricoin EF, Maitra A, Rajapakse V, King C, Jacobetz MA, et al. Preinvasive and invasive ductal pancreatic cancer and its early detection in the mouse. Cancer Cell. 2003 Dec;4(6):437-50.

243. Oliver MH, Harrison NK, Bishop JE, Cole PJ, Laurent GJ. A rapid and convenient assay for counting cells cultured in microwell plates: application for assessment of growth factors. J Cell Sci. 1989 Mar;92 (Pt 3)(Pt 3):513-8.

244. Drake CG. Combination immunotherapy approaches. Ann Oncol. 2012 Sep;23 Suppl 8:viii41-6.

245. Frese KK, Neesse A, Cook N, Bapiro TE, Lolkema MP, Jodrell DI, et al. nab-Paclitaxel potentiates gemcitabine activity by reducing cytidine deaminase levels in a mouse model of pancreatic cancer. Cancer Discov. 2012 Mar;2(3):260-9.

246. Xu Z, Pothula SP, Wilson JS, Apte MV. Pancreatic cancer and its stroma: a conspiracy theory. World J Gastroenterol. 2014 Aug 28;20(32):11216-29.

247. Wilson JS, Pirola RC, Apte MV. Stars and stripes in pancreatic cancer: role of stellate cells and stroma in cancer progression. Front Physiol. 2014 Feb 14;5:52.

248. Gomes FG, Nedel F, Alves AM, Nor JE, Tarquinio SB. Tumor angiogenesis and lymphangiogenesis: tumor/endothelial crosstalk and cellular/microenvironmental signaling mechanisms. Life Sci. 2013 Feb 7;92(2):101-7.

249. Ando N, Nakao A, Nomoto S, Takeda S, Kaneko T, Kurokawa T, et al. Detection of mutant K-ras in dissected paraaortic lymph nodes of patients with pancreatic adenocarcinoma. Pancreas. 1997 Nov;15(4):374-8.

250. Sohn TA, Yeo CJ, Cameron JL, Koniaris L, Kaushal S, Abrams RA, et al. Resected adenocarcinoma of the pancreas-616 patients: results, outcomes, and prognostic indicators. J Gastrointest Surg. 2000 Nov-Dec;4(6):567-79.

251. Kayahara M, Nagakawa T, Ohta T, Kitagawa H, Ueno K, Tajima H, et al. Analysis of paraaortic lymph node involvement in pancreatic carcinoma: a significant indication for surgery? Cancer. 1999 Feb 1;85(3):583-90.

252. Madsen CD, Sahai E. Cancer dissemination--lessons from leukocytes. Dev Cell. 2010 Jul 20;19(1):13-26.

253. St Hill CA. Interactions between endothelial selectins and cancer cells regulate metastasis. Front Biosci (Landmark Ed). 2011 Jun 1;16:3233-51.

254. Patel KD, Cuvelier SL, Wiehler S. Selectins: critical mediators of leukocyte recruitment. Semin Immunol. 2002 Apr;14(2):73-81.

255. Sperandio M. Selectins and glycosyltransferases in leukocyte rolling in vivo. FEBS J. 2006 Oct;273(19):4377-89.

256. Rigby DA, Ferguson DJ, Johnson LA, Jackson DG. Neutrophils rapidly transit inflamed lymphatic vessel endothelium via integrin-dependent proteolysis and lipoxin-induced junctional retraction. J Leukoc Biol. 2015 Dec;98(6):897-912.

257. Gout S, Tremblay PL, Huot J. Selectins and selectin ligands in extravasation of cancer cells and organ selectivity of metastasis. Clin Exp Metastasis. 2008;25(4):335-44.

258. Taniguchi S, Iwamura T, Kitamura N, Yamanari H, Kojima A, Hidaka K, et al. Protein-free culture of the human pancreatic cancer cell line, SUIT-2. Hum Cell. 1994 Dec;7(4):207-14.

259. Taniguchi S, Iwamura T, Katsuki T. Correlation between spontaneous metastatic potential and type I collagenolytic activity in a human pancreatic cancer cell line (SUIT-2) and sublines. Clin Exp Metastasis. 1992 Jul;10(4):259-66.

260. Reymond N, d'Agua BB, Ridley AJ. Crossing the endothelial barrier during metastasis. Nat Rev Cancer. 2013 Dec;13(12):858-70.

261. Balkwill F. The significance of cancer cell expression of the chemokine receptor CXCR4. Semin Cancer Biol. 2004 Jun;14(3):171-9.

262. Balkwill F. Cancer and the chemokine network. Nat Rev Cancer. 2004 Jul;4(7):540-50.

263. Koshiba T, Hosotani R, Miyamoto Y, Ida J, Tsuji S, Nakajima S, et al. Expression of stromal cell-derived factor 1 and CXCR4 ligand receptor system in pancreatic cancer: a possible role for tumor progression. Clin Cancer Res. 2000 Sep;6(9):3530-5.

264. Thomas RM, Kim J, Revelo-Penafiel MP, Angel R, Dawson DW, Lowy AM. The chemokine receptor CXCR4 is expressed in pancreatic intraepithelial neoplasia. Gut. 2008 Nov;57(11):1555-60.

265. Salvucci O, Bouchard A, Baccarelli A, Deschenes J, Sauter G, Simon R, et al. The role of CXCR4 receptor expression in breast cancer: a large tissue microarray study. Breast Cancer Res Treat. 2006 Jun;97(3):275-83.

266. Mirisola V, Zuccarino A, Bachmeier BE, Sormani MP, Falter J, Nerlich A, et al. CXCL12/SDF1 expression by breast cancers is an independent prognostic marker of disease-free and overall survival. Eur J Cancer. 2009 Sep;45(14):2579-87.

267. Yu S, Wang X, Liu G, Zhu X, Chen Y. High level of CXCR4 in triple-negative breast cancer specimens associated with a poor clinical outcome. Acta Med Okayama. 2013;67(6):369-75.

268. Minamiya Y, Saito H, Takahashi N, Ito M, Imai K, Ono T, et al. Expression of the chemokine receptor CXCR4 correlates with a favorable prognosis in patients with adenocarcinoma of the lung. Lung Cancer. 2010 Jun;68(3):466-71.

269. Otsuka S, Klimowicz AC, Kopciuk K, Petrillo SK, Konno M, Hao D, et al. CXCR4 overexpression is associated with poor outcome in females diagnosed with stage IV non-small cell lung cancer. J Thorac Oncol. 2011 Jul;6(7):1169-78.

270. Wagner PL, Hyjek E, Vazquez MF, Meherally D, Liu YF, Chadwick PA, et al. CXCL12 and CXCR4 in adenocarcinoma of the lung: association with metastasis and survival. J Thorac Cardiovasc Surg. 2009 Mar;137(3):615-21.

271. Wehler TC, Graf C, Biesterfeld S, Brenner W, Schadt J, Gockel I, et al. Strong expression of chemokine receptor CXCR4 by renal cell carcinoma correlates with advanced disease. J Oncol. 2008;2008:626340.

272. Kim J, Takeuchi H, Lam ST, Turner RR, Wang HJ, Kuo C, et al. Chemokine receptor CXCR4 expression in colorectal cancer patients increases the risk for recurrence and for poor survival. J Clin Oncol. 2005 Apr 20;23(12):2744-53.

273. Liberman J, Sartelet H, Flahaut M, Muhlethaler-Mottet A, Coulon A, Nyalendo C, et al. Involvement of the CXCR7/CXCR4/CXCL12 axis in the malignant progression of human neuroblastoma. PLoS One. 2012;7(8):e43665.

274. Taichman RS, Cooper C, Keller ET, Pienta KJ, Taichman NS, McCauley LK. Use of the stromal cell-derived factor-1/CXCR4 pathway in prostate cancer metastasis to bone. Cancer Res. 2002 Mar 15;62(6):1832-7.

275. Gao Z, Wang X, Wu K, Zhao Y, Hu G. Pancreatic stellate cells increase the invasion of human pancreatic cancer cells through the stromal cell-derived factor-1/CXCR4 axis. Pancreatology. 2010;10(2-3):186-93.

276. Torzicky M, Viznerova P, Richter S, Strobl H, Scheinecker C, Foedinger D, et al. Platelet endothelial cell adhesion molecule-1 (PECAM-1/CD31) and CD99 are critical in lymphatic transmigration of human dendritic cells. J Invest Dermatol. 2012 Apr;132(4):1149-57.

277. Marchesi F, Monti P, Leone BE, Zerbi A, Vecchi A, Piemonti L, et al. Increased survival, proliferation, and migration in metastatic human pancreatic tumor cells expressing functional CXCR4. Cancer Res. 2004 Nov 15;64(22):8420-7.

278. Mori T, Doi R, Koizumi M, Toyoda E, Ito D, Kami K, et al. CXCR4 antagonist inhibits stromal cell-derived factor 1-induced migration and invasion of human pancreatic cancer. Mol Cancer Ther. 2004 Jan;3(1):29-37.

279. Shakir M, Tang D, Zeh HJ, Tang SW, Anderson CJ, Bahary N, et al. The chemokine receptors CXCR4/CXCR7 and their primary heterodimeric ligands CXCL12 and CXCL12/high mobility group box 1 in pancreatic cancer growth and development: finding flow. Pancreas. 2015 May;44(4):528-34.

280. Matsuo Y, Ochi N, Sawai H, Yasuda A, Takahashi H, Funahashi H, et al. CXCL8/IL-8 and CXCL12/SDF-1alpha co-operatively promote invasiveness and angiogenesis in pancreatic cancer. Int J Cancer. 2009 Feb 15;124(4):853-61.

281. Singh S, Srivastava SK, Bhardwaj A, Owen LB, Singh AP. CXCL12-CXCR4 signalling axis confers gemcitabine resistance to pancreatic cancer cells: a novel target for therapy. Br J Cancer. 2010 Nov 23;103(11):1671-9.

282. Ho TK, Shiwen X, Abraham D, Tsui J, Baker D. Stromal-Cell-Derived Factor-1 (SDF-1)/CXCL12 as Potential Target of Therapeutic Angiogenesis in Critical Leg Ischaemia. Cardiol Res Pract. 2012;2012:143209.

283. Janowski M. Functional diversity of SDF-1 splicing variants. Cell Adh Migr. 2009 Jul-Sep;3(3):243-9.

284. Yu L, Cecil J, Peng SB, Schrementi J, Kovacevic S, Paul D, et al. Identification and expression of novel isoforms of human stromal cell-derived factor 1. Gene. 2006 Jun 7;374:174-9.

285. Zhuo W, Jia L, Song N, Lu XA, Ding Y, Wang X, et al. The CXCL12-CXCR4 chemokine pathway: a novel axis regulates lymphangiogenesis. Clin Cancer Res. 2012 Oct 1;18(19):5387-98.

286. Liu KK, Dorovini-Zis K. Regulation of CXCL12 and CXCR4 expression by human brain endothelial cells and their role in CD4+ and CD8+ T cell adhesion and transendothelial migration. J Neuroimmunol. 2009 Oct 30;215(1-2):49-64.

287. Jin F, Brockmeier U, Otterbach F, Metzen E. New insight into the SDF-1/CXCR4 axis in a breast carcinoma model: hypoxia-induced endothelial SDF-1 and tumor cell CXCR4 are required for tumor cell intravasation. Mol Cancer Res. 2012 Aug;10(8):1021-31.

288. Mukherjee S, Manna A, Bhattacharjee P, Mazumdar M, Saha S, Chakraborty S, et al. Non-migratory tumorigenic intrinsic cancer stem cells ensure breast cancer metastasis by generation of CXCR4(+) migrating cancer stem cells. Oncogene. 2016 Sep 15;35(37):4937-48.

289. Scala S. Molecular Pathways: Targeting the CXCR4-CXCL12 Axis--Untapped Potential in the Tumor Microenvironment. Clin Cancer Res. 2015 Oct 1;21(19):4278-85.

290. Puchert M, Engele J. The peculiarities of the SDF-1/CXCL12 system: in some cells, CXCR4 and CXCR7 sing solos, in others, they sing duets. Cell Tissue Res. 2014 Feb;355(2):239-53.

291. Morimoto M, Matsuo Y, Koide S, Tsuboi K, Shamoto T, Sato T, et al. Enhancement of the CXCL12/CXCR4 axis due to acquisition of gemcitabine resistance in pancreatic cancer: effect of CXCR4 antagonists. BMC Cancer. 2016 May 12;16:305,016-2340-z.

292. Detoraki A, Staiano RI, Granata F, Giannattasio G, Prevete N, de Paulis A, et al. Vascular endothelial growth factors synthesized by human lung mast cells exert angiogenic effects. J Allergy Clin Immunol. 2009 May;123(5):1142,9, 1149.e1-5.

293. Raica M, Cimpean AM, Ceausu R, Ribatti D, Gaje P. Interplay between mast cells and lymphatic vessels in different molecular types of breast cancer. Anticancer Res. 2013 Mar;33(3):957-63.

294. Brideau G, Makinen MJ, Elamaa H, Tu H, Nilsson G, Alitalo K, et al. Endostatin overexpression inhibits lymphangiogenesis and lymph node metastasis in mice. Cancer Res. 2007 Dec 15;67(24):11528-35.

295. Gagliostro V, Seeger P, Garrafa E, Salvi V, Bresciani R, Bosisio D, et al. Pro-lymphangiogenic properties of IFN-gamma-activated human dendritic cells. Immunol Lett. 2016 May;173:26-35.

296. Isaka N, Padera TP, Hagendoorn J, Fukumura D, Jain RK. Peritumor lymphatics induced by vascular endothelial growth factor-C exhibit abnormal function. Cancer Res. 2004 Jul 1;64(13):4400-4.

297. Ochi N, Matsuo Y, Sawai H, Yasuda A, Takahashi H, Sato M, et al. Vascular endothelial growth factor-C secreted by pancreatic cancer cell line promotes lymphatic endothelial cell migration in an in vitro model of tumor lymphangiogenesis. Pancreas. 2007 May;34(4):444-51.

298. Tao J, Li T, Li K, Xiong J, Yang Z, Wu H, et al. Effect of HIF-1alpha on VEGF-C induced lymphangiogenesis and lymph nodes metastases of pancreatic cancer. J Huazhong Univ Sci Technolog Med Sci. 2006;26(5):562-4.

299. Ikenaga N, Ohuchida K, Mizumoto K, Cui L, Kayashima T, Morimatsu K, et al. CD10+ pancreatic stellate cells enhance the progression of pancreatic cancer. Gastroenterology. 2010 Sep;139(3):1041,51, 1051.e1-8.

300. Yuzawa S, Kano MR, Einama T, Nishihara H. PDGFRbeta expression in tumor stroma of pancreatic adenocarcinoma as a reliable prognostic marker. Med Oncol. 2012 Dec;29(4):2824-30.

301. Nakai K, Tanaka T, Murai T, Ohguro N, Tano Y, Miyasaka M. Invasive human pancreatic carcinoma cells adhere to endothelial tri-cellular corners and increase endothelial permeability. Cancer Sci. 2005 Nov;96(11):766-73.

302. Aceto N, Bardia A, Miyamoto DT, Donaldson MC, Wittner BS, Spencer JA, et al. Circulating tumor cell clusters are oligoclonal precursors of breast cancer metastasis. Cell. 2014 Aug 28;158(5):1110-22.

303. Hou JM, Krebs MG, Lancashire L, Sloane R, Backen A, Swain RK, et al. Clinical significance and molecular characteristics of circulating tumor cells and circulating tumor microemboli in patients with small-cell lung cancer. J Clin Oncol. 2012 Feb 10;30(5):525-32.

304. Burns AR, Walker DC, Brown ES, Thurmon LT, Bowden RA, Keese CR, et al. Neutrophil transendothelial migration is independent of tight junctions and occurs preferentially at tricellular corners. J Immunol. 1997 Sep 15;159(6):2893-903.

305. Walker DC, MacKenzie A, Hosford S. The structure of the tricellular region of endothelial tight junctions of pulmonary capillaries analyzed by freeze-fracture. Microvasc Res. 1994 Nov;48(3):259-81.

306. Sumagin R, Sarelius IH. Intercellular adhesion molecule-1 enrichment near tricellular endothelial junctions is preferentially associated with leukocyte transmigration and signals for reorganization of these junctions to accommodate leukocyte passage. J Immunol. 2010 May 1;184(9):5242-52.

307. Duda DG, Duyverman AM, Kohno M, Snuderl M, Steller EJ, Fukumura D, et al. Malignant cells facilitate lung metastasis by bringing their own soil. Proc Natl Acad Sci U S A. 2010 Dec 14;107(50):21677-82.

308. Laferriere J, Houle F, Taher MM, Valerie K, Huot J. Transendothelial migration of colon carcinoma cells requires expression of E-selectin by endothelial cells and activation of stress-activated protein kinase-2 (SAPK2/p38) in the tumor cells. J Biol Chem. 2001 Sep 7;276(36):33762-72.

309. Kim YJ, Varki A. Perspectives on the significance of altered glycosylation of glycoproteins in cancer. Glycoconj J. 1997 Aug;14(5):569-76.

310. Sawa Y, Tsuruga E. The expression of E-selectin and chemokines in the cultured human lymphatic endothelium with lipopolysaccharides. J Anat. 2008 May;212(5):654-63.

311. Kawarada Y, Ishikura H, Kishimoto T, Kato H, Yano T, Kato H, et al. The role of sialylated Lewis antigens on hematogenous metastases of human pancreas carcinoma cell lines in vivo. Pathol Res Pract. 2000;196(4):259-63.

312. Iwai K, Ishikura H, Kaji M, Sugiura H, Ishizu A, Takahashi C, et al. Importance of E-selectin (ELAM-1) and sialyl Lewis(a) in the adhesion of pancreatic carcinoma cells to activated endothelium. Int J Cancer. 1993 Jul 30;54(6):972-7.

313. Nozawa F, Hirota M, Okabe A, Shibata M, Iwamura T, Haga Y, et al. Tumor necrosis factor alpha acts on cultured human vascular endothelial cells to increase the adhesion of pancreatic cancer cells. Pancreas. 2000 Nov;21(4):392-8.

314. Kijima H, Kashiwagi H, Dowaki S, Ohtani Y, Tobita K, Matsubayasi H, et al. Stromal sialyl Le(a) expression is correlated with vascular invasion of human gallbladder adenocarcinoma. Int J Oncol. 2000 Jul;17(1):55-60.

315. Wei J, Cui L, Liu F, Fan Y, Lang R, Gu F, et al. E-selectin and Sialyl Lewis X expression is associated with lymph node metastasis of invasive micropapillary carcinoma of the breast. Int J Surg Pathol. 2010 Jun;18(3):193-200.

316. Sheen-Chen SM, Eng HL, Huang CC, Chen WJ. Serum levels of soluble E-selectin in women with breast cancer. Br J Surg. 2004 Dec;91(12):1578-81.

317. Numahata K, Satoh M, Handa K, Saito S, Ohyama C, Ito A, et al. Sialosyl-Le(x) expression defines invasive and metastatic properties of bladder carcinoma. Cancer. 2002 Feb 1;94(3):673-85.

318. Alexiou D, Karayiannakis AJ, Syrigos KN, Zbar A, Sekara E, Michail P, et al. Clinical significance of serum levels of E-selectin, intercellular adhesion molecule-1, and vascular cell adhesion molecule-1 in gastric cancer patients. Am J Gastroenterol. 2003 Feb;98(2):478-85.

319. Bal N, Kocer NE, Ertorer ME, Canpolat ET, Kayaselcuk F. Maspin, E-selectin, and P-selectin expressions in papillary thyroid carcinomas and their correlation with prognostic parameters. Pathol Res Pract. 2008;204(10):743-50.

320. Nakamori S, Nishihara S, Ikehara Y, Nagano H, Dono K, Sakon M, et al. Molecular mechanism involved in increased expression of sialyl Lewis antigens in ductal carcinoma of the pancreas. J Exp Clin Cancer Res. 1999 Sep;18(3):425-32.

321. Woodman N, Pinder SE, Tajadura V, Le Bourhis X, Gillett C, Delannoy P, et al. Two E-selectin ligands, BST-2 and LGALS3BP, predict metastasis and poor survival of ER-negative breast cancer. Int J Oncol. 2016 Jul;49(1):265-75.

322. Schultz MJ, Swindall AF, Bellis SL. Regulation of the metastatic cell phenotype by sialylated glycans. Cancer Metastasis Rev. 2012 Dec;31(3-4):501-18.

323. Ben-David T, Sagi-Assif O, Meshel T, Lifshitz V, Yron I, Witz IP. The involvement of the sLe-a selectin ligand in the extravasation of human colorectal carcinoma cells. Immunol Lett. 2008 Mar 15;116(2):218-24.

324. Julien S, Ivetic A, Grigoriadis A, QiZe D, Burford B, Sproviero D, et al. Selectin ligand sialyl-Lewis x antigen drives metastasis of hormone-dependent breast cancers. Cancer Res. 2011 Dec 15;71(24):7683-93.

325. Khatib AM, Kontogiannea M, Fallavollita L, Jamison B, Meterissian S, Brodt P. Rapid induction of cytokine and E-selectin expression in the liver in response to metastatic tumor cells. Cancer Res. 1999 Mar 15;59(6):1356-61.

326. Mannori G, Santoro D, Carter L, Corless C, Nelson RM, Bevilacqua MP. Inhibition of colon carcinoma cell lung colony formation by a soluble form of E-selectin. Am J Pathol. 1997 Jul;151(1):233-43.

327. Brodt P, Fallavollita L, Bresalier RS, Meterissian S, Norton CR, Wolitzky BA. Liver endothelial E-selectin mediates carcinoma cell adhesion and promotes liver metastasis. Int J Cancer. 1997 May 16;71(4):612-9.

328. Laubli H, Borsig L. Selectins as mediators of lung metastasis. Cancer Microenviron. 2010 Feb 27;3(1):97-105.

329. Roussos ET, Balsamo M, Alford SK, Wyckoff JB, Gligorijevic B, Wang Y, et al. Mena invasive (MenaINV) promotes multicellular streaming motility and transendothelial migration in a mouse model of breast cancer. J Cell Sci. 2011 Jul 1;124(Pt 13):2120-31.

330. Strell C, Lang K, Niggemann B, Zaenker KS, Entschladen F. Surface molecules regulating rolling and adhesion to endothelium of neutrophil granulocytes and MDA-MB-468 breast carcinoma cells and their interaction. Cell Mol Life Sci. 2007 Dec;64(24):3306-16.

331. Winkler IG, Barbier V, Nowlan B, Jacobsen RN, Forristal CE, Patton JT, et al. Vascular niche E-selectin regulates hematopoietic stem cell dormancy, self renewal and chemoresistance. Nat Med. 2012 Nov;18(11):1651-7.

332. Kitamura T, Qian BZ, Pollard JW. Immune cell promotion of metastasis. Nat Rev Immunol. 2015 Feb;15(2):73-86.

333. Winkler IG, Barbier V, Nutt HL, Hasnain SZ, Levesque J, Magnani JL, et al. **Administration Of E-Selectin Antagonist GMI-1271 Improves Survival After High-Dose Chemotherapy By Alleviating Mucositis and Accelerating Neutrophil Recovery**. Blood. 2013(122):2266.

334. Winkler IG, Barbier V, Perkins AC, Magnani JL, Levesque J. **Mobilisation of Reconstituting HSC Is Boosted By Synergy Between G-CSF and E-Selectin Antagonist GMI-1271.**. Blood. 2014(124):317.

335. Du LL, Liu P. CXCL12/CXCR4 axis regulates neovascularization and lymphangiogenesis in sutured corneas in mice. Mol Med Rep. 2016 Jun;13(6):4987-94.

336. Lechertier T, Berard M, Vassy R, Herve MA, Crepin M. Transendothelial migration of two metastatic breast carcinoma cells depend on the SDF-lalpha-CXCR4 complexes. Anticancer Res. 2004 Nov-Dec;24(6):4011-7.

337. Hamada T, Mohle R, Hesselgesser J, Hoxie J, Nachman RL, Moore MA, et al. Transendothelial migration of megakaryocytes in response to stromal cell-derived factor 1 (SDF-1) enhances platelet formation. J Exp Med. 1998 Aug 3;188(3):539-48.

338. Bryant J, Ahern DJ, Brennan FM. CXCR4 and vascular cell adhesion molecule 1 are key chemokine/adhesion receptors in the migration of cytokine-activated T cells. Arthritis Rheum. 2012 Jul;64(7):2137-46.

339. Phillips R, Ager A. Activation of pertussis toxin-sensitive CXCL12 (SDF-1) receptors mediates transendothelial migration of T lymphocytes across lymph node high endothelial cells. Eur J Immunol. 2002 Mar;32(3):837-47.

340. van Buul JD, Voermans C, van Gelderen J, Anthony EC, van der Schoot CE, Hordijk PL. Leukocyte-endothelium interaction promotes SDF-1-dependent polarization of CXCR4. J Biol Chem. 2003 Aug 8;278(32):30302-10.

341. Liu Z, Teng XY, Meng XP, Wang BS. Expression of stromal cell-derived factor 1 and CXCR7 ligand receptor system in pancreatic adenocarcinoma. World J Surg Oncol. 2014 Nov 18;12:348,7819-12-348.

342. Guo JC, Li J, Zhou L, Yang JY, Zhang ZG, Liang ZY, et al. CXCL12-CXCR7 axis contributes to the invasive phenotype of pancreatic cancer. Oncotarget. 2016 Aug 17.

343. Liu ZJ, Tian R, An W, Zhuge Y, Li Y, Shao H, et al. Identification of E-selectin as a novel target for the regulation of postnatal neovascularization: implications for diabetic wound healing. Ann Surg. 2010 Oct;252(4):625-34.

344. Singh AP, Arora S, Bhardwaj A, Srivastava SK, Kadakia MP, Wang B, et al. CXCL12/CXCR4 protein signaling axis induces sonic hedgehog expression in pancreatic cancer cells via extracellular regulated kinase- and Akt kinase-mediated activation of nuclear factor kappaB: implications for bidirectional tumor-stromal interactions. J Biol Chem. 2012 Nov 9;287(46):39115-24.

345. Hirakawa S, Kodama S, Kunstfeld R, Kajiya K, Brown LF, Detmar M. VEGF-A induces tumor and sentinel lymph node lymphangiogenesis and promotes lymphatic metastasis. J Exp Med. 2005 Apr 4;201(7):1089-99.

346. Liersch R, Hirakawa S, Berdel WE, Mesters RM, Detmar M. Induced lymphatic sinus hyperplasia in sentinel lymph nodes by VEGF-C as the earliest premetastatic indicator. Int J Oncol. 2012 Dec;41(6):2073-8.

347. Jeong HS, Jones D, Liao S, Wattson DA, Cui CH, Duda DG, et al. Investigation of the Lack of Angiogenesis in the Formation of Lymph Node Metastases. J Natl Cancer Inst. 2015 Jun 10;107(9):10.1093/jnci/djv155. Print 2015 Sep.

348. Yeo CJ, Cameron JL. Prognostic factors in ductal pancreatic cancer. Langenbecks Arch Surg. 1998 Apr;383(2):129-33.

349. Zuckerman DS, Ryan DP. Adjuvant therapy for pancreatic cancer: a review. Cancer. 2008 Jan 15;112(2):243-9.

350. Konstantinidis IT, Warshaw AL, Allen JN, Blaszkowsky LS, Castillo CF, Deshpande V, et al. Pancreatic ductal adenocarcinoma: is there a survival difference for R1 resections versus locally advanced unresectable tumors? What is a "true" R0 resection? Ann Surg. 2013 Apr;257(4):731-6.

351. Chang DK, Johns AL, Merrett ND, Gill AJ, Colvin EK, Scarlett CJ, et al. Margin clearance and outcome in resected pancreatic cancer. J Clin Oncol. 2009 Jun 10;27(17):2855-62.

352. Tempero MA, Malafa MP, Behrman SW, Benson AB,3rd, Casper ES, Chiorean EG, et al. Pancreatic adenocarcinoma, version 2.2014: featured updates to the NCCN guidelines. J Natl Compr Canc Netw. 2014 Aug;12(8):1083-93.

353. Gresham GK, Wells GA, Gill S, Cameron C, Jonker DJ. Chemotherapy regimens for advanced pancreatic cancer: a systematic review and network meta-analysis. BMC Cancer. 2014 Jun 27;14:471,2407-14-471.

354. Hurwitz H, Fehrenbacher L, Novotny W, Cartwright T, Hainsworth J, Heim W, et al. Bevacizumab plus irinotecan, fluorouracil, and leucovorin for metastatic colorectal cancer. N Engl J Med. 2004 Jun 3;350(23):2335-42.

355. Saltz LB, Clarke S, Diaz-Rubio E, Scheithauer W, Figer A, Wong R, et al. Bevacizumab in combination with oxaliplatin-based chemotherapy as first-line therapy in metastatic colorectal cancer: a randomized phase III study. J Clin Oncol. 2008 Apr 20;26(12):2013-9.

356. Sandler A, Gray R, Perry MC, Brahmer J, Schiller JH, Dowlati A, et al. Paclitaxel-carboplatin alone or with bevacizumab for non-small-cell lung cancer. N Engl J Med. 2006 Dec 14;355(24):2542-50.

357. Goel S, Wong AH, Jain RK. Vascular normalization as a therapeutic strategy for malignant and nonmalignant disease. Cold Spring Harb Perspect Med. 2012 Mar;2(3):a006486.

358. Goel S, Duda DG, Xu L, Munn LL, Boucher Y, Fukumura D, et al. Normalization of the vasculature for treatment of cancer and other diseases. Physiol Rev. 2011 Jul;91(3):1071-121.

359. Sahora K, Schindl M, Kuehrer I, Eisenhut A, Werba G, Brostjan C, et al. A phase II trial of two durations of Bevacizumab added to neoadjuvant gemcitabine for borderline and locally advanced pancreatic cancer. Anticancer Res. 2014 May;34(5):2377-84.

360. Sohal DP, Metz JM, Sun W, Giantonio BJ, Plastaras JP, Ginsberg G, et al. Toxicity study of gemcitabine, oxaliplatin, and bevacizumab, followed by 5-fluorouracil, oxaliplatin, bevacizumab, and radiotherapy, in patients with locally advanced pancreatic cancer. Cancer Chemother Pharmacol. 2013 Jun;71(6):1485-91.

361. Kindler HL, Niedzwiecki D, Hollis D, Sutherland S, Schrag D, Hurwitz H, et al. Gemcitabine plus bevacizumab compared with gemcitabine plus placebo in patients with advanced pancreatic cancer: phase III trial of the Cancer and Leukemia Group B (CALGB 80303). J Clin Oncol. 2010 Aug 1;28(22):3617-22.

362. Van Cutsem E, Vervenne WL, Bennouna J, Humblet Y, Gill S, Van Laethem JL, et al. Phase III trial of bevacizumab in combination with gemcitabine and erlotinib in patients with metastatic pancreatic cancer. J Clin Oncol. 2009 May 1;27(13):2231-7.

363. Bergers G, Hanahan D. Modes of resistance to anti-angiogenic therapy. Nat Rev Cancer. 2008 Aug;8(8):592-603.

364. Tamburrino A, Piro G, Carbone C, Tortora G, Melisi D. Mechanisms of resistance to chemotherapeutic and anti-angiogenic drugs as novel targets for pancreatic cancer therapy. Front Pharmacol. 2013 Apr 30;4:56.

365. Chien MH, Ku CC, Johansson G, Chen MW, Hsiao M, Su JL, et al. Vascular endothelial growth factor-C (VEGF-C) promotes angiogenesis by induction of COX-2 in leukemic cells via the VEGF-R3/JNK/AP-1 pathway. Carcinogenesis. 2009 Dec;30(12):2005-13.

366. Scavelli C, Vacca A, Di Pietro G, Dammacco F, Ribatti D. Crosstalk between angiogenesis and lymphangiogenesis in tumor progression. Leukemia. 2004 Jun;18(6):1054-8.

367. Cao Y, Linden P, Farnebo J, Cao R, Eriksson A, Kumar V, et al. Vascular endothelial growth factor C induces angiogenesis in vivo. Proc Natl Acad Sci U S A. 1998 Nov 24;95(24):14389-94.

368. Karpanen T, Wirzenius M, Makinen T, Veikkola T, Haisma HJ, Achen MG, et al. Lymphangiogenic growth factor responsiveness is modulated by postnatal lymphatic vessel maturation. Am J Pathol. 2006 Aug;169(2):708-18.

369. Lin J, Lalani AS, Harding TC, Gonzalez M, Wu WW, Luan B, et al. Inhibition of lymphogenous metastasis using adeno-associated virus-mediated gene transfer of a soluble VEGFR-3 decoy receptor. Cancer Res. 2005 Aug 1;65(15):6901-9.

370. He XW, Liu T, Chen YX, Cheng DJ, Li XR, Xiao Y, et al. Calcium carbonate nanoparticle delivering vascular endothelial growth factor-C siRNA effectively inhibits lymphangiogenesis and growth of gastric cancer in vivo. Cancer Gene Ther. 2008 Mar;15(3):193-202.

371. Roberts N, Kloos B, Cassella M, Podgrabinska S, Persaud K, Wu Y, et al. Inhibition of VEGFR-3 activation with the antagonistic antibody more potently suppresses lymph node and distant metastases than inactivation of VEGFR-2. Cancer Res. 2006 Mar 1;66(5):2650-7.

372. Krishnan J, Kirkin V, Steffen A, Hegen M, Weih D, Tomarev S, et al. Differential in vivo and in vitro expression of vascular endothelial growth factor (VEGF)-C and VEGF-D in tumors and its relationship to lymphatic metastasis in immunocompetent rats. Cancer Res. 2003 Feb 1;63(3):713-22.

373. Karpanen T, Egeblad M, Karkkainen MJ, Kubo H, Yla-Herttuala S, Jaattela M, et al. Vascular endothelial growth factor C promotes tumor lymphangiogenesis and intralymphatic tumor growth. Cancer Res. 2001 Mar 1;61(5):1786-90.

374. Stacker SA, Caesar C, Baldwin ME, Thornton GE, Williams RA, Prevo R, et al. VEGF-D promotes the metastatic spread of tumor cells via the lymphatics. Nat Med. 2001 Feb;7(2):186-91.

375. He Y, Kozaki K, Karpanen T, Koshikawa K, Yla-Herttuala S, Takahashi T, et al. Suppression of tumor lymphangiogenesis and lymph node metastasis by blocking vascular endothelial growth factor receptor 3 signaling. J Natl Cancer Inst. 2002 Jun 5;94(11):819-25.

376. Chen Z, Varney ML, Backora MW, Cowan K, Solheim JC, Talmadge JE, et al. Down-regulation of vascular endothelial cell growth factor-C expression using small interfering RNA vectors in mammary tumors inhibits tumor lymphangiogenesis and spontaneous metastasis and enhances survival. Cancer Res. 2005 Oct 1;65(19):9004-11.

377. Shimizu K, Kubo H, Yamaguchi K, Kawashima K, Ueda Y, Matsuo K, et al. Suppression of VEGFR-3 signaling inhibits lymph node metastasis in gastric cancer. Cancer Sci. 2004 Apr;95(4):328-33.

378. Burton JB, Priceman SJ, Sung JL, Brakenhielm E, An DS, Pytowski B, et al. Suppression of prostate cancer nodal and systemic metastasis by blockade of the lymphangiogenic axis. Cancer Res. 2008 Oct 1;68(19):7828-37.

379. Thelen A, Scholz A, Benckert C, von Marschall Z, Schroder M, Wiedenmann B, et al. VEGF-D promotes tumor growth and lymphatic spread in a mouse model of hepatocellular carcinoma. Int J Cancer. 2008 Jun 1;122(11):2471-81.

380. Yang F, Jin C, Yang D, Jiang Y, Li J, Di Y, et al. Magnetic functionalised carbon nanotubes as drug vehicles for cancer lymph node metastasis treatment. Eur J Cancer. 2011 Aug;47(12):1873-82.

381. Caunt M, Mak J, Liang WC, Stawicki S, Pan Q, Tong RK, et al. Blocking neuropilin-2 function inhibits tumor cell metastasis. Cancer Cell. 2008 Apr;13(4):331-42.

382. Ou JJ, Wei X, Peng Y, Zha L, Zhou RB, Shi H, et al. Neuropilin-2 mediates lymphangiogenesis of colorectal carcinoma via a VEGFC/VEGFR3 independent signaling. Cancer Lett. 2015 Mar 28;358(2):200-9.

383. Neal J, Wakelee H. AMG-386, a selective angiopoietin-1/-2-neutralizing peptibody for the potential treatment of cancer. Curr Opin Mol Ther. 2010 Aug;12(4):487-95.

384. Holopainen T, Saharinen P, D'Amico G, Lampinen A, Eklund L, Sormunen R, et al. Effects of angiopoietin-2-blocking antibody on endothelial cell-cell junctions and lung metastasis. J Natl Cancer Inst. 2012 Mar 21;104(6):461-75.

385. Da MX, Wu Z, Tian HW. Tumor lymphangiogenesis and lymphangiogenic growth factors. Arch Med Res. 2008 May;39(4):365-72.

386. Cao R, Ji H, Feng N, Zhang Y, Yang X, Andersson P, et al. Collaborative interplay between FGF-2 and VEGF-C promotes lymphangiogenesis and metastasis. Proc Natl Acad Sci U S A. 2012 Sep 25;109(39):15894-9.

387. Chen HM, Tsai CH, Hung WC. Foretinib inhibits angiogenesis, lymphangiogenesis and tumor growth of pancreatic cancer in vivo by decreasing VEGFR-2/3 and TIE-2 signaling. Oncotarget. 2015 Jun 20;6(17):14940-52.

388. Heckman CA, Holopainen T, Wirzenius M, Keskitalo S, Jeltsch M, Yla-Herttuala S, et al. The tyrosine kinase inhibitor cediranib blocks ligand-induced vascular endothelial growth factor receptor-3 activity and lymphangiogenesis. Cancer Res. 2008 Jun 15;68(12):4754-62.

389. Padera TP, Kuo AH, Hoshida T, Liao S, Lobo J, Kozak KR, et al. Differential response of primary tumor versus lymphatic metastasis to VEGFR-2 and VEGFR-3 kinase inhibitors cediranib and vandetanib. Mol Cancer Ther. 2008 Aug;7(8):2272-9.

390. Grunwald V, Merseburger AS. Axitinib for the treatment of patients with advanced metastatic renal cell carcinoma (mRCC) after failure of prior systemic treatment. Onco Targets Ther. 2012;5:111-7.

391. Spano JP, Chodkiewicz C, Maurel J, Wong R, Wasan H, Barone C, et al. Efficacy of gemcitabine plus axitinib compared with gemcitabine alone in patients with advanced pancreatic cancer: an open-label randomised phase II study. Lancet. 2008 Jun 21;371(9630):2101-8.

392. Rixe O, Bukowski RM, Michaelson MD, Wilding G, Hudes GR, Bolte O, et al. Axitinib treatment in patients with cytokine-refractory metastatic renal-cell cancer: a phase II study. Lancet Oncol. 2007 Nov;8(11):975-84.

393. Reataza M, Imagawa DK. Advances in managing hepatocellular carcinoma. Front Med. 2014 Jun;8(2):175-89.

394. Procopio G, Verzoni E, Testa I, Nicolai N, Salvioni R, Debraud F. Experience with sorafenib in the treatment of advanced renal cell carcinoma. Ther Adv Urol. 2012 Dec;4(6):303-13.

395. Wilhelm SM, Carter C, Tang L, Wilkie D, McNabola A, Rong H, et al. BAY 43-9006 exhibits broad spectrum oral antitumor activity and targets the RAF/MEK/ERK pathway and receptor tyrosine kinases involved in tumor progression and angiogenesis. Cancer Res. 2004 Oct 1;64(19):7099-109.

396. Khagi S, Saif MW. Pancreatic neuroendocrine tumors: targeting the molecular basis of disease. Curr Opin Oncol. 2015 Jan;27(1):38-43.

397. Detry B, Blacher S, Erpicum C, Paupert J, Maertens L, Maillard C, et al. Sunitinib inhibits inflammatory corneal lymphangiogenesis. Invest Ophthalmol Vis Sci. 2013 May 3;54(5):3082-93.

398. Mankal P, O'Reilly E. Sunitinib malate for the treatment of pancreas malignancies--where does it fit? Expert Opin Pharmacother. 2013 Apr;14(6):783-92.

399. Kodera Y, Katanasaka Y, Kitamura Y, Tsuda H, Nishio K, Tamura T, et al. Sunitinib inhibits lymphatic endothelial cell functions and lymph node metastasis in a breast cancer model through inhibition of vascular endothelial growth factor receptor 3. Breast Cancer Res. 2011 Jun 21;13(3):R66.

400. Ahn HK, Choi JY, Kim KM, Kim H, Choi SH, Park SH, et al. Phase II study of pazopanib monotherapy in metastatic gastroenteropancreatic neuroendocrine tumours. Br J Cancer. 2013 Sep 17;109(6):1414-9.

401. Verweij J, Sleijfer S. Pazopanib, a new therapy for metastatic soft tissue sarcoma. Expert Opin Pharmacother. 2013 May;14(7):929-35.

402. Schutz FA, Choueiri TK, Sternberg CN. Pazopanib: Clinical development of a potent anti-angiogenic drug. Crit Rev Oncol Hematol. 2011 Mar;77(3):163-71.

403. Baker CH, Solorzano CC, Fidler IJ. Blockade of vascular endothelial growth factor receptor and epidermal growth factor receptor signaling for therapy of metastatic human pancreatic cancer. Cancer Res. 2002 Apr 1;62(7):1996-2003.

404. Solorzano CC, Baker CH, Bruns CJ, Killion JJ, Ellis LM, Wood J, et al. Inhibition of growth and metastasis of human pancreatic cancer growing in nude mice by PTK 787/ZK222584, an inhibitor of the vascular endothelial growth factor receptor tyrosine kinases. Cancer Biother Radiopharm. 2001 Oct;16(5):359-70.

405. Sini P, Samarzija I, Baffert F, Littlewood-Evans A, Schnell C, Theuer A, et al. Inhibition of multiple vascular endothelial growth factor receptors (VEGFR) blocks lymph node metastases but inhibition of VEGFR-2 is sufficient to sensitize tumor cells to platinum-based chemotherapeutics. Cancer Res. 2008 Mar 1;68(5):1581-92.

406. Lin B, Podar K, Gupta D, Tai YT, Li S, Weller E, et al. The vascular endothelial growth factor receptor tyrosine kinase inhibitor PTK787/ZK222584 inhibits growth and migration of multiple myeloma cells in the bone marrow microenvironment. Cancer Res. 2002 Sep 1;62(17):5019-26.

407. Drevs J, Hofmann I, Hugenschmidt H, Wittig C, Madjar H, Muller M, et al. Effects of PTK787/ZK 222584, a specific inhibitor of vascular endothelial growth factor receptor tyrosine kinases, on primary tumor, metastasis, vessel density, and blood flow in a murine renal cell carcinoma model. Cancer Res. 2000 Sep 1;60(17):4819-24.

408. Dragovich T, Laheru D, Dayyani F, Bolejack V, Smith L, Seng J, et al. Phase II trial of vatalanib in patients with advanced or metastatic pancreatic adenocarcinoma after first-line gemcitabine therapy (PCRT O4-001). Cancer Chemother Pharmacol. 2014 Aug;74(2):379-87.

409. Kindler HL, Ioka T, Richel DJ, Bennouna J, Letourneau R, Okusaka T, et al. Axitinib plus gemcitabine versus placebo plus gemcitabine in patients with advanced pancreatic adenocarcinoma: a double-blind randomised phase 3 study. Lancet Oncol. 2011 Mar;12(3):256-62.

410. Cardin DB, Goff L, Li CI, Shyr Y, Winkler C, DeVore R, et al. Phase II trial of sorafenib and erlotinib in advanced pancreatic cancer. Cancer Med. 2014 Jun;3(3):572-9.

411. Goncalves A, Gilabert M, Francois E, Dahan L, Perrier H, Lamy R, et al. BAYPAN study: a double-blind phase III randomized trial comparing gemcitabine plus sorafenib and gemcitabine plus placebo in patients with advanced pancreatic cancer. Ann Oncol. 2012 Nov;23(11):2799-805.

412. Hoshida T, Isaka N, Hagendoorn J, di Tomaso E, Chen YL, Pytowski B, et al. Imaging steps of lymphatic metastasis reveals that vascular endothelial growth factor-C increases metastasis by increasing delivery of cancer cells to lymph nodes: therapeutic implications. Cancer Res. 2006 Aug 15;66(16):8065-75.

413. Nune SK, Gunda P, Majeti BK, Thallapally PK, Forrest ML. Advances in lymphatic imaging and drug delivery. Adv Drug Deliv Rev. 2011 Sep 10;63(10-11):876-85.

414. Sevick-Muraca EM, Kwon S, Rasmussen JC. Emerging lymphatic imaging technologies for mouse and man. J Clin Invest. 2014 Mar;124(3):905-14.

415. Witte MH, Dellinger MT, McDonald DM, Nathanson SD, Boccardo FM, Campisi CC, et al. Lymphangiogenesis and hemangiogenesis: potential targets for therapy. J Surg Oncol. 2011 May 1;103(6):489-500.

416. Michalski CW, Kleeff J, Wente MN, Diener MK, Buchler MW, Friess H. Systematic review and meta-analysis of standard and extended lymphadenectomy in pancreaticoduodenectomy for pancreatic cancer. Br J Surg. 2007 Mar;94(3):265-73.

417. O'Hagan D, Christy N, Davis S. Particulates and lymphatic drug delivery. In: Charman W, Stella V, editors. Lymphatic transport of drugs. Boca Raton, FL, USA: CRC Press Inc.; 1992. p. 279,280-315.

418. Singh I, Swami R, Khan W, Sistla R. Lymphatic system: a prospective area for advanced targeting of particulate drug carriers. Expert Opin Drug Deliv. 2014 Feb;11(2):211-29.

419. Ali Khan A, Mudassir J, Mohtar N, Darwis Y. Advanced drug delivery to the lymphatic system: lipid-based nanoformulations. Int J Nanomedicine. 2013;8:2733-44.

420. Li X, Dong Q, Yan Z, Lu W, Feng L, Xie C, et al. MPEG-DSPE polymeric micelle for translymphatic chemotherapy of lymph node metastasis. Int J Pharm. 2015 Jun 20;487(1-2):8-16.

421. Kaminskas LM, Ascher DB, McLeod VM, Herold MJ, Le CP, Sloan EK, et al. PEGylation of interferon alpha2 improves lymphatic exposure after subcutaneous and intravenous administration and improves antitumour efficacy against lymphatic breast cancer metastases. J Control Release. 2013 Jun 10;168(2):200-8.

422. Dunne AA, Boerner HG, Kukula H, Schlaad H, Wiegand S, Werner JA, et al. Block copolymer carrier systems for translymphatic chemotherapy of lymph node metastases. Anticancer Res. 2007 Nov-Dec;27(6B):3935-40.

423. Radomski M, Zeh HJ, Edington HD, Pingpank JF, Butterfield LH, Whiteside TL, et al. Prolonged intralymphatic delivery of dendritic cells through implantable lymphatic ports in patients with advanced cancer. J Immunother Cancer. 2016 Apr 19;4:24,016-0128-y. eCollection 2016.

424. Zor M, Yildirim I, Basal S, Yaman H, Ozturk M, Irkilata CH, et al. Intralymphatic delivery of platinum-based chemotherapeutics is possible: an experimental study. J Cancer Res Clin Oncol. 2012 Oct;138(10):1679-82.